Performance of 2D geometric morphometric analysis in hominin taxonomy and its application to the mandibular molar sample from Lomekwi, Kenya

Mykolas Dovydas Imbrasas

Student No. 17905401

School of Anthropology and Conservation

University of Kent

Project supervisor – Dr. Matthew Skinner

Submitted November 2018

Acknowledgements

I would like to thank Matthew Skinner for introducing me to the world of hominin dentition, and for providing detailed instruction regarding the current techniques (geometric morphometrics, micro-CT scanning, and software used for visualizing 3D data) used in studies of hominin tooth morphology. I would also like to thank Matthew Skinner for his support and guidance throughout this research and beyond it. I would like to thank Tracy Kivell for providing me with the opportunity to work with fossil hominin hands, which was a welcomed change of scenery from teeth.

Lastly, I would like to thank my parents for their financial and moral support throughout this year.

Abstract

The Lomekwi area, situated west of Late Turkana, Kenya, has yielded numerous hominin fossil specimens, mostly isolated teeth, dated to between 3.5 to 3.2 million years ago. The isolated dental remains from Lomekwi have been tentatively attributed to *Kenyanthropus platyops*, whereas a number of specimens (KNM-WT 8556 and KNM-WT 16006) have been referred to as *Australopithecus afarensis*. However, the type specimens of *K. platyops* do not have sufficient dental material preserved, which does not allow the direct comparison of the isolated Lomekwi teeth to the dentition *of K. platyops*. In this study, 2D geometric morphometric (GM) data of the occlusal enamel surface of the crown have been used to compare the crown morphology of eleven mandibular molars from Lomekwi to specimens attributed to *Au. afarensis* (n=26), *Au. africanus* (n=35), and *Au. anamensis* (n=11). The current study also compared the performance of 2D GM data to traditional crown morphology measurements (cusp areas and mesiodistal and buccolingual dimensions) in classifying molars to their correct taxon by use of a canonical variate analysis (CVA), and finding differences between taxa in MANOVAs and permutational MANOVAs. The results showed that the Lomekwi sample was not exclusively linked to any of the comparative *Australopithecus* taxa, and exhibited some degree of morphological uniqueness. With regards to the data type comparisons, 2D GM data has been shown to be able to more accurately classify specimens to their correct taxonomic groups, and find a larger number of significant differences between taxa than traditional crown morphology measurements.

Table of Contents

CHAPTER 1: INTRODUCTION, AIMS, TERMINOLOGY, AND LITERATURE REVIEW

1.1 Introduction

Teeth constitute a major part of the hominin fossil record (Guatelli-Steinberg, 2016). Teeth are compact, strong, and made of mineralized tissue, which renders them relatively resilient to weathering, and allows them to be found in a particularly well preserved condition. Their direct contact with the environment during the lifespan of an individual can provide insights about diet and behavior (Ungar, 2011), and the strong genetic control of their development and morphology makes teeth useful for inferring taxonomic affinities and phylogenetic relationships (Irish et al., 2013).

Crown and root morphology (Dart, 1934; Robinson, 1956; Manthi, Plavcan and Ward, 2012; Wood, Abbott and Uytterschaut, 1988), crown size (e.g. Tobias, 1966), cusp size and fissure patterns (Wood, Abbot and Graham, 1983; Grine, Delanty and Wood, 2013), cusp angles (e.g. Suwa, 1988), and the enamal-dentine junction (Skinner et al., 2008) have been used in studies of hominin taxonomy. However, the majority of hominin dentition studies focus on the outer enamel surface, mainly due to three reasons: 1) micro-computed tomography imaging techniques are relatively new, and became accessible only recently (Swain and Xue, 2009); 2) diagenetic processess can result in enamel and dentine having similar gray scale values, which could both preclude segmentation of dental tissues and diminish sample size (Skinner, 2008); 3) the majority of dental remains do not maintain any roots.

1.2 Lomekwi and *Kenyanthropus platyops*

Fieldwork in 1998 and 1999 was being undertaken at the site of Lomekwi, situated west of Lake Turkana, Kenya, in an attempt to find evidence for hominin diversity between four and three mya (million years ago). Isolated teeth and parts of two maxillae were recovered. However, the most significant finding was that of an almost complete, albeit distorted, cranium (KNM-WT 4000) dated to 3.5mya, which became the holotype for the new hominin species *Kenyanthropus platyops* (Leakey et al., 2001). The two most distinguishable features of the holotype are its reduced sub-nasal prognathism, and the very small upper second molar. White (2003) questioned the validity of creating a new genus for the Lomekwi specimens, and argued that the cranium is that of a distorted *Australopithecus afarensis*. Spoor, Leakey and Leakey (2010) countered the claims made by White (2003) by conducting a comparative geometric morphometric (GM) analysis of the maxilla of KNM-WT 40000, and finding support for the assertions made by Leakey and colleagues (2011) about the uniqueness of the cranium.

In their initial description of the Lomekwi material, Leakey et al. (2001) reserved judgement about the taxonomy of the KNM-WT 8556 mandible and the isolated teeth. Partly because no morphological comparisons could be made with the holotype and paratype specimens, and in part because some of the lower isolated molars were considered to be too big for the small upper molars of KNM-WT 40000 and KNM-WT 38350. However, Leakey et al. (2001) did note that the morphology of the KNM-WT 8556 mandible showed features that distinguished it from *Au. afarensis*, and the crowns of the lower third premolar and lower third molar were enlarged relative to the lower first molar, a condition comparable to that of *Paranthropus boisei*. A GM

analysis of the lower fourth premolars by Haile-Selassie and Melillo (2015) supports the claim that the lower fourth premolars of KNM-WT 8556 are unusually large when compared to those of *Au. afarensis*. Furthermore, the isolated molars had numerous secondary fissures, low relief, and some exhibited a protostylid, which is absent in *Au. afarensis*. In a later publication, Wood and Leakey (2011) assigned the dental material from Lomekwi to cf. *Kenyanthropus platyops*, whereas Brown, Brown and Walker (2001) refer to KNM-WT 8556 and KNM-WT 16006 as *Au. afarensis*. To date, only one study has been conducted on the dental sample from Lomekwi (Skinner et al., in preparation). The results suggest that the teeth are similar to those of *Au. afarensis*, albeit inconclusively. The uncertainty in the results mainly comes from the use of mesiodistal (MD) and buccolingual (BL) measurements, which are limited in their ability to capture tooth crown morphology.

1.3 Geometric morphometrics

Various methodologies have been employed in studies of hominin dentition for assessing taxonomy and evaluating relationships between taxa (e.g. Robinson, 1956; Ashton and Zuckerman, 1950; Clark, 1950b; Wood, Abbot and Graham, 1983; Suwa, 1988). However, most studies have relied on descriptive and qualitative data (e.g. Robinson, 1956), MD and BL dimensions (Robinson, 1956; Tobias, 1966), measurements of cusp areas and angles (Suwa, 1988), and ASUDAS (Arizona State University Dental Anthropology System) (e.g. Irish et al., 2013). While these methodological approaches have provided important insights about the taxonomic affinities of fossil hominins, they, nevertheless, have limitations. Relying mostly on linear measurements, and at times on cusp ratios and angles (e.g. Suwa, 1988), the ability to

comprehensively capture crown shape is limited. While the ASUDAS is a powerful tool for assessing morphological variability (e.g. Irish et al., 2013; Irish and Guatelli-Steinberg, 2003), it does not fully succeed in capturing the full range of morphological variation in hominin fossil teeth, and established criteria for scoring dental traits present in hominins but not in *Homo sapiens* are still lacking (Hlusko, 2004; Gomez-Robles et al, 2007). An additional limitation of these methods is the difficulty in accounting for size and orientation (Martinon-Torres et al., 2006). As these shortcomings have been outlined in other, non-paleoanthropological, biometric studies, statisticians sought to develop better tools for capturing biological shape. This quest culminated in what is called "The Geometric Morphometric Revolution" beginning in the early 1990s (Adams, Rohlf and Slice, 2004).

In geometric morphometric analysis, the definition of shape is "all the geometric information that remains when location, scale and rotational effects are filtered from an object" (Kendall, 1977). Shape can be understood as the configuration of landmarks, and the relationship between them, that are present within and between populations (Bookstein, 1991). Bookstein (1991) described three different types of landmarks. The first is a point that is homologous between biological forms and is biologically unique and significant; the second is a point that is homologous between biological forms but its significance is geometric rather than biological (e.g. the point of maximum curvature along a boundary); and the third is a landmark that has at least one deficient point (e.g. end of the longest diameter). The third type can characterize more than one region of the form. In current usage, Type I and Type II landmarks are often referred to as "fixed landmarks", "anatomical landmarks" or simply "landmarks", while Type III are known as "semi-landmarks" (Adams, Rohlf and Slice, 2004).

Location, size, and rotation are filtered out with the use of a Generalized Procrustes Analysis (GPA), where least square methods fit a configuration of landmarks of a single target on a reference structure, by rotating, translating and scaling it, through a process called superimposition (Bookstein, 1991). During the GPA, a centroid size is obtained, which is the square root of the sum of the square roots of the distances between each landmark and the center point (centroid) (Zelditch, Swiderski and Sheets, 2004). The centroid size is a measure of size that is independent of shape (Zelditch Swiderski and Sheets, 2004). Thin plate splines can then visualize and quantify the relationship between landmarks through a Procrustes fit between the objects by deforming one into the other (Bookstein, 1991).

While each semilandmark by itself does not carry meaningful biological information, a set of semilandmarks can carry information about the shape of the object that is biologically useful (Martinon-Torres et al., 2006). Because the spacing of semilandmarks is arbitrary, and consequently can result in inaccurate differences between objects, sliding procedures are often employed (Gunz and Mitteroecker, 2013). During the sliding procedure, the semilandmarks of one specimen slide along the curve, following lines tangent to the curve, until the criteria of bending energy, or Procrustes distance, is achieved (Gunz and Mitteroecker, 2013). This process is repeated with each specimen with respect to the reference template, until their bending energy or Procrustes distances are minimized. The new shape and coordinates can then be used for a principal components analysis or canonical variate analysis (Gunz and Mitteroecker, 2013).

Geometric morphometrics in paleoanthropological studies have been successfully applied in comparative studies of hominin 2D outer enamel surface morphology (e.g. Wood, Abbott and

Graham, 1983; Martinon-Torres et al., 2006; Gomez-Robles et al., 2007, 2008, 2011; Haile-Selassie and Melillo, 2015), and 3D enamel-dentine junction morphology (e.g. Skinner et al., 2008; Martin et al., 2017).

1.4 Aims

The main aim of the thesis is to shed light on the taxonomy of the fossil hominin mandibular molars from Lomekwi, which are currently attributed to *Kenyanthropus platyops* (Wood and Leakey, 2011), using 2D geometric morphometric data.

First, 2D geometric morphometric data are compared to linear measurements (MD and BL dimensions, crown shape, and crown size) and relative and absolute cusp areas data. The aim is to test how well each data type is able to correctly classify mandibular molars to their correct taxonomic group, and how well can the data types differentiate between four taxa in multivariate analyses. This assessment is described in Chapter two.

Second, using 2D GM data, the question is asked: to which known *Australopithecus* taxa is the Lomekwi sample most similar?

Third, using 2D GM data, the question is asked: does the Lomekwi sample exhibit lower molar crown shape morphology that distinguishes it from known *Australopithecus* taxa?

The analyses dedicated to answering the questions pertaining to the Lomekwi sample are undertaken in Chapter three.

1.5 Terminology

In the following thesis the terms describing taxonomic membership are used following Wood and Richmond (2010). Hominid refers to any member of the family Hominidae which includes all extant great apes (*Pongo*, *Pan*, *Gorilla,* and modern humans). Hominin referes to any members of the tribe Hominini, which includes taxa that are more closely related to modern humans than to extant non-human apes. These are divided into two subtribes: Australopithecina, which contains the genera *Paranthropus*, *Australopithecus*, *Kenyanthropus,* and *Ardipitheucs*; and Hominina, which comprises of the genus *Homo*.

The mandibular molars of hominids usually exhibit five main cusps: the metaconid and protoconid, which are situated in the mesial half of the crown, or the trigonid; and the hypoconulid, hypoconid, and entoconid, which are located in the distal half of the crown, or the talonid (Figure 1.1). Hominid lower molars sometimes express accessory cusps: a C6, which usually lies within the distal fovea between the entoconid and hypoconulid; a C7, which lies on the lingual border of the crown between the entoconid and metaconid; and a protostylid, which is a cuspular enamel ridge that forms on the buccal surface of the protoconid. Seven main fissures (or grooves) delineate the main five cusps (Figure 1.2). The terminology used to describe the fissures in the thesis follows Wood, Abbott and Graham (1983). However, in order to increase the capacity to describe the fissure morphology in greater detail, the distal longitudinal fissure, which refers to the fissure that runs from the start of the lingual fissure and terminate at the distal fovea, has been divided into two section. The first section of the fissure, which will be referred to as the distal longitudinal fissure, starts at the base of the lingual

fissure and terminates where it intersects with the distobuccal fissure. The second section of the fissure, which will be referred to as the distolingual fissure, starts at the point where the distal longitudinal fissure and distobuccal fissure meet, and terminates at the distal fovea. The mesial longitudinal fissure has also been divided into two sections: the first represents part of the fissure that emanates from the mesial fovea and terminates at the intersection with the mesiobuccal fissure. This fissure will be referred to as the mesial longitudinal fissure; the second section refers to the fissure that begins at the point where the mesial longitudinal and mesiobuccal fissures meet, and terminates at the central pit. This fissure will be referred to as the longitudinal fissure.

In the thesis the lower dentition will be described using a subscript. That is, a lower second left molar would be referred to as LM_2, and a lower second molar will be written as M_2. Upper molars will be referred to using a superscript. Thus, an upper right second molar wil be referred to as RM^2, and an upper second molar would be written as M^2.

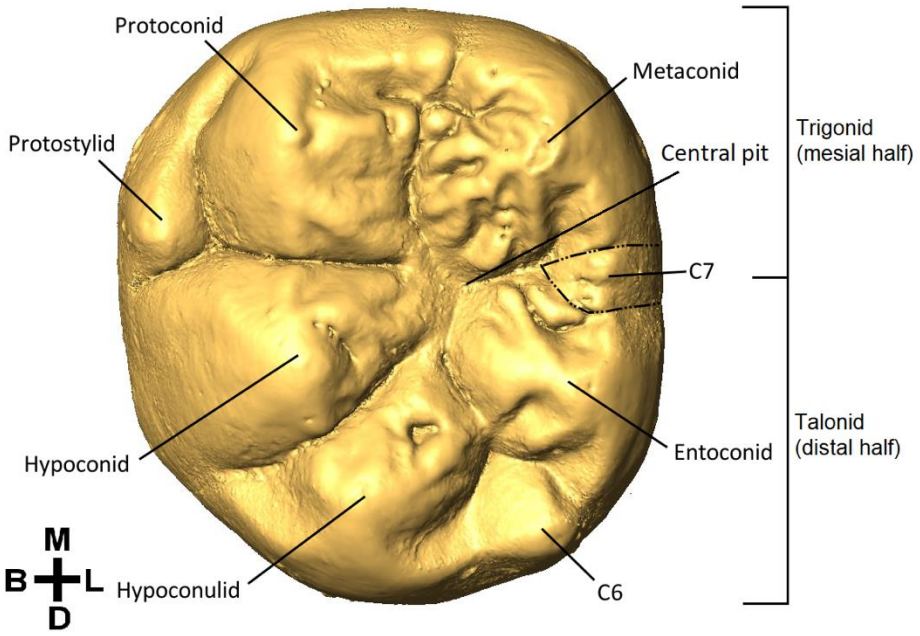

Figure 1.1. A hominin mandibular molar that has a C6, a C7, and a protosylid in addition to the main five cusps. Orientation: M – mesial; B – buccal; D – distal; L – lingual.

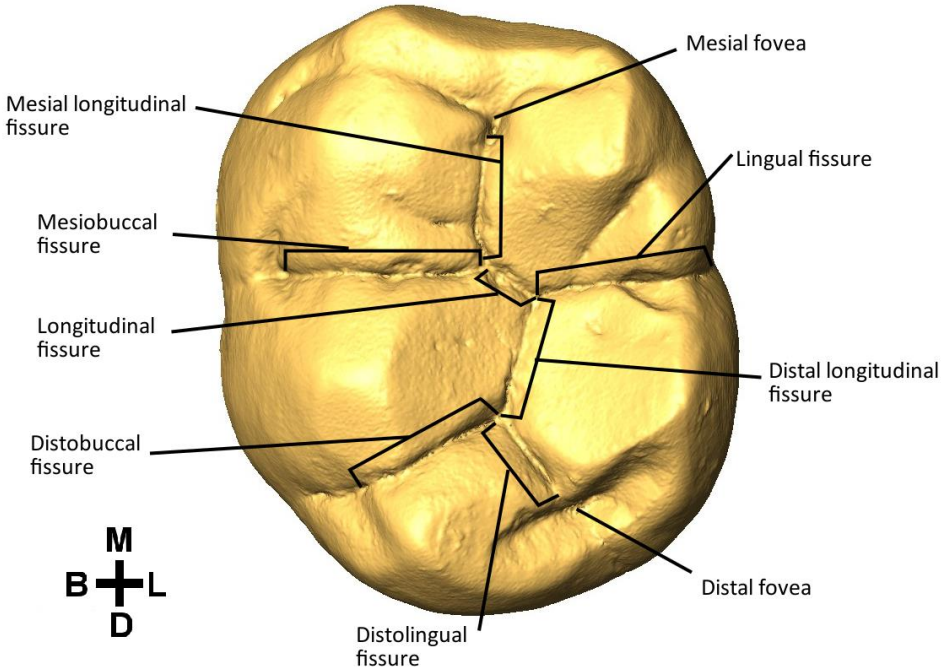

Figure 1.2. The fissures of a hominin mandibular molar. Orientation: M – mesial; B – buccal; D – distal; L – lingual.

1.6. Literature Review: The Role of Teeth in Studies of Hominin Taxonomy

The literature review aims to provide a short summary of the tooth morphology of Pliocene to mid-Pleistocene hominins, with a focus on the outer enamel surface of *Australopithecus* dentition.

First discoveries: Au. africanus and P. robustus.

In 1925, Raymond Dart discovered the fossilized skull of a juvenile hominin (Dating to ~2.8 million years ago (mya)) at Taung, South Africa, which subsequently became known as the 'Taung child'. Dart (1925) asserted that the Taung child was ancestral to *Homo sapiens* due to specific characteristics of the skull and dentition that he deemed to be more human-like than ape-like. Specific distinct dental traits included small canines, short diastema, slight projection of the upper incisors, vertical lower incisors, and the parabolic shape of the upper jaw. Based on these and the cranial traits, Dart (1925) concluded that the Taung child was a "man-like ape", and assigned it to the genus *Australopithecus* and species *africanus* (meaning "southern ape of Africa"). Later, Dart (1934), after separating the upper jaw from the lower jaw in 1929, published a detailed report on the morphology of the dentition of the Taung child. While the teeth were larger than those of *Homo sapiens*, their form was similar: the upper first deciduous molars (sometimes also referred to as deciduous third premolars) had three cusps, while those of chimpanzees and gorillas have only two, and the first lower deciduous molar (sometimes called deciduous third premolar) had four well-developed cusps, whereas in chimpanzees the

protoconid is the largest and most developed cusp among the four, giving the tooth a canine-like appearance.

Controversy arose due to the claims made by Dart about the role of the Taung child in human evolution, partly fueled by the resistance to accept Africa as the origin of *Homo sapiens*, and partly because it was assumed that humans split from non-human great apes during the late Oligocene (Keith and Smith, 1925). However, some of the contemporaries of Dart agreed with his conclusions. Arthur Keith (1931) eventually recognized that the teeth were human-like based on the bicanine width and the size of the deciduous molars, and Robert Broom (1929) provided illustrations of the jaw of the Taung Child from lateral view, comparing it against the morphology of the jaws of juvenile extant non-human apes, agreeing with the interpretation of Dart regarding the significance of the hominin in the evolution of *Homo sapiens*. In an essay, Alsberg (1934) argued that in the absence of large canines, to which he referred to as "fighting teeth", the presence of large molars, a reduced jaw, and large cranial size, the Taung Child belonged to a very early evolutionary human stage. As the morphology of the teeth of the Taung Child led Dart (1934) to speculate about the diet of *Au. africanus*, Alsberg interpreted the small canines as tentative evidence for the use of tools by the hominin.

Subsequent discoveries by Broom in South Africa further consolidated the view for the existence of Pliocene apes that were morphologically more similar to *Homo sapiens* than to extant non-human apes. These include the partial adult skull from Sterkfontein (Broom, 1936) to which Broom assigned the species *Australopithecus transvaalensis* for its distinct cranial and maxillary molar crown morphology compared to the Taung Child. Later, Broom (1938) created a new genus, *Plesianthropus,* to accommodate the Sterkfontein skull after the discovery of

additional fossils from the same site in 1938. During the same year Broom (1938) discovered another well-preserved skull at Kromdraai, situated a few kilometers away from Sterkfontein. The large premolars, relatively small canines, rhomboidal M^1s (contra the square *Plesianthropus* upper molars), and small incisors convinced Broom to place the skull in the new genus *Paranthropus* and species *robustus*. Shortly after, Gregory and Hellman (1939) ventured to compare the morphology of the three then known South African hominin genera to *Sinanthropus* (i.e. *Homo erectus*), fossil apes, and modern humans, reaching similar conclusions as those voiced by Dart and Broom regarding the intermediate position of the South African hominins in human evolution, and placing the three in a single sub-family, the *Australopithecinae*. Following this study, Gregory and Williams (1939) carried out the first quantitative systematic analysis of the dentition of the South African hominins. Their study mainly aimed to determine the phylogenetic relationships between the South African hominins, Asian hominins (*Pithecanthropus* and *Sinanthropus*), extant non-human apes, and *Homo sapiens*. Their conclusions were in concordance with those of Dart and Broom - that these South African "man-apes" represented an early stage of human evolution, who probably evolved from a stock of *Dryopithecus* or *Sivapithecus*. Furthermore, Gregory and Williams (1939) were first to note through metric measurements that the M_3 was greater in proportion to the M_1 in the South African hominins compared to Asian hominins and *Homo sapiens*.

In 1946, Broom and Schepers published a monograph on the South African hominins, which contained the most detailed descriptions of the fossils yet. In the monograph, Broom and Schepers (1946) also reported on a recently found hominin juvenile mandible with a preserved right dentition that was recovered from the site of Kromdraai, and assigned to *Paranthropus*

robustus. The deciduous molars "are of the greatest scientific interest" wrote Broom and Schepers (1946), in that they are distinguished from *Australopithecus africanus* by having cusps of equal size, a well-developed fifth cusp (hypoconulid), and a deep anterior fovea. The second molar lacked a sixth cusp, which is present in *Au. africanus*, and was narrower than the corresponding tooth in *Au. africanus*. Broom and Schepers (1946) argued that these differences between the deciduous dentition of *Paranthropus* and *Australopithecus* warrant the creation of two separate sub-families, contra the views of Gregory and Williams (1939). Broom and Schepers (1946) also claimed that the South African hominins could be viewed as ancestral to modern humans, slightly more primitive than *Pithecanthropus*. Keith (1948) and Clark (1947) agreed with the conclusions of Broom and Schepers (1946), with Clark (1947) further contributing weight to their claims by examining the wear on the deciduous teeth. Their high degree of wear compared to that of extant non-human apes suggested to Clark (1947) that *Australopithecus* and *Paranthropus* had a prolonged adolescence period, comparable to that of modern humans. Clark wrote: "In other words, if only the evidence of the teeth were to be taken into account, the allocation of these fossil creatures to the *Hominidae* rather than to the *Pongidae,* would seem a logical necessity" (1947, pp. 318).

The next significant discovery came from Makapansgat, South Africa, in 1947, where James Kitching discovered a hominin occipital bone (Dart, 1948a), and subsequently an adolescent mandible (Dart, 1948b), part of a maxilla and two lower molars (Dart, 1949). The unique features of the mandible and the dentition led Dart (1948a; 1948b) to assign the fossils to a new species, *Australopithecus prometheus*. Dart (1948b) noted that the adolescent mandible showed an eruption pattern different than that of modern humans, specifically in that the M_2

erupted before both P_4s. Slight wear on the first permanent molars and severe wear on the first deciduous molars in conjunction with the eruption pattern constituted an individual with an extended childhood, which was more akin to the developmental pattern observed in modern humans than in any extant non-human apes. The teeth were broader and cubical, slightly larger, permanent molars lacked a sixth cusp, and exhibited a protostylid, all features that distinguished *Au. prometheus* from *Au. africanus*. Dart (1948b) described the P_4 as "ultra-human", as no ridge connected the buccal and lingual cusps, both anterior and posterior foveas were of similar depth, and the lingual cusp was low. Dart (1948b) argued that while the teeth of *Au. prometheus* displayed some unique characteristics, it also shared many with the then known fossil hominins, suggesting that they might all be placed under the genus *Australopithecus*.

However, Ashton and Zuckerman (1950) were convinced that a quantitative examination of the fossils was warranted in order to support the assertation made by Broom and Dart about the human-shaped teeth of the South African hominins. To test that, they compiled a large sample of extant and fossil non-human ape teeth, and took measurements of their mesiodistal (MD) and buccolingual (BL) dimensions, height, and the size of the talonid and trigonid of the upper molars (though in the case of fossil hominins, the type of measurements taken varied; for example, only the breadth and length of the Taung canine was measured, while the height, breadth and length of the Kromdraai canine was taken). Their results challenged the claims made by Dart and Broom, “Indeed, hardly one of the teeth considered in this paper cannot be matched in dimensions and shape by the corresponding tooth of at least one type of extant great ape” (Ashton and Zuckerman, 1950:517). In a letter to Nature sent before the publication

of the study by Ashton and Zuckerman (1950), Clark (1950a) argued that the teeth of the South African hominins consistently showed a "combination of traits that were remarkably hominid in character" (1950a, 893-894), and questioned the assertion that dimensions and indices of individual teeth could provide information about the taxonomic affinities of the fossils. In a later publication, Clark (1950b) claimed that a descriptive or qualitative approach to assessing the taxonomy of fossils is sufficient when differences are marked, as in the australopith teeth compared to those of extant non-human apes. Furthermore, Clark (1950b) argued that for a proper statistical analysis of the fossil dental material, one would need to take measurements of morphological traits that are markedly different between taxa. Thus, measuring the most antero-posterior dimension of an *Australopithecus* and chimpanzee canine and comparing them, as Ashton and Zuckerman (1950) did, was inappropriate since their shape was so fundamentally different (*Australopithecus* canine is "spatulate" in form, while that of chimpanzees is "conical") that comparison between these measurements becomes meaningless. Instead, Clark (1950b) took three measurements on the canine, each corresponding to homologous inter-genera morphological traits. His study of both the permanent and deciduous dentition of hominins confirmed that the teeth were significantly different from those of extant non-human apes, and more similar to those of *Homo sapiens*.

Excavations at the South African hominin fossil sites mostly halted during the war, but resumed shortly after, yielding additional hominin fossil material (e.g. Broom, 1943; Broom and Robinson, 1947; Broom, 1947). During this period, two significant discoveries were made at Swartkrans - that of a mandible, which was assigned by Broom (1949) to the new species of *Paranthropus crassidens*, due to the large teeth and jaw; and an additional lower jaw that was

placed in the genus *Telanthropus capensis* due to its small molars and distinct mandibular morphology (Broom and Robinson, 1949). Broom and Robinson continued their work at Swartkrans recovering a large number of skulls, jaws, and over 200 teeth, culminating with the publication of the monograph *Swartkrans Ape-Man* (Broom and Robinson, 1952). In it, they argued that *Paranthropus crassidens* should be placed in the superfamily *Hominoidea* due to the following dental traits: small canines that show wear on the tip rather on the distal face as in extant non-human apes; a lower third premolar (P_3) that is bicuspid compared to the unicuspid anthropoid P_3; small upper and lower incisors that are comparable in their size to those of *Homo sapiens*; lower and upper dental arcades that are parabolic in shape. Features separating *Paranthropus crassidens* from other hominins were the deep fissures of the upper molars; extremely reduced metacone of the M^3; the mesial-ward orientation of the lingual cusp of the P_3; highly variable, crenulated, and multi-cusped third lower molars that are distally narrow; and the markedly asymmetrical deciduous lower canines. In the same monograph and in a later publication by Robinson (1953), the *Telanthropus* mandible and its associated dentition were compared to those of *P. crassidens*. Apart from the small size of the teeth of *Telanthropus*, the P_3 root morphology was deemed distinct by having a reduced root both in BL and MD dimensions. Furthermore, the size gradient of the lower molar row was $M_1 < M_2 > M_3$, which is distinct from all the other South African hominins, where the size gradient is $M_1 < M_2 < M_3$. An additional feature distinguishing *Telanthropus* from *P. crassidens* was the lack of a sixth cusp on the M_1, whereas in *Paranthropus crassidens* the accessory cusp was present in all M_1s. For Robinson (1953), these unique traits suggested that from an evolutionary perspective,

Telanthropus was more closely related to modern humans than *P. crassidens*. Currently, *Telanthropus capensis* is considered to be either *Homo erectus*, or *H. erectus*-like (Anton, 2012).

The increasing number of new genera and species of hominins led to a debate about their taxonomic status, where some considered the existence of three subfamilies: the *Australopithecinae*, *Paranthropinae*, and *Archanthropinae* (Broom, 1950), while others lumped all fossil hominins and modern humans into the single genus *Homo* (Mayr, 1950). The dissatisfaction with these classifications led Robinson (1954) to devise a new taxonomic system. Robinson (1954) argued that all fossil hominins fall into two different groups, heavily relying on differences in dental morphology between the Sterkforntein and Swartkrans specimens. He found that the DM_1s from Sterkfontein had a poorly developed hypoconulid, while the DM_1s from Swartkrans were broader posteriorly and had a larger hypoconulid. Furthermore, he noted that specimens from Sterkfontein had a more derived P^3 root morphology by having two separate roots but a more primitive canine, while the P^3 of the specimens from Swartkrans had three roots and their canines were more derived. Robinson (1954) then placed all fossil hominins in the family of *Hominidae*, with the subfamily *Australopithecinae* that contained two genera: 1) *Australopithecus* (with *Plesianthropus transvaalensis* and *Au. prometheus* being subsumed under *Au. africanus*), and 2) *Paranthropus* (with *P. crassidens* combined with *P. robustus*). Later, Robinson (1972) placed the *Au. africanus* material in *Homo*, a proposal that never gained traction.

The decision by Robinson (1954) to "simplify" the taxonomic diversity of the South African hominins has been largely supported by subsequent comparative studies of *P. robustus* and *Au. africanus*. Wood, Abbott and Graham (1983) found that the cusp areas of the metaconid and

protoconid of the M_1 are reduced, and the hypoconulid in M_1 , M_2, and M_3 is enlarged in *P. robustus* compared to *Au. africanus*. Suwa et al. (1994) found a similar pattern, but added that the entoconid increases in size as well. Skinner and colleagues (2008), in a study of the morphology of the enamel-dentine junction of the lower molars of *P. robustus* and *Au. africanus*, found that the dentine horns are consistently higher in *Au. africanus* compared to *P. robustus*, confirming earlier observations made by Robinson (1963).

Robinson (1956), in his seminal monograph on australopith dentition, *The Dentition of the Australopithecinae,* noted that the mean enamel thickness of six *Paranthropus* molars was 2.3mm and did not differ markedly from that of *Australopithecus* (though he did not provide measurements for the latter taxon). Later studies of two-dimensional (Grine and Martin, 1988) and three-dimensional (Olejniczak et al., 2008) enamel thickness showed that *Paranthropus* have significantly thicker enamel than *Australopithecus*.

Tobias (1967) noted that the Makapansgat *Au. africanus* material showed more robust features (large, buccolingually expanded molars and a robust jaw) that aligned them with *P. robustus*. However, he considered it part of the intra-species variation in *Au. africanus*. Aguirre (1970) on the other hand, argued that these robust features suggest the presence of two distinct species in Makapansgat – *Au. africanus* and *P. robustus*. Indeed, he considered the MLD2 mandible to belong to a juvenile *P. robustus*. Clarke (1985) agreed that some *Au. africanus* specimens showed robust features, however he divluged that they might belong to a second, *Paranthropus*-like, *Australopithecus* species in South Africa. In 1988, Clarke argued for the presence of two species in the Sterkfontein Member 4 assemblage that can be defined by: 1) specimens that possess a thick supra-orbital ridge and small teeth, and 2) specimens with large

teeth and thin supraorbital ridge). Later, Clarke (2008) expanded the number of characters distinguishing the two proposed taxa. In terms of dental morphology, Clarke (2008) noted that the more robust species have large and bulbous molars and premolars, with cusps oriented towards the centre of the crown, and canines and incisors that are large relative to the postcanine dentition. However, to date there is still no agreement about whether the *Au. africanus* sample represents two taxa. Studies have yet to be conducted that directly attempt to address this issue. The reasons for that might be the fragmentary nature of the fossils, the small sample size, and the presence of immature individuals (Grine, 2013). An exception is a study by Grine, Delanty and Wood (2013) of the cusp areas of the mandibular postcanine teeth of the Sterkfontein hominins, which did not find support for the two-species hypothesis. The current consensus is that *Au. africanus* represents a single, highly variable taxon.

Australopithecus sediba

In 2010, Berger and colleagues reported the discovery of a new hominin species, *Australopithecus sediba* (~1.97mya), found at Malapa, South Africa. The sample consisted of the postcranial and cranial remains of two individuals, a juvenile (MH1) and an adult (MH2). The fossils presented a mosaic of primitive and derived dental, cranial, and post-skeletal traits, characteristic of both *Homo* and *Australopithecus* (Berger et al., 2010). Dental features aligning *Au. sediba* with *Homo* are the absolute small size of the postcanine dentition, the weakly defined grooves of the upper maxillary molars, and the lack of a lingual relief on the mandibular canines, while those that align it with *Au. africanus* are the smaller M^3s in relation to the M^2s,

closely spaced mandibular and premolar cusps, and a mandibular canine that in size falls within the range of *Au. africanus* (Berger et al., 2010).

In their analysis of the mandibular corpus of *Au. sediba*, de Ruiter et al. (2013) also reported on additional measurements of the dentition of the new hominins, with the inclusion of the dental remains of MH2. The MD and BL measurements of the anterior dentition and the premolars of *Au. sediba* all fall within the range of *H. erectus* and *H. sapiens*, while the size gradient of the mandibular molars maintains the primitive condition seen in australopiths (i.e. $M_1 < M_2 < M_3$). Furthermore, an analysis of the occlusal outline of the premolars showed that their shape is unique when compared to *P. robustus* and *Au. africanus* (de Ruiter et al., 2013). Irish et al. (2013) conducted a detailed comparative morphological analysis of the *Au. sediba* dentition by employing the ASUDAS (Arizona State University Dental Anthropology System) for recording dental traits and their degree of expression. Their study showed that *Au. sediba* shares the most traits with *Au. africanus*, and a phylogenetic analysis places *Au. sediba* as a sister taxon to *Au. africanus*. However, some dental features of *Au. sediba* are derived: slight shoveling of the I^1, an increase in the expression of Carabelli's trait on the M_1, and the presence of a portostylid and a seventh cusp on the M_1s (Irish et al., 2013).

East African hominins

Paranthropus boisei

The discovery of a new robust australopith occurred in 1955, when Louis Leakey found two deciduous hominin teeth, a canine and second lower molar, at Olduvai Gorge, Tanzania (Leakey, 1958). As the deciduous molar was morphologically unique by being incredibly large

and multi-cusped, Leakey (1958) did not assign the teeth to any species. However, he did comment on the possibility that the tooth could be that of an australopith due to its short buccal fissures, which are characteristic of the subtribe. Excavations commenced at Olduvai Gorge and in 1959, Leakey reported the discovery of a well preserved cranium (OH 5) of an immature individual. Leakey (1959) placed the skull in a new genus, *Zinjanthropus*, while recognizing its affinity to *Paranthropus* due the robustness of the skull and the significant reduction in canine size, while distinguishing it from the genus for expressing an M^3 that is smaller than the M^2 - a condition that is characteristic of *Australopithecus*. Robinson (1960) argued on the contrary, that the dentition of *Zinjanthropus* is very reminiscent of that of *Paranthropus* and does not warrant the creation of a new genus, and that instead, the skull should belong to the species *Paranthropus boisei*.

In 1967, Tobias published a series of monographs on the then available material of *Paranthropus boisei*. The MD and BL dimensions of the upper premolars were significantly larger than in any known australopith, while those of the upper molars either slightly exceeded them or were within the upper limit. The most significant feature of *P. boisei* upper dentition is their incredible breadth. Tobias (1967) also omitted the subgenera *Zinjanthropus* and proposed to designate it to *Australopithecus boisei*.

Additional discoveries of the megadont australopith came from the site of Peninj, when in 1964, a team lead by Leakey found a well preserved mandible (Peninj I), and referred to it as a late representative of *P. boisei* (Tobias, 1965). In 1971 excavations at Chesowanja, Kenya, culminated with the discovery of a partial skull of a late Pleistocene australopith (KNM-CH 1). The incomplete cranium showed features that resembled those of *P. robustus*, *P. boisei*, and

Au. africanus, whereas the teeth were large and fell within the range of *P. boisei* and *P. robustus* (Carney et al., 1971). The relatively young age of the skull and its suite of derived and primitive traits led Carney et al. (1971) to refer to it as a member of "a population evolved from robust australopothecines, most likely descended from *A. boisei*" (pp. 513). Currently, KNM-CH 1 is considered to be a female *P. boisei* (Wood and Leakey, 2011). The next significant *P. boisei* discovery came from Konso, Ethiopa, where Suwa and colleagues (1997) found a nearly complete cranium with an associated mandible (KGA10-525). This specimen, dated at ~1.4mya, is also one of the latest *P. boisei* specimens. Generally, many specimens from Koobi Fora, Kenya, represent the *P. boisei* hypodigm (Wood and Constantino, 2007).

Homo habilis

In 1961 a juvenile mandible (OH7) was discovered in Olduvai Gorge, however the premolars and molars were smaller and significantly narrower than that of any known australopith (Leakey, 1961). Further excavations at the site yielded additional hominin fossils with hand, feet, and teeth morphology distinguishable from those of any known australopiths. Leakey, Tobias and Napier (1964) created a new species, *Homo habilis,* to accommodate the new morphologically unique fossils, while also relegating *Zinjanthropus* to a subgenus. However, Robinson (1965) contested the decision to place these hominins in a new species. His measurements of the dimensions of the lower premolars and molars yielded length/breadth indices that were within the range of those of australopiths. Furthermore, Robinson (1965) argued that reliance on the length/breadth index in determining taxonomy is misguided, as it has no phyletic significance in hominins. Instead, he suggested treating the fossils as

Australopithecus africanus. Tobias (1966) criticized the methodology employed by Robinson (1965), calling into question the inexplicable omission of the measurements of the P_4s, and the inclusion of a not fully erupted and thus not fully mineralized *Paranthropus* tooth (SK96). In his analysis, Tobias (1966) expanded the sample of hominin teeth, and found that the length/breadth indices of the lower premolars of *Homo habilis* were much higher (i.e. narrower and longer) than in any other australopith in the sample.

Australopithecus afarensis

In 1973, the site of Hadar, Ethiopia, was selected as a potential location for finding fossil hominins for its antiquity and the presence of many well-preserved fossils deposited in low-energy environments (Johanson and Taieb, 1976). The site turned out to be fruitful, and many fossil hominins were excavated during 1973 and 1974. Initial assessment of the specimens suggested that they showed affinities with *P. robustus*, *Au. africanus*, and material attributed to *Homo*, especially two well-preserved maxillae with large canines, broad incisors, and large posterior dentition (Johanson and Taieb, 1976). A similar expedition took place in Laetoli, Tanzania, from 1974 to 1975 (Leakey et al., 1976). The site was surveyed in the late 1930s by Kohl-Larsen who collected many fossils, including a fragment of a hominin maxilla with both premolars preserved, that was later placed in the species *Meganthropus africanus* by Weinert (1950). In the 1974 and 1975 field work seasons thirteen additional new hominin fossils were recovered, mainly teeth, mandibles and a maxilla (Leakey et al., 1976). While the question of the taxonomic affinities of the fossils remained open, the dentition showed traits that were aligned with both the 'gracile' South African australopiths (non-molarized premolars, and

smaller, narrower, molars that lacked accessory cusps) and some of the *Homo* East African material and early African and Asian *Homo erectus* (absolutely and relatively large canines and central incisors). Furthermore, some dental features were considered primitive and consistent with the old age of the fossils (~3.55mya), mainly a P_3 with a small mesially placed lingual cusp, buccolingually elongate upper molars, a large canine with a distal wear surface, and a "V-shaped" dental arcade (Leakey et al., 1976). Even though the remains exhibited a mosaic of primitive and derived traits, Leakey and colleagues (1976) claimed that the specimens were of "only one phylogenetic entity or lineage" (p. 466).

In 1978 Johanson, White and Coppens created the new species *Australopithecus afarensis* to accommodate the hominin fossils from Hadar and Laetoli, with the Laetoli mandible LH4 becoming the type specimen. In terms of dental morphology, Joahnson and White (1979) initially described *Au. afarensis* as having a P_3 with an MD elongated buccal cusp that shows vertical wear due to occlusion with the upper canine; a P^3 larger than the P^4, with a pointed buccal cusp and assymetric elongated buccal face, and a mesially oriented lingual crown, giving the tooth an asymmetric appearance; molars with a square outline and a simple Y-5 pattern (especially M_1 and M_2); and a lower molar row gradient size of $M_1<M_2<M_3$. In general, tooth size is considered highly variable in this species (Johanson, White and Coppens, 1978; Johanson and White, 1979). However, Tobias (1980) questioned whether some of the traits claimed to be unique to *Au. afarensis* were indeed so, and found that most were present in *Au. africanus* as well. Another concern was raised about the validity of assigning the hominins from Hadar and Laetoli to the same species (e.g. Tobias, 1980; Wolpoff, 1980).

In 1983, Blumenberg and Lloyd conducted one of the most comprehensive statistical analyses of hominin metric dental traits to date, that aimed to determine whether the variability in these traits is within their assigned taxonomic limits. Contrary to claims made by Tobias (1980) about the similarities between the *Au. afarensis* and *Au. africanus* dentition, Blumenberg and Lloyd (1983) found the percentage of significant differences between the taxa high enough (63%) to not include *Au. afarensis* with *Au. africanus*, and small enough between the Hadar and Laetoli specimens to regard them as one species. White (1985), in a subsequent dental analysis of the Hadar and Laetoli specimens, came to a similar conclusion. However, there are some differences between the two samples: in Hadar maxillary canines, the mesial shoulder is positioned more apically compared to the distal shoulder, and the crowns have smaller MD dimensions compared to the Laetoli canines (Kimbel and Delzene, 2009). P_3s are also more elongated (KImbel et al., 2006), and the M^3s are both mesiodistally and buccolingually smaller in the Laetoli sample (Lockwood, Kimbel and Johanson, 2000). An especially distinct feature of *Au. afarensis* dentition is the absolutely and relatively small size of the lower and upper incisors (Ward, Leakey and Walker, 2001), and the larger medial incisors compared to the lateral ones (Kimbel and Delezene, 2009). Another diagnostic feature of the *Au. afarensis* dentition is the distal wear facet on the upper maxillary canines, whereas in other *Australopithecus* the wear is apical (Johanson and White, 1978). While the condition is similar to wear patterns observed in extant non-human apes, it is not homologous (Joahnson and White, 1978; Greenfield, 1990). Instead, the wear on the distal edge of the maxillary canines served to blunt them so their occlusion with the P_3 would be consistent with the occlusion of the posterior teeth (Greenfield, 1990). With additional findings of *Au. afarensis* specimens, Guatelli-Steinberg and Irish (2005)

found that the frequency of a sixth cusp in the M_1s was similar between the Hadar *Au. afarensis* sample and *Paranthropus*, contradicting previous claims that this trait is unique to the latter genus (e.g. Wood, Abbot and Graham, 1983).

Additional *Au. afarensis* material has been recovered from the site of Maka, Ethiopia (White et al., 2000), and Woranso-Mille (Haile-Selassie, 2010a). However, the taxonomic affinities of the Woranso-Mille specimens are yet unclear. Haile-Selassie and Melillo (2015) did find the morphology of the P_4s to be more similar to that of *Au. afarensis*, but only marginally so.

Australopithecus bahrelghazali

In 1995, Brunet and colleagues found part of a hominin mandible (KT 12/H1) west of the Rift Valley, at the site of KT 12 (dated at 3.0-3.5mya), Chad. The mandible was similar to *Au. afarensis*; however, it did differ from it by having three rooted premolars with thin enamel. Brunet et al. (1995) initially refrained from assigning the mandible to a new species, but later they created *Australopithecus bahrelghazali* to accommodate the fossil while also reporting on the discovery of an upper premolar (Brunet et al., 1996). In 1996, a maxillary fragment was found at site of K13, and in 2000, an additional mandibular fragment was recovered from the site KT 40 (Lee-Thorp et al., 2012). However, White et al. (2000) note that P_3 root polymorphism is present *Au. afarensis* as well, with LH-24 having the same root pattern that is diagnostic of *A. bahrelghazali.* Wood and Lonergan (2008) also consider *Australopithecus bahrelghazali* to be a regional variant of *Au. afarensis*, while Ward et al. (2001) claim the mandible to be morphologically equivalent to that of *Au. afarensis* (but see Guy et al. (2008) for a view that supports the distinctiveness of the KT 12/H1 mandible). The only study to date to

run a comparative analysis of the *Au. bahrelghazali* dentition is by Delezene and Kimbel (2011), who found the P_3 crown morphology of KT 12/H1 to be similar to that of *Au. afarensis*.

Australopithecus anamensis

In 1995, Leakey and colleagues reported the discovery of new hominin fossils (~4.2mya) at Kanapoi and Allia Bay, Kenya, which were subsequently placed in the new species of *Australopithecus anamensis*. Specific dental characters that led Leakey and colleagues to distinguish *Au. anamensis* from *Au. afarensis* included: pronounced sloping buccal faces of the lower premolars and upper and lower molars, large upper and lower canines with long roots, upper molars with wider trigons than talons, and asymmetrical P_3s and lower canines. Furthermore, the shape of the maxillary and mandibular dental arcades exhibited a distinct U-form, a condition considered primitive (Ward, Leakey and Walker, 2001). However, in their initial assessment Leakey et al. (1995) observed that many features of *Au. anamensis* dentition were similar to those of *Au. afarensis* specimens from Laetoli, especially the tapering of the upper molars, large lower canines with accessory cusps, and vertically oriented upper canines. Senut (1996) argued that these similarities in conjunction with *Au. anamensis* postcranial morphology were evidence that the Laetoli and Kanapoi specimens are congeneric, and should be assigned to the genus *Praeanthropus* and species *africanus*, a taxon that was proposed half a century ago by Weinert (1950). In a later publication, Ward, Leakey and Walker (2001) provided a detailed description and a comparative analysis of all then known specimens from Kanapoi and Allia Bay attributed to *Au. anamensis*. A major difference between *Au. anamensis* and *Au. afarensis* is the C/P_3 complex, which is much more primitive in *Au. anamensis*, resembling that

of *Ardipithecus ramidus*, with the almost unicuspid shape of the P_3 displaying a metaconid only as a small lingual tubercle, and canines that are blade-like when viewed lingually with strong basal tubercles. Thus, Ward and colleagues (2001) argued that *Au. anamensis* presents a suite of derived and primitive traits that place the taxon as the evolutionary link between *Ar. ramidus* and *Au. afarensis*. Recovery of new specimens from Kanapoi supported the hypothesis that the basal dimensions of *Au. anamensis* canine teeth are larger relative to the size of the postcanine dentition (Ward, Manthi and Plavcan, 2013). Furthermore, the new canines confirmed that *Au. anamensis* had longer and larger (by volume) canines than *Au. afarensis*, and that their shape could be considered as intermediate between *Ardipithecus ramidus* and *Au. afarensis*. While the canines of *Au. anamensis* are not as asymmetrical as the canines of *Ar. ramidus,* they are also not as symmetrical and diamond-shaped as the canines of *Au. afarensis* (Manthi, Plavcan and Ward, 2012; Ward, Manthi and Plavcan, 2013). The canines were not significantly longer in *Au. anamensis*, but the roots were, which suggests that reduction in crown height occurred before reduction in root length and size (Ward, Plavcan and Manthi, 2010). Furthermore, *Au. anamensis* exhibits an evolutionary trend in the lineage of *Au. anamensis-Au. afarensis* through a reduction in the basal shape of the upper canines and P_3s (the honing complex), and no reduction in the size of the mandibular canine and P^3. This suggests that it was not a selection towards an absolute reduction in tooth size, but rather a selection specifically against the honing complex. Ward, Plavcan and Manthi (2010) further noted that the anterior dentition of *Au. anamensis* tends to be more worn than in *Au. afarensis*, suggesting that their diets probably differed.

The addition of *Au. anamensis* to the diversity of *Australopithecus* was not only important for understanding early hominin evolution, but also for resolving taxonomic questions pertaining to fossil teeth recovered decades ago (Ward, Manthi and Plavcan, 2013). The hominin teeth from Fejej that were initially assigned to *Au. afarensis* (Fleagle et al., 1991) have been allocated to *Au. anamensis* due to their temporal overlap (4.0-4.2mya) with the taxon (Haile-Selassie, 2010). However, Grine, Ungar and Teaford (2006) disagree with the allocation of the Fejej teeth to *Au. anamensis* solely based on their age, as some are too worn to be used for a proper morphological comparison, and some are morphologically distinct from *Au. anamensis* teeth. Additional *Au. anamensis* fossils have been recovered from Assa Issie and Aramis, Ehtiopia (White et al., 2006).

Australopithecus gahri

In 1999, Asfaw and colleagues discovered a cranium and dental remains of an australopith dated to 2.5mya, that were assigned to the species *Australopithecus gahri*. The upper dentition of *Au. gahri* is unique among australopiths. While the teeth are remarkably large, with the canine breadth exceeding that of any known australopith, and the size of the postcanine dentition falling within the range of *P. robustus*, the canine to premolar/molar ratio is as in *Australopithecus* (Asfaw et al., 1999).

Australopithecus deyiremada

Field work in Burtele, Ethiopia, further expanded the known hominin diversity in the Pliocene with the discovery of two mandibles (BR BRT-VP-3/14 and YT-VP-2/10), two maxillary fragments (BRT-VP-3/1 the holotype, and BRT-VP-3/37), and a number of isolated teeth, dated at 3.3-

3.5mya, all of which have been assigned to *Australopithecus deyiremada* (Haile-Selassie, 2015). In terms of its dentition, *Au. deyiremada* can be distinguished from *Au. afarensis* for its absolutely small upper postcanine dentition and a mesiodistally narrow upper canine, which lacks lingual relief. *Au. deyiremada* is distinguished from the other contemporaneous australopith *A. anamensis* for its bicuspid P_3s. In general, the canine crown of BRT-VP-3/1 is the smallest among almost all *Australopithecus*, comparable in size only to *Paranthropus*, with a root that is almost as long as in *Au. anamensis*. The M^1 of BRT-VP-3/1 is the smallest among all known Pliocene hominins, whereas the M^2 is slightly larger than that of *K. Platyops* (Haile-Selassie, 2015).

Comparative studies of hominin mandibular postcanine morphology

Since the first palaeoanthropological studies and up until the beginning of the 1980s, most of the work that focused on questions pertaining to hominin taxonomy using teeth relied on quantitative assessment of the crown by experts, or linear measurements such as MD and BL dimensions. Both were considered to be lacking – the former approach suffered from a lack of quantitative and statistical analysis, and the latter captured only a small portion of the morphology of the crown. In order to improve and expand the tools available to palaeoanthropologists for studying hominin dentition, Wood, Abbott and Graham (1983), drawing from a methodological foundation laid by Biggerstaff (1969), developed a method for measuring relative and absolute cusp areas, fissure patterns, and the cross-sectional shape of the crown.

In the first study (Wood, Abbott and Graham, 1983), they compared the relative and absolute cusp areas of the M_1s, M_2s, and M_3s of *Paranthropus boisei*, *Paranthropus robustus*, *Australopithecus africanus, Homo erectus*, and *Homo habilis*, with the former two species considered 'robust' and *Au. africanus* referred to as 'gracile'. They found that across the three mandibular molars the 'robust' taxa had reduced protoconids and metaconids and larger hypoconulids and entoconids compared to the 'gracile' australopithecines and *Homo*. A subsequent study of the relative and absolute cusp areas of the P_3 and P_4 of the same taxa revealed that the 'robust' australopithecines had a significantly larger talonid than the 'gracile' and *Homo* taxa (Wood and Uytterschaut, 1987). In a later publication the samples were expanded and *Au. afarensis* was included in the analysis (Suwa, Wood and White, 1994). While the results were similar to the previous studies, they were refined. In the M_1s it was specifically the small size of the protoconid that distinguished the 'robust' taxa from the 'gracile' australopithecines (including *Au. afarensis*) and *Homo*, whereas in the M_2s the larger size of the entoconid and hypoconulid separated the 'robust' australopithecines from the other taxa, while in the M_3s it was the small protoconids and hypoconulids. Across this series of studies the presence of a C6 was observed in high frequencies on the M_1s and M_2s of the 'robust' taxa, and in low frequencies on the molars of 'gracile' australopithecines and *Homo*. The cusp was also larger in the 'robust' hominins. Of note is that while relative cusp areas were able to distinguish well between 'robust' and other taxa, there was a significant overlap in cusp areas between the 'garcile' and *Homo* species.

More recent GM studies that looked at cusp and crown shape (Dykes, 2016), and other traits, such as the position of the mesial and distal foveas and cusp tips, in hominin postcanine

dentition (Gomez-Robles et al., 2007, 2008, 2011, 2015) support the conclusions of previous cusp area studies. In the series of studies by Gomez-Robles and colleagues referenced above, the focus was on *Homo*, especially *Homo heidelbergensis*, and as such most of the trends that were detected in the analyses were related to the derived condition of later *Homo* dentition. However, because early hominins (*Au. afarensis*, *Au. africanus*, *P. robustus*, and *P. boisei*) were included in the analyses, some morphological dental trends in those taxa have been observed as well. An analysis of the P_3s showed that the tooth in early hominins is relatively asymmetrical compared to that in *Homo*, has a pronounced talonid, and a larger occlusal polygon (a four sided polygon where the corners represent the two cusp tips and the mesial and distal foveas). A 2D GM study of the mandibular molars (Gomez-Robles et al., 2015) found that the crown shape of *Au. afarensis* M_1s is square and buccolingually broad, whereas *P. robustus* and some *Au. africanus* M_1s have a more elongated crown that is characterized by lingual cusps that are larger and more distantly spaced than the buccal cusps. The M_2s of *P. robustus* and *P. boisei* have a large distal moiety that most likely indicates the presence of a C6 (something that was not measured in the study due to methodological limitations), and a rounded symmetrical crown. The M_2s of *Au. afarensis* are more variable, as some are more buccolingually expanded, whereas other specimens show only a slight buccolingual expansion in the mesial part of the trigonid. *Au. africanus* M_2s are buccolingually broad with some exhibiting a broad distal moiety as well, which, similarly to *P. robustus* and *P. boisei*, might be due to the presence of a C6. The M_3s of both *P. robustus* and *P. boisei* maintain the trend of having a large distal moiety, which likely indicates the presence of a C6 or multiple accessory cusps. The crown shape is variable,

ranging from being buccolingually narrow to average. In contrast, the M_3s of the 'gracile' taxa are buccolingually broader, with only some specimens exhibiting a large distal moiety.

The ASUDAS (Arizona State University Dental Anthropology System) aims to standardize the scoring of key morphological features of the dentition. The system was initially developed for scoring the variation of modern traits in the dentition of *H. sapiens*, but later expanded to include traits that are present in other hominins (Bailey and Wood, 2007; Irish et al., 2013). The traits are generally considered to be highly heritable, easily identifiable, exhibit little to no sexual dimorphism, and can be found in most tooth types (Irish et al., 2013). Irish and colleagues (2013) scored traits present in the dentition of both *Paranthropus* taxa, *Au. afarensis* and *Au. anamensis* (which were pooled together and referred to as East African australopiths), *Au. africanus*, *Au. sediba*, all early *Homo* species, *H. sapiens*, and *Gorilla gorilla*. Some of the traits present in the dentition of early hominins could be briefly mentioned here.

The mesial fovea in East African australopiths and *Au. sediba* is weak, while moderate in *Au. africanus* and *Paranthropus*. Cusp numbers on the M_1 generally mirror previous studies, although Irish et al. (2013) note that East African australopiths have 6 cusps, the same as in *Paranthropus*, while *Au. africanus* and *Au. sediba* have 5. The protostylid in East African australopiths and *P. robustus* is absent or pit-like, whereas in *Au. africanus* it is expressed as a small cusp, and in *P. boisei* it is characterized by curved mesial and distal grooves. In *Au. sediba* the protostylid is only a trace cusp. A C7 on the M_1s is absent in East African australopiths, but present in *Au. africanus* and *Au. sediba* as a small cusp. It is absent from the M_1s of *P. boisei*, and expressed only as a faint cusp on the M_1s of *P. robustus*. Some M_2s of East African australopiths have an X fissure pattern, whereas the fissure pattern in *Paranthropus*, *Au.*

africanus, and *Au. sediba* is Y. The cusp number on the M_2s of *Au. africanus* and *Au. sediba* is five, whereas East African australopiths and *P. robustus* have six, and *P. boisei* has ≥ six.

CHAPTER 2: METHODS COMPARISON

2.1 Materials and Methods

2.1.1 Materials

The sample consists of mandibular molars (n=108) belonging to *Australopithecus afarensis*, *Australopithecus africanus*, *Homo neanderthalensis*, and *Pan troglodytes* (Table 2.1). These taxa were selected to test the performance of data types that capture the shape of the crown due to the evolutionary distance between them, and the vast amount of research detailing their dental morphological distinctiveness. *Au. afarensis* and *Au. africanus* were chosen to assess how well the methodologies can distinguish between taxa on the species level.

The *H. neanderthalensis* sample consists of a variety of European specimens that are derived from the following sites: Abri Suard, Combe-Grenal, Le Moustier, Regourdou, Roc de Marsal, and Saint-Cesare, France; El Sidron, Spain; Scaldina, Belgium; Krapina and Vindija, Croatia; and Ehringsdorf, Germany. *P. troglodytes* specimens are derived from the Max Planck Institute (MPI) and Museum for Natural History (ZMB), Berlin, Germany collections. The majority of the *Au. afarensis* sample is derived from the National Museum of Ethiopia (NME), apart from one specimen (LH4) derived from the National Museum of Tanzania (NMT). The *Au. africanus* sample consists of specimens from Sterkfontein, Makapansgat, and Kromdraai that are derived from University of Witwatersrand, Johannesburg, South Africa, and the Ditsong National Museum of Natural History, Pretoria, South Africa.

Table 2.1
Composition of the study sample for comparison of methods*

Taxon	M_1	M_2	M_3	Total
Pan troglodytes	7	10	7	24
Australopithecus afarensis	7	12	7	26
Australopithecus africanus	10	14	11	35
Homo neanderthalensis	7	10	6	23
Total	31	46	31	108

*The sample is detailed in full in Table A1 in the Appendix.

The *Au. africanus* sample was initially composed of specimens of either known tooth type (i.e. in jaws), or when the tooth position was considered to be known based on a number of criteria, that is, isolated teeth that have matching interproximal wear facets; teeth that show distinct morphological similarities; or whose tooth position has been assessed by Skinner et al. (2008). Additional isolated teeth were then added to these samples based on the classification results of this study (see methods section). The *Au. afarensis*, *P. troglodytes*, and *H. neanderthalensis* samples were not subjected to molar position evaluation analyses since their specimens match the criteria for known tooth position described above.

2.1.2 Methods

Micro-computed tomography

Each molar was scanned with a microcomputed tomography scanner to produce a series of TIFF image stacks. The image stacks of each molar were imported to Avizo 6.3 (FEI Visualization Sciences Group) to create a 3D surface model (isosurface module). In order to generate a morphologically accurate model, a greyscale threshold value was set for each molar based on the greyscale value required to produce an accurate model of the enamel surface. Severely cracked teeth (e.g. Sts 18) were refitted in Geomagic Wrap 2014.

Orientation

Each molar was rotated to its correct anatomical position in Avizo 6.3 with the aid of three aspects: 1) occlusal, 2) mesial, and 3) buccal, taking into account the general tendency of the lingual cusps to be taller than the buccal cusps, and the mesial cusps to be the tallest. Teeth were also rotated so that the mesiodistal and buccolingual planes would be in the correct anatomical orientation, as the teeth were also used for taking MD (mesiodistal) and BL (buccolingual) measurements. This procedure differs slightly (though is broadly comparable) to two commonly employed protocols for rotating teeth, the first relying on the plane of the cervical line to be horizontally aligned with the camera lens (Wood, Abbott and Graham, 1983), while the second uses the plane of the maximum exposure of the occlusal fovea to align with the camera lens (Suwa, 1994). In this study a rotation protocol that relies on anatomical knowledge was preferred over the two methodologies described above (i.e. Wood, Abbot and Graham (1983) and Suwa (1994)) due to three reasons: 1) the cervix may not always be fully preserved, which may preclude the application of Wood, Abbot and Graham's methodology to the whole sample; 2) variation in the morphology of the cervix may lead to non-homologous rotations; 3) occlusal wear may preclude the fitting of a plane using the occlusal fovea as per Suwa (1994). While the anatomical approach could be considered less objective, as it does not rely on quantifiable criteria for orienting teeth, it overcomes the issues that may be present in the methodologies described above. Differences in orientation between the methodologies that rely on the plane of the cervical line and the exposure of the occlusal fovea are generally considered to be very slight (Bailey et al., 2004). After rotating each molar to its anatomical

position, a scale was added, and a screenshot of the occlusal enamel surface was taken to produce a 2D image of the tooth.

Landmarking

Two sets of 2D landmarks were collected. The first set consists of eight anatomical landmarks that were defined as follows :

1) The point on the buccal border of the crown located opposite the termination of the mesiobuccal fissure (Wood, Abbott and Graham, 1983). When a protosylid is present, it is the point that is opposite the point where the mesiobuccal fissure bifurcates. In cases when the point at which the fissure terminates is not visible due to wear, the first landmark is opposite the corrected continuation of the fissure.

2) The point on the distobuccal border of the crown at the termination of the distobuccal fissure (Wood, Abbott and Graham, 1983). When the marginal ridge between the hypoconulid and hypoconid results in a mesial deflection of the fissure, the landmark is defined as opposite the point at which the distobuccal fissure begins to deflect.

3) The point on the distolingual border of the crown located opposite the distal fovea or the termination of the distolingual fissure. When a C6 (or accessory cusps) are present, it is the point that is opposite the point at which the distolingual fissure bifurcates (Wood, Abbott and Graham, 1983).

4) The point on the lingual border of the crown, which is located opposite the termination of the lingual fissure (Wood, Abbott and Graham, 1983). When a C7 is

present the fissures delimiting it are ignored, and the reference point is located opposite the point where the main lingual fissure bifurcates around the C7.

5) The point on the mesial border of the crown opposite the centre of the mesial fovea (Wood, Abbott and Graham, 1983). When the mesial fovea is not visible due to wear, it is the point on the mesial border of the crown opposite the termination of the mesial longitudinal fissure.

6) The intersection of the mesial longitudinal fissure with the mesiobuccal fissure (Wood, Abbott and Graham, 1983).

7) The centre of the central fossa (central pit), or the junction of the lingual fissure with the mesiobuccal and distobuccal fissures (Wood, Abbott and Graham, 1983).

8) The posterior fovea, or the intersection of the distal longitudinal fissure with the buccal and lingual foveal fissure, or, in teeth with C6, the intersection of the distal longitudinal fissure with the fissure delimiting the C6 (Wood, Abbott and Graham, 1983).

The second set of landmarks consists of 121 semilandmarks, or type III landmarks (Bookstein, 1990), that are distributed across 12 curves. The curves can be divided into two sets: 1) semilandmarks that capture the occlusal shape of the crown, and 2) semilandmarks the capture the shape of the fissures. The first set consists of five curves each defined by 15 semilandmarks:

1) The buccal face of the hypoconid delimited by main landmarks one and two.

2) The distal face of the hypoconulid delimited by main landmarks two and three. When a C6 or accessory cusps are present, the curve also includes part of the distal face of the C6/accessory cusps.

3) The lingual face of the entoconid delimited by main landmarks three and four. When a C6, C7, or accessory cusps are present, the curve also includes part of the accessory cusps.

4) The mesiolingual face of the crown delimited by main landmarks four and five.

5) The mesiobuccal face of the crown delimited by main landmarks five and one.

The second set consists of seven curves each defined by a different number of semilandmarks:

6) The mesial longitudinal fissure delimited by main landmarks five and six (eight semilandmarks).

7) The mesiobuccal fissure delimited by main landmarks six and one (eight semilandmarks).

8) The section of the longitudinal fissure that connects the mesiobuccal fissure with the lingual fissure, or the longitudinal fissure, as delimited by main landmarks six and seven (three semilandmarks).

9) The lingual fissure delimited by main landmarks seven and four (eight semilandmarks).

10) The distal longitudinal fissure as delimited by main landmarks seven and eight (three semilandmarks).

11) The distobuccal fissure delimited by main landmarks eight and two (eight semilandmarks).

12) The distolingual fissure delimited by main landmarks eight and three (eight semilandmarks).

The 2D image of each molar was imported to ImageJ 1.51j8 (Schneider et al., 2012), where each curve was individually traced using the segmented line tool, converted into points, and exported as a .txt file that contained the X and Y coordinates of each point along the curve. Prior to the tracing procedure, each right molar was mirrored so that all molars in the sample would be of the same side. The .txt files were then imported to R 3.4.3 (R core team, 2017), where each curve was converted into equidistant semilandmarks (Figure 2.1) using a customized R code from the package 'geomorph' (Adams et al., 2018). Semilandmarks were allowed to slide only within their respective curve in order to maintain an accurate representation of the shape. After the sliding procedure, a Generalized Procrustes Analysis (GPA) was conducted in order to correct for orientation, location, and remove geometric size (Zelditch et al., 2004). Both the sliding and GPA were performed in R 3.4.3 (R core team, 2017) using the package 'geomorph' (Adams et al., 2018).

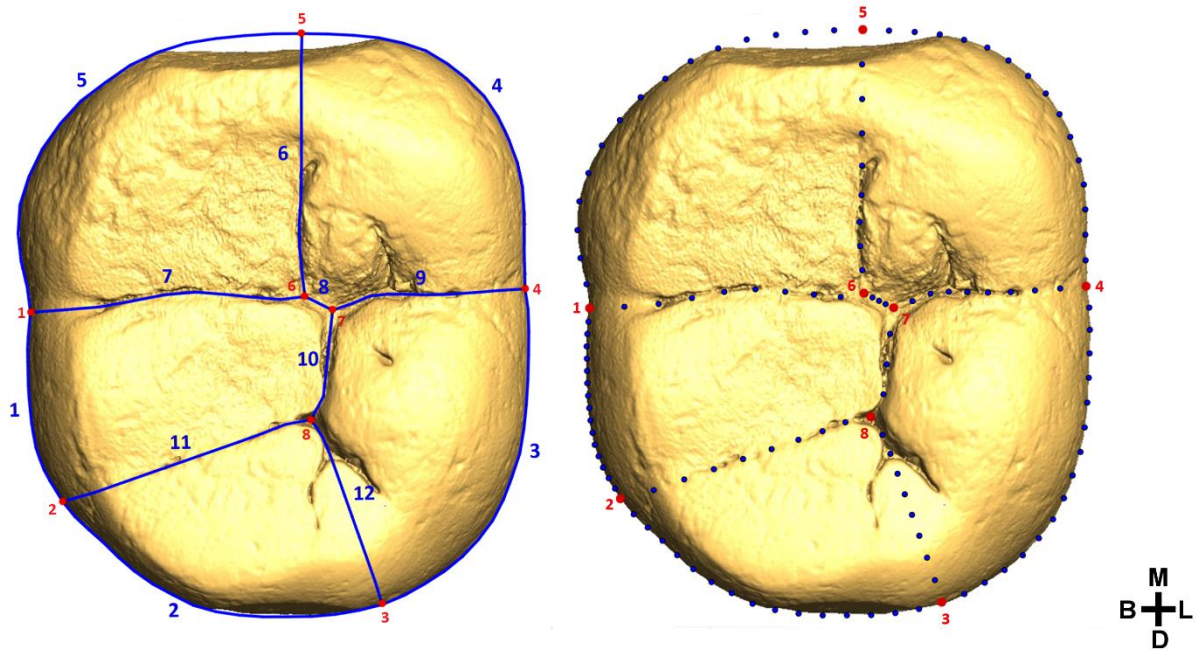

Figure 2.1. Left: a molar after the fissures and the outline of the crown have been traced in ImageJ. In blue are the curves, and in red are the positions of the fixed landmarks. Note the correction for interproximal wear (curves two, four, and five; fixed landmark five) and the continuation of the distolingual fissure (curve 12) through the C6. Right: a molar with the final configuration of landmarks after the curves have been converted into equidistant semilandmarks and fixed landmarks. In blue are the semilandmarks, in red are the fixed landmarks. Orientation: M = mesial; L = lingual; D = distal; B = buccal.

MD/BL dimensions and cusp area measurements

The MD and BL dimensions were measured as the distance between the smallest and largest X and Y values, respectively, of the raw (i.e. pre GPA) landmark coordinates. Crown shape index was dervied from MD and BL measurements using the formula MD*BL/100. The returned value can provide rudimentary information about crown shape. For example, a value of a 100 would indicate that the crown is as long as it is wide and could be described as square-shaped. A value above 100 would indicate that the crown is longer than it is wide, and a value below 100 means the crown is wider than it is long. Crown size index was derived from MD and BL measurements using the formula (MD+BL)/2. The value returned by the formula is the average of the width

(BL) and length (MD) of the tooth, and can be useful for comparing the overall size of different teeth. Because the landmark coordinates that make up each cusp could be considered as the coordinates of the vertices of a polygon, the function 'areapl', which finds the area of a non-self-intersecting polygon from the R package 'Splancs' (Bivand et al., 2017), was used to calculate absolute cusp areas (ACA). Relative cusp areas (RCA) were calculated by dividing the absolute area of the respective cusp by total crown area.

Multivariate analyses

Assessing the position of isolated Au. africanus mandibular molars

As described above, the *Au. africanus* sample was initially composed only of lower molars of known position. To maximize sample size for the taxon, 2D GM data were used to assess the tooth position of isolated *Au. africanus* (Moggi-Cecchi, 2006) molars. First, principal component analyses (PCA) were conducted using both the Procrustes coordinates of shape (also referred to as an analysis in shape space), and then using the Procrustes coordinates as well as the natural log of the centroid size in order to introduce size as a variable (also referred to as an analysis in form space). In Procrustes form space analysis, size accounts for all the variation in PC1, whereas in other PCs its loadings are smaller than those of most shape variables. Generally, Procrustes form space could be considered as a shape + size analysis. In the present study, Procrustes shape space and form space data would be referred to as GM shape and GM form data, respectively. A canonical variate analysis (CVA) was then conducted with the isolated molars treated as an unknown for tooth position. Following previous studies (Gomez-Robles et al., 2007, 2008, 2011, 2012; Skinner et al., 2008) only a subset of the total number of PCs was used in the CVA. A total of 13 CVAs were conducted using the first 2 to the first 14 PCs. The first

14 PCs accounted for ~96% and ~98% of the morphological variation for the shape space and form space data, respectively. A molar was deemed to be of known position if its classification results were consistent at 70% in both shape space and form space analyses. Molars whose positions were previously assessed by Skinner et al. (2008) via a 3D GM analysis of the EDJ were also assessed using the 2D GM data. If there was a disagreement between the 3D GM and 2D GM results, the tooth type was inferred from the 3D GM results by Skinner et al. (2008). The molar would then be added to the knowns sample and the process repeated for each unknown molar. Results are presented in Table 2.2.

Table 2.2
Classification results of isolated *Au. africanus* mandibular molars.

		Shape space			Form space		
Specimen	**Status**	**M_1**	**M_2**	**M_3**	**M_1**	**M_2**	**M_3**
Sts9[a,c]	M_1	100.0%			92.3%	7.7%	
STW 145[b]*	M_2	46.2%	53.8%		69.2%	30.8%	
STW 234[b]	M_2		100.0%		7.7%	92.3%	
STW 237[b]	M_3	92.3%	7.7%		84.6%	15.4%	
STW 280[b]*	M_3		53.8%	46.2%		38.5%	61.5%
STW 285b[b]	M_2	92.3%	7.7%		100.0%		
STW 291[b]	M_1		100.0%		38.5%	61.5%	
STW 364[b]	M_1	69.2%	30.8%		100.0%		
STW 412B[b]	M_2	76.9%	23.1%		100.0%		
STW 424[b]	M_2	100.0%			84.6%	15.4%	
STW 520[b]	M_3	15.4%	46.2%	38.5%		46.2%	53.8%
STW 529[b]	M_3			100.0%			100.0%
STW 537[b]	M_2 (M_3**)		100.0%			100.0%	
STW 555[b]	M_2	76.9%	23.1%		53.8%	46.2%	
STW 123[b]	M_1	23.1%	76.9%		92.3%	7.7%	
STW 133[b]	M_2		76.9%	23.1%		69.2%	30.8%
STW 421B[b]	M_1	100.0%			100.0%		
TM 1518[c]	M_3	84.6%		15.4%	23.1%		76.9%

*indicates specimens that were added to the sample based on the results in Skinner et al. (2008) despite their incorrect classification with 2D GM data in the current study. ** the molar was assigned an M_3 position by Moggi-Cecchi et al. (2006), however it is most likely an M_2 based on Skinner et al. (2008). Light shaded cells show the classification results for the assigned molar position by past research. Dark shaded cells indicate which specimens were omitted from the analysis. Citation: a – Suwa, 1996; b – Moggi-Cecchi et al., 2006; c – Robinson, 1956.

Assessing the performance of the methodologies

The different data types that capture tooth crown shape (2D GM shape space, 2D GM form space, relative cusp areas, absolute cusp areas, MD and BL dimension, crown shape and crown size indices) were evaluated as to how well they 1) differentiate between the four hominid taxa (*Au. afarensis, Au. africanus, H. neanderthalensis, and P. troglodytes*) at each lower molar position, and 2) between the mandibular molar types of *Au. afarensis*. The aim of the latter analysis was to identify which data types show the highest rates of correctly classified molars to their respective type, and use them in the subsequent analysis for determining the position of isolated Lomekwi molars.

Canonical variate analyses

A Canonical variate analysis (CVA) was used to assess how well the different data types correctly classify the taxa, and a CVA with leave-one-out cross validation (CV) was used to evaluate the reliability of the classification results (Kovarovich et al., 2011). In a CVA without cross validation the canonical variates are generated using all the specimens in the sample, and then each specimen is classified according to the values of the canonical variates. This process is circular, but it allows for the assessment of the precision of the model in correctly assigning specimens to their respective groups. This is useful, because knowing how precise a model is helps in interpreting the classification results of data that we wish to classify. In a CVA with leave-one-out cross validation, one specimen is omitted from the generation of canonical variates and *then* classified. This is repeated for each specimen in the sample. This process avoids the circularity that is innate to a CVA without cross validation, and assesses how reliable the classification results of unknown specimens would be. Thus, a CVA without cross validation

provides a better sense of the behavior of all the data that is used in the analysis and the precision of the model, whereas a CVA with cross validation assesses how generalizable the model is. This approach has been successfully applied in past studies of hominin dentition (Skinner, 2008; Grine et al., 2009; Turvey et al., 2018), and is particularly useful in the case of Lomekwi as both it and the comparative samples are small. PCs derived from GM shape space, form space, relative and absolute cusp area data were used to assess the classification performance of each type of data. The number of PCs for the analyses of the absolute and relative cusp area data was chosen based on the maximum number of variables (PCs) before they became collinear. In a linear discriminant analysis (which a CVA is a type of), a least squares method is used to estimate a regression vector using the moment matrix X^TX. If two explanatory variables have a highly linear relationship they cannot be assigned a rank, which then does not allow for the inversion of the moment matrix and the derivation of the regression vector. In this instance, a predictor cannot be obtained to classify the data (Naes and Mevik, 2001). Thus, for the relative cusp area data three CVAs were conducted: using PCs 1-2, 1-3, and 1-4. For absolute cusp area data four CVAs were conducted: PCs 1-2, 1-3, 1-4, and 1-5. The presence of more variables than observations in a CVA can lead to unstable degrees of discrimination, expressed mostly as overfitting and clustering of random data (Mitteroecker and Bookstein, 2011). This is a particular issue for GM analyses in which there tends to be more landmarks than specimens. For CVAs of GM data in both shape and form space the number of PCs chosen explained ~99% of the variance. The raw MD, BL, crown shape, and crown size data were also used in the CVA analyses to evaluate the performance of these methodologies.

Pairwise permutational MANOVAs, also known as PERMANOVA (Anderson, 2001), with 1000 permutations were run to test for group differences using the GM shape and form space data, and the relative and absolute cusp area data. PERMANOVA is a non-parametric multivariate tets that tests for similarity based on a chosen distance measure (in this analysis it is Euclidean distances between Procrustes coordinates and cusp areas for the GM and cusp area data, respectively), which neither assumes normal distribution nor requires the number of variables to not exceed the number of sampling units - both common issues in palaeonathropological GM studies, and have been encountered in the current study as well. Because PERMANOVA does not limit the number of variables in the analysis, it allows for the use of the whole landmark dataset and overcomes the need to reduce the dimensionality of the data via PCA or other means. As such, it is a powerful tool for testing for group differences in a GM setting. MANOVAs were used to test for MD/BL and crown shape + crown size mean group differences, whereas t-tests were run to test for group differences using the crown shape data. Prior to running the t-tests an ANOVA was perfromed and these results are reported as well. The decision to carry out individual t-tests rather than performing an ANOVA with pairwise post-hoc tests was based on the need to maintain an inter-statistical comparable approach. That is, since all the other statistical tests are concerned with the specific pairwise group results rather than with the question of whether all group means are identical or not, running pairwise t-tests rather than an ANOVA with pairwise post-hoc tests was deemed to be more appropriate. Furthermore, most ANOVA post-hoc tests employ some form of p-value adjustment to control for Type I errors (or false positives), which is not necessarily needed for the analyses at hand (see below).

Generally, controlling for Type I errors may not be necessary for the purpose of this study, since the analyses use independent data from independent groups. However, because p-value corrections are relatively common in GM studies (e.g. Buchanan and Collard, 2010; Sanchez et al., 2013; Nicholson and Harvati, 2006; Changbunjong et al., 2016; Cocos and Halazonetis, 2017), the Bonferroni correction was performed. While Bonferroni correction is considered to be overly conservative and more powerful procedures for controlling for Type I errors have been developed (Narum, 2006), it was chosen specifically for its conservative nature. Because the methods comparison analyses are concerned with assessing the performance of different data types in various scenarios, Bonferroni correction could inform which data types manage to perform well under some constraints. The p-values were adjusted using the function 'p.adjust' from the package 'stats' (R core team, 2017). Bonferroni correction is traditionally performed by dividing the alpha value by the number of tests, with the returned value constituting the new significance threshold. In contrast, the 'p.adjust' function multiplies each non-adjusted p-value by the number of tests and returns adjusted p-values where the significance threshold of 0.05 is maintained. All multivariate analyses were carried out in R 3.4.3 (R core team, 2017).

Intra observer error

The projection of the fissures may change between rotations of the same molar, which could lead to inconsistent, and in turn unreliable, classification results. Thus, the degree of acceptable rotation and fissure delineation errors should be estimated. Ten random molars from the whole sample were rotated and landmarked three times. Then, they were added to the whole sample and a PCA using Procrustes shape coordinates was conducted to reduce the dimensionality of the data. The molars of each specimen were then assigned to their own group, and CVAs using

the first 3-4, 3-5, 3-6, ..., and 3-15 PCs, were used to determine how often each molar classified correctly with the other two molars. A classification accuracy of 85% was deemed to be acceptable. Results are presented in Table 3A in the Appendix.

2.2 Results

2.2.1 First molars

Figure 2.2 presents graphical comparisons of the crown morphology between taxa using each dataset. The GM form space data show the best separation between the taxa among the data types, with the first two PCs accounting for 83.3% of the variation. Absolute cusp areas and MD and BL data performed well, both showing little overlap between the species. GM shape and relative cusp areas performed the poorest, both exhibiting significant overlap, with an exception for the GM shape data, which separates *Au. afarensis* from the other taxa. This could be explained by the square shaped molars of *Au. afarensis* compared to the more oval-rectangular shape of the molars in the other taxa (see Figure 1 in Appendix). The third PC is not shown as it does not significantly change the results of either the GM or cusp area data. The PCA results suggests that size is the main variable that drives the separation between the hominids, with a size pattern of *P. troglodytes* < *H. neanderthalensis* < *Au. afarensis* < *Au. africanus*.

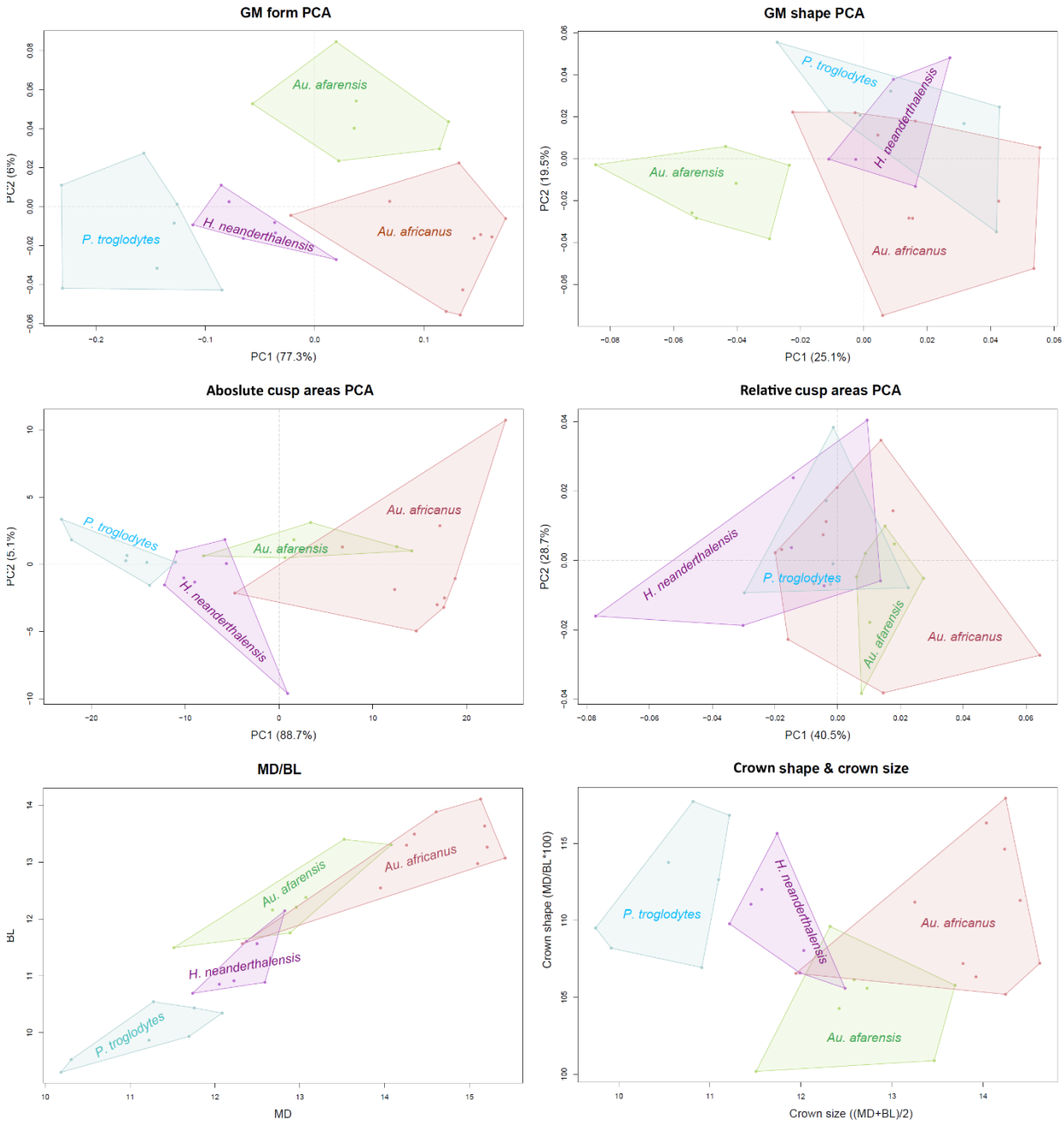

Figure 2.2. PCA and bivariate plots of the first lower molars of each taxon. Upper row: PCA plots visualizing the first two principal components of GM form (left) and shape (right) data. Middle row: PCA plots visualizing the first two principal components of absolute cusp area (left) and relative cusp area (right) data. Bottom row: bivariate plots of the MD and BL data (left) and crown shape and crown size data (right).

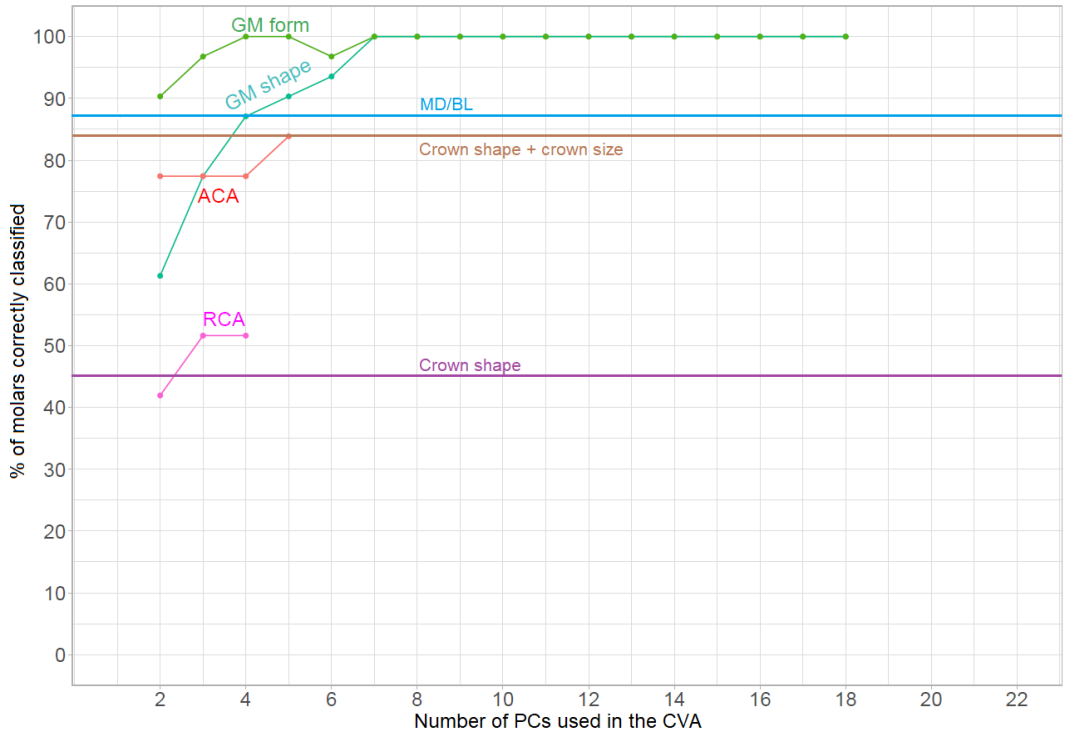

A)

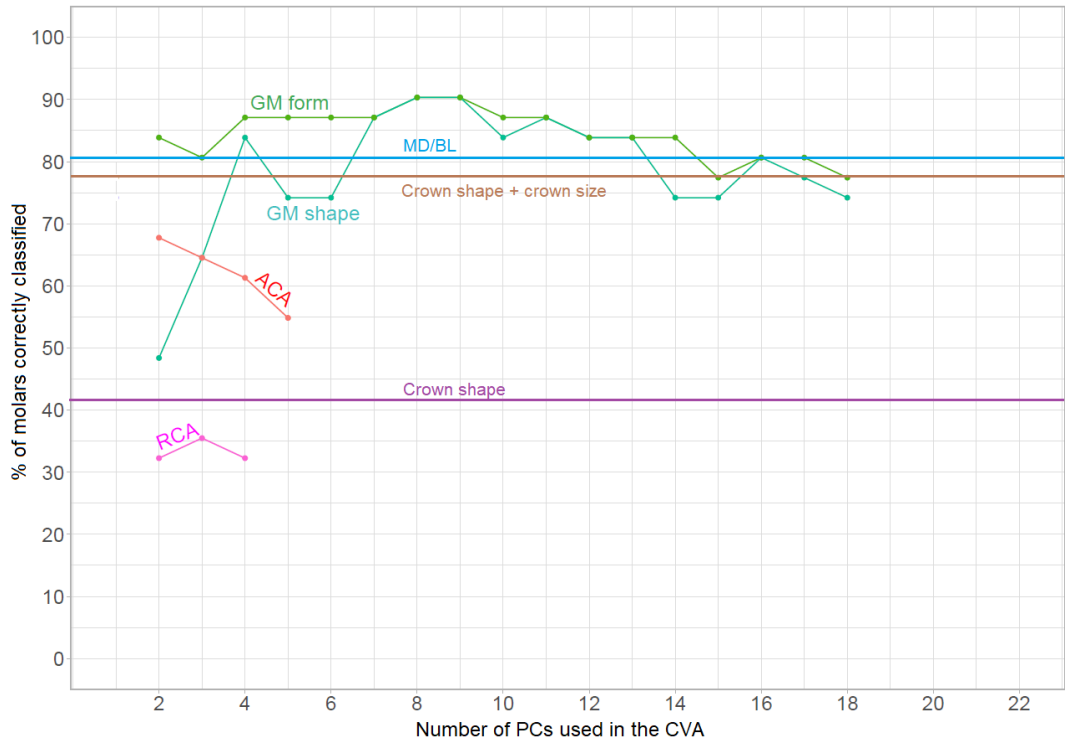

B)

Figure 2.3. A) Classification results without using cross-validation and B) with cross-validation of the lower first molar sample. ACA – absolute cusp areas; RCA – relative cusp areas.

In the CVAs without cross-validation (Figure 2.3; A), GM form had the best performance with a correct classification rate consistent at above 90%. GM shape shows a relatively poor correct classification rate for the first two PCs at 61.5%, but an improvement at three PCs with a classification accuracy rate of 78%, and above 85% for the first 4-18 PCs. Absolute cusp area data performed well across all PCs with a consistent classification accuracy rate of above 75%, peaking at 87% with five PCs. Relative cusp area performed the poorest at correctly classifying the molars, with correct classification rates of 42%, 51%, and 51% for the first two, three, and four PCs, respectively. MD and BL data correctly classified 87% of the molars, whereas crown shape + crown size had a classification accuracy of 81%. Crown shape alone managed to classify correctly only 45% of the molars. The CVAs with cross-validation results show a similar pattern (Figure 2.3; B). GM form performed the best among all data types with a correct classification accuracy consistent at 75% or above for the first 2-14 PCs, and two peaks of 90% at eight and nine PCs. As with the CVA without cross-validation results, GM shape shows initial poor classification results of 48% and 65% with the first two and three PCs, respectively. The percentage of correctly classified molars increases to and maintained at 73% for the first 4-18 PCs, with two peaks of 90% at eight and nine PCs. Absolute cusp area data displayed the best classification rate at two PCs, with a steady decline in accuracy bottoming at 55% with five PCs. Relative cusp area data exhibited the poorest performance of all datasets, with a correct classification accuracy range of 32%-35%. Crown shape correctly classified 42% of the molars. Generally, the CVA with CV results show an inverse trend to that of the CVA without CV, with a decreasing classification accuracy as the number of variables increases.

PERMANOVA results reveal that the GM form data found statistically significant differences between all taxa, even when p-values were corrected for multiple comparisons using Bonferroni correction (Table 2.3). Significant differences between most groups were found using absolute cusp area and GM shape data, although differences between *Au. afarensis* and *Au. africanus* (p=0.136; unadjusted p=0.018, df=(1,15), Pseudo-F=4.8771, SS=437.99, R^2=0.245), and *Au. africanus* and *P. troglodytes* (p=0.186; unadjusted p=0.038, df=(1,15), Pseudo-F=2.3071, SS=0.0089, R^2=0.133) become non-significant when p-values are Bonferroni adjusted, respectively. Significant differences between all taxa were found in the MANOVAs using MD and BL, and crown shape and crown size data, apart from between *Au. afarensis* and *H. neanderthalensis* which becomes non-significant with Bonferroni correction (p=0.091; unadjusted p=0.015, df=(1,12), Pillai's trace=0.53, F=6.253). PERMANOVAs using RCA data detected statistically significant differences between the means of the relative cusp areas of only *H. neanderthalensis* and *Au. afarensis* (p=0.009, df=(1,12), Pseudo-F=3.5713, SS=0.0042, R^2=0.229) and *P. troglodytes* and *Au. afarensis* (p=0.024, df=(1,12), Pseudo-F=3.1564, SS=0.0025, R^2=0.208), and t-test using crown shape data found significant differences only between the first lower molars of *Au. afarensis* and the three other taxa.

The interpretation of the GM shape and form results is aided by the comparison between the mean shapes of the M_1s of each taxon (Figure 2.4). Generally, the mean shapes of the M_1s exhibit little overlap between the taxa, except for those of *Au. africanus* and *P. troglodytes*, which may explain why when the p-value is Bonferroni corrected it becomes non-significant in the GM shape PERMANOVA. Boxplots comparing the relative and absolute cusp areas between the taxa are shown in Figure 2.5. The small number of significant differences found in the RCA

PERMANOVAs can be explained by the large overlap in the relative cusp areas between the species (Figure 2.5; A). Only *Au. afarensis* departs from the other groups by exhibiting marked differences between the relative areas of the hypoconid and entoconid. The inclusion of size increases the variability in the ACA data, which may have led to the large number of significant differences found in the PERMANOVA.

Table 2.3.
Results of pairwise permutational MANOVAs (1000 permutations), MANOVAs, and t-test for the lower first molars. Numbers in brackets are Bonferroni corrected p-values. Significant p-values are in bold.

	Relative cusp areas		
	Au. afarensis	*Au. africanus*	*H. neanderthalensis*
Au. africanus	0.502 (1.000)	-	-
H. neanderthalensis	**0.009** (0.072)	0.227 (1.000)	-
P. troglodytes	**0.024** (0.108)	0.460 (1.000)	0.412 (1.000)
	Absolute cusp areas		
	Au. afarensis	*Au. africanus*	*H. neanderthalensis*
Au. africanus	**0.018** (0.136)	-	-
H. neanderthalensis	**0.011** (0.066)	**0.001** (**0.006**)	-
P. troglodytes	**0.002** (**0.006**)	**0.001** (**0.006**)	**0.002** (**0.036**)
	GM shape		
	Au. afarensis	*Au. africanus*	*H. neanderthalensis*
Au. africanus	**0.003 (0.006)**	**-**	**-**
H. neanderthalensis	**0.003 (0.012)**	**0.005 (0.024)**	**-**
P. troglodytes	**0.003 (0.024)**	**0.038** (0.186)	**0.003 (0.012)**
	GM form (log centroid size)		
	Au. afarensis	*Au. africanus*	*H. neanderthalensis*
Au. africanus	**0.005 (0.024)**	**-**	**-**
H. neanderthalensis	**0.002 (0.006)**	**0.001 (0.006)**	**-**
P. troglodytes	**0.003 (0.018)**	**0.001 (0.006)**	**0.001 (0.018)**
	MD/BL MANOVAs		
	Au. afarensis	*Au. africanus*	*H. neanderthalensis*
Au. africanus	**0.004 (0.044)**	-	-
H. neanderthalensis	**0.015** (0.091)	**0.003 (0.005)**	-
P. troglodytes	**0.001 (0.001)**	**0.001 (0.001)**	**0.003 (0.022)**
	Crown shape pairwise t-test (ANOVA p=0.009)		
	Au. afarensis	*Au. africanus*	*H. neanderthalensis*
Au. africanus	**0.007 (0.041)**	-	-
H. neanderthalensis	**0.022** (0.134)	0.773 (1.000)	-
P. troglodytes	**0.001 (0.008)**	0.358 (1.000)	0.264 (1.000)
	Crown shape + crown size MANOVAs		
	Au. afarensis	*Au. africanus*	*H. neanderthalensis*
Au. africanus	**0.007 (0.046)**	-	-
H. neanderthalensis	**0.014** (0.085)	**0.001 (0.001)**	-
P. troglodytes	**0.001 (0.001)**	**0.001 (0.001)**	**0.003 (0.02)**

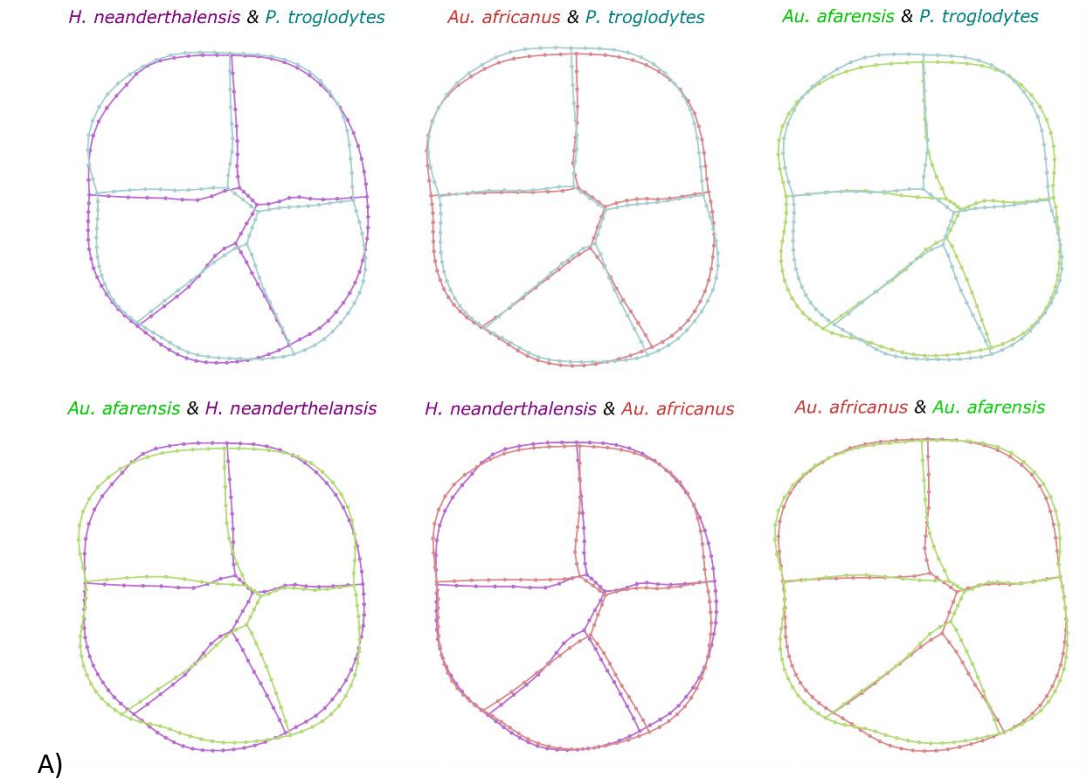

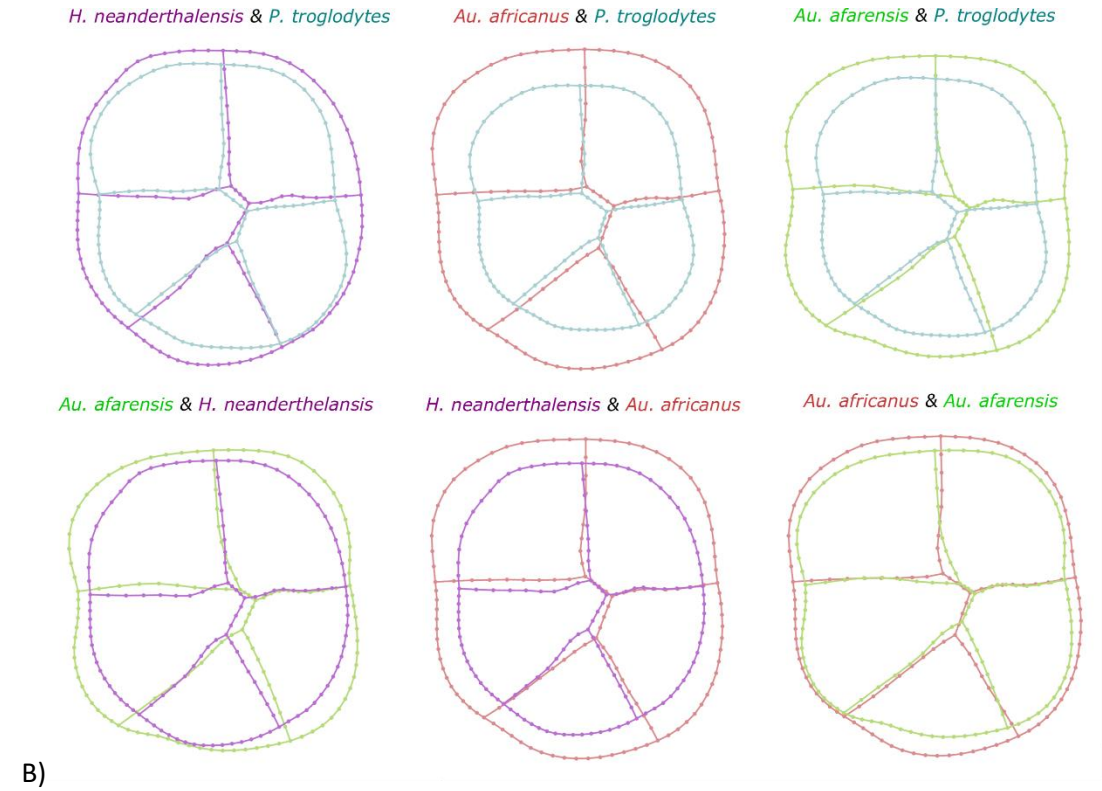

Figure 2.4. A) mean shapes of the first lower molars of each taxon. B) mean shapes and size of the first lower molars of each taxon.

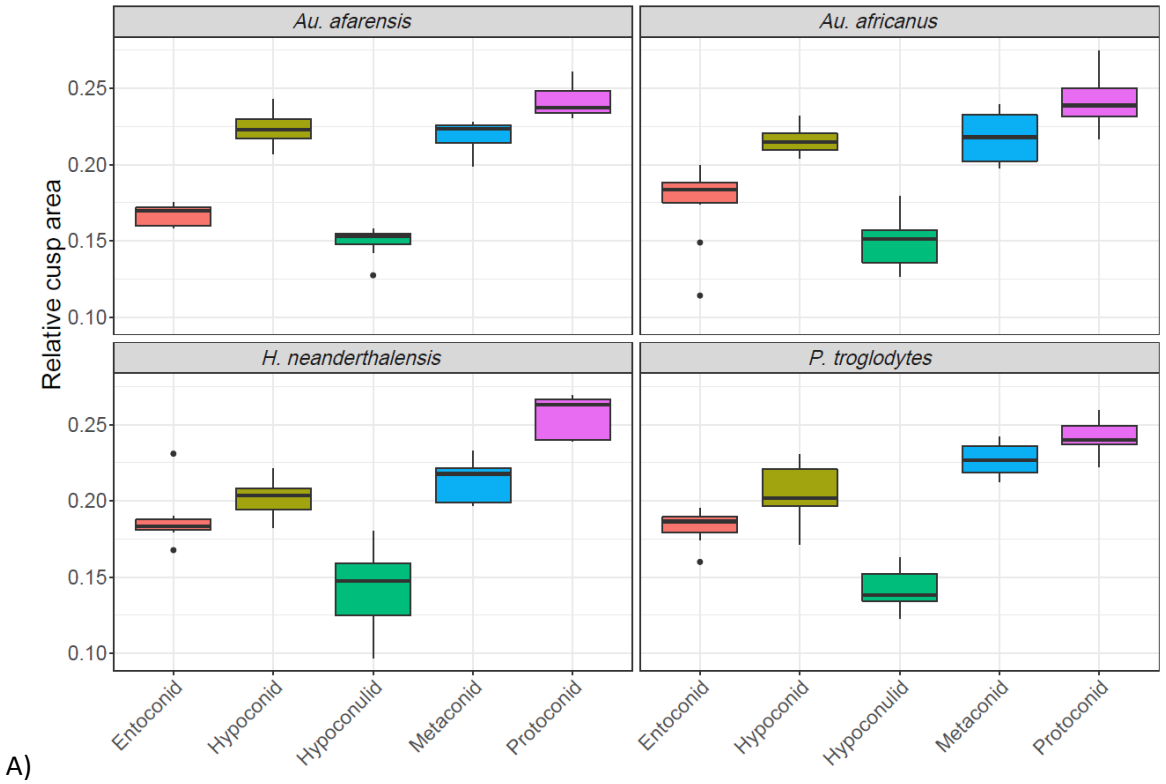

A)

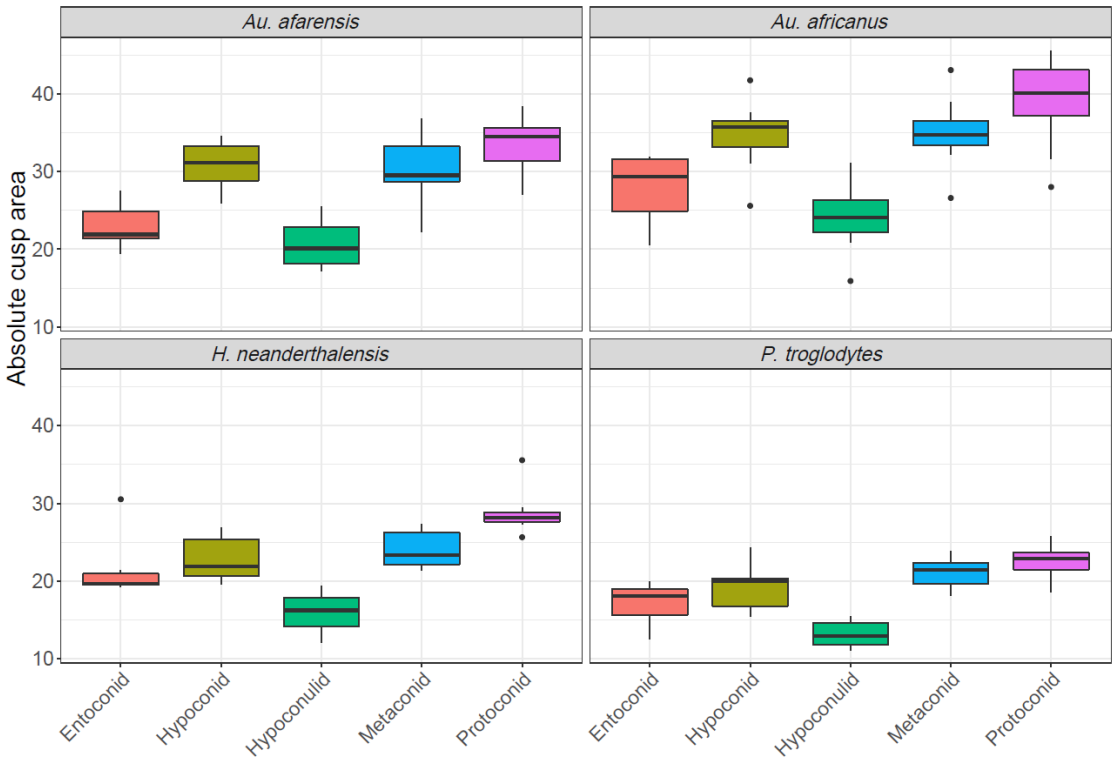

B)

Figure 2.5. A) Boxplots of the A) relative cusp areas and B) absolute cusp areas for the first lower molars of each taxon.

2.2.2 Second molars

PCA plots of the first two PCs of the GM shape and form data are compared to the PCA plots of the first two PCs of the relative and absolutes cusp areas data, and to the MD and BL data in Figure 2.6. The first two PCs of GM form, which account for 86.2% of the morphological variation, show the best separation between the taxa among all data types, with an overlap only between *Au. africanus and Au. afarensis*. The first two PCs (94.2% of the variation) of the absolute cusp area PCA exhibit a good separation between the molars of the four taxa as well, with clustering similar to that observed in the PCA plot of the GM form data. The first two PCs of GM shape space, which account for a combined variation of 50.1%, only distinguish *H. neanderthalensis* from the other taxa. Thin plate spline (TPS) grids depicting the morphological variation along PC1 (Figure 2. Appendix) show that *H. neanderthalensis* M_2s are distinguished from those of *P. troglodytes*, *Au. afarensis*, and *Au. africanus*, by having an oval shape, whereas the mesial half of the crown in *P. troglodytes* and *Australopithecus* is expanded buccolingually giving the molars a more ovoid shape. The PCA plot of the first two principal components of the relative cusp area data show a similar pattern, with *H. neanderthalensis* specimens clustering in the positive range of PC1 (49.2% of the variation), and the other taxa in the negative range. The relative cusp areas results somewhat mirror those of GM shape data, which is expected since the major difference between *H. neanderthalensis* and the other taxa is in the relative shape of the metaconid and protoconid. The bivariate plots of MD and BL and crown shape and crown size data show relatively good separation between the taxa, with size being the main variable accounting for the separation. According to the crown shape index, apart from a few *P.*

troglodytes and *Au. afarensis* specimens, shape does not appear to be different between the species, as the M_2s are all longer than they are wide.

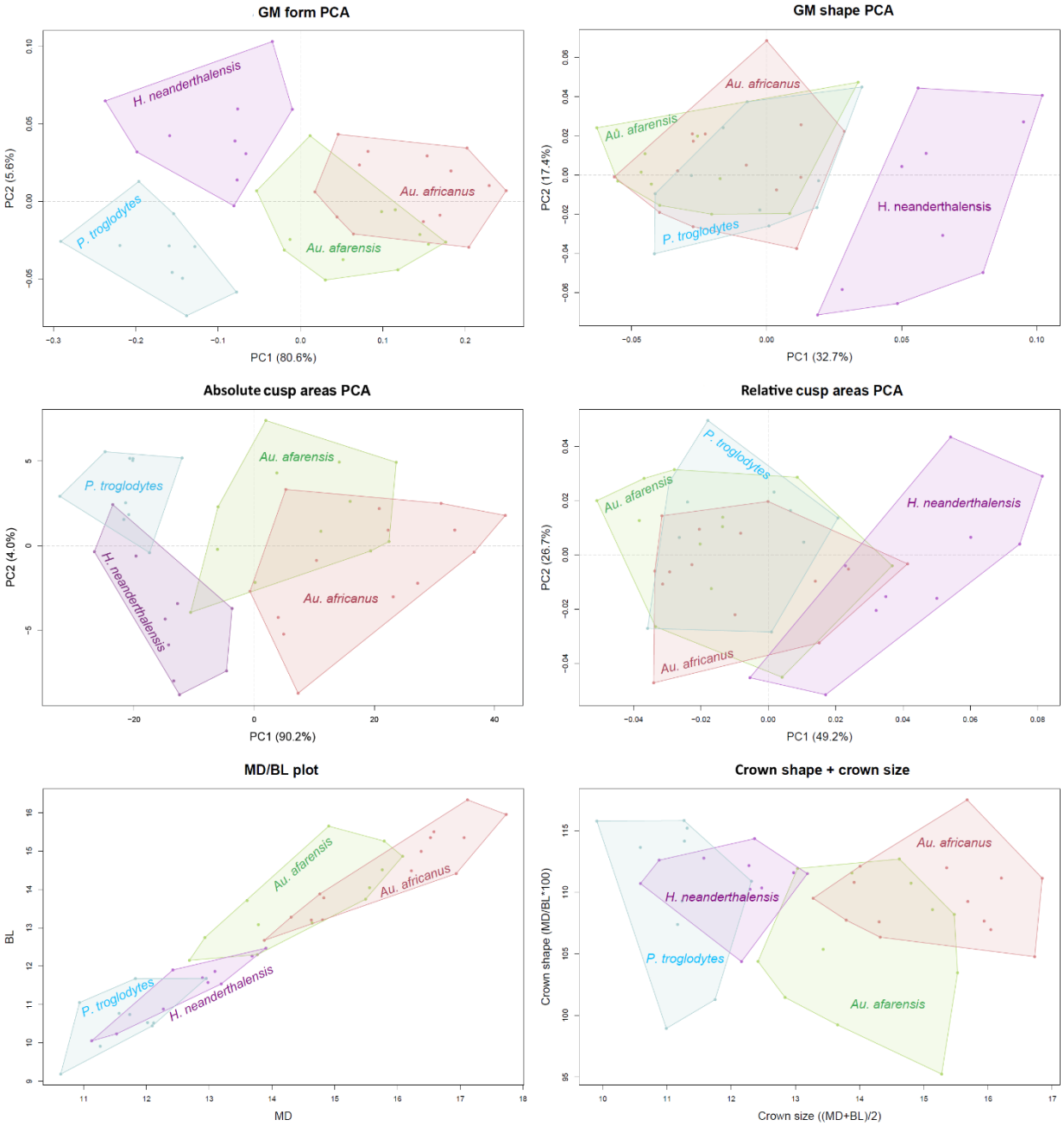

Figure 2.6. PCA and bivariate plots of the second lower molars of each taxon. Upper row: PCA plots visualizing the first two principal components of GM form (left) and shape (right) data. Middle row: PCA plots visualizing the first two principal components of absolute cusp area (left) and relative cusp area (right) data. Bottom row: bivariate plots of the MD and BL data (left) and crown shape and crown size data (right).

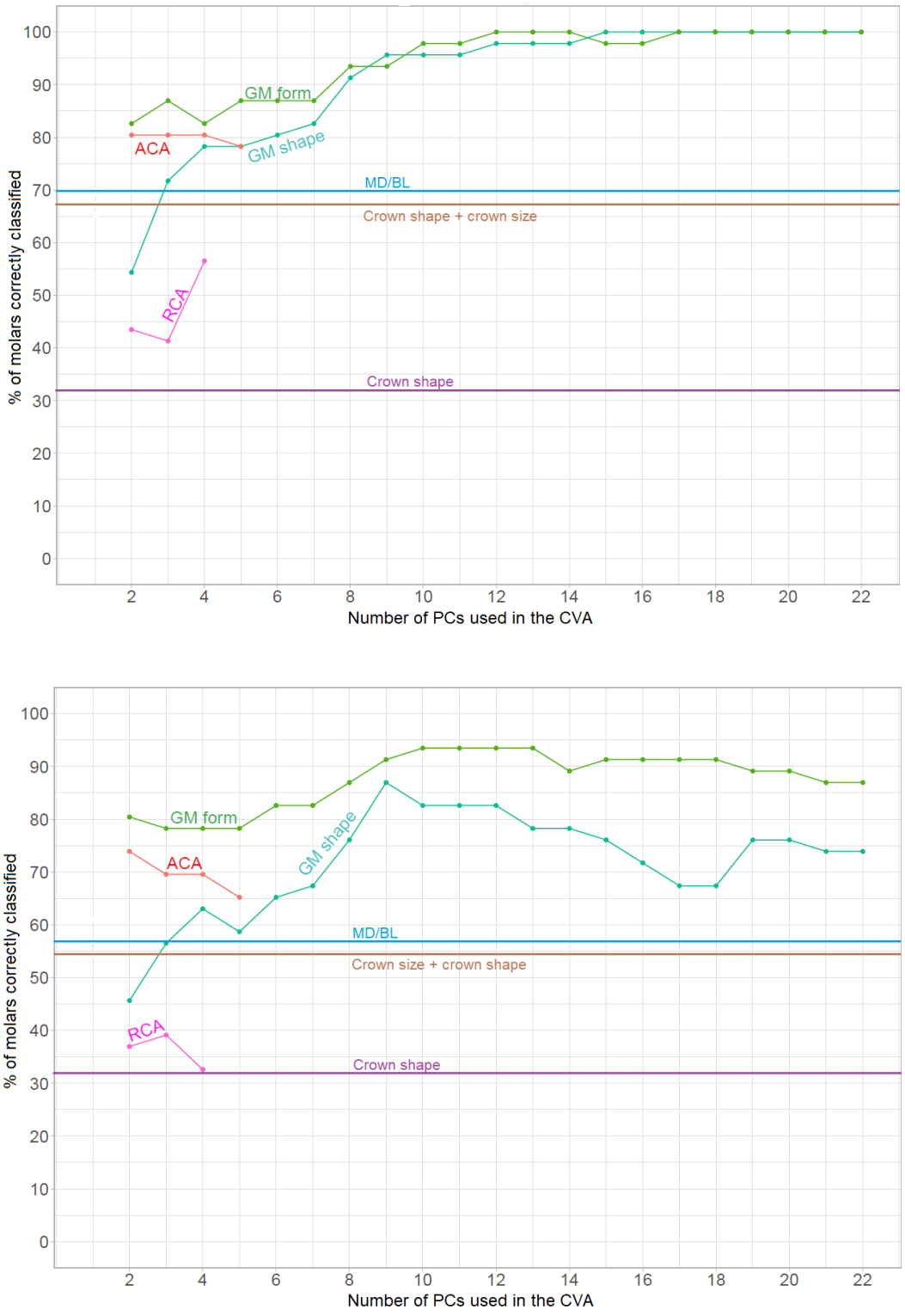

Figure 2.7. A) Classification results without using cross-validation and B) with cross-validation for the lower second molar sample. ACA – absolute cusp areas; RCA – relative cusp areas.

In the CVA without cross-validation results, GM form showed the best performance with a consistently correct classification accuracy rate at above 80% for the first two to 21 PCs (Figure 2.7; A). The performance of GM shape displayed a similar pattern to the M_1s results. Classification accuracy is poor (54.4%) for the first two PCs, increases to 72.4% with three PCs, and maintained at a level of above 75% in subsequent CVAs. Absolute cusp area data performed well as well, exhibiting a consistent classification accuracy of ~80% for the first four PCs, and a slight decline to 78% with five PCs. Relative cusp area data performed poorly, with a classification accuracy below 45% for the first two to three PCs, and a slight increase to 52% at four PCs. MD and BL data correctly classified ~70% of the specimens, and crown size + crown shape correctly classified ~68% of the specimens. Crown shape data performed the poorest, with a correct classification rate of only 32%.

In the CVA with cross-validation (Figure 2.7; B), GM form performed the best, with a consistently correct classification rate of 78%, and peaks of 94% with the first 10 to 13 PCs. The initial performance of GM shape is relatively poor, with a classification accuracy of below 70% for the first two to six PCs. The accuracy increases to 70% with seven PCs and maintained at this level or above up to 21 PCs, with a peak of 86% with nine PCs. Absolute cusp area data performed relatively well, with a correct classification rate of 74%-70% for the first 2-4 PCs, and a slight dip with five PCs to 65%. The performance of relative cusp area data is poor, with a consistent correct classification rate below 40%. MD and BL data correctly classified 57% of the specimens, and crown shape + crown size indices had a classification accuracy of 55%. Crown shape data performed the poorest of all data types, with a correct classification rate of 32%.

In the PERMANOVAs using GM form and absolute cusp areas data significant differences were observed between most taxa, and were maintained even when p-values were Bonferroni corrected (Table 2.4). The only differences that became non-significant are between *Au. afarensis* and *Au. africanus*. Significant differences between the M_2s of the two species have also not been detected with GM shape data (both corrected and non-corrected p-values). The significant overlap between the shape (Figure 2.8) and relative cusp areas (Figure 2.9) of the M_2s in these hominins can explain the results. MD and BL, and crown shape + crown size data performed as well as GM form and absolute cusp area data. The performance of the relative cusp area and crown shape data was the poorest, finding the least amount of significant differences between the taxa. The poor ability of relative cusp area data to detect differences between the groups is most likely driven by the marked overlap between the four taxa (Figure 2.9).

Table 2.4.
Results of pairwise permutational MANOVAs (1000 permutations), MANOVAs, and t-test for the lower second molars. Numbers in brackets are Bonferroni corrected p-values. Significant p-values are in bold.

	Relative cusp areas		
	Au. afarensis	*Au. africanus*	*H. neanderthalensis*
Au. africanus	0.330 (1.000)	-	-
H. neanderthalensis	**0.001 (0.006)**	**0.001 (0.006)**	-
P. troglodytes	0.614 (1.000)	0.329 (1.000)	**0.001 (0.006)**
	Absolute cusp areas		
	Au. afarensis	*Au. africanus*	*H. neanderthalensis*
Au. africanus	**0.037** (0.180)	-	-
H. neanderthalensis	**0.001** (**0.006**)	**0.001** (**0.006**)	-
P. troglodytes	**0.001** (**0.006**)	**0.001** (**0.006**)	**0.004** (**0.012**)
	GM shape		
	Au. afarensis	*Au. africanus*	*H. neanderthalensis*
Au. africanus	0.122 (0.821)	-	-
H. neanderthalensis	**0.001 (0.006)**	**0. 001 (0.006)**	-
P. troglodytes	**0.001 (0.012)**	**0. 001 (0.006)**	**0. 001 (0.006)**
	GM form (log centroid size)		
	Au. afarensis	*Au. africanus*	*H. neanderthalensis*
Au. africanus	**0.031** (0.246)	-	-
H. neanderthalensis	**0.001 (0.006)**	**0.001 (0.006)**	-
P. troglodytes	**0.001 (0.018)**	**0.001 (0.006)**	**0.002 (0.012)**
	MD/BL MANOVAs		
	Au. afarensis	*Au. africanus*	*H. neanderthalensis*
Au. africanus	**0.026** (0.156)	-	-
H. neanderthalensis	**0.001 (0.006)**	**0.001 (0.006)**	-
P. troglodytes	**0.001 (0.006)**	**0.001 (0.006)**	**0.042** (0.253)
	Crown shape pairwise t-test (ANOVA p=0.059)		
	Au. afarensis	*Au. africanus*	*H. neanderthalensis*
Au. africanus	0.054 (0.324)	-	-
H. neanderthalensis	**0.014 (**0.083**)**	0.442 (1.000)	-
P. troglodytes	**0.038** (0.227)	0.739 (1.000)	0.685 (1.000)
	Crown shape + crown size MANOVAs		
	Au. afarensis	*Au. africanus*	*H. neanderthalensis*
Au. africanus	**0.027** (0.165)	-	-
H. neanderthalensis	**0.001 (0.006)**	**0.001 (0.006)**	-
P. troglodytes	**0.001 (0.006)**	**0.001 (0.006)**	**0.043** (0.258)

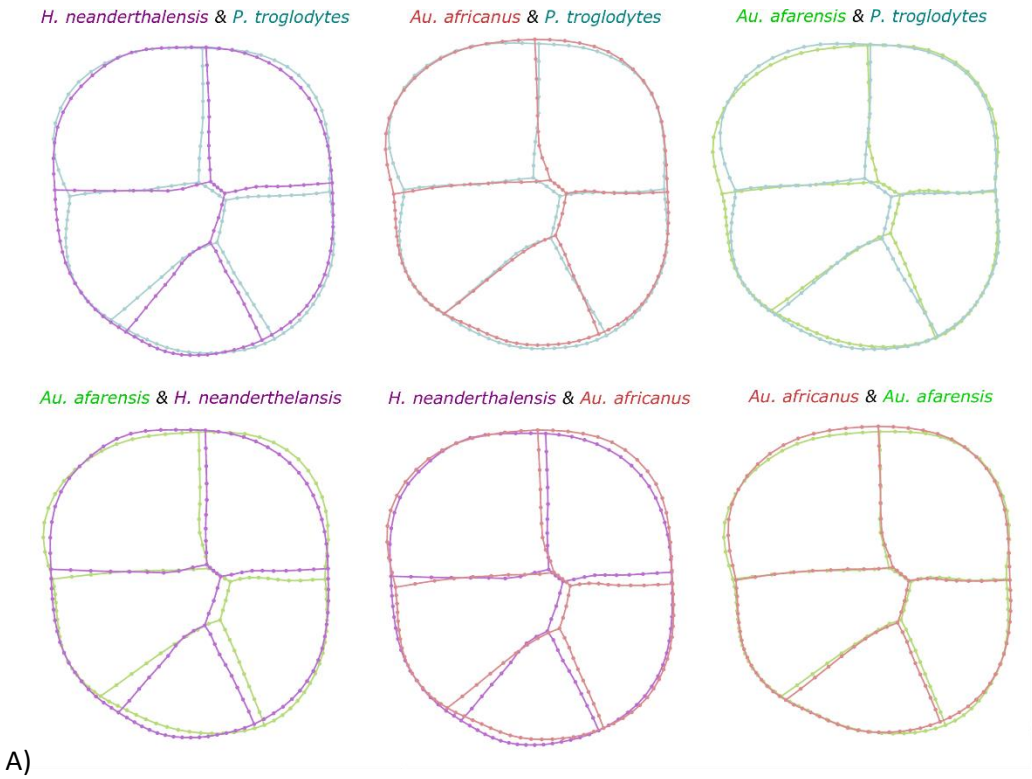

A)

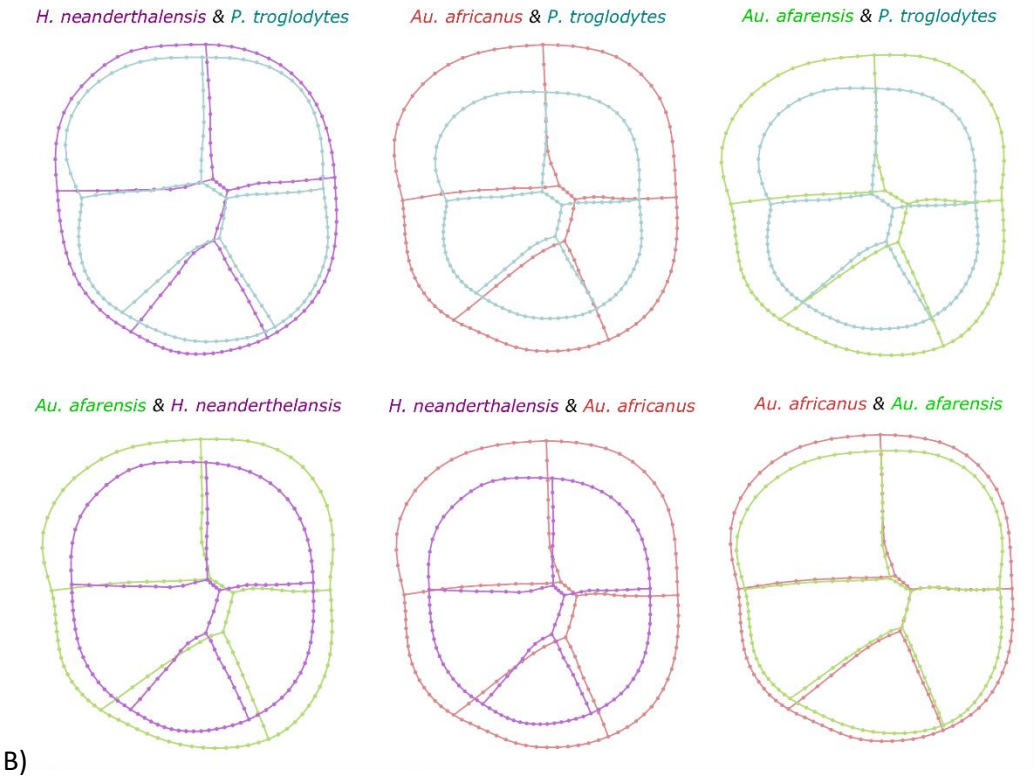

B)

Figure 2.8. A) mean shapes of the second lower molars of each taxon. B) mean shapes and size of the second lower molars of each taxon.

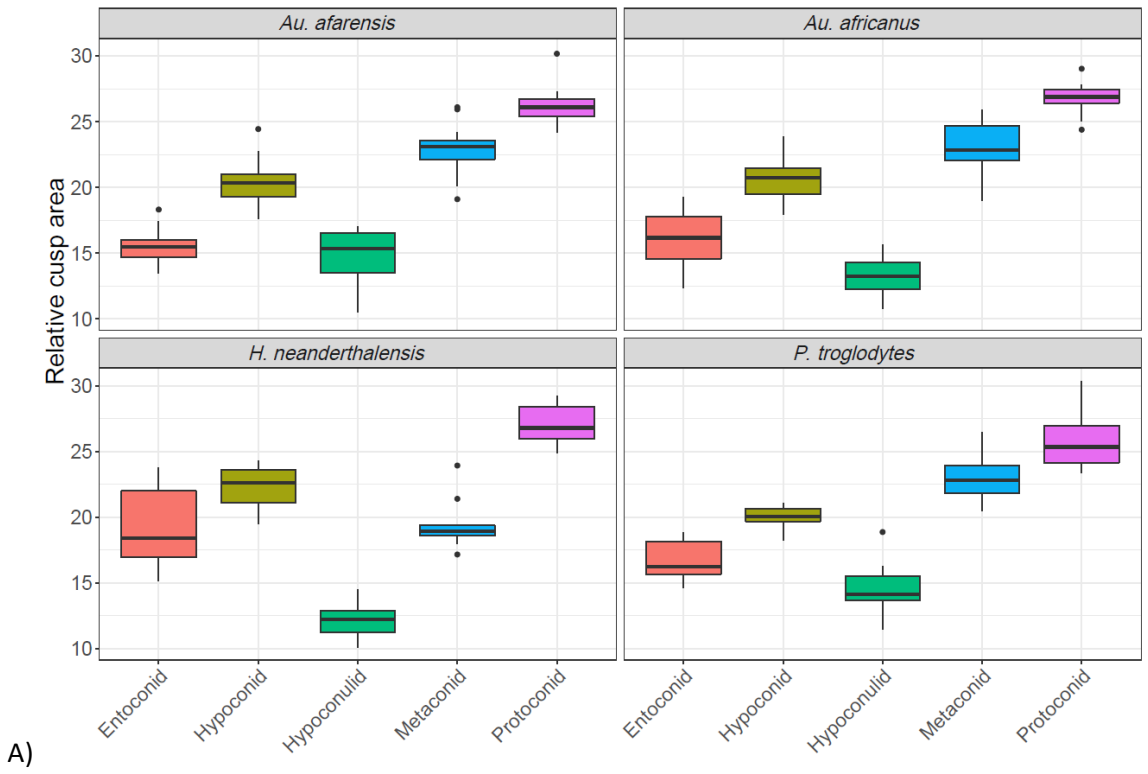

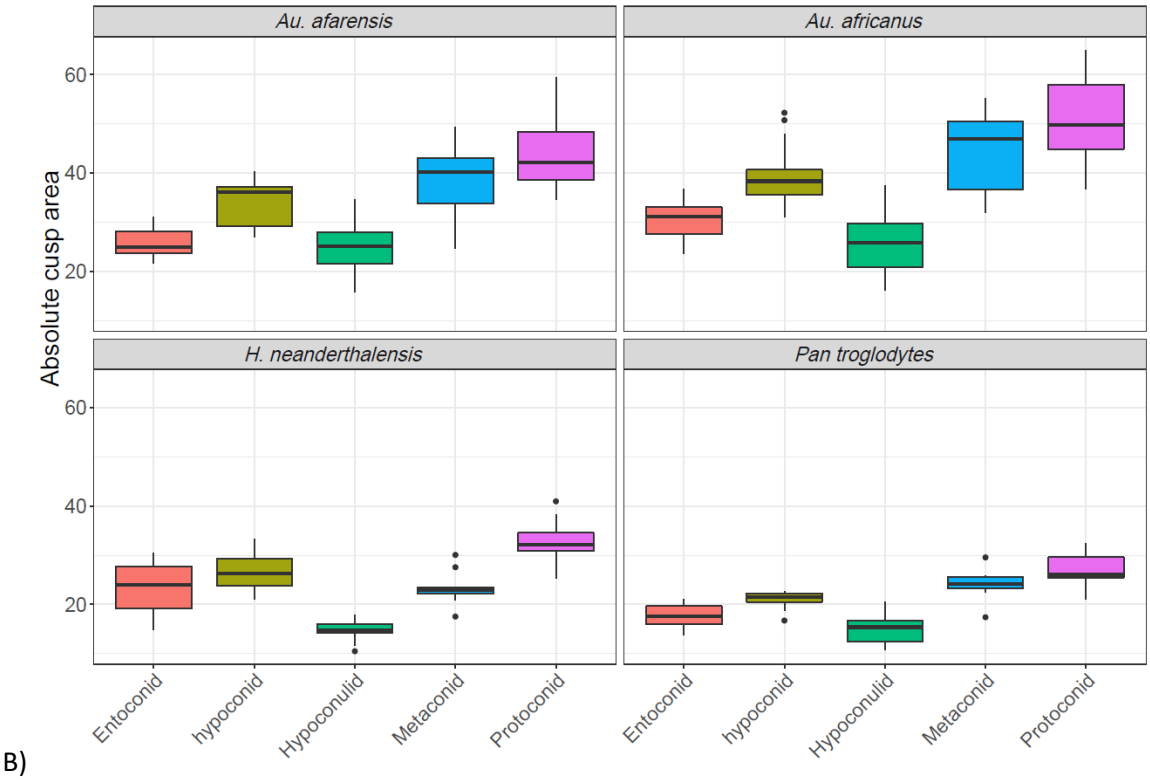

Figure 2.9. A) Boxplots of the A) relative cusp areas and B) absolute cusp areas of the second molar in each taxon in the sample.

2.2.3 Third molars

All datasets, apart from the first two PCs of GM shape space and relative cusp areas, are able differentiate between the taxa relatively well and all plots show a similar pattern of separating *P. troglodytes* and *H. neanderthalensis* from *Au. afarensis* and *Au. africanus* (Figure 2.10). Size is the main variable driving this distinction in these datasets. However, the same separation between the taxa can be observed in a less noticeable manner in the first two PCs of GM shape data, which account for 54.9% of the morphological variation. The TPS grids that depict the crown shape morphological variation across PC1 (Figure 3A. Appendix), suggest that *Australopithecus* M_3s are distinguished from *H. neanderthalensis* and *P. troglodytes* for their small entoconid, relatively parallel distobuccal and mesiobuccal fissures, large hypoconulid (or more likely the presence of multiple accessory cusps), and the subrectangular outline of the crown. The third PC, which explains 11.4% of the variation, further distinguishes between *H. neanderthalensis* and *P. troglodytes*. TPS grids that correspond to the morphological variation in this PC (Figure 4A. Appendix), distinguish *P. troglodytes* M_3s from *H. neanderthalensis* for their large protoconid, a more bucally positioned mesial longitudinal fissure, and their overall square shaped crown which tapers at the midpoint. The first two PCs (~77% of the morphological variation) of relative cusp area data show a similar grouping to GM shape, but with more significant overlap between the taxa. The third PC of relative cusp area data, which accounts for 11.4% of the variation, is also included since it slightly improves the separation between the groups. Overall, both GM datasets are able to distinguish between the four taxa based on the morphology of their M_3 relatively well. Furthermore, GM shape space data were able to convey more information about crown shape morphology than the other shape-based datasets.

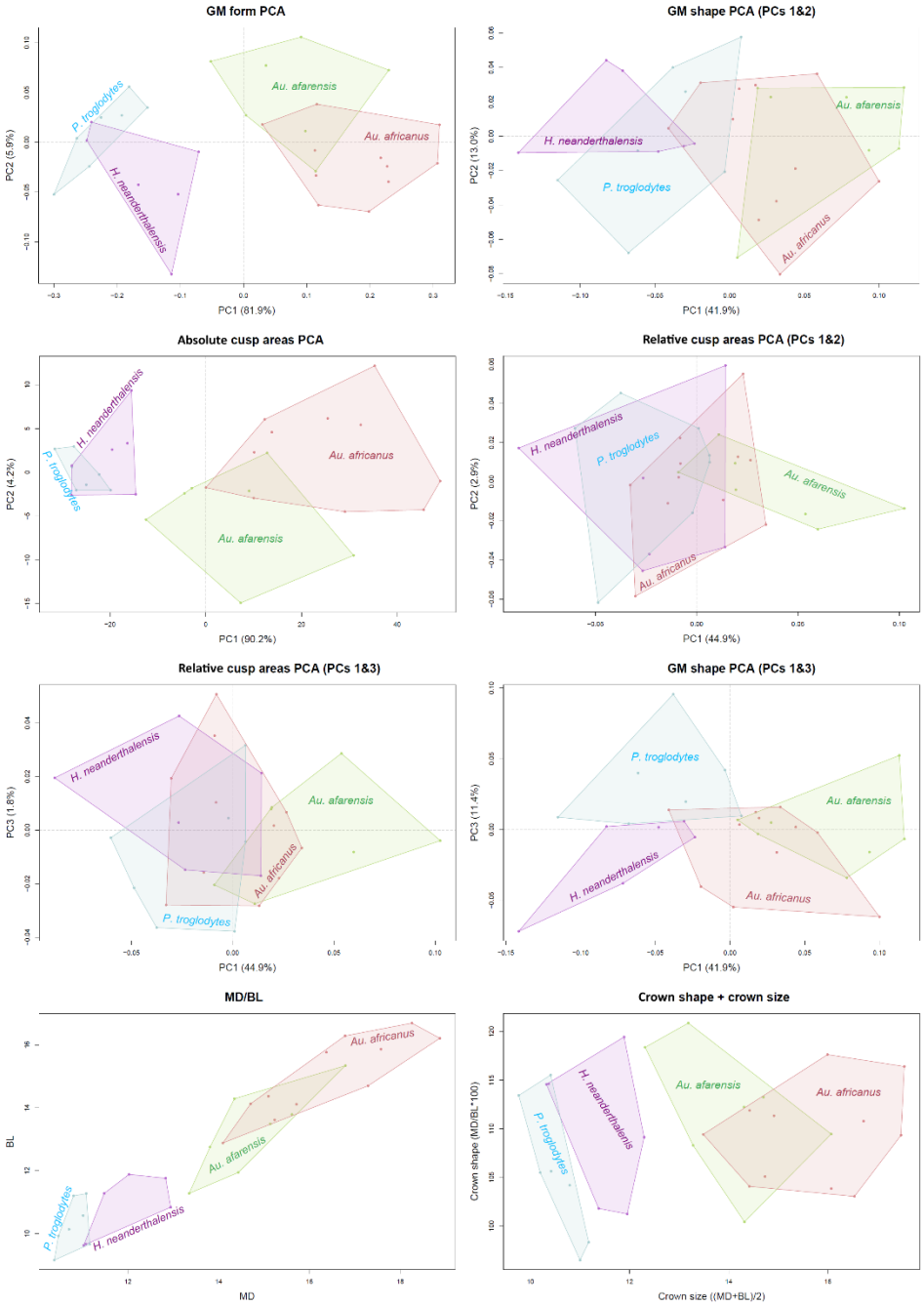

Figure 2.10. PCA and bivariate plots of the third lower molars of each taxon. Upper row: PCA plots visualizing the first two principal components of GM form (left) and shape (right) data. Second row from the top: PCA plots visualizing the first two principal components of absolute cusp area (left) and relative cusp area (right) data. Third row from the top: PCA plots visualizing the first and third principal components of relative cusp area (left) and GM shape (right) data. Bottom row: bivariate plots of the MD and BL data (left) and crown shape and crown size data (right).

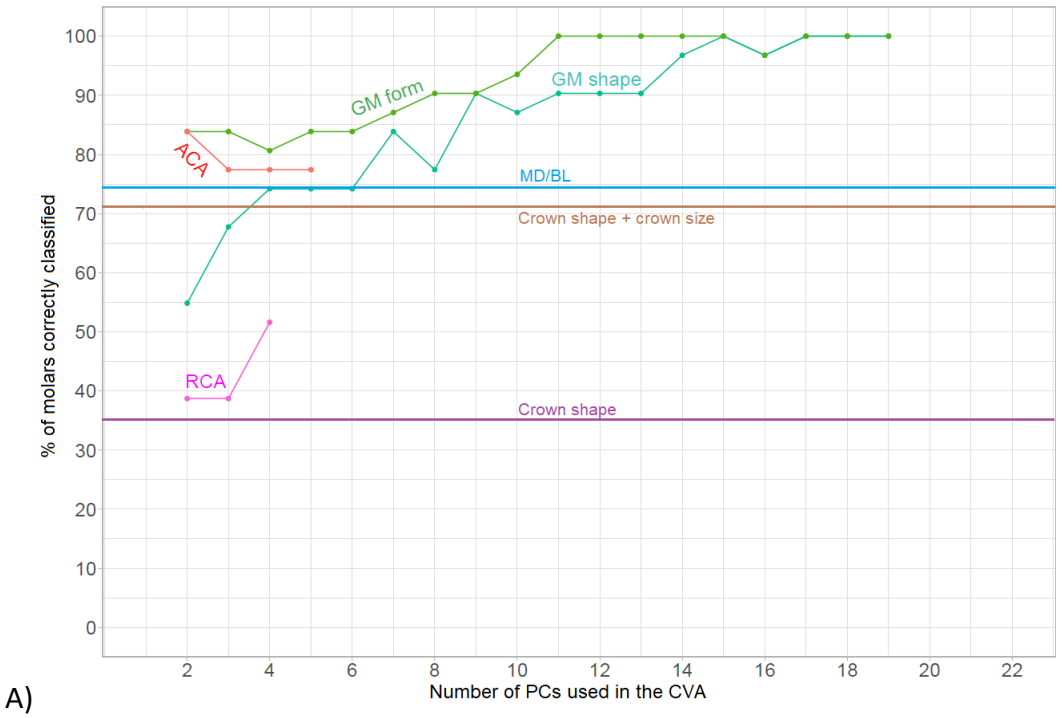

A)

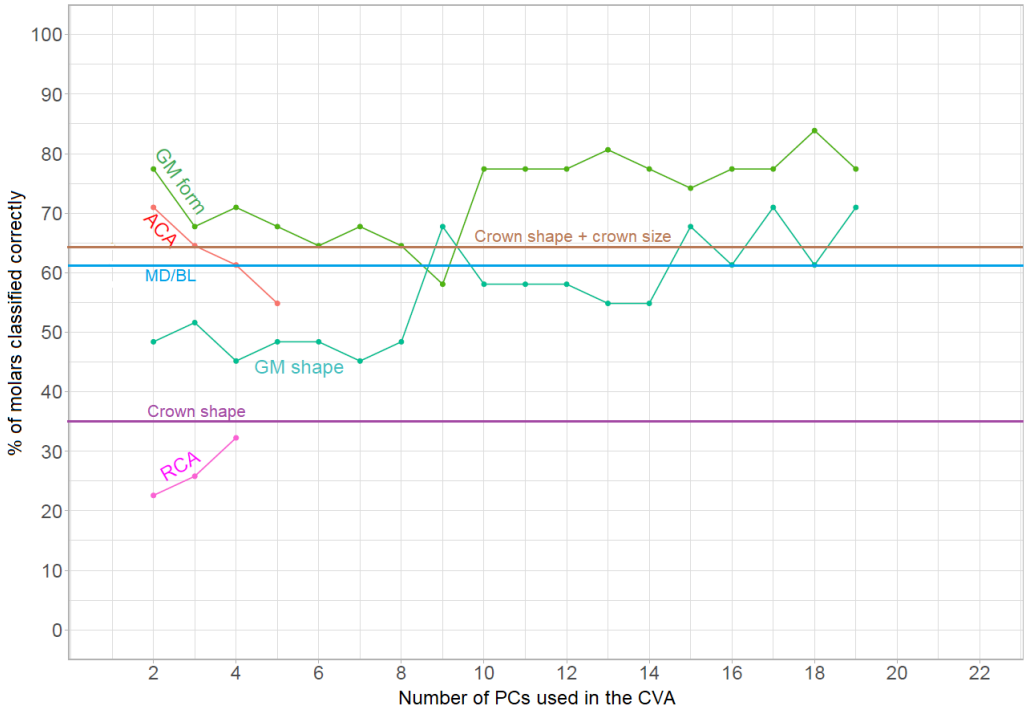

B)

Figure 2.11. A) Classification results without using cross-validation and B) with cross-validation of the lower third molar sample. ACA – absolute cusp areas; RCA – relative cusp areas.

CVA without cross-validation results are presented in Figure 2.11 (A). Absolute cusp area and GM form data display the highest correct classification rates among all datasets at ~84% with the first two PCs. However, at three PCs the data types depart, with GM form retaining a classification accuracy of > 80% in all subsequent CVAs and peaking at 100% with 11 PCs, whereas the classification accuracy of the absolute cusp area data dips to ~78% and maintained at the same level throughout the following CVAs. GM shape data correctly classified only 55% of the molars using the first two PCs. However, the classification accuracy steadily increases with the addition of each subsequent PC, and peaks at 100% with 15, and 17-19 PCs. Relative cusp area data showed consistently poor classification results, correctly classifying ~38% of the molars with the first 2-3 PCs, and ~52% with the first four. MD and BL data performed relatively well, classifying correctly 74% of the molars, and crown shape + crown size had a correct classification rate of ~71%. Crown shape performed the poorest of all datasets, with only 35% of molars having been assigned to their correct taxonomic group.

Compared to the other two molar type (M_1 and M_2) analyses, the classification results of CVAs with cross-validation of the M_3s showed the lowest accuracy rates for all datasets (Figure 2.11; B). GM form data have the highest correct classification rate for the first two PCs at 78%, but the accuracy steadily declines with the addition of each subsequent PC, bottoming at nine PCs, which correctly classified 58% of the molars. There is a sharp increase in accuracy at the first ten PCs to 78% and a maintenance of an accuracy rate of 75% and above in the following analyses. Absolute cusp area data exhibited the highest correct classification rate of 72% with the first two PCs. The accuracy then consistently declines and bottoms at 55% with the first five PCs. GM shape had a poor classification accuracy of ~45-52% for the first eight PCs, an increase

to ~68% with nine PCs, and then a decline. The highest classification accuracy rates (~72%) for the GM shape data are achieved with the first 17 and 19 PCs. MD and BL data correctly classified ~62% of the molars, and crown shape + crown had a classification accuracy of ~64%. Crown shape correctly classified 35% of the molars, and RCA data had the poorest classification results of all data types, with a lowest frequency of ~22% using the first two PCs and the highest at ~32% using the first four. Overall, the CVA without CV results are similar to those of the first and second molar analyses, with GM shape and form data having classified correctly most molars with different configuration of PCs. The CVA with cross-validation results of the third molars are poorer than those of the first and second molars, however the pattern is similar in that that GM form had the highest correct classification rates, although it did exhibit a somewhat erratic behavior in the frequency of correctly classified molars across the CVAs. GM shape did not perform as well as absolute cusp areas, and did better than MD and BL data only with a few configurations of PCs. *Australopithecus* M_3s tend to be quite variable which may increase the difficulty of finding morphological configurations that would allow for best separation between the hominins, and it is likely that most misclassifications occurred between *Au. africanus* and *Au. afarensis*.

The PERMANOVAs (Table 2.5) using GM form and absolute cusp area data found the highest number of significant differences. Surprisingly, both datasets did not find a significant difference between *P. troglodytes* and *H. neanderthalensis*, whereas crown shape + crown size and MD and BL data did (though the p-values become non-significant when Bonferroni corrected). This suggests that while size was able to differentiate between the two taxa, shape was not, as can be seen from the GM shape and RCA results. The mean shapes of the third

lower molars of *P. troglodytes* and *H. neanderthalensis* (Figure 2.12) show a substantial overlap between the shapes of the entoconid and hypoconulid, and there is a very slight overlap in the shape of the crowns as well. Relative cusp area data boxplots also exhibit an overlap between the cusp areas of the taxa (Figure 2.13; A), with a minor difference in the area of the protoconid, which can be observed in the GM mean shapes as well.

Table 5.
Results of pairwise permutational MANOVAs (1000 permutations), MANOVAs, and t-test for the lower third molars. Numbers in brackets are Bonferroni corrected p-values. Significant p-values are in bold.

	Relative cusp areas		
	Au. afarensis	*Au. africanus*	*H. neanderthalensis*
Au. africanus	0.061 (0.320)	-	-
H. neanderthalensis	**0.015** (0.110)	0.309 (1.000)	-
P. troglodytes	**0.011** (0.120)	0.424 (1.000)	0.682 (1.000)
	Absolute cusp areas		
	Au. afarensis	*Au. africanus*	*H. neanderthalensis*
Au. africanus	**0.017** (0.156)	-	-
H. neanderthalensis	**0.002** (**0.024**)	**0.001** (**0.006**)	-
P. troglodytes	**0.001** (**0.006**)	**0.001** (**0.006**)	0.105 (0.683)
	GM shape		
	Au. afarensis	*Au. africanus*	*H. neanderthalensis*
Au. africanus	0.107 (0.647)	**-**	**-**
H. neanderthalensis	**0.001 (0.030)**	**0. 001 (0.006)**	**-**
P. troglodytes	**0.003 (0.018)**	**0. 001 (0.006)**	0. 076 (0.402)
	GM form (log Centroid size)		
	Au. afarensis	*Au. africanus*	*H. neanderthalensis*
Au. africanus	**0.014** (0.108)	**-**	**-**
H. neanderthalensis	**0.001 (0.012)**	**0.001 (0.006)**	**-**
P. troglodytes	**0.001 (0.006)**	**0.001 (0.006)**	0.055 (0.252)
	MD/BL MANOVAs		
	Au. afarensis	*Au. africanus*	*H. neanderthalensis*
Au. africanus	0.061 (0.368)	-	-
H. neanderthalensis	**0.002 (0.014)**	**0.001 (0.006)**	-
P. troglodytes	**0.001 (0.006)**	**0.001 (0.006)**	**0.030** (0.181)
	Crown shape pairwise t-test (ANOVA p=0.059)		
	Au. afarensis	*Au. africanus*	*H. neanderthalensis*
Au. africanus	0.426 (1.000)	-	-
H. neanderthalensis	0.632 (1.000)	0.812 (1.000)	-
P. troglodytes	0.077 (0.460)	0.232 (1.000)	0.211 (1.000)
	Crown shape + crown size MANOVAs		
	Au. afarensis	*Au. africanus*	*H. neanderthalensis*
Au. africanus	0.059 (0.358)	-	-
H. neanderthalensis	**0.002 (0.013)**	**0.001 (0.006)**	-
P. troglodytes	**0.001 (0.006)**	**0.001 (0.006)**	**0.026** (0.161)

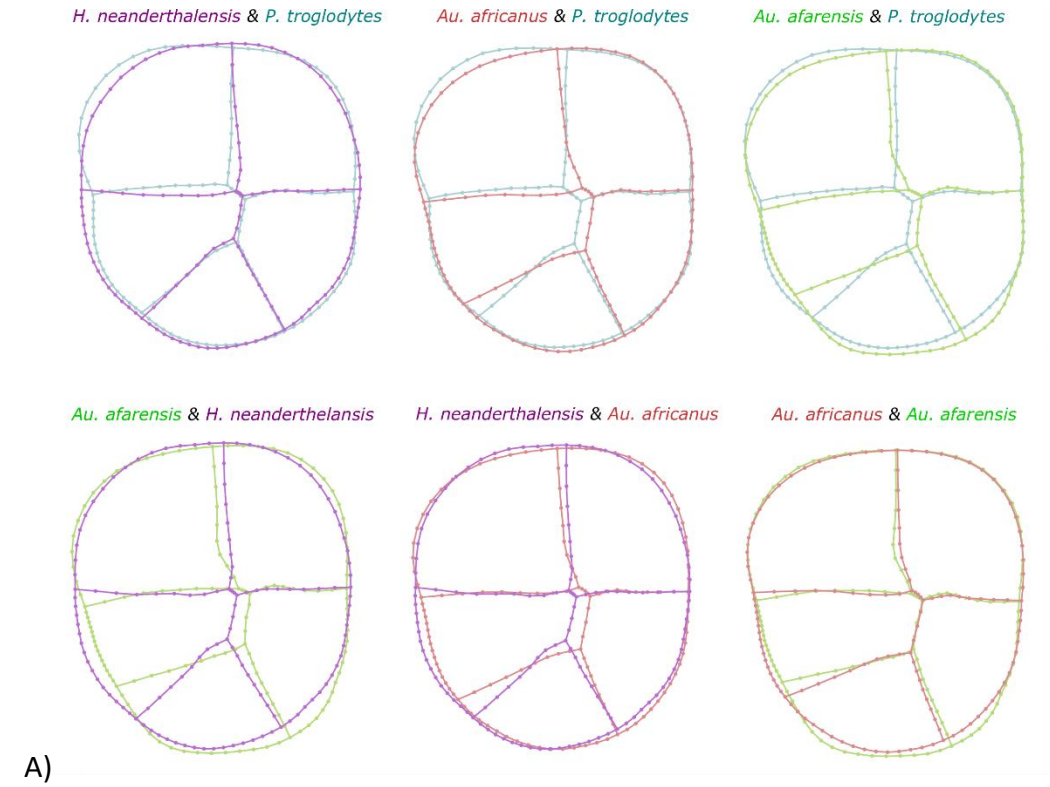

A)

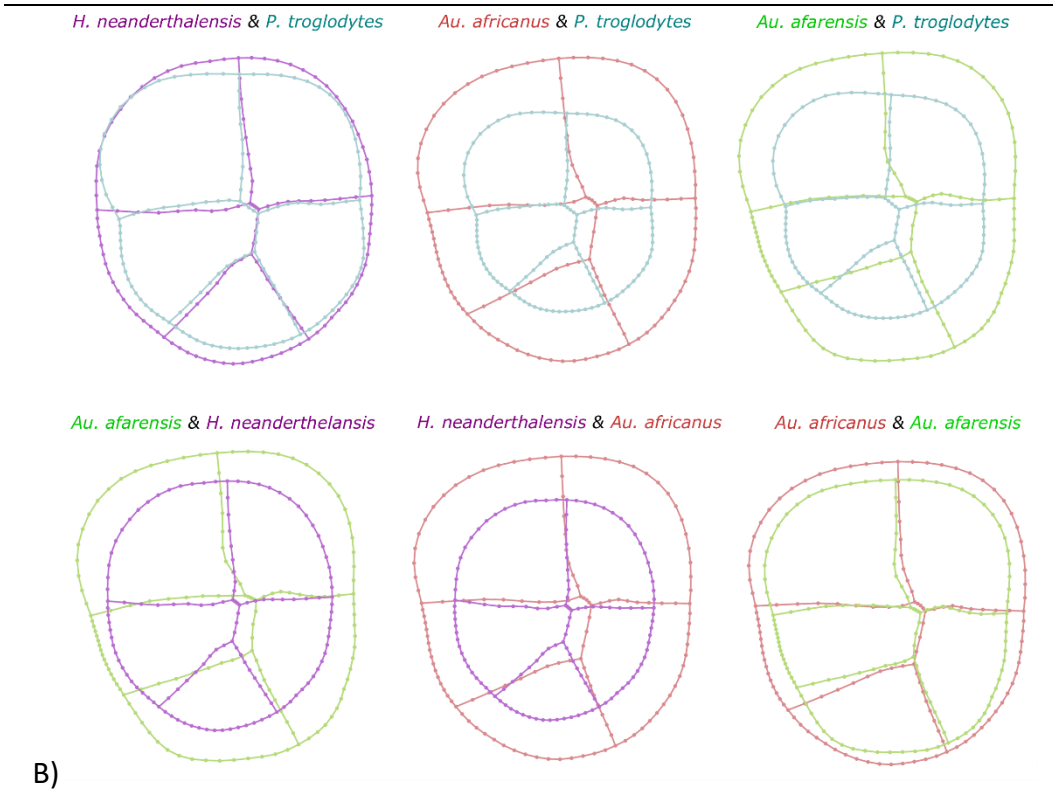

B)

Figure 2.12. A) mean shapes of the third lower molars of each taxon. B) mean shapes and size of the third lower molars of each taxon.

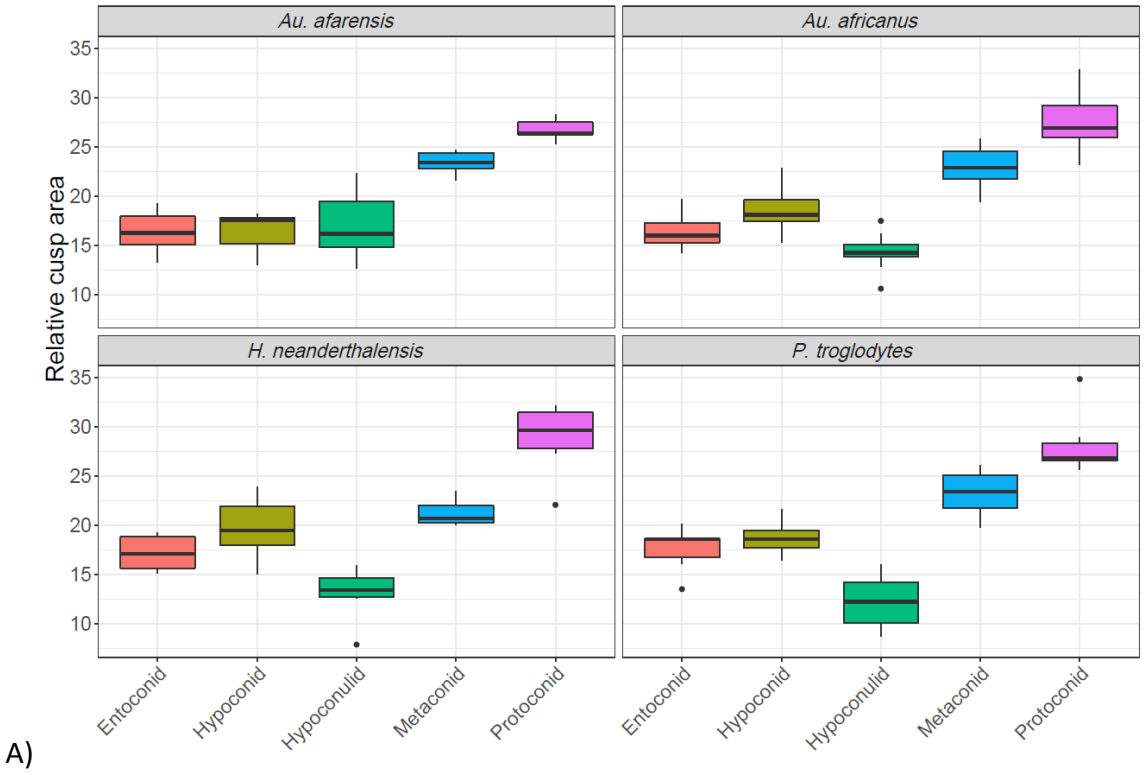

A)

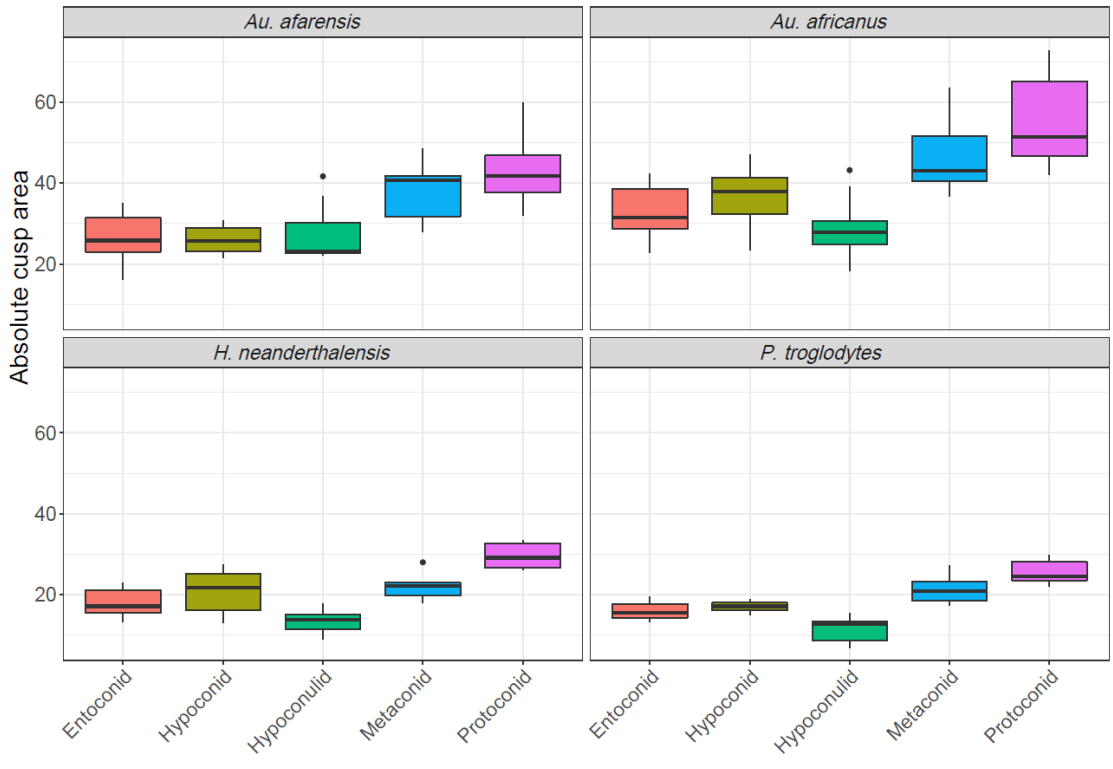

B)

Figure 2.13. A) Boxplots of the A) relative cusp areas and B) absolute cusp areas of the third molar of each taxon in the sample.

2.2.4 *Au. afarensis* molar types

Figure 2.14 presents graphical comparisons of the crown morphology between the mandibular molars of *Au. afarensis* using each dataset. GM and cusp area data show very similar scatter patterns, with relatively little overlap between the tooth types. In the GM shape and relative cusp areas PCAs, the M_1s and M_2s have negative PC1 values, whereas M_3s have positive values. TPS grids that correspond to the morphological variation in this PC (Figure 5, Appendix) show that M_3s are separated from the M_1s and M_2s for their subrectangular crown shape, small entoconid, and large hypoconulid, which appears expanded due to the presence of accessory cusps. GM shape also shows some separation between the M_1s and M_2s along PC2, which accounts for 15.2% of the variation. The shape variation along the negative scores of this PC is associated with a square shaped crown, a lingually positioned mesial longitudinal fissure, and reduced longitudinal fissure. Size does not separate well between the molar types, as can be seen from the first PC in the GM form PCA, which explains 55.3% of the variation, and the MD and BL bivariate plot. The variability in the size of the molars is most likely to be due to sexual dimorphism.

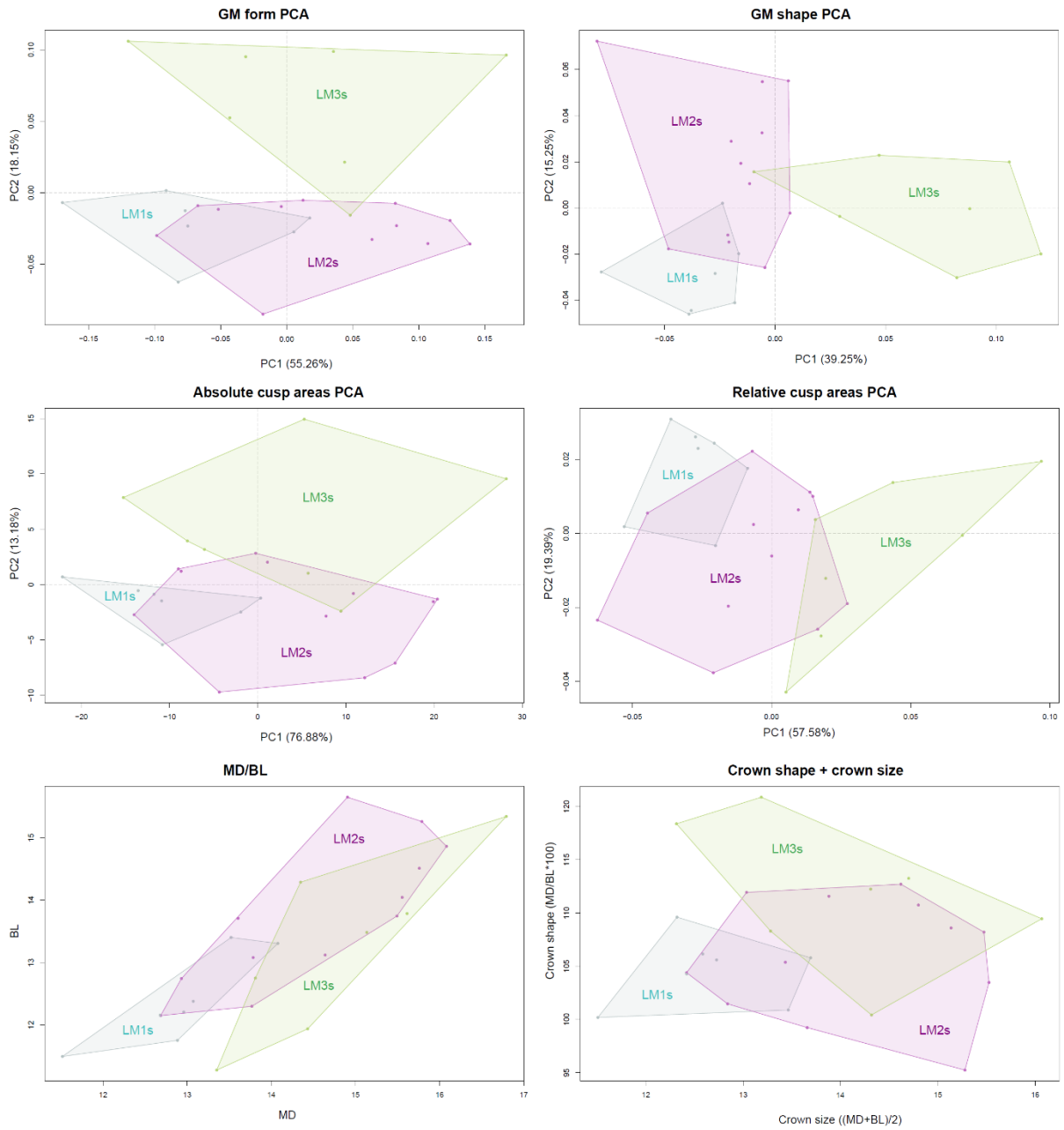

Figure 2.14. PCA and bivariate plots of the molar types of *Au. afarensis*. Upper row: PCA plots visualizing the first two principal components of GM form (left) and shape (right) data. Middle row: PCA plots visualizing the first two principal components of absolute cusp area (left) and relative cusp area (right) data. Bottom row: bivariate plots of the MD and BL data (left) and crown shape and crown size data (right).

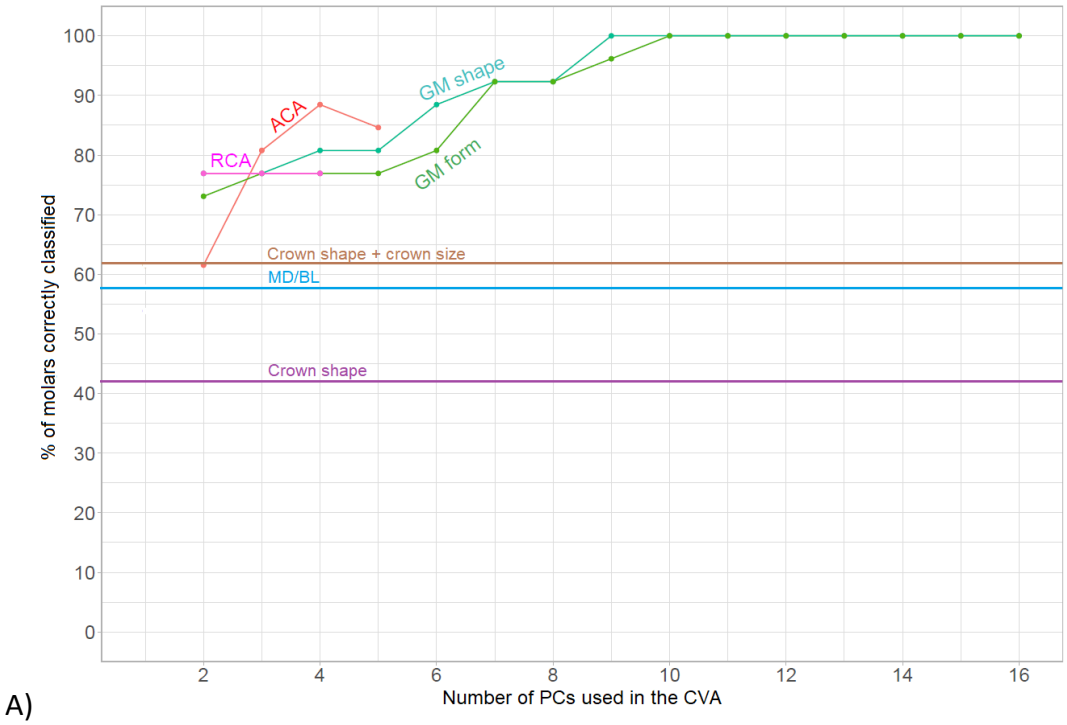

A)

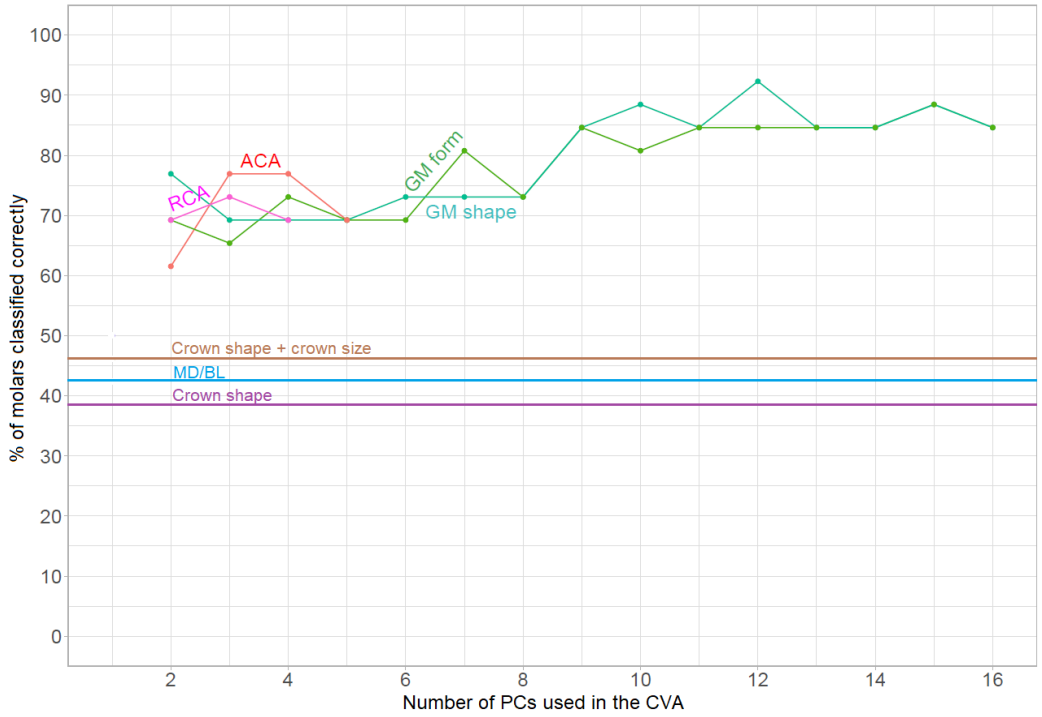

B)

Figure 2.15. A) Classification results without using cross-validation and B) with cross-validation for the mandibular molars of *Au. afarensis* sample. ACA – absolute cusp areas; RCA – relative cusp areas.

In the CVA without cross-validation (Figure 2.15; A), GM shape and form data correctly classified a similar number of molars using the first two PCs (~73%), and showed a steady increase in accuracy with each subsequent analysis. GM shape data had a peak at 100% with nine PCs, and GM form peaked with 10 PCs, correctly classifiying 100% of the molars. In contrast to the results of the CVAs for classifying the molars based on taxonomic affiliation, both relative and absolute cusp area data performed well at correctly classifying the molar types of *Au. afarensis*. Relative cusp area data maintained a correct classification rate of ~78% across all analyses, and absolute cusp area data correctly assigned ~81-89% of the molars to the their respective groups across the CVAs that used more than two PCs.

In the CVA with cross-validation (Figure 12.5; B), GM shape data had the highest correct classification rate (~78%) with the fewest variables (first two PCs). The percentage of correctly classified molars drops to ~68% and remains at a similar level until nine PCs, where it increases to 85%. The classification accuracy is then maintained across all CVAs, with a peak of ~92% at 12 PCs. GM form data shows a similar pattern to GM shape, with slightly lower classification results in the range of ~65%-68% for the first six PCs, and then a steady increase in accuracy with the addition of each subsequent PC. The highest percentage of correctly classified molars is 89% with 15 PCs. Relative cusp area data performed well across all three CVAs, having correctly classified ~68%-72% of the molars. Absolute cusp area data had a relatively poor classification accuracy with the first two PCs (62%), however it increased to ~77% with the first three and four PCs, and then dipped at five PCs (70%). The MD and BL data, crown shape + crowns and crown shape data were able to correctly classify only ~38-47% of the molars.

Pairwise PERMANOVA, MANOVA, and t-test results are presented in Table 2.6. In contrast to the results of the analyses for detecting differences between the molars of different taxa, crown shape rather than size, was the most important variable in differentiating between the mandibular molar types of *Au. afarensis*. This is reflected by the PERMANOVA results of relative cusp area and GM shape data, that found signficant differnces between all molars, even with Bonferroni adjustment. The differences in the crown shape and size between the molars are illustrated in Figure 2.16, and the differences in relative and absolute cusp areas are depicted in Figure 2.17.

Table 2.6.
Results of pairwise permutational MANOVAs (1000 permutations), MANOVAs, and t-test for the mandibular molars of *Au. afarensis*. Numbers in brackets are Bonferroni corrected p-values. Significant p-values are in bold.

	Relative cusp areas		**Absolute cusp areas**	
	M_1	M_2	M_1	M_2
M_2	**0.011 (0.036)**	-	**0.011 (0.048)**	-
M_3	**0.002 (0.003)**	**0.004 (0.003)**	**0.020 (0.036)**	0.210 (0.582)
	GM shape		**GM form (og centroid size)**	
	M_1	M_2	M_1	M_2
M_2	**0.003 (0.003)**	-	**0.013** (0.051)	-
M_3	**0.002 (0.003)**	**0.001 (0.003)**	**0.005 (0.021)**	0.028 (0.120)
	MD/BL MANOVAs		**Pairwise t-tests crown shape (ANOVA p=0.0433)**	
	M_1	M_2	M_1	M_2
M_2	**0.021** (0.064)	-	0.583 (1.000)	-
M_3	**0.006 (0.020)**	0.213 (0.641)	**0.021** (0.062)	**0.035** (0.105)

	Crown shape + crown size MANOVAs	
	M_1	M_2
M_2	**0.021** (0.063)	-
M_3	**0.005 (0.016)**	0.177 (0.532)

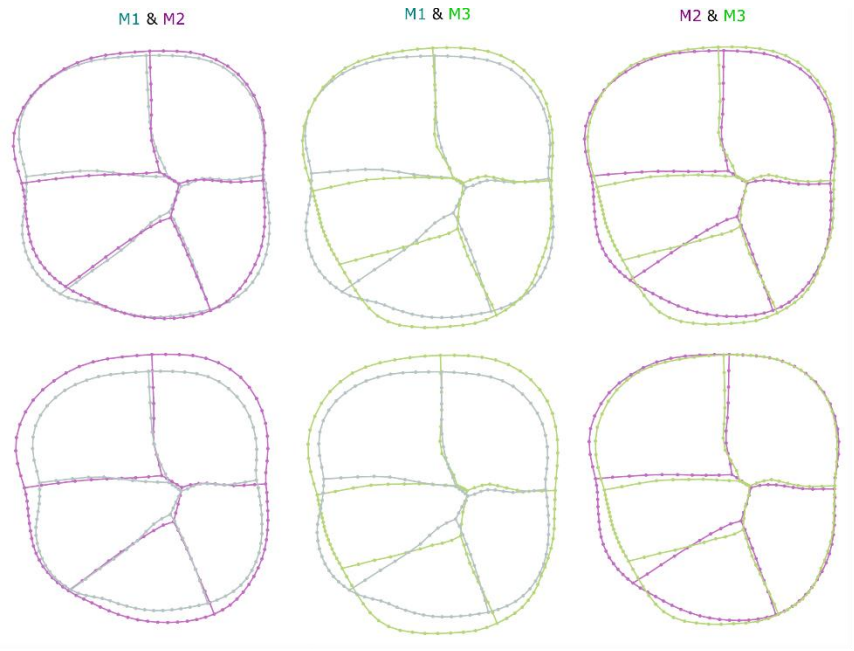

Figure 2.16. A) mean shapes of the mandibular molars of *Au. afarensis*. B) mean shapes and size of the mandibular molars of *Au. afarensis*.

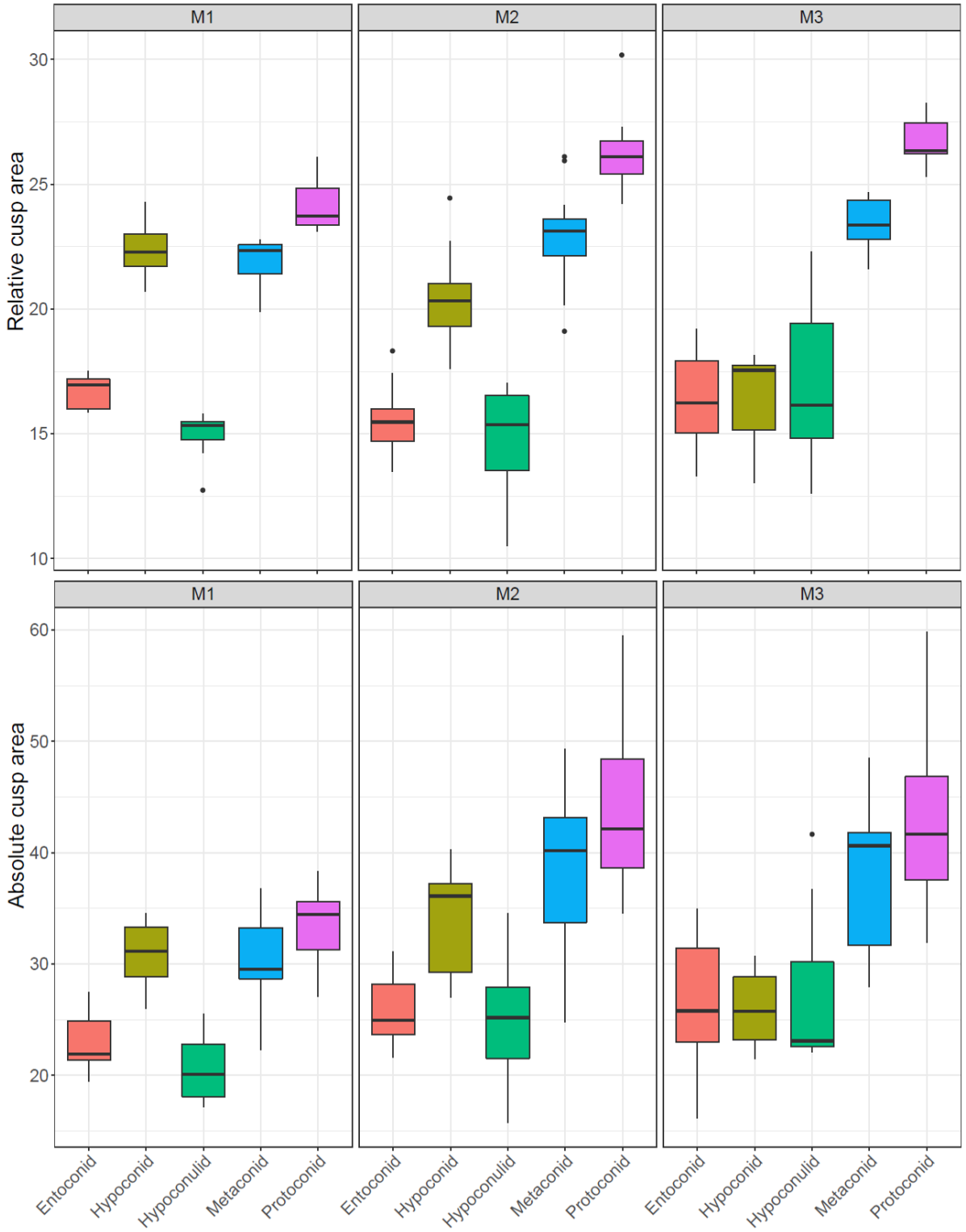

Figure 2.17. A) Boxplots of the relative cusp areas (top) and absolute cusp areas (bottom) for each mandibular molar of *Au. afarensis*.

2.2.5 Summary

A summary of the classification results for each data type is presented in Table 2.7. Overall, both GM form and shape data reached a classification accuracy of 100% in all the CVAs without cross-validation. Because the number of variables (PCs) eventually exceeds the size of the smallest group in the GM CVAs, some of the high classification results are most likely due to the overfitting of data (Kovarovich et al., 2011; Mitteroecker and Bookstein, 2011). However, because the GM data also displayed relatively high correct classification rates in the CVAs with cross-validation, the degree of overfitting may be not be substantial. Generally, the number of PCs to be used in a CVA, or any other multivariate analysis, can be determined by finding a balance between generality, i.e. how reliable the model is at classifying specimens that are not used to form the canonical variates, which can be tested by running a CVA with cross-validation; and precision, which is the rate of correct assignments of specimens used to form the CVA axes (Sheets et al., 2006). Thus, among all data types that capture the shape of the crown used in this study, 2D GM had the highest precision and generality.

The classification accuracy of absolute cusp area data was relatively high as well across all analyses. The performance of the absolute cusp area data in the CVAs with cross-validation was consistent with an overall range of 55-77%, and exhibited the highest correct classification rates in distinguishing between the molar types of *Au. afarensis*. Relative cusp area data consistently displayed low classification rates of <52% in the CVAs with and without cross-validation for classifying the molars of the four taxa. However, the classification accuracy of the data in the *Au. afarensis* molar types CVAs was within the range of the GM data.

The performance of MD and BL, and crown shape + crown size data in the CVAs was similar, which is to be expected since the crown shape + crown size indices are derived from the MD and BL data. Generally, the classification rates of the two data types in the CVAs without CV for the taxonomic classification of the molars was good (67-87%). The smallest number of correctly classified molars occurred in the *Au. afarensis* molar types CVAs. The MD and BL data and the indices derived from it (crown shape and crown size) capture the least amount of crown shape morphology, and account mainly for tooth size. Because the molar types of *Au. afarensis* are highly variable in their size, MD and BL data lacked a sufficient amount of information about crown shape to be able to distinguish between the molars. This is exemplified by the high correct classification rates of the molar types using GM shape, and to some degree, relative cusp area data. The relatively good performance of the MD and BL data in the other CVAs is probably due to the composition of the sample – the molars of the taxa used are all markedly different in size from each other, which allows molar size alone to be a good predictor of group membership. In this respect, the PERMANOVA, MANOVA, and t-test results mirror to some degree the CVA results. MD and BL data found as many (sometimes more) significant differences between the molars of the taxa as GM and ACA data, but had greater difficulty finding significant differences between the molar types of *Au. afarensis*.

Overall, among the data types that capture only the shape of the crown (GM shape space, relative cusp areas, and crown shape), GM shape displayed the highest correct classification rates and found the most significant results in the PERMANOVAs. Furthermore, mean shapes

using Procrustes coordinates were also able to convey a higher degree of morphological detail than relative cusp areas or crown shape data. The high classification rates using GM shape and form data stem from the large number of morphologically meaningful variables available for generating canonical variates that can discriminate between groups on a finer level than cusp area or MD and BL data. This capacity is translated to some degree to the ability of PERMANOVA to find more significant differences between molar crown shape and tooth type of different taxa using GM data compared to other traditional methods for capturing tooth crown morphology.

Table 2.7
Summary of the classification results

	Classification accuracy in a CVA without CV				Classification accuracy in a CVA with CV			
Data type	**M_1**	**M_2**	**M_3**	**Molar types**	**M_1**	**M_2**	**M_3**	**Molar types**
GM shape	62-100%	54-100%	55-100%	73-100%	48-90%	46-87%	45-71%	69-93%
GM form	90-100%	83-100%	81-100%	73-100%	77-90%	78-94%	58-84%	65-89%
Relative cusp areas	42-52%	41-56%	38-52%	78%	32-35%	33-39%	23-32%	69-73%
Absolute cusp areas	78-84%	78-80%	78-84%	61-89%	55-68%	65-74%	55-71%	62-77%
MD/BL	87%	70%	75%	57%	80%	57%	61%	43%
Crown shape + crown size	84%	67%	71%	62%	77%	55%	64%	46%
Crown shape	45%	32%	35%	42%	42%	32%	35%	38%

CVA - canonical variate analysis; CV – cross validation.

Table 2.8
Summary of the pairwise PERMANOVAs, MANOVAs, and t-tests results

	Percentage of significant differences found			
Data type	**M_1**	**M_2**	**M_3**	**Molar types**
GM shape	100% (83.3%)	83.3% (83.3%)	66.7% (66.7%)	100% (100%)
GM form	100% (100%)	100% (83.3%)	83.3% (66.7%)	100% (33.3%)
Relative cusp areas	33.3% (0%)	50% (50%)	33.3% (0%)	100% (100%)
Absolute cusp areas	100% (83.3%)	100% (83.3%)	83.3% (66.7%)	66.6% (66.6%)
MD/BL	100% (83.3%)	100% (66.7%)	83.3% (66.7%)	66.6% (33.3%)
Crown shape + crown size	100% (83.3%)	100% (83.3%)	83.3% (66.7%)	66.6% (33.3%)
Crown shape	33.3% (33.3%)	33.3% (16.7%)	16.7% (0%)	66.6% (0%)

CHAPTER 3: COMPARATIVE ANALYSIS OF THE LOMEKWI MANDIBULAR MOLARS

3.1 Materials and methods

3.1.1 Materials

The Lomekwi sample has a temporal and spatial overlap with *Au. afarensis*, and some of the specimens (e.g. KNM-WT 8556 and KNM-WT 16006) have been previously published as either *Au. afarensis*, or a regional variant of the taxon (Brown, Brown and Walker, 2001). Others have attributed the isolated teeth found in Lomekwi to *Kenyanthropus platyops* (Wood and Leakey, 2011), whose type specimen KNM-WT 40000 was found nearby (Leakey et al., 2001). The size of the teeth and their spatial and temporal distribution suggests morphological affinities with *Australopithecus*. Thus, the comparative sample consists of the M_1s, M_2s, and M_3s of *Au. afarensis*, *Au. africanus*, and *Au. anamensis*. Specimens of *Au. deyiremada* and *Au. bahreghazali* were not included in the analysis because the sample sizes for various molar positions are very small and we do not have access to either CT data or photos of sufficient quality. While *Au. africanus* does not have temporal and spatial overlap with Lomekwi, the taxon was included in the sample since it is generally considered to be a sister taxon of *Au. afarensis* (Strait and Grine, 2004, or other relevant cladistics analysis), and there is a relatively larger sample of molars of known tooth position. The *Au. afarensis* and *Au. africanus* samples (Table 3.1) consist of the same specimens from Chapter 2. The *Au. anamensis* sample is relatively small and all teeth are confidently assigned to particular molar positions. Eleven Lomekwi lower molars were used in the analysis, of which two are of known position (KNM-WT 8556 and KNM-WT 16006) because they are located in mandibles, and two are isolated but associated (KNM-WT 38359a and KNM-WT 38359b) and considered as a lower right M_1 and M_2 respectively, due to their close proximity to each

other during their discovery and the morphological similarities between them (Leakey et al., 2001).

Table 3.1
Composition of the comparative sample for the Lomekwi analysis and the Lomekwi sample*

Taxon	**M_1**	**M_2**	**M_3**	**Total**
Australopithecus afarensis	7	12	7	26
Australopithecus africanus	10	14	11	35
Australopithecus anamensis	5	3	3	11
Total	22	29	21	72
Lomekwi				
KNM-WT 8556	X			
KNM-WT 16006			X	
KNM-WT 38333		Unknown		
KNM-WT 38334		Unknown		
KNM-WT 38339		Unknown		
KNM-WT 38342		Unknown		
KNM-WT 38347		Unknown		
KNM-WT 38349		Unknown		
KNM-WT 38359a	X			
KNM-WT 38359b		X		
KNM-WT 66291		Unknown		

*The sample is detailed in full in Table 1 in the Appendix.

3.1.2 The Lomekwi sample

The following section provides a short description of the Lomekwi molars in the sample. When micro-CT scans of the teeth were available, the molars were landmarked and rotated according to the protocol described in Chapter 2. When micro-CT scans of the molars were not available, photos of the molars taken by Fred Spoor were used.

KNM-WT 8556

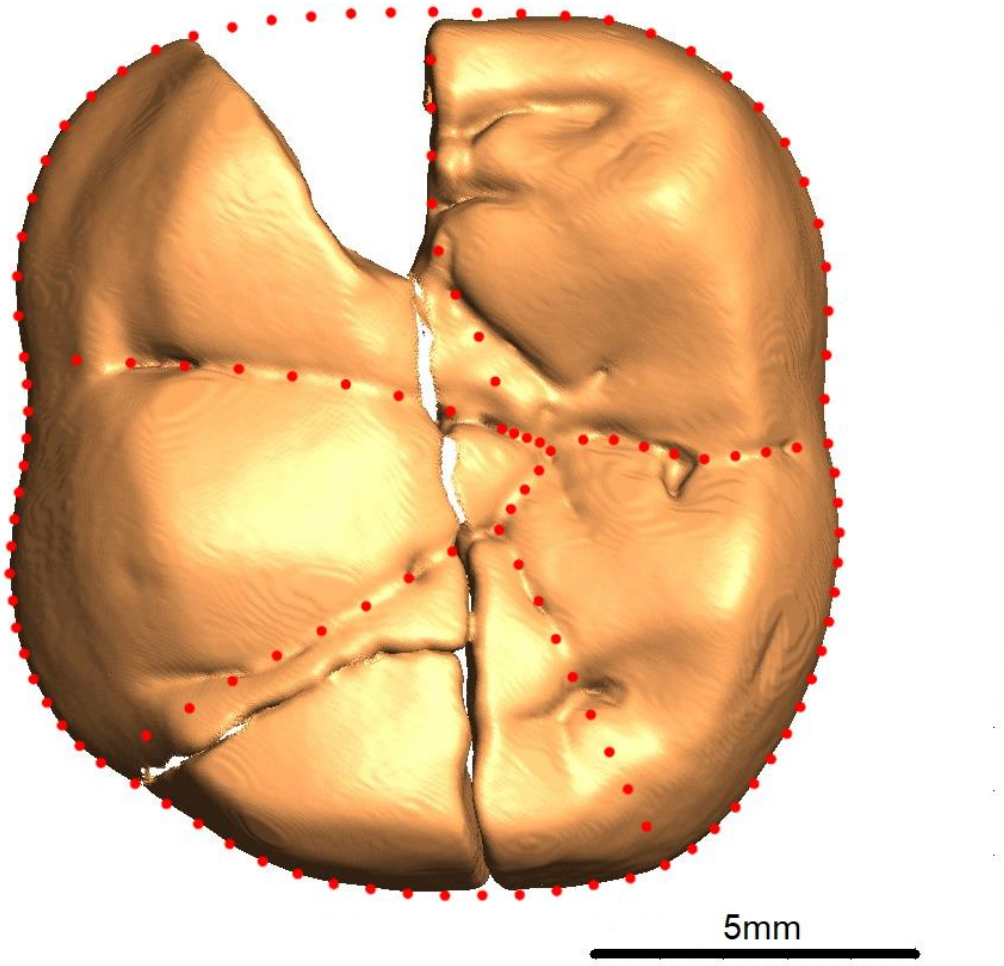

Figure 3.1. The landmarked RM_1 of KNM-WT 8556 (mirrored). The mesial longitudinal fissure is landmarked at roughly the midpoint between the mesiodistal crack and the groove at the base of the metaconid due to the uncertainty in the position of fissure.

Figure 3.1 shows KNM-WT 8556, a first right lower molar that sits in a mandible which has the RP_4 and RP_3 preserved. A fragment of an RM_2, an almost complete crown of an RM_3, and a complete LP_3 are associated with the mandible. There is a mesiodistal crack that runs through the crown, which is associated with a missing triangular piece from the protoconid. An additional crack runs distobuccally through the hypoconulid. There is an oblique slit at the base of the metaconid, which probably corresponds to the distal portion of the mesial longitudinal fissure. The hypoconulid is relatively large compared to the entoconid, and

there is a small protostylid that emanates from the base of the mesiobuccal fissure. The crown shape is square, with waisting at its midpoint.

KNM-WT 16006

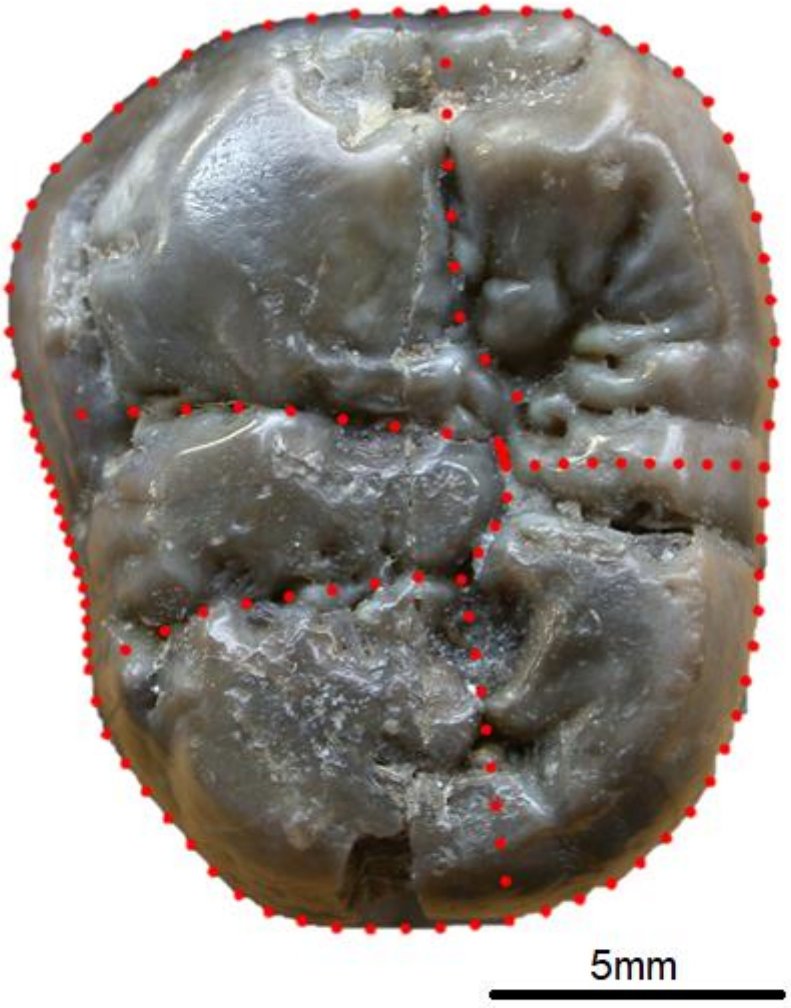

Figure 3.2. The landmarked LM_3 KNM-WT 16006.

KNM-WT 16006 (Figure 3.2) is a LM_3 that sits in a mandibular fragment, which has only portion of the distal crown of the M_2 preserved. The molar exhibits light wear on the buccal side, and there is a small piece missing from the distal border of the crown. The crown has a subrectangular shape and displays tapering that begins at the base of the mesial cusps,

which is common in *Australopithecus* M_3s. There is a well-defined C7 that is bordered by a small tubercle distal to the metaconid, and there is evidence for the presence of a small C6 that sits near the centre of the distal border of the crown. The occlusal basin of the metaconid exhibits numerous secondary fissures, and vertical grooves are present on the buccal faces of the protoconid, hypoconid, and hypoconulid. A marked protostylid extends from near the base of the mesiobuccal fissure and terminates opposite the mesial marginal ridge. The mesial fovea is shallow, and there is a tubercle situated at the distolingual border of the protoconid, which results in the lingual deflection of the mesial longitudinal fissure. The fissure pattern is Y-5.

KNM-WT 38333

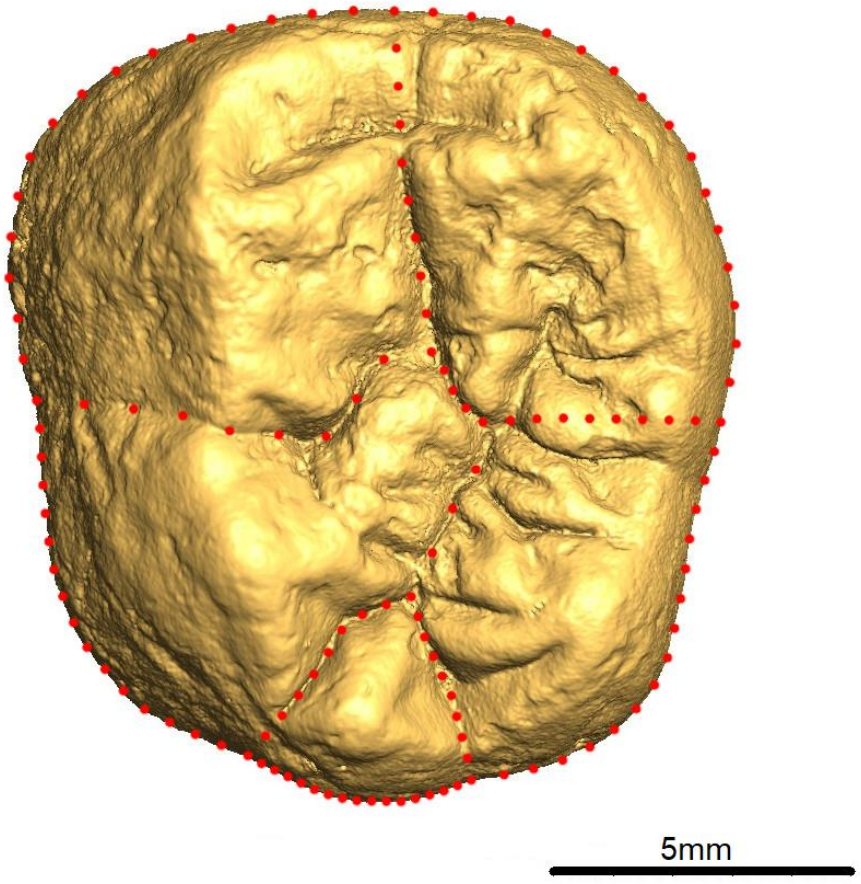

Figure 3.3. The left lower molar KNM-WT 38333. Note the small hypoconulid and the upward deflection of the mesiobuccal fissure.

KNM-WT 38333 (Figure 3.3) is an isolated unassociated unworn left lower molar, that is considered to be either an M_1 or an M_2 based largely on size (Wood and Leakey, 2011). The crown shape is ovoid and tapers distally from the base of the mesial cusps. The mesial fovea is a long and asymmetrical slit, with the buccal groove being slightly longer than the lingual. There is a C7 that is delimited by two small lingual fissures, but no C6. The hypoconid is irregular in shape due to a mesial expansion of the cusp towards the centre of the crown. The hypoconulid is distinct and very small, and the protoconid is the largest cusp. The enamel surface is highly crenulated.

KNM-WT 38334

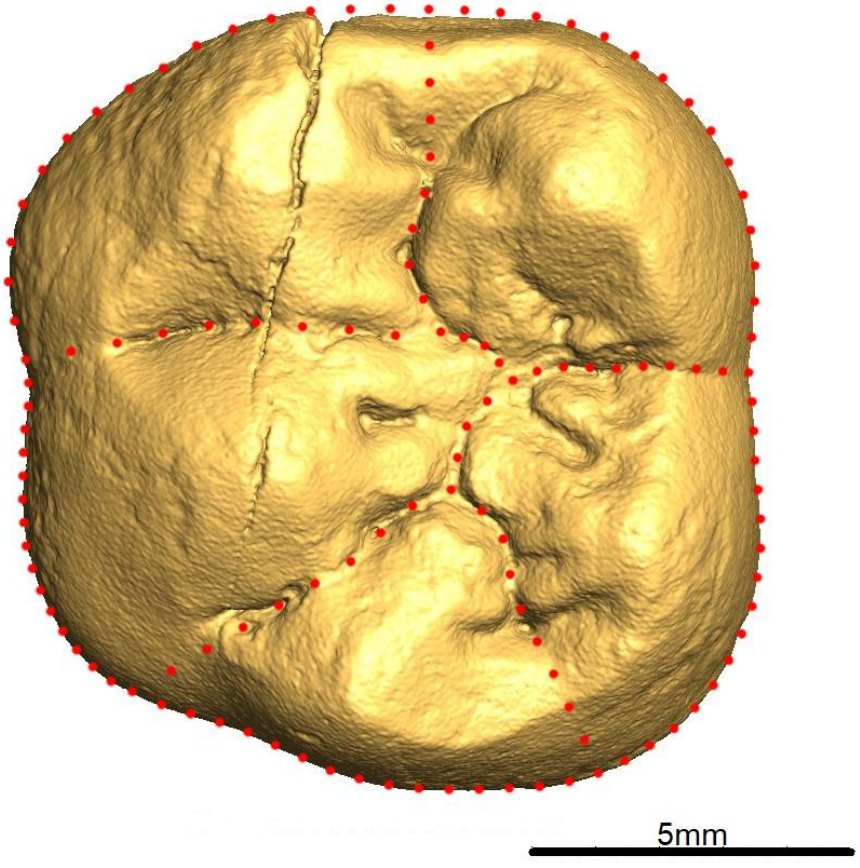

Figure 3.4. The left lower molar KNM-WT 38334.

Figure 3.4 shows KNM-WT 38334, an isolated, well preserved and lightly worn left lower molar that is either an M_1 or an M_2 (Wood and Leakey, 2011). The protoconid has been most affected by wear, with the tip of the cusp eroded away. The distal and mesial foveas are pit-like, with the mesial being slightly larger. Secondary fissures in the occlusal basin emanate from all cusps, and the fissure pattern is Y-5. There are no C6, C7, or a protostylid. A mesiodistal crack runs through the buccal portion of the crown and terminates near the tip of the hypoconid.

KNM-WT 38339

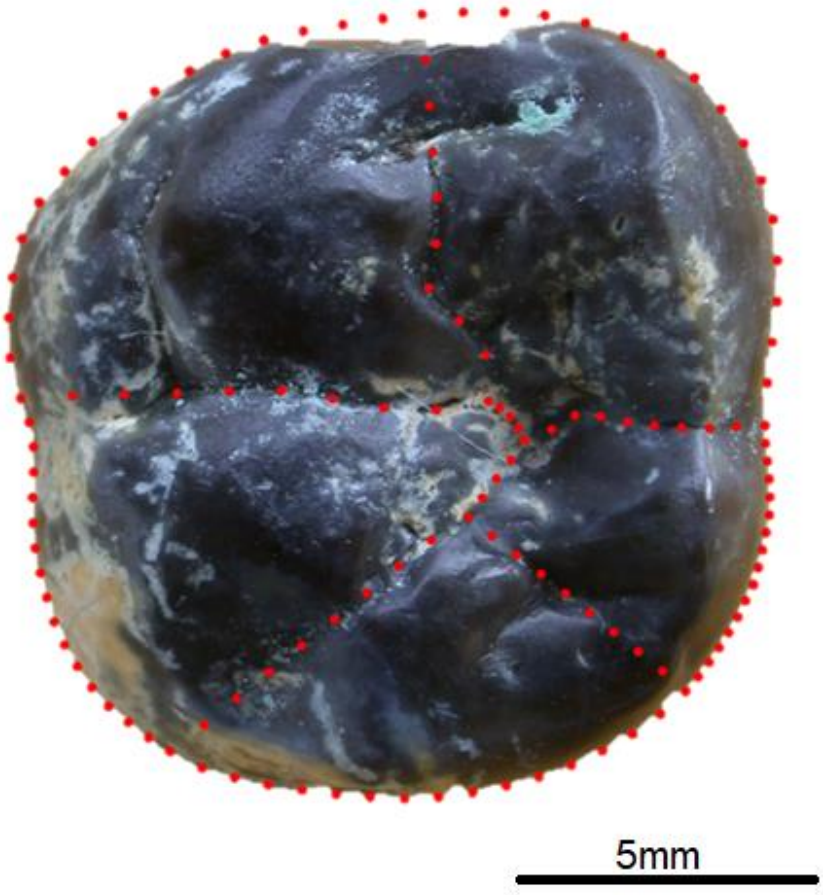

Figure 3.5. The landmarked isolated lower left molar KNM-WT 38339. Note the small entoconid and the large protostylid.

KNM-WT 38339 (Figure 3.5) is an isolated, moderately worn left M_2 or M_1 (Wood and Leakey, 2011). The crown is square shaped, with the buccolingual dimension being relatively

large mesially. A large protostylid runs from the base of the mesiobuccal fissure and terminates opposite the mesial marginal ridge. The entoconid is relatively small, and the distolingual border of the protoconid extends lingually towards the occlusal basin, which leads to the lingual deflection of the mesial longitudinal fissure. The mesial fovea is slit-like and asymmetrical, with the lingual side being slightly longer than the buccal. The fissure pattern is Y-5.

KNM-WT 38342

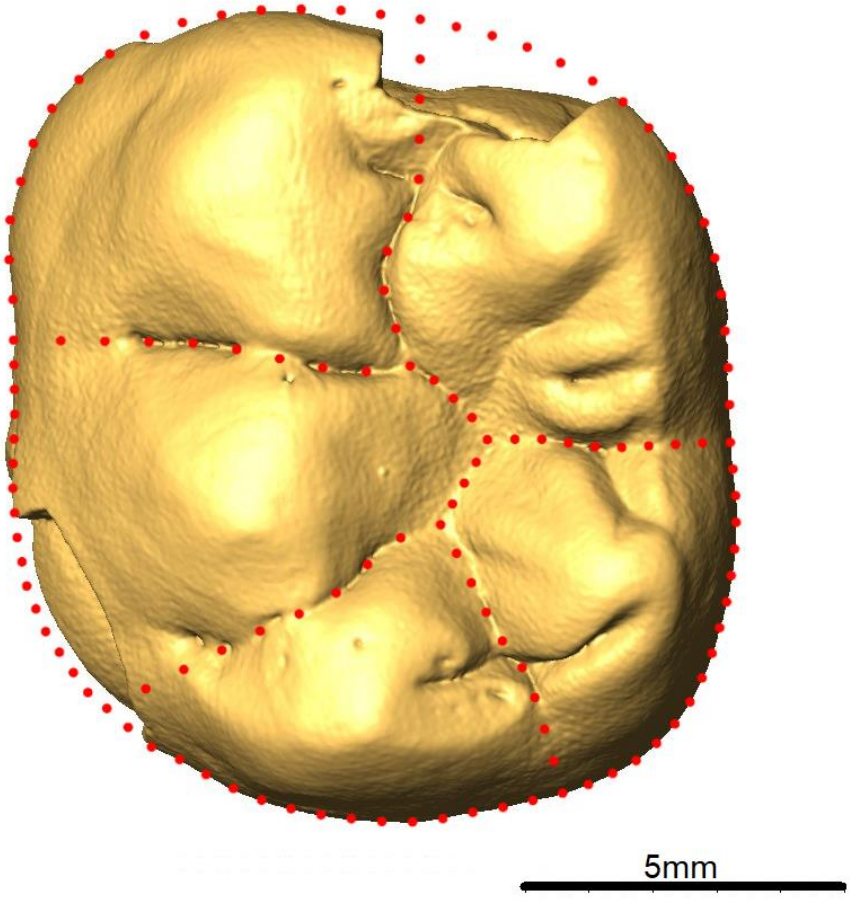

Figure 3.6. The landmarked isolated lower left molar KNM-WT 38342.

KNM-WT 38342 (Figure 3.6) exhibits light wear with an inferred tooth position of an M_1 or an M_2 based on crown size (Wood and Leakey, 2011). The crown has an oval occlusal outline, and enamel has been fractured off the mesial and distobuccal faces of the crown.

The metaconid is positioned slightly distally compared to the protoconid, giving the mesiolingual face of the crown a compressed shape. The mesial and distal foveas are slit-like, with the distal being slightly longer. There is no C6 or a protostylid. Two tubercles are present on the ridge of the metaconid that are reminiscent of a C7. There are no secondary fissures, and the fissure pattern is Y-5.

KNM-WT 38347

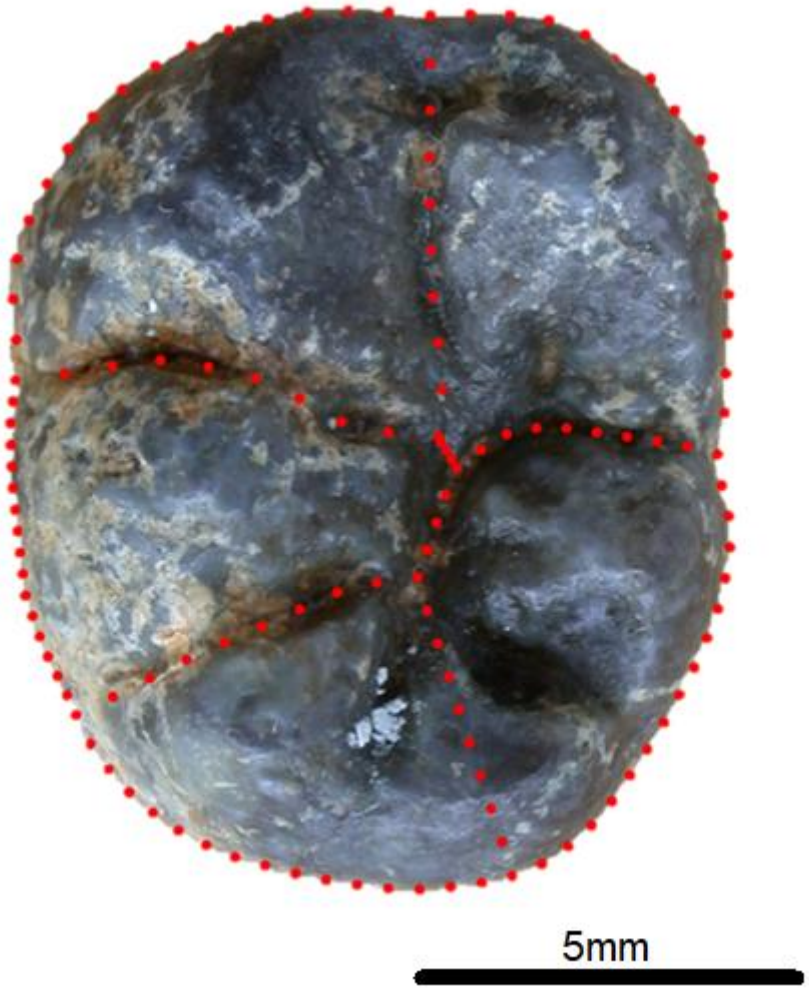

Figure 3.7. The landmarked isolated lower left molar KNM-WT 38347.

KNM-WT 38347 (Figure 3.7) is an isolated mandibular left molar that was inferred as being a deciduous molar due to its small size (Wood and Leakey, 2011). However, enamel thickness

and the height of the dentine horns are not consistent with those of a deciduous molar (Matthew Skinner, personal communication). Based on crown shape alone, in this study it is considered as a permanent M_2 or an M_3. The crown has a subrectangular shape, and the enamel surface is pitted as a result of weathering. There is no C7 or protostylid, but a distinct C6 that is as large as the hypoconulid is present in the distolingual half of the crown. The mesial fovea is deep and extends towards the metaconid. The fissure pattern is Y-5.

KNM-WT 38349

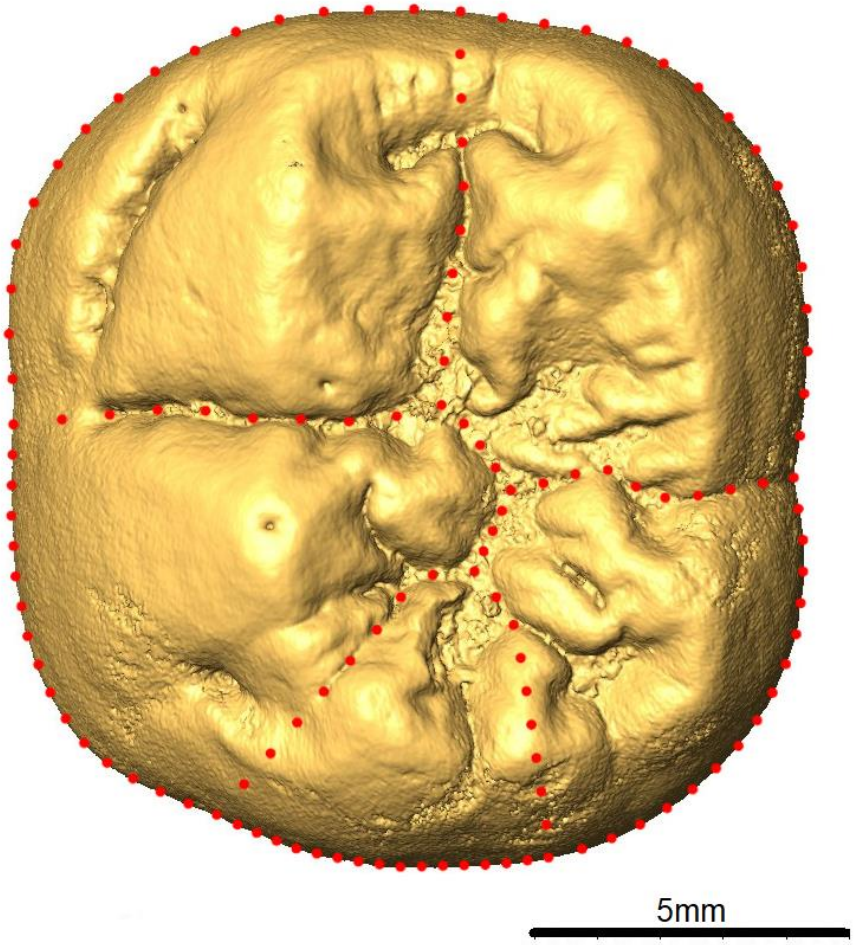

Figure 3.8. The landmarked isolated lower left molar KNM-WT 38349. Note the small hypoconulid, the relatively large C6, and the protostylid.

Figure 3.8 shows KNM-WT38349, an isolated, unworn, right mandibular molar that is listed as an ambiguous M_2 by Wood and Leakey (2011). The crown has an oval square outline,

with a mesiolingual face that slightly slopes distally. There are numerous secondary fissures emanating from all cusps into the occlusal basin, and the fissure pattern is Y-5. There is no C7, but a relatively large C6 is present on the lingual half of the distal crown. The hypoconulid and entoconid are relatively small. There is a deep, symmetrical mesial fovea, and a protostylid runs from opposite the mesial marginal ridge and terminates before the mesiobuccal fissure.

KNM-WT 38359a

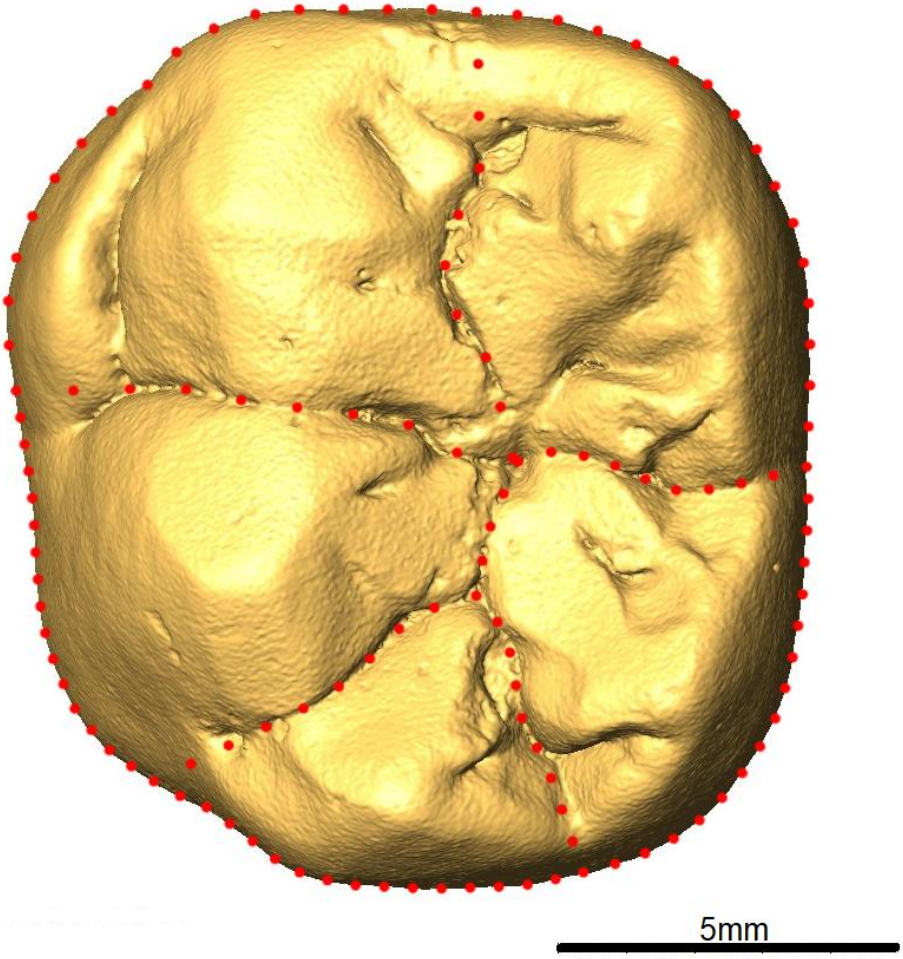

Figure 3.9. The landmarked first right mandibular molar KNM-WT 38359a (mirrored). Note the well developed protostylid.

KNM-WT 38359a (Figure 3.9) is an isolated, lightly worn right mandibular molar of an inferred position of an M_1 based on the morphological similarities and the close proximity to

KNM-WT 38359b during their discovery. The crown has an elongated oval shape that displays a slight bossing of the mesiobuccal face, which is caused by a marked, crest-like protostylid that emanates from the mesiobuccal fissure and terminates opposite the mesial marginal ridge. Secondary fissures run into the occlusal basin from all cusps, and the fissure pattern is +. There are no C6 or C7. The mesial fovea is slit-like and asymmetrical, with a preference towards the metaconid. The distal fovea is slightly smaller, and is associated with both the hypoconulid and entoconid.

KNM-WT 38359b

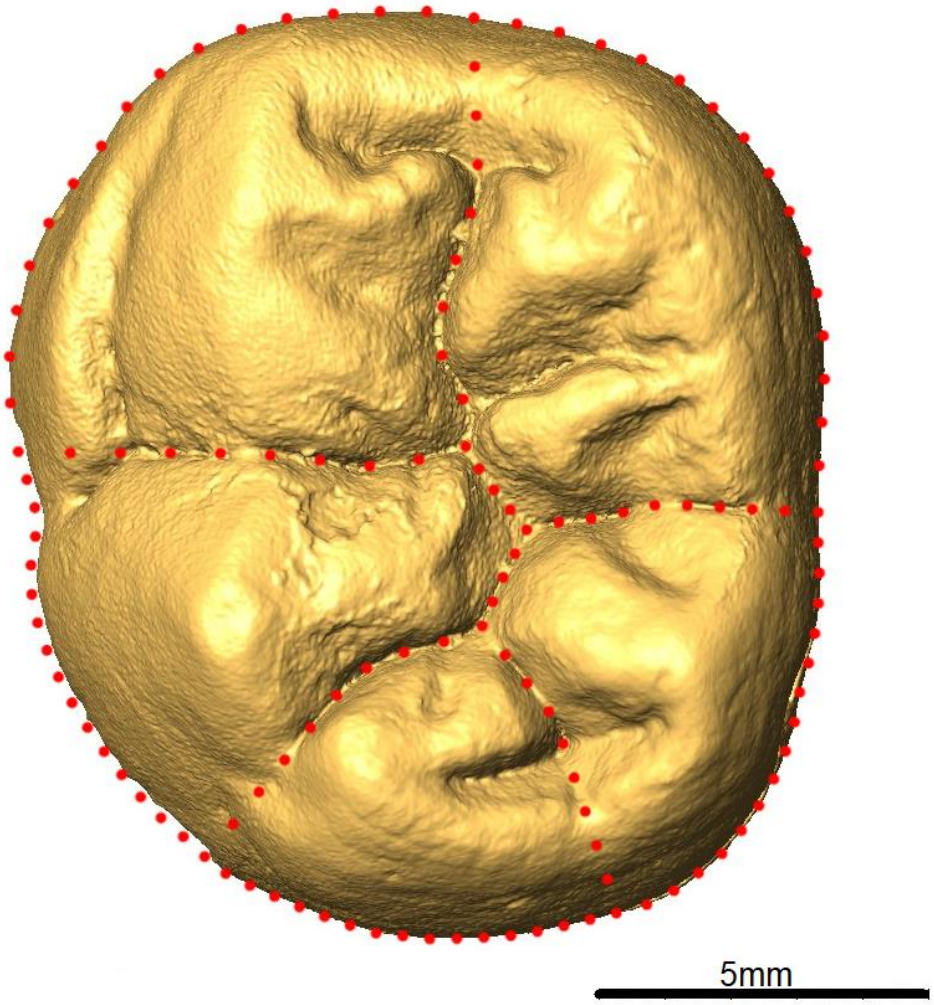

Figure 3.10. The landmarked associated lower second right molar KNM-WT 38359b (mirrored). Note the well developed, crest-like protosylid that is shared with KNM-WT 38359a.

KNM-WT 38359b (Figure 3.10) is an isolated mandibular RM_2, which is associated with KNM-WT 38359a. The shape of the crown is an enlongated oval, with a slight bossing of the mesiobuccal face which is caused by a marked, crest-like protostylid that runs from opposite the mesial marginal ridge and terminates at the mesiobuccal fissure. A thin strip of enamel is missing from the distobuccal face of the crown in occlusal view. There are no C6 or C7, but there is a distinct distal ridge on the metaconid. The distal fovea is deep, and slit-like, and is associated with both the entoconid and hypoconulid. The mesial fovea is slit-like and exhibits a slight preference towards the protoconid. The enamel surface is relatively simple, with only a few secondary fissures. The fissures display a Y-5 pattern.

KNM-WT 66291

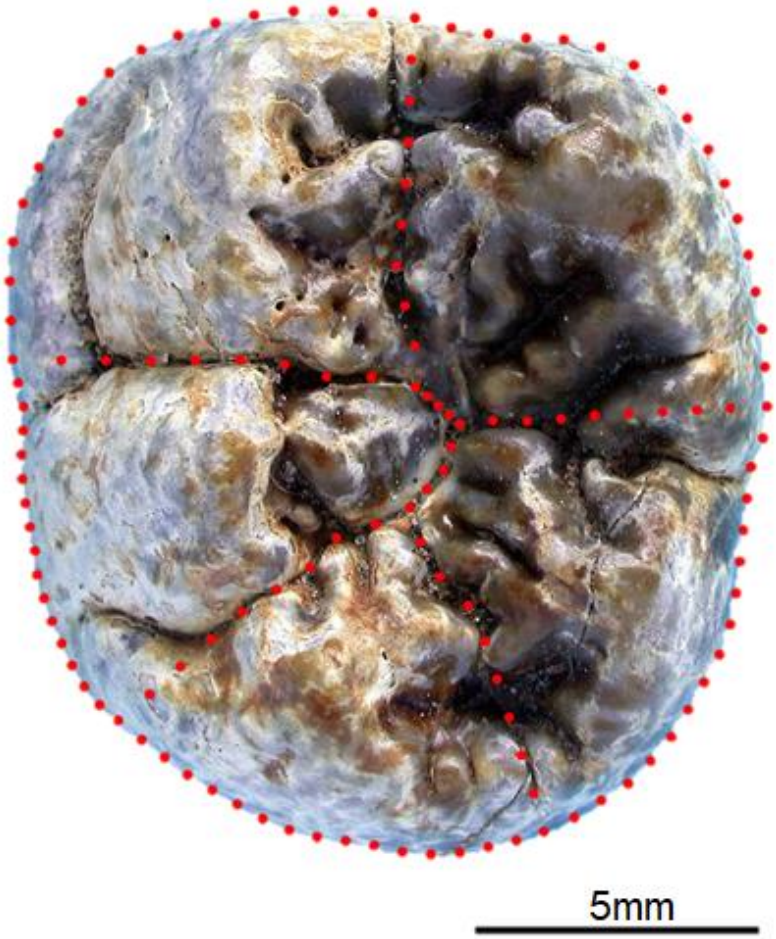

Figure 3.11. The landmarked isolated lower left molar KNM-WT 66291. Note the distinct C7, the three distal accessory cusps, the well-developed protostylid, and the numerous secondary fissures.

Figure 3.11 shows KNM-WT 66291, an unworn left lower molar with an inferred position of M_2 or 3 based on size (Wood and Leakey, 2011). The crown shape is oval, albeit slightly irregular. There is a well-defined metaconulid type C7 that is positioned at the middle of the lingual face of the crown. There are three accessory cusps located below the distal fovea on the distal marginal ridge. A marked protostylid runs from opposite the mesial marginal ridge and terminates at the mesiobuccal fissure. The enamel surface is complex and exhibits multiple secondary fissures that run from all cusps. The distal fovea is deep, short and

symmetrical. The mesial fovea is slit-like and wide, and extends towards the cusp tips of the protoconid and metaconid. The fissure pattern is Y-5.

3.1.3 Methods

Determining the position of isolated molars

Prior to making taxonomic comparisons, it is important to be as certain as one can about the position a particular tooth has in the molar row (Skinner et al., 2008). Since the taxonomic affinities of the Lomekwi sample are unclear (and in principle they could sample more than one taxon), a determination of tooth position of the isolated molars was based on comparison to a combined M_1 (n=22), M_2 (n=29), and M_3 (n=21) sample of the three *Australopithecus* taxa. Determination of tooth type was conducted with CVAs using the GM landmark data (both form and shape), and the relative and absolute cusp area data. The decision to use these data types was based on their performance in Chapter two (Methods Comparison). Similarly, CVAs were conducted on principal components to reduce the dimensionality of the data. Inclusive sets of the first twenty PCs (i.e., 1-2, 1-3, 1-4…1-20 PCs) derived from the GM shape and form data were used, accounting for 98% and 99% of the variance, respectively. The decision to use the first 20 PCs was based on the smallest group size in the analysis - the M_3s (n=21). While the number of variables does not exceed the group size, which in turn avoids the issue of potentially overfitting of the results (Mitteroecker and Bookstein, 2011), a slightly smaller number of variables was decided upon for conservative purposes. In contrast to the GM CVAs, a single CVA was run for each cusp area data using the first four (relative cusp areas) and five (absolute cusp areas) PCs, respectively. In each CVA the combined sample of *Australopithecus* molars were treated as having known molar position and the Lomekwi molar positions were treated as unknowns.

Assessing to which known Australopithecus taxa the Lomekwi molars are most similar

After determining the position of the isolated Lomekwi molars, known molars were assigned to either one of three group: "Lomekwi M_1s", "Lomekwi M_2s", and "Lomekwi M_3s".Each Lomekwi sample was then included in a PCA of both shape and form space with the relevant comparative sample. Thin plate spline (TPS) grids were used to visual the morphological variation across the first three PCs in the shape space PCAs. CVAs using PCs derived from GM shape and form data with Lomekwi molars treated as unknowns were conducted for each molar type to determine to which taxon (*Au. anamensis, Au. afarensis, or Au. africanus*) each molar is most similar. The number of PCs used differed for each molar type analysis, but they all explained ~95% of the total variation of the respective PCA.

Assessing whether the Lomekwi molars may be taxonomically distinct

Apart from depicting the morphological relationship of the Lomekwi molars to the three *Australopithecus* taxa, PCA/CVA were also used to assess whether the Lomekwi molars show unique morphological patterns. After PCA, CVAs of PC scores with leave one out cross-validation were conducted on both shape and form data. In each case, Lomekwi molars were treated as of known taxonomy (i.e., their own group) in order to assess whether Lomekwi molars tend to classify amongst themselves or other *Australopithecus* species. Lomekwi molars of uncertain tooth type were not included in these CVAs. Instead, they were treated as unknowns in a CVA without cross-validation, with the known Lomekwi tooth type specimens treated as a group along with *Au. afarensis*, *Au. africanus*, and *Au. anamensis*. Furthermore, PERMANOVAs with 1000 permutations using GM shape and form data were run to determine if there are differences between the group means of Lomekwi and *Au. afarensis*, *Au. africanus*, and *Au. anamensis*. Molars that were concluded to be of uncertain tooth type were excluded from the PERMANOVA analyses. As discussed in the

Methods section of Chapter 2, controlling for Type I errors may not be necessary for this type of analysis, yet p-value adjustments are still common in GM studies. For the Lomekwi analysis, the FDR (False Discovery Rate, or the Benjamini-Hochberg Procedure (Benjamini and Hochberg, 1995)) p-value adjustment was performed. In contrast to the Bonferroni correction, FDR is less conservative and has a smaller probability of experiencing Type II errors (also known as false negatives). Consequently, the test benefits from greater power (Narum, 2006). As the name of the procedure suggests, it allows for the probability of obtaining false positive results, but at the rate chosen by the user. For these reasons FDR is often preferred over Bonferroni, and it is commonly used in exploratory studies. As such, it was deemed to be a more appropriate approach for controlling for Type I errors in the Lomekwi analysis than Bonferroni correction. Since the p-value adjustments were carried out in R using the function 'p.adjust' from the package 'stats' (R core team, 2017), the false discovery rate was set at 5%. All analyses were carried out in R 3.4.3 (R core team, 2017).

3.2 Results

3.2.1 Determining the position of isolated Lomekwi molars

The first goal is to attempt to clarify the molar positions of the isolated teeth in the Lomekwi sample. GM data tooth type classification results are presented in Table 3.2, and tooth type classification results using cusp area data are presented in Table 3.3. A summary of the classification results is presented in Table 3.4. A scatter plot of the centroid sizes of the specimens in the sample is presented in Figure 3.12. The shape of each Lomekwi molar laid over the mean shapes of the combined *Australopithecus* M_1s, M_2s, and M_3s are presented in Figure 3.13.

Table 3.2
Results of the canonical variate analyses to determine the tooth position of the Lomekwi molars using GM data

Data type	GM shape			GM form		
Specimen	**M_1**	**M_2**	**M_3**	**M_1**	**M_2**	**M_3**
KNM-WT 8556	100%			94.7%	5.3%	
KNM-WT 16006			100%			100%
KNM-WT 38333		100%		31.6%	68.4%	
KNM-WT 38334	100%			100%		
KNM-WT 38339	47.4%	52.6%		94.7%	5.3%	
KNM-WT 38342	100%			100%		
KNM-WT 38347	5.3%	15.8%	78.9%	100%		
KNM-WT 38349		100%		5.3%	94.7%	
KNM-WT 38359a	5.3%	94.7%		42.1%	57.9%	
KNM-WT 38359b		100%		15.8%	84.2%	
KNM-WT 66291	89.5%	10.5%		73.3%	26.3%	

Dark shaded cells indicate conclusive tooth type results. Light shaded cells indicate the majority, but inconclusive, of the classification results.

Table 3.3
Results of the canonical variate analyses to determine the tooth position of the Lomekwi molars using relative and absolute cusp data

Data type	Relative cusp areas			Absolute cusp areas		
Specimen	**M_1**	**M_2**	**M_3**	**M_1**	**M_2**	**M_3**
KNM-WT 8556	X			X		
KNM-WT 16006			X			X
KNM-WT 38333		X			X	
KNM-WT 38334	X			X		
KNM-WT 38339		X			X	
KNM-WT 38342	X			X		
KNM-WT 38347		X		X		
KNM-WT 38349		X			X	
KNM-WT 38359a		X			X	
KNM-WT 38359b		X			X	
KNM-WT 66291	X			X		

Table 3.4
A summary of the CVA classification results with the final determination on the position of each Lomekwi molar.

Specimen	Status	GM shape	GM form	RCA	ACA	Final
KNM-WT 8556	M_1	M_1	M_1	M_1	M_1	M_1
KNM-WT 16006	M_3	M_3	M_3	M_3	M_3	M_3
KNM-WT 38333	M_1/M_2	M_2	M_1/M_2	M_2	M_2	M_2
KNM-WT 38334	M_1/M_2	M_1	M_1	M_1	M_1	M_1
KNM-WT 38339	M_1/M_2	M_1/M_2	M_1	M_2	M_2	$M_1/_2$
KNM-WT 38342	M_1/M_2	M_1	M_1	M_1	M_1	M_1
KNM-WT 38347	M_2/M_3	M_3	M_1	M_2	M_1	M_3*
KNM-WT 38349	M_1/M_2	M_2	M_2	M_2	M_2	M_2
KNM-WT 38359a	M_1	M_2	M_1/M_2	M_2	M_2	M_2*
KNM-WT 38359b	M_2	M_2	M_2	M_2	M_2	M_2
KNM-WT 66291	M_2/M_3	M_1	M_1	M_1	M_1	M_1

RCA: relative cusp areas; ACA: absolute cusp areas; *: see text.

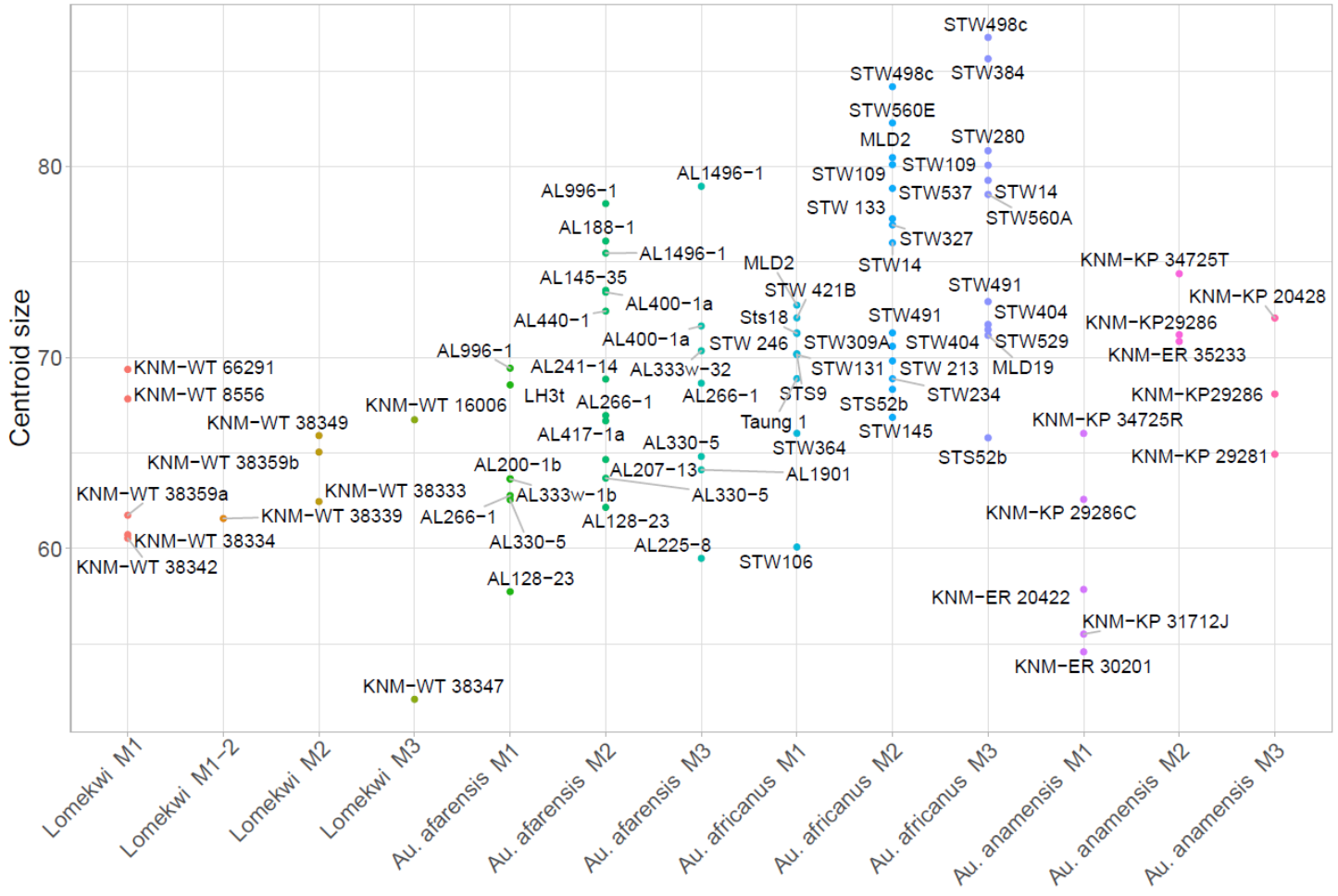

Figure 3.12. A centroid size plot that depicts the size of the molar types in each taxa and the Lomekwi sample. Note the small centroid size of KNM-WT 38347, and the overall relatively small size of the Lomekwi molars.

The two molars of known tooth type (KNM-WT 8556 and KNM-WT 16006) consistently classified correctly, and their shape compared to the mean shapes of the respective *Australopithecus* molar types exhibits significant overlap. KNM-WT 8556 has a rounded square outline, which is characteristic of *Australopithecus* M_1. However, the molar is slightly larger than the mean *Australopithecus* M_1 size, and it is the second largest M_1 in the Lomekwi sample (Figure 3.12). KNM-WT 16006 has a subrectangual crown shape that exhibits distal tapering, and a small hypoconid, both characteristic of *Australopithecus* M_3s.

KNM-WT 38333 is unusual by having a very small hypoconulid, and a mesiobuccal fissure that sharply curves mesially to the right before intersecting with the mesial longitudinal fissure. The GM shape classification results suggests that it is an M_2, whereas the GM form results classified it as an M_1 31.5% of the time. It is highly likely that the shape classification results are mostly based on the occlusal outline of the molar, as the crown base tapers distally from the metaconid and protoconid, and the mesial half is buccolingually expanded, which is characteristic of *Australopithecus* M_2s. The small size of the molar drives the GM form data to classify it as an M_1 some of the time.

KNM-WT 38334 has a rounded square outline, which is characteristic of *Australopithecus* M_1s, while it is slightly smaller than the mean size of the molar in this genus. The classification results of KNM-WT 38339 using GM shape data are split between M_1 and M_2, while in CVAs using GM form data the molar classified as an M_1, most likely due to its relatively small size. The molar is unusual by being buccolingually wide and having a relatively small entoconid. It is similar to an M_1 mostly for its square shaped crown, and the position of the mesiobuccal fissure. It is similar to an M_2 mostly for its buccolingually expanded trigonid. KNM-WT 38342 consistently classified as an M_1 in both GM shape and

form canonical variate analyses. The molar exhibits an oval square outline, which is characteristic of *Australopithecus* M_1s. The fissure pattern is consistent with the mean pattern of *Australopithecus* M_1s, albeit the mesial longitudinal fissure deflects buccally before intersecting with the mesiobuccal fissure. The metaconid is also slightly smaller than that in *Australopithecus*. The molar is smaller than the mean size of *Australopithecus* M_1s.

KNM-WT 38347 classified the majority of the time (80%) as an M_3 in the Procrustes shape CVAs, and 100% of the time as an M_1 in the Procrustes form CVAs. The similarities of the molar to *Australopithecus* M_3s are the subrecangular shape of the crown, and the shape of the entoconid. It departs from the mean shape of *Australopithecus* M_3s by having a slightly smaller hypoconulid and protoconid, and a larger hypoconid. The size and shape of these cusps might explain why the molar classified once as an M_1, and twice as an M_2. Procrustes form CVAs classified the tooth as an M_1 100% of the time due its very small size. Thus, the molar is unusual by exhibiting a typical *Australopithecus* M_3 crown shape morphology while being significantly smaller than expected. Due to its characteristic M_3 crown morphology, it will be regarded as such in subsequent analyses.

In both Procrustes shape and form CVAs, KNM-WT 38349 consistently classified as an M_2. The molar shares a slightly buccolingually expanded mesial half and the patterning of the mesiobuccal and longitudinal fissures with *Australopithecus* M_2s, although it is slightly smaller than the mean size of M_2s in the genera. It is unusual by having a small hypoconulid. KNM-WT 38359a classified the majority of the time as an M_2 (94.7%) in Procrustes shape CVAs, whereas the results of the Procrustes form CVAs did not show a marked preference for either tooth position. The molar is similar to an M_2 mostly for the buccal expansion of the mesiobuccal face of the crown, which is uncommon in M_1s. The size of the molar,

however, is similar to that of M_1s, which may have influenced the classification results in the Procrustes form CVAs. The molar will be regarded as an M_1 in subsequent analyses regardless of the present tooth type classification results due its known association with the M_2 KNM-WT 38359b.

KNM-WT 38359b classified 100% of the time as an M_2 in Procrustes shape CVAs, and 84.2% in Procrustes form CVAs. The shape results can be explained by the occlusal outline of the crown of the molar, as it is an elongated oval, which exhibits a buccolingual expansion of the mesial half and slight tapering of the distal half that begins at the base of the metaconid and protoconid. These traits are characteristic of *Australopithecus* M_2s. The Procrustes form classification results are mostly driven by the relatively small size of the molar compared to *Australopithecus* M_2s, as can be seen in Figure 3.13. KNM-WT 66291 classified the majority of the time as an M_1 in both Procrustes shape (89.5%) and form CVAs (73.3%). The molar is similar to *Australopithecus* M_1s for its fissure pattern and to some degree the occlusal outline of the crown. Compared to the mean shape of the M_1s of this genus, KNM-WT 66291 does not exhibit bossing of the buccal face of the hypoconid. However, this trait is more common in *Au. afarensis* and *Au. anamensis* than in *Au. africanus*. Thus, the molar could be more similar to the M_1s of the latter taxon than to those of the former taxa. The somewhat elongated crown of KNM-WT 66291 may have resulted in the molar classifying as an M_2 10.5% of the time in Procrustes shape CVAs. In Procrustes form CVAs, KNM-WT 66291 classified as an M_2 26.3% of the time mostly likely due to its relatively large size. It is the largest molar in the Lomekwi sample (Figure 3.12). However, the relatively high frequency at which the molar classified as an M_1 in the form CVAs (73.3%) suggests that regardless of the its size, it shares a crown shape morphology with M_1s.

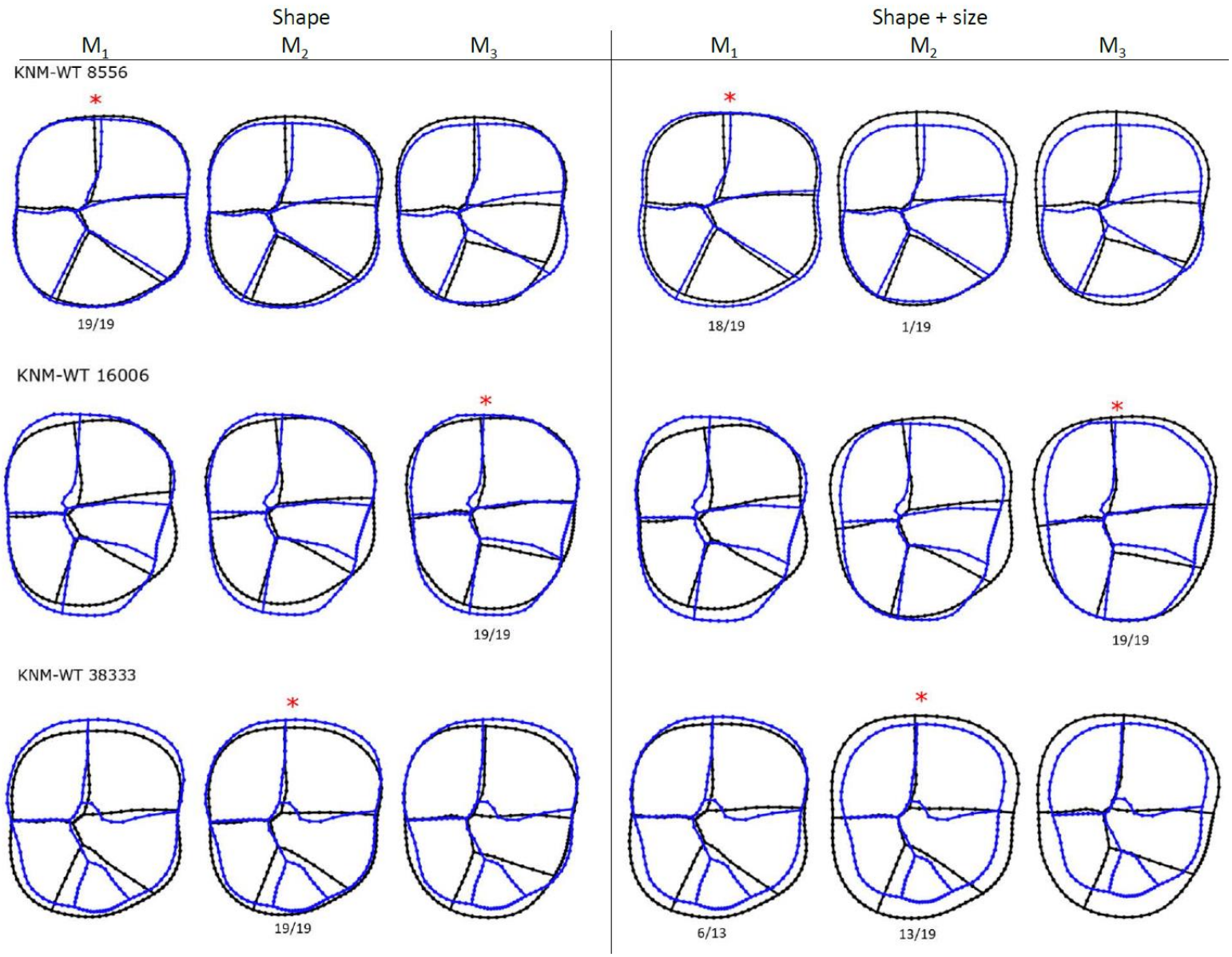
Shape
Shape + size
M1
M2
M3
M1
M2
M3
KNM-WT 8556
19/19
18/19
1/19
KNM-WT 16006
19/19
19/19
KNM-WT 38333
19/19
6/13
13/19

KNM-WT 38334

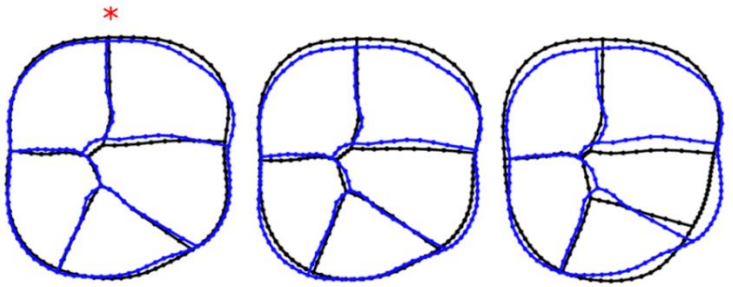

19/19

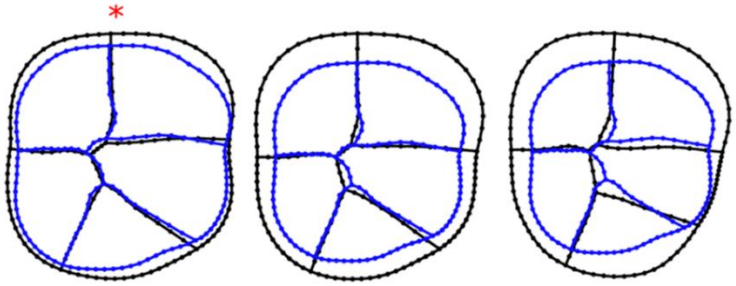

19/19

KNM-WT 38339

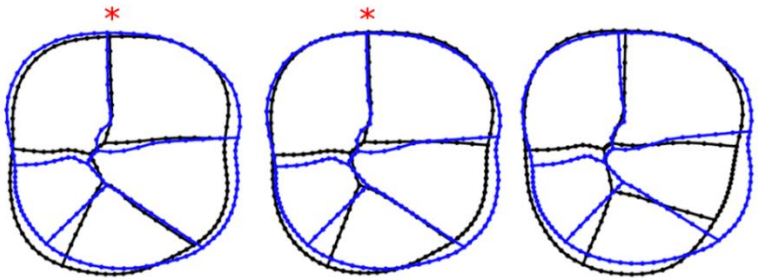

9/19 10/19

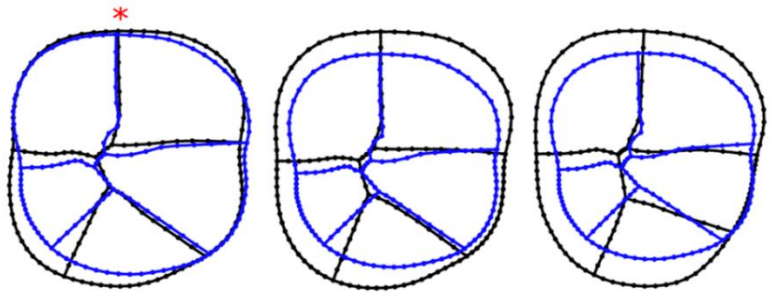

18/19 1/19

KNM-WT 38342

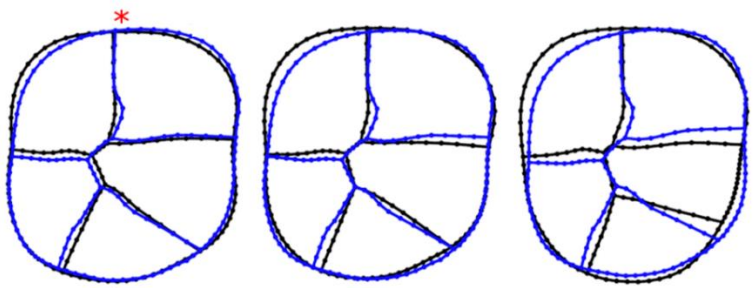

19/19

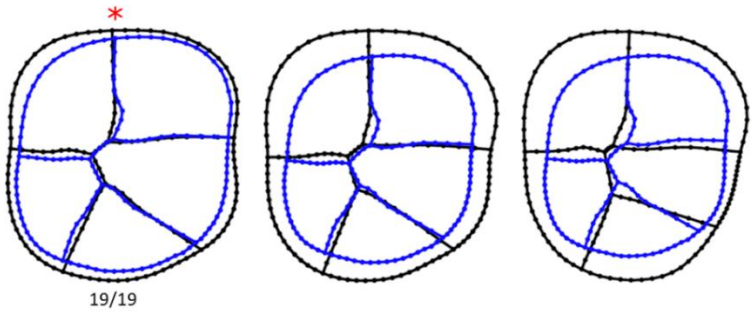

19/19

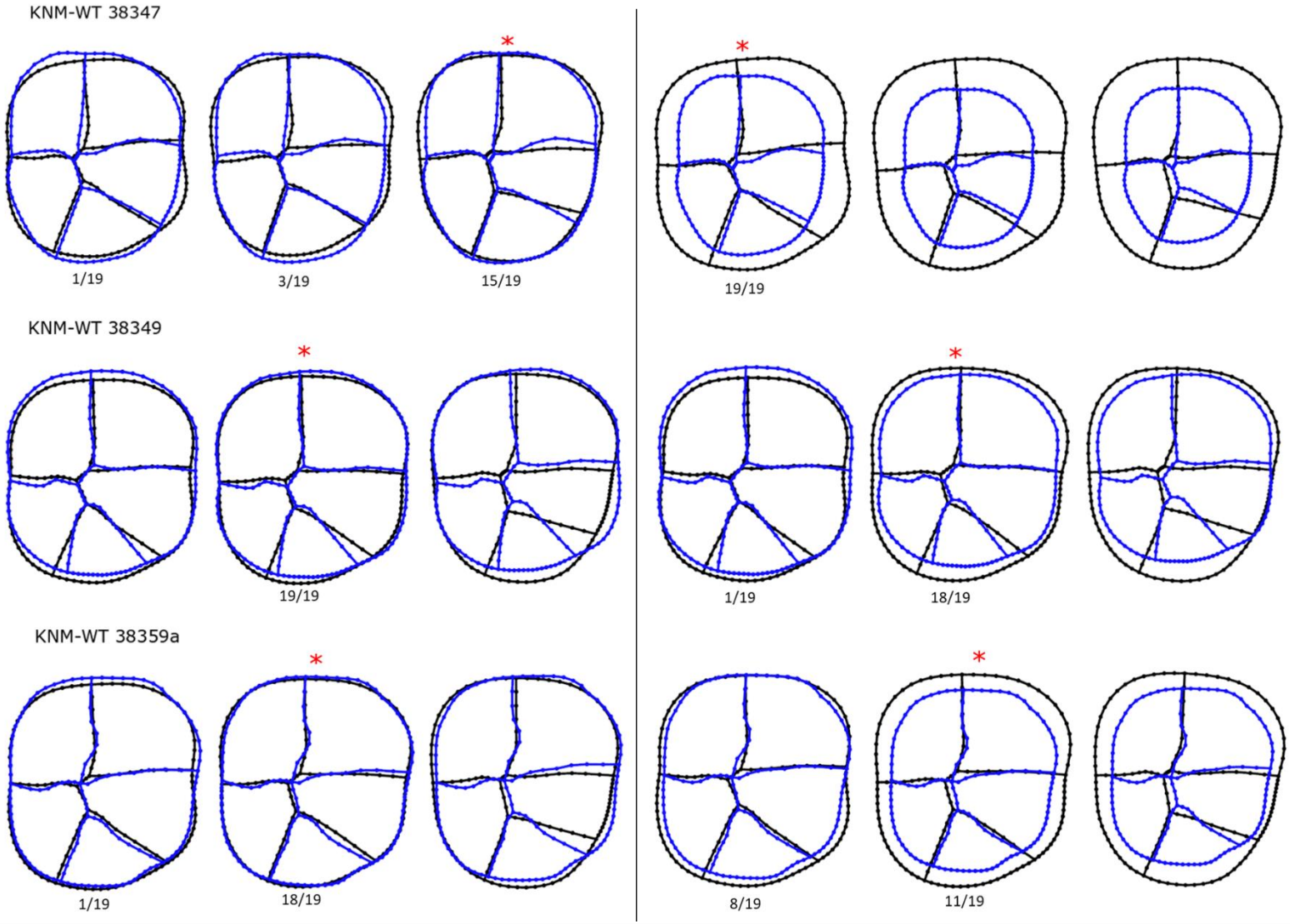
KNM-WT 38347
1/19
3/19
15/19
19/19
KNM-WT 38349
19/19
1/19
18/19
KNM-WT 38359a
1/19
18/19
8/19
11/19

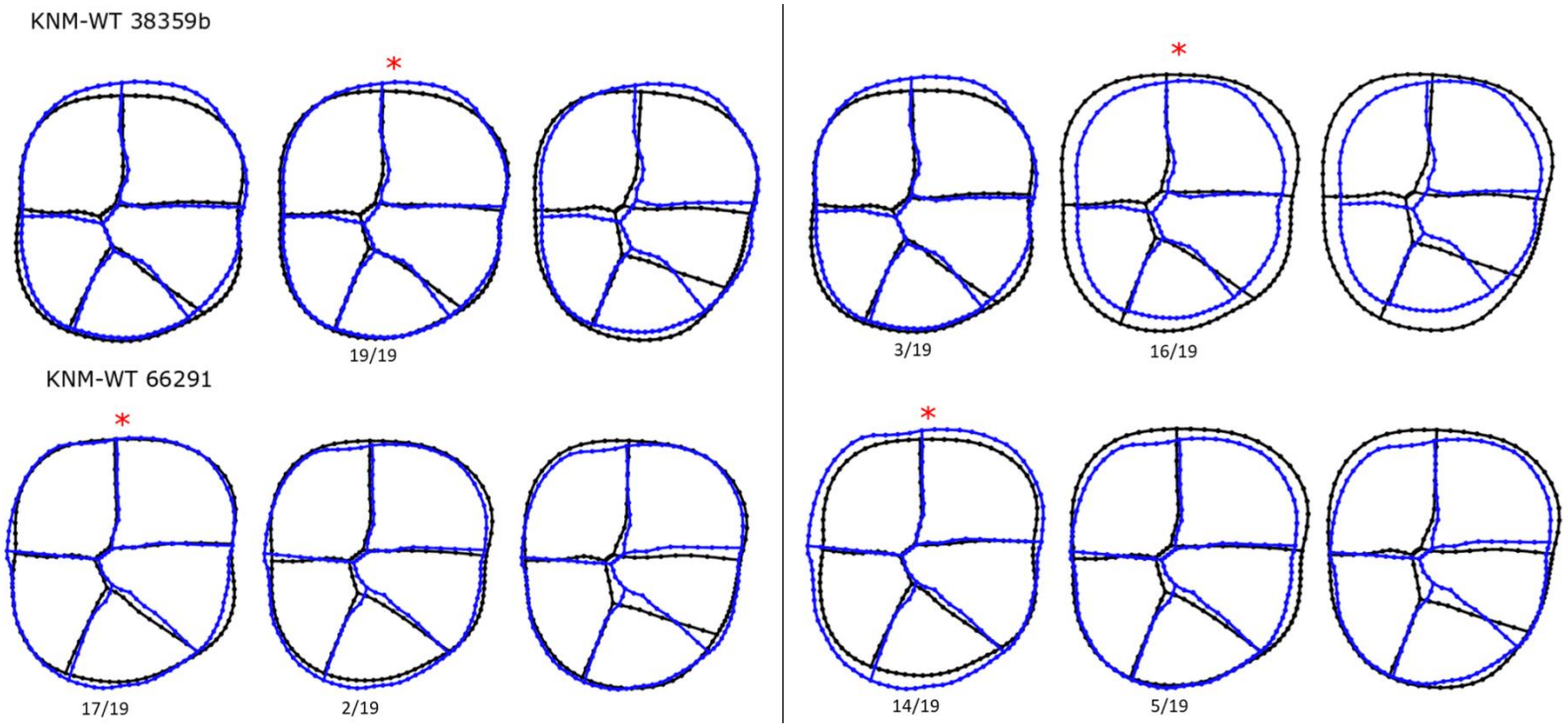

Figure 3.13. The shape of Lomekwi molars is visualized in blue, *Australopithecus* molar type mean shapes are depicted in black. The shapes on the left are Procrustes shape data. Procrustes form data, visualizing the relative size of each Lomekwi molar compared to mean size of each *Australopithecus* molar type, are on the right. Red stars represent the final tooth type classification results, and the ratios at the bottom show the classification results.

3.2.2 Assessing to which known *Australopithecus* taxa the Lomekwi molars are most similar

After clarifying the molar positions (to the best degree possible), the second goal is to determine to which of the well-established *Australopithecus* species (i.e., *Au. anamensis, Au. afarensis, and Au. africanus*) the Lomekwi material is most similar. If, for example, they tend to classify as *Au. afarensis* then this would lend support to the hypothesis that they are simply a regional population of that species. However, if they classify as *Au. africanus*, then it would suggest that the differences between Lomekwi and *Au. afarensis* are at a level similar to that between recognized *Australopithecus* species. Each molar position is examined in turn below.

First molars

The first two PCs of Shape space PCA are presented in Figure 3.14 and the first and third PCs are presented in Figure 3.15. The first two PCs of form space PCA are presented in Figure 3.16. TPS grids illustrate that negative PC1 values are associated with a large reduction of the entoconid, and separate KNM-WT 38339 from the rest of the sample, including the known Lomekwi M_1s. This PC accounts for 27.1% of the morphological variation. PC2 (24.4% of the variation) corresponds to a square shaped crown outline and shortened longitudinal fissure that results in a + fissure pattern. This PC contributes to the separation of *Au. afarensis* M_1s from those of *Au. africanus* and *Au. anamensis*. Apart from KNM-WT 38339, the Lomekwi M_1s do not contribute to the morphological variation across the first two PCs, and exhibit a central distribution in the PCA.

KNM-WT 8556 plots near *Au. afarensis* but does not overlap. Its position near *Au. afarensis* can be explained by the square shape of the crown, which is characteristic of the M_1s in this

species. The lack of overlap with *Au. afarensis* is most likely due to the relatively expanded hypoconulid of the molar, which is associated with positive scores in PC3 (13.1% of the variation). KNM-WT 38359a does not overlap with *Au. afarensis*, or any other taxa, as can be seen from PC3. Its position in the negative half of PC2 can be explained by the extremely reduced, or absent, central fissure. However, it drives the morphological variation along PC3, which is due to its slightly buccolingualy expanded mesial half and elongated oval shape. KNM-WT 38342 is positioned on the positive half of PC2, which can be explained by its buccally deflecting mesial longitudinal fissure, a feature that is characteristic of *Au. africanus* M_1s in the sample. KNM-WT 38334 plots within *Au. afarensis* in PC3 due to its square shaped crown. KNM-WT 66291 overlaps only with *Au. africanus* across the first 3 PCs, most likely due to its elongated oval shape. Overall, a few of the Lomekwi M_1s show morphological features that may be unique among the *Australopithecus* specimens in the sample.

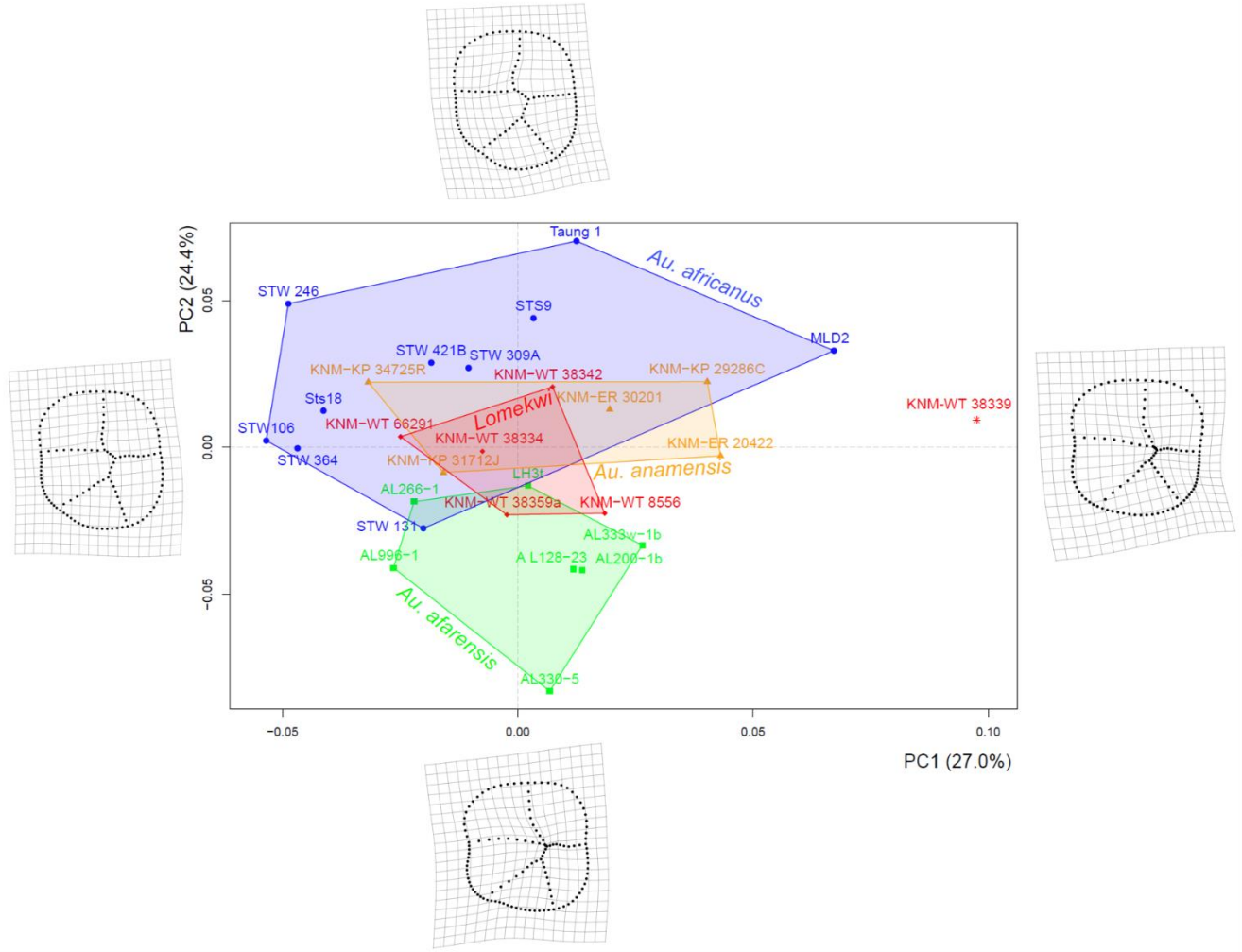

Figure **3.14**. Scatter plot of principal component axis one (PC1) and axis two (PC2) based on the Procrustes shape data of M_1s. TPS grids represent the morphological variation trends of the specimens along the principal component axes. KNM-WT 38339 is not included within Lomekwi M_1s due to the ambiguity in the position of molar.

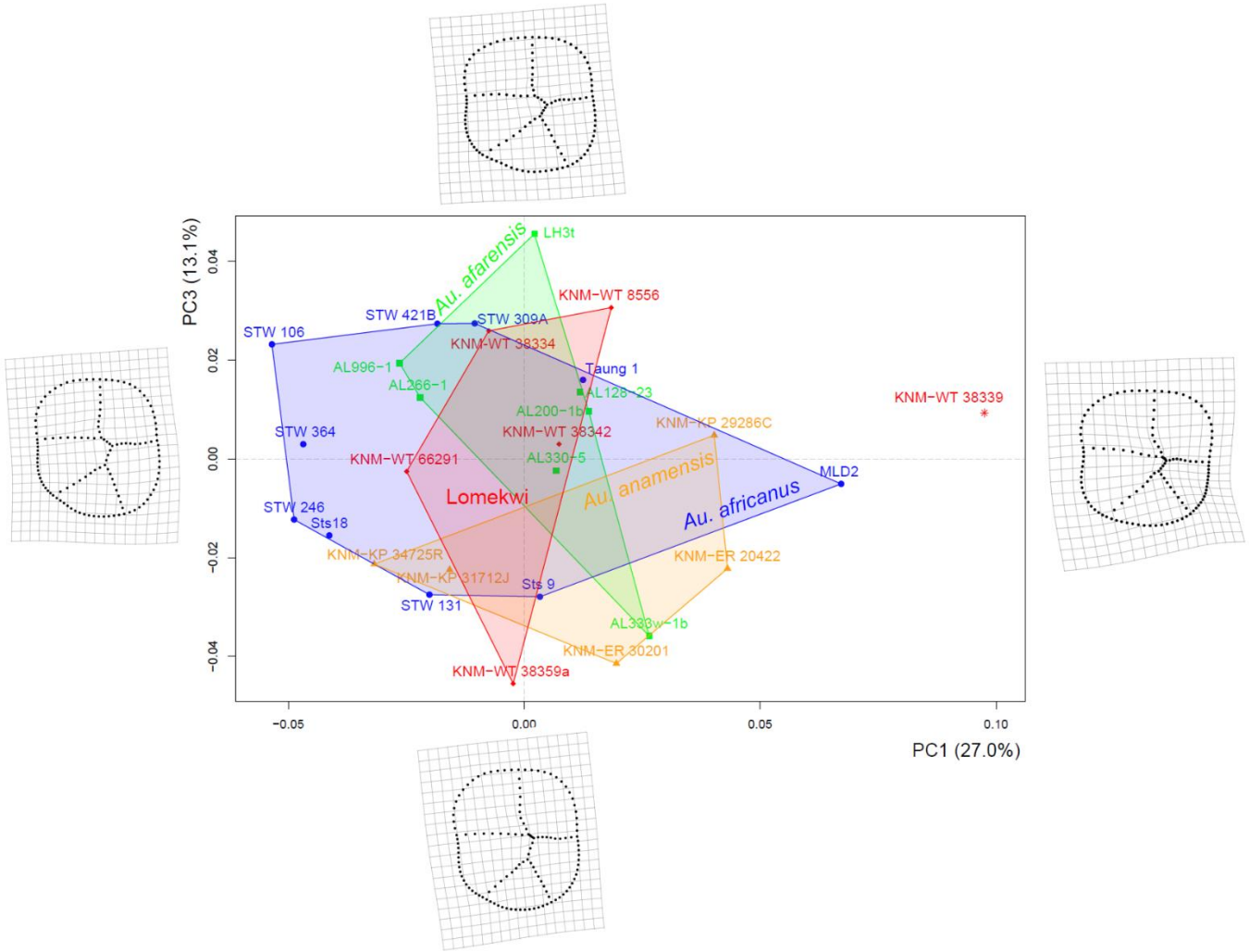

Figure **3.15**. Scatter plot of principal component axis one (PC1) and axis three (PC3) based on the Procrustes shape data of M_1s. TPS grids represent the morphological variation trends of the specimens along the principal component axes KNM-WT 38339 is not included within Lomekwi M_1s due to the ambiguity in the position of molar.

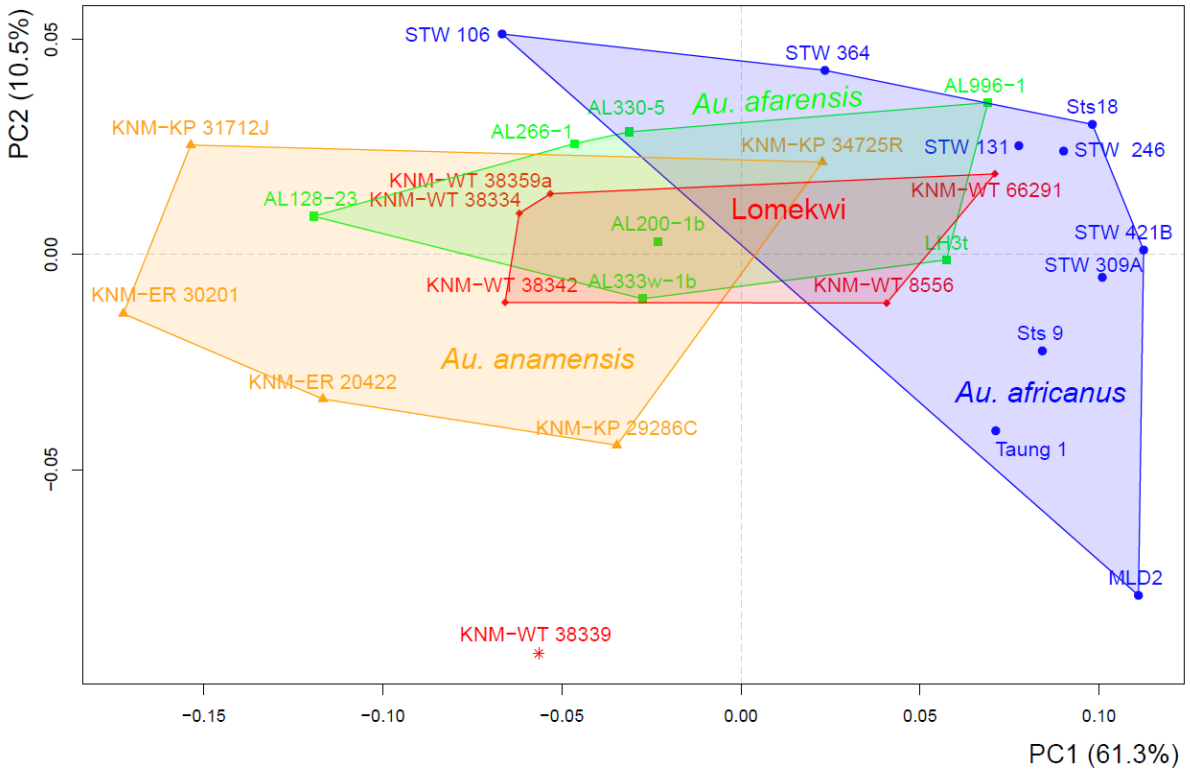

Figure 3.16. Scatter plot of principal component axis one (PC1) and axis two (PC2) based on the Procrustes form data of the M_1s. PC1 accounts only for size. KNM-WT 38339 is not included within Lomekwi M_1s due to the ambiguity in the position of molar

Table 3.5

Classification results of CVAs using M_1s Procrustes form and shape data with Lomekwi molars treated as unknown. Shaded cells indicate the majority of the classification results. KNM-WT 38339 is separated from the sample due to the uncertainty in the position of the molar.

	Procrustes shape (2-11 PCs)		
Specimen	*Au. afarensis*	*Au. africanus*	*Au. anamensis*
KNM-WT 8556	100.0%		
KNM-WT 38334	22.2%	66.7%	11.1%
KNM-WT 38342		44.4%	55.6%
KNM-WT 38359a	11.1%		88.9%
KNM-WT 66291		66.7%	33.3%
KNM-WT 38339	77.8%	11.1%	11.1%

	Procrustes form (2-8 PCs)		
Specimen	*Au. afarensis*	*Au. africanus*	*Au. anamensis*
KNM-WT 8556	83.3%	16.7%	
KNM-WT 38334	66.7%	16.7%	16.7%
KNM-WT 38342			100.0%
KNM-WT 38359a	33.3%		66.7%
KNM-WT 66291		100.0%	
KNM-WT 38339	66.7%		33.3%

Procrustes shape CVA results (Table 3.5) do not suggest that the Lomekwi M_1s, as a sample, are more similar to a specific taxon. The classification results of KNM-WT 8556, KNM-WT 66291, and KNM-WT 38359a are consistent with the PCA shape space results. It is unclear why KNM-WT 38334 would classify mostly as *Au. africanus* given its square shaped crown, or why KNM-WT 38339 classify the majority of the time as *Au. afarensis* based on the PCA results. It is possible that fissure patterning, or minute crown shape sections, become more prominent after the first three PCs and may lead to unexpected classification results, especially with specimens that do not show a tendency towards any specific morphological configuration within the sample. Procrustes form CVA results (Table 3.5) show a trend for Lomekwi to classify as either *Au. afarensis* or *Au. anamensis*, and are consistent with the PCA form space results. The classification of KNM-WT 8556 as *Au. afarensis,* KNM-WT 38359a as *Au. anamensis*, and KNM-WT 66291 as *Au. africanus* can be explained by the morphological and size similarities between the three specimens and the three taxa. The classification results of the rest of the Lomekwi specimens are mostly driven by size, classifying as either one of the smaller hominins (*Au. afarensis* and *Au. anamensis*).

Second molars

Negative scores on the first PC (Figure 3.17) correspond to a reduced hypoconulid, elongated crown shape, and a mesial deflection of the mesiobuccal fissure. This PC explains 34.5% of the morphological variation. The Lomekwi specimens drive most of the morphological variation along this PC, and neither overlap with other taxa. Molars with positive scores along PC2 (17.2% of the variation) have a reduced entoconid, a larger hypoconid, and a mesial longitudinal fissure that turns sharply lingually before intersecting with the mesiobuccal fissure. KNM-WT 38333 is positioned at the negative extreme of PC1 due to its small hypoconulid and the mesially deflecting mesiobuccal fissure. KNM-WT

38349 plots in the negative half of PC1 due to its small hypoconulid, and in the positive half of PC2 due to its relatively square shaped crown. A relatively small hypoconulid lends KNM-WT 38359b a negative PC1 score, and its larger hypoconid places it in the positive half of PC2. KNM-WT 38339 plots at the positive extremes of both PC1 and PC2. Compared to the other M_2s, it has a strongly reduced entoconid, and enlarged protoconid and hypoconid. Its crown shape is square-like, in contrast to the elongated ovoid shape of M_2s. Positive scores in PC3 (Figure 3.18), which account for 11.9% of the variation, correspond to a more square-shaped crown with reduced entoconid and hypoconid, and expanded protoconid and metaconid. KNM-WT 38333 and KNM-WT 38359b have negative PC3 scores due to their relatively enlogated-oval crown shape, whereas KNM-WT 38339 and KNM-WT 38349 have positive PC3 scores because of their square shaped crown. There is a significant overlap between *Au. afarensis*, *Au. anamensis*, *and Au. africanus* across all 3 PCs. Form space PCA (Figure 3.19) suggests that Lomekwi M_2s and KNM-WT 38339 not only exhibit unique crown morphology among the M_2s of *Australopithecus*, but they are also very small compared to the tooth types in these taxa.

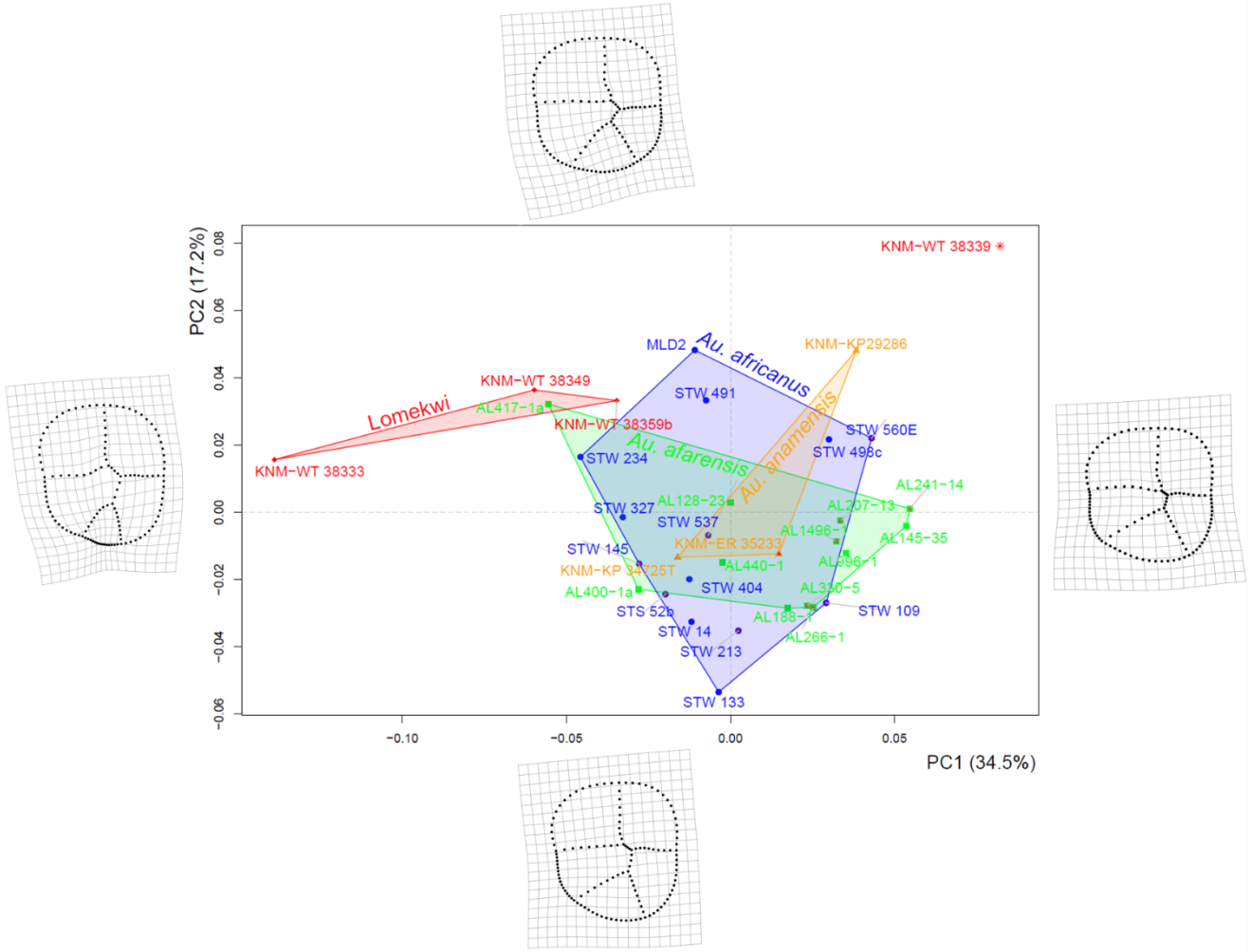

Figure 3.17. Scatter plot of principal component axis one (PC1) and axis two (PC2) based on the Procrustes shape data of M_2s. TPS grids represent the morphological variation trends of the specimens along the principal component axes. KNM-WT 38339 is not included within Lomekwi M_2s due to the ambiguity in the position of molar. Note the virtual lack of overlap between the Lomekwi M_2s and the M_2s of *Australopithecus*.

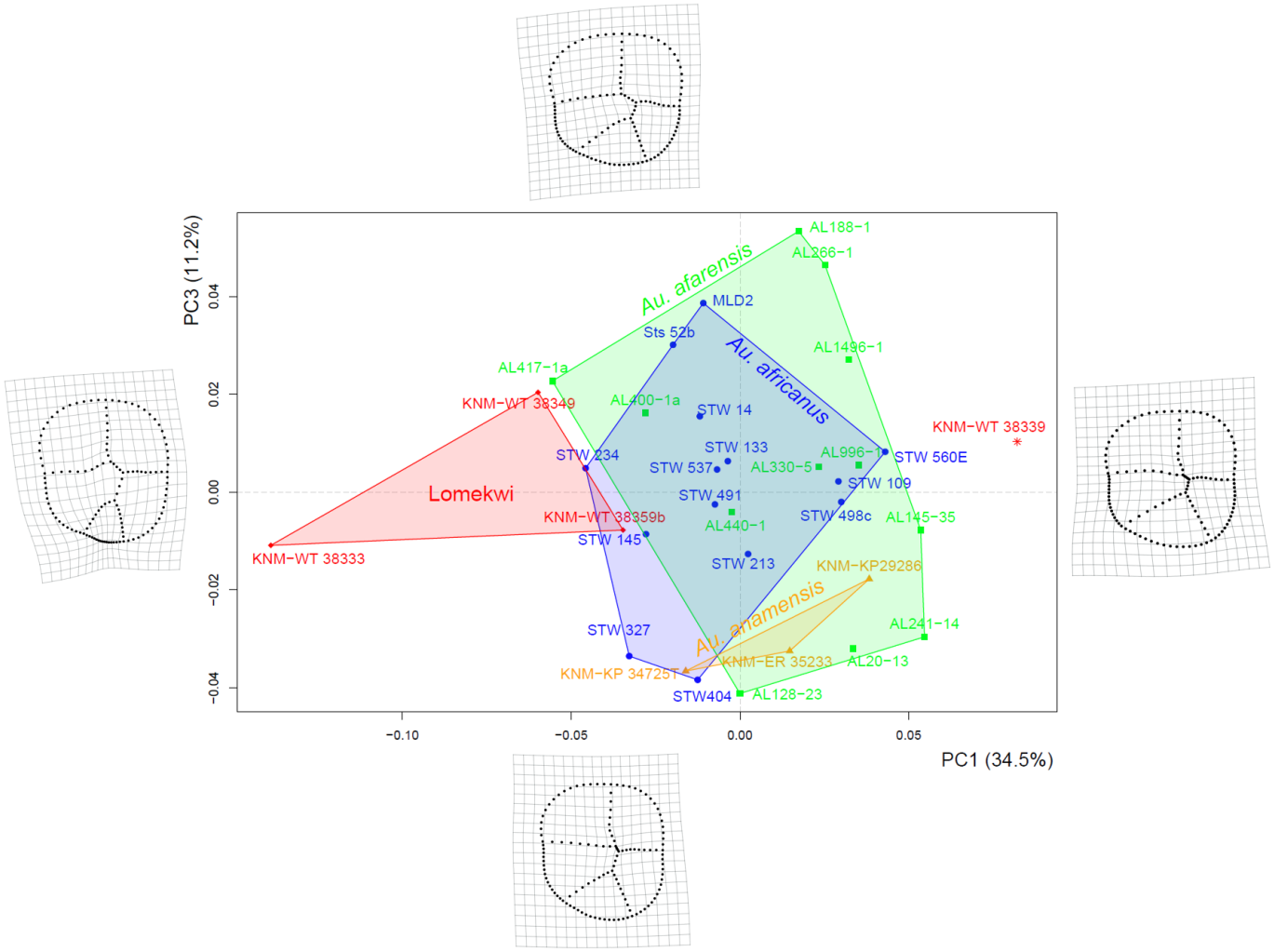

Figure 3.18. Scatter plot of principal component axis one (PC1) and axis three (PC3) based on the Procrustes shape data of M_2s. TPS grids represent the morphological variation trends of the specimens along the principal component axes. KNM-WT 38339 is not included within Lomekwi M_2s due to the ambiguity in the position of molar. Note the virtual lack of overlap between the Lomekwi M_2s and the M_2s of *Australopithecus*.

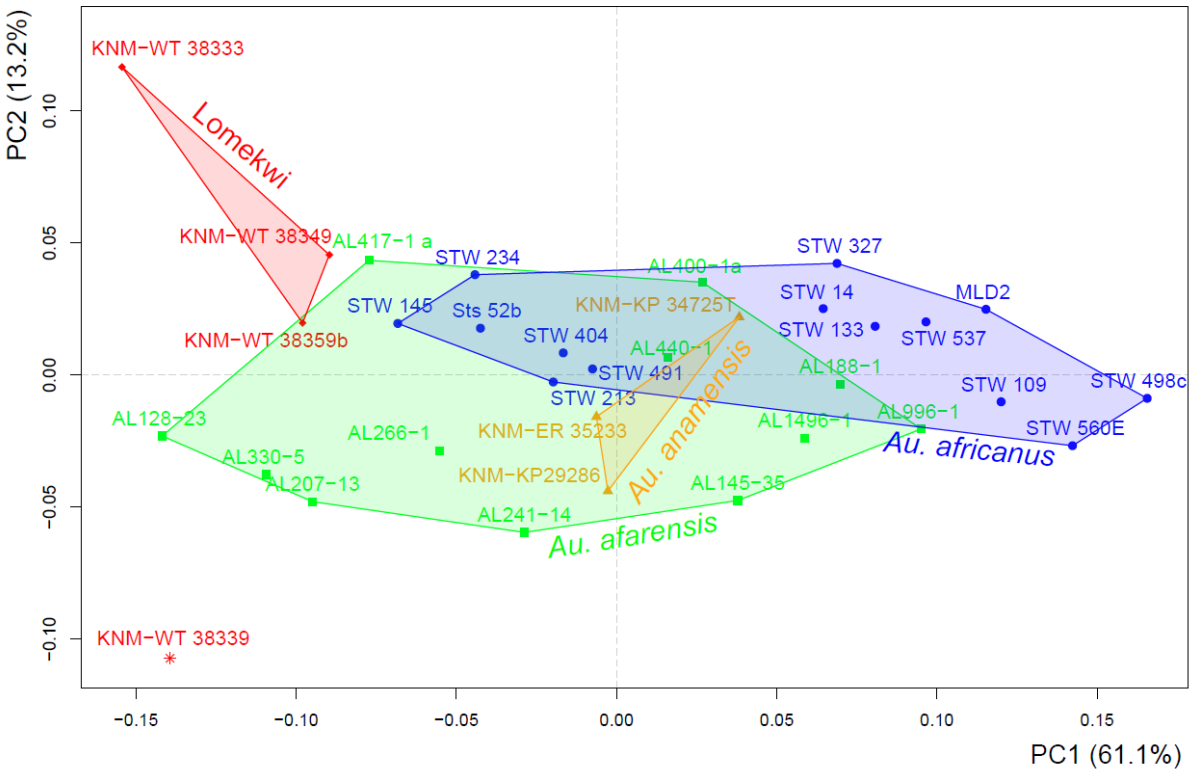

Figure 3.19. Scatter plot of principal component axis one (PC1) and axis two (PC2) based on the Procrustes form data of the M_2s. PC1 accounts only for size. Note the relatively small size of the Lomekwi sample. KNM-WT 38339 is not included within Lomekwi M_2s due to the ambiguity in the position of molar.

Table 3.6

Classification results of CVAs using M_2s Procrustes form and shape data with Lomekwi molars treated as unknown. Shaded cells indicate the majority of the classification results. KNM-WT 38339 is separated from the sample due to the uncertainty in the position of the molar.

	Procrustes shape (2-13)		
Specimen	*Au. afarensis*	*Au. africanus*	*Au. anamensis*
KNM-WT 38333		100.0%	
KNM-WT 38349		100.0%	
KNM-WT 38359b		83.3%	16.7%
KNM-WT 38339		66.7%	33.3%

	Procrustes form (2-9)		
Specimen	*Au. afarensis*	*Au. africanus*	*Au. anamensis*
KNM-WT 38333		100.0%	
KNM-WT 38349	12.5%	87.5%	
KNM-WT 38359b	50.0%	12.5%	37.5%
KNM-WT 38339	75.0%	12.5%	12.5%

Procrustes shape CVA results (Table 3.6) show that the Lomekwi sample has a tendency to classify as *Au. africanus*, with none of the specimens classifying as *Au. afarensis*. The preference to classify as *Au. africanus* over *Au. anamensis* and *Au. afarensis* might be due to the large morphological variability present in this species and the larger sample size. Data that exhibits a wide spread in multivariate space would likely find more commonalities with the Lomekwi sample. The bias to classify as *Au. africanus* disappears in the Procrustes form CVAs (Table 3.6). The classification of KNM-WT 38339 as either *Au. afarensis* or *Au. anamensis* is most likely driven largely by size, as it is morphologically distinguished from other molars in the sample. It is unclear why KNM-WT 38333 and KNM-WT 38349 classify as *Au. africanus*, considering their small size and a closer clustering towards *Au. afarensis* in the form PCAs. It is possible that the contribution of size in PCs 4 -9 diminishes, and shape becomes more prominent in the canonical variates.

Third molars

Negative scores in the first PC (Figure 3.20), which accounts for 32.2% of the morphological variation, correspond to a reduced hypoconid with the mesiobuccal and distobuccal fissures running parallel to each other, a large hypoconulid that is buccally expanded, which is likely to be associated with the presence of multiple or large distal accessory cusps, and a subrectangular crown shape. Negative scores along PC2 (17.3% of the variation) are associated with a large entoconid that is distally expanded, which likely indicates the presence of distal accessory cusps and their position relative to the other cusps, and a slight reduction in the size of the hypoconid and protoconid, which gives the mesial half of the crown an asymmetrical shape. There is a significant overlap between *Au. africanus* and *Au. afarensis* along PC1, and it mostly separates between *Au. anamensis* and *Au. africanus*. In

the second PC, *Au. anamensis* representatives plot only in the positive half. The negative values in the third PC (Figure 3.21), which accounts for 12.4% of the variation, are associated with an X fissure pattern, a wide buccal face of the hypoconid, and a relatively small metaconid.

The distance between KNM-WT 16006 and KNM-WT 38347 is large, and both are positioned near opposite ends of PC1. KNM-WT 16006 plots near *Au. afarensis* and *Au. africanus* in PC1 and PC2 but does not overlap, and near *Au. anamensis* and *Au. afarensis* in PC3 (Figure 3.21). The almost vertical position of the distolingual fissure, the relatively small entoconid, and the subrectangular crown shape explain the negative PC1 and PC2 values of the molar. In PC1 and PC2 KNM-WT 38347 overlaps with *Au. africanus*, which is most likely due to the relatively large hypoconid and the position of the hypoconulid near the midpoint of the distal half the crown. Neither molar shows a marked tendency to plot in either the positive or the negative range of PC3. In the form PCA (Figure 3.22), KNM-WT 38347 is an outlier, as it is the smallest M_3 in the sample, whereas the size of KNM-WT 16006 is within the range of *Au. anamensis* and *Au. afarensis*.

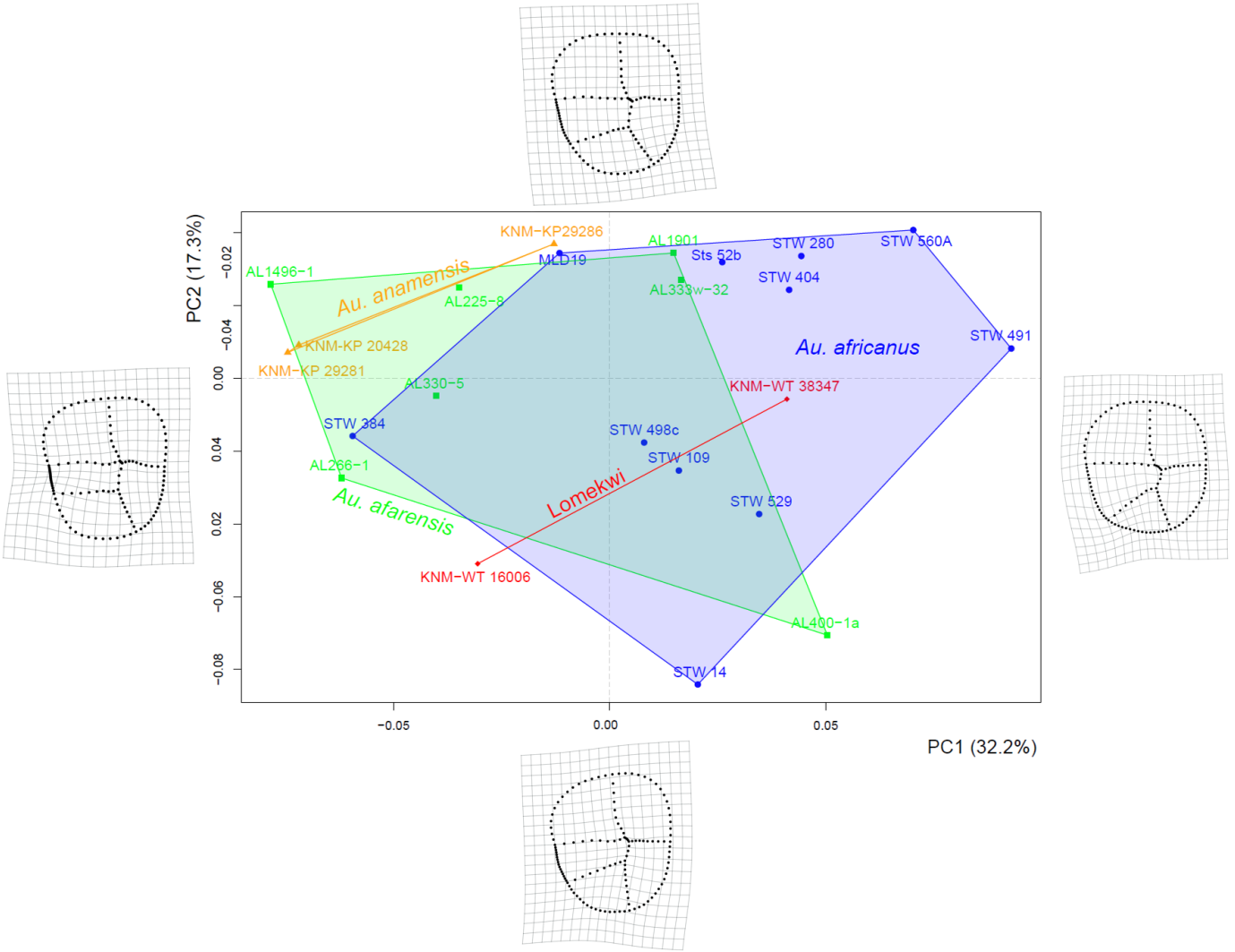

Figure 3.20. Scatter plot of principal component axis one (PC1) and axis two (PC2) based on the Procrustes shape data of M_3s. TPS grids represent the morphological variation trends of the specimens along the principal component axes.

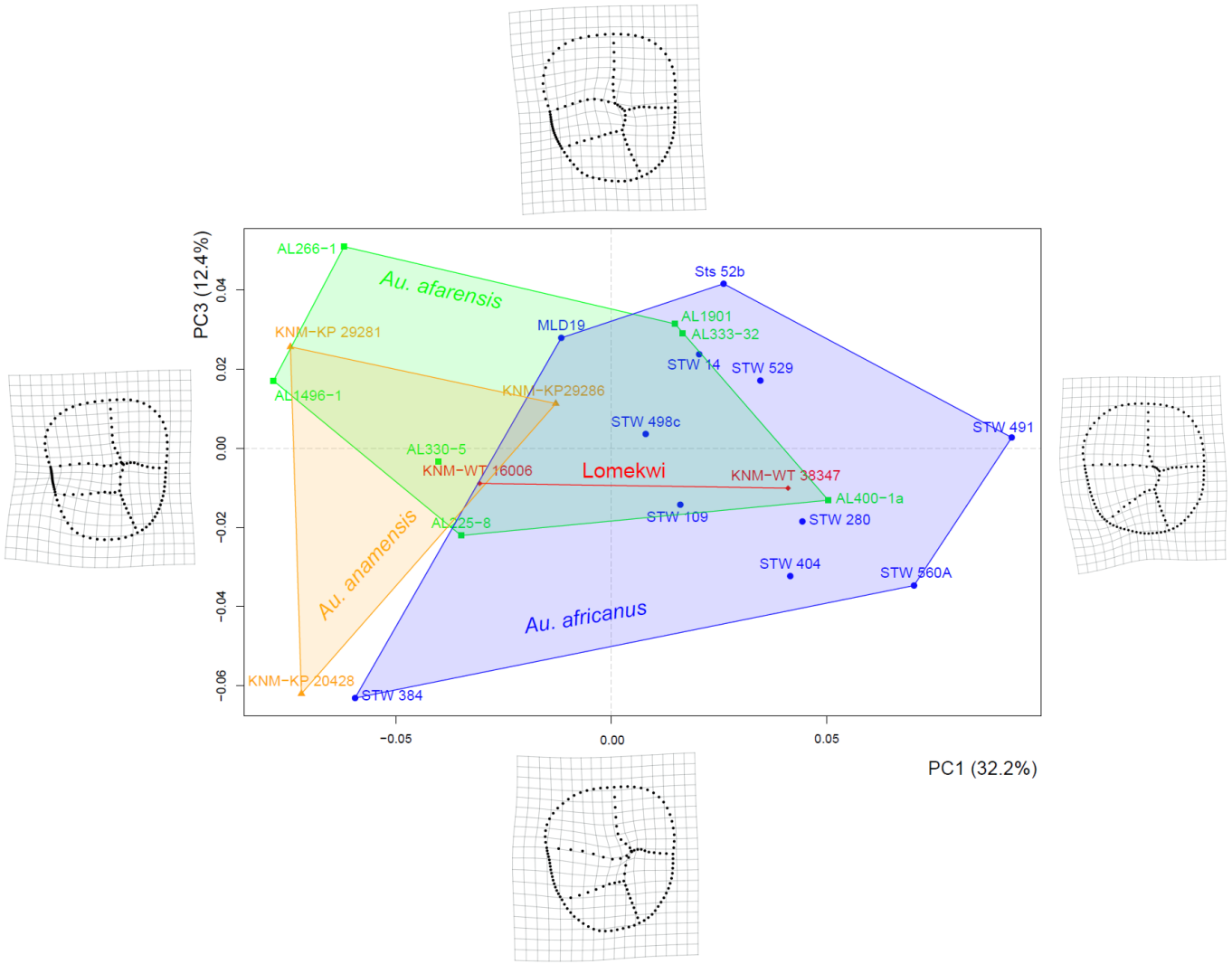

Figure 3.21. Scatter plot of principal component axis one (PC1) and axis three (PC3) based on the Procrustes shape data of M_3s. TPS grids represent the morphological variation trends of the specimens along the principal component axes.

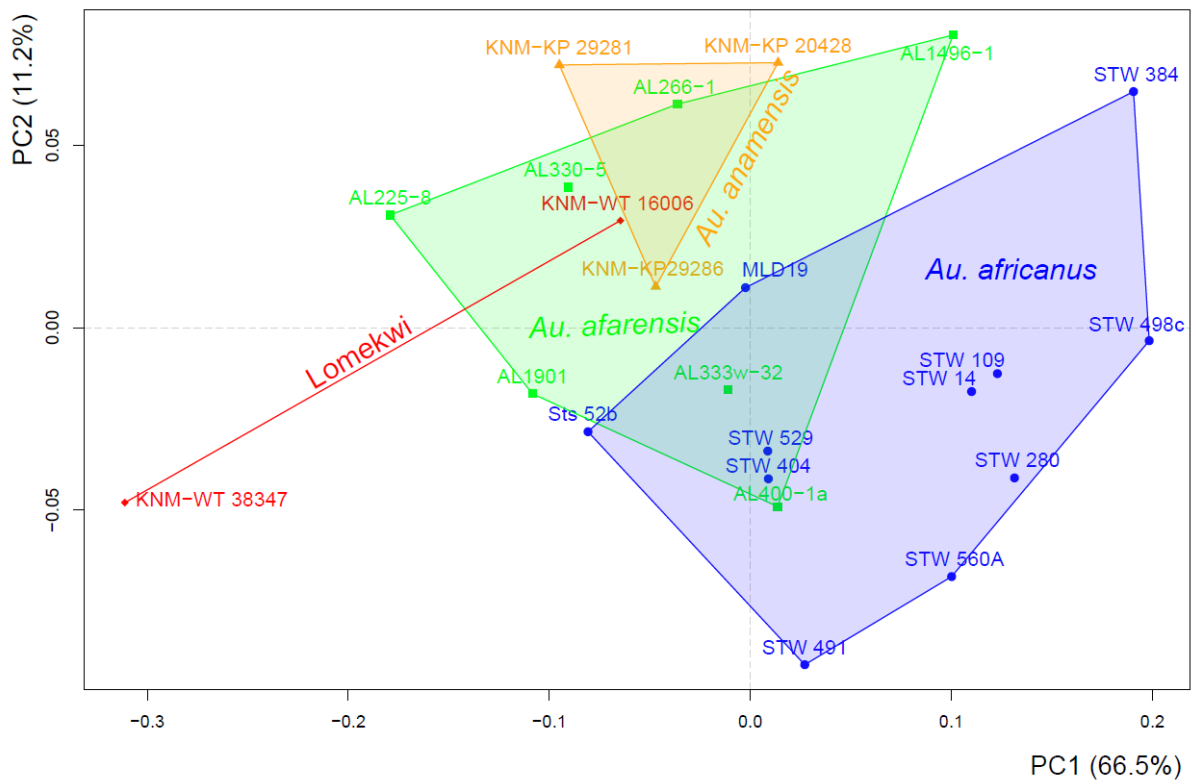

Figure 3.22. Scatter plot of principal component axis one (PC1) and axis two (PC2) based on the Procrustes form data of the M_3s. PC1 accounts only for size. Note the particularly small size of KNM-WT 38347.

Table 3.7
Classification results of CVAs using M_3s Procrustes form and shape data with Lomekwi molars treated as unknown. Shaded cells indicate the majority of the classification results.

	Procrustes shape (2-11 PCS)		
Specimen	*Au. afarensis*	*Au. africanus*	*Au. anamensis*
KNM-WT 16006	40.0%		60.0%
KNM-WT 38347	10.0%	50.0%	40.0%

	Procrustes form (2-8 PCs)		
Specimen	*Au. afarensis*	*Au. africanus*	*Au. anamensis*
KNM-WT 16006	71.4%		28.6%
KNM-WT 38347	85.7%		14.3%

In Procrustes shape CVAs (Table 3.7), KNM-WT 16006 exhibited a tendency to classify as *Au. anamensis* (60%) over *Au. afarensis* (40%), but only by a small margin. KNM-WT 38347 classified half of the time (50%) as *Au. africanus*, 40% as Au. anamensis, and 10% of the time as *Au. afarensis*. In terms of crown shape, neither molar showed a strong tendency to classify as one of the *Australopithecus* taxa. The Procrustes shape classification results are largely in agreement with the PCA results, albeit KNM-WT 38347 classified as *Au. anamensis*, which is unexpected based on the values of the first three PCs of the molar. While the fissure pattern is similar to that of *Au. africanus* M_3s, as can be observed in the PCA plots, the crown shape of KNM-WT 38347 is subrectangular with distal tapering, which more closely resembles the crown shape of *Au. anamensis and Au. afarensis*. It is likely that landmarks that are associated with crown outline become more prominent in PCs 4-11, and may lead KNM-WT 38347 to classify as these taxa. Procrustes form CVA results (Table 3.7) reveal that Lomekwi molars tended to classify as the M_3s of the two smaller taxa – *Au. afarensis* and *Au. anamensis*. This could be mostly explained by the relatively small size of the Lomekwi molars compared to that of *Au. africanus* M_3s.

3.2.3 Assessment of whether the Lomekwi sample exhibits morphological uniqueness

This final section expands on the previous analysis that found that the Lomekwi sample was not exclusively linked to any of the comparative *Australopithecus* taxa. Specifically it treats the Lomekwi material as a distinctive group and, using cross-validation, assesses how often each molar of the Lomekwi sample classifies with the remaining Lomekwi molars (as opposed to with the comparative taxa) when it is treated as of unknown taxonomic affinity.

First molars

As described above, some of the Lomekwi M_1s and KNM-WT 38339 do not overlap with other taxa in the shape space PCA, and appear to exhibit morphological features that distinguish them from *Au. anamensis*, *Au. afarensis*, and *Au. africanus*.

Table 3.8
Classification results of CVAs with cross-validation using M_1s Procrustes form and shape data with Lomekwi molars treated as known. Shaded cells indicate the majority of the classification results.

	Procrustes shape (2-10 PCs)			
Specimen	*Au. afarensis*	*Au. africanus*	*Au. anamensis*	Lomekwi
KNM-WT 8556	100.0%			
KNM-WT 38334		77.8%		22.2%
KNM-WT 38342		22.2%	77.8%	
KNM-WT 38359a	11.1%		88.9%	
KNM-WT 66291		66.7%	22.2%	11.1%
KNM-WT 38339			11.1%	88.9%

	Procrustes form (2-7 PCs)			
Specimen	*Au. afarensis*	*Au. africanus*	*Au. anamensis*	Lomekwi
KNM-WT 8556	100.0%			
KNM-WT 38334		33.3%		66.7%
KNM-WT 38342			100.0%	
KNM-WT 38359a			66.7%	33.3%
KNM-WT 66291		100.0%		
KNM-WT 38339			16.7%	83.3%

CVA results with CV treating the Lomekwi molars as known (Table 3.8) suggest that Lomekwi M_1s may be slightly more similar in size to each other than to other taxa. It is not quite clear why KNM-WT 38339 classifies as Lomekwi in Procrustes shape CVAs. A possible explanation could be the relatively large hypoconulid of the molar, which is shared, to some extent, with KNM-WT 8556 and KNM-WT 38334. Another that KNM-WT 38339 was classified with the Lomekwi sample is the small size of the entoconid. The size of the cusp in KNM-WT 38342 is also relatively small compared to *Australopithecus* M_1s (Figure 3.13). Thus, the relatively small size of the cusp in the molars may allow KNM-WT 38339 to plot near the Lomekwi sample in multivariate space and classify as the group. KNM-WT 38334 classified as Lomekwi 22.2% of time in Procrustes shape CVAs, which may be explained by the slightly enlarged hypoconulid of the molar that is shared with KNM-WT 8556, and the depression on the mesial border of the protoconid, which can be observed in KNM-WT 38359a as well.

Procrustes shape PERMANOVA (Table 3.9) did not find statistically significant differences between the mean shapes of Lomekwi M_1s and the M_1 samples of *Au. afarensis*, *Au. africanus*, and *Au. anamensis.* A significant difference between the group means of Lomekwi M_1s and *Au. africanus* M_1s was found (p=0.027, df=(1,13), Pseudo-F=3.4004, SS=0.0255, R^2=0.207) when size was introduced, although the difference becomes non-significant when the p-value is FDR corrected (p=0.066). The mean shape of Lomekwi M_1s is compared to the mean shapes of *Au. anamensis*, *Au. afarensis*, and *Au. africanus* M_1s in Figure 3.23. Overall, Lomekwi M_1s are similar to the first molars of other taxa, although there are subtle differences. Lomekwi M_1s are more oval than *Au. afarensis* M_1s, which may explain the low, although non-significant, p-value (p=0.08, df=(1,10), Pseudo-F=1.601, SS=0.004811, R^2=0.138) in the Procrustes shape

PERMANOVA. The difference is mostly expressed as a reduced flaring of the hypoconid and metaconid. The fissure pattern is similar to that of *Au. afarensis*, especially the reduced longitudinal fissure and the lingual deflection of the distal portion of the mesial longitudinal fissure. Lomekwi M_1s differ from *Au. africanus* M_1s by having a slightly larger protoconid that expands buccally, a short longitudinal fissure in the mesial half of the crown to the lingually rotated mesial longitudinal fissure, a smaller entoconid, and a larger metaconid. Compared to *Au. anamensis* M_1s, Lomekwi M_1s have slightly larger hypoconulid and entoconid. The fissure pattern is similar, and both exhibit a reduced longitudinal fissure.

Table 3.9
Results of pairwise PERAMNOVAs using Procrustes shape and form data for testing whether the mean shape of Lomekwi M_1s differ from the M_1s of *Au. anamensis*, *Au. afarensis*, *Au. africanus*. P-values in bold are significant. FDR corrected values are presented inside the parentheses. Note that KNM-WT 38339 was not included in the analyses due to the uncertainty regarding the position of the molar.

Procrustes shape pairwise permutational MANOVAs (10000 permutations)

Taxon	*Au. afarensis*	*Au. africanus*	*Au. anamensis*
Au. africanus	**0.002 (0.006)**	-	-
Au. anamensis	**0.003 (0.012)**	0.107 (0.177)	-
Lomekwi	0.080 (0.177)	0.344 (0.370)	0.512 (0.490)

Procrustes form pairwise permutational MANOVAs (10000 permutations)

Taxon	*Au. afarensis*	*Au. africanus*	*Au. anamensis*
Au. africanus	**0.002 (0.015)**	-	-
Au. anamensis	**0.032** (0.066)	**0.002 (0.006)**	-
Lomekwi	0.565 (0.562)	**0.027** (0.066)	0.135 (0.181)

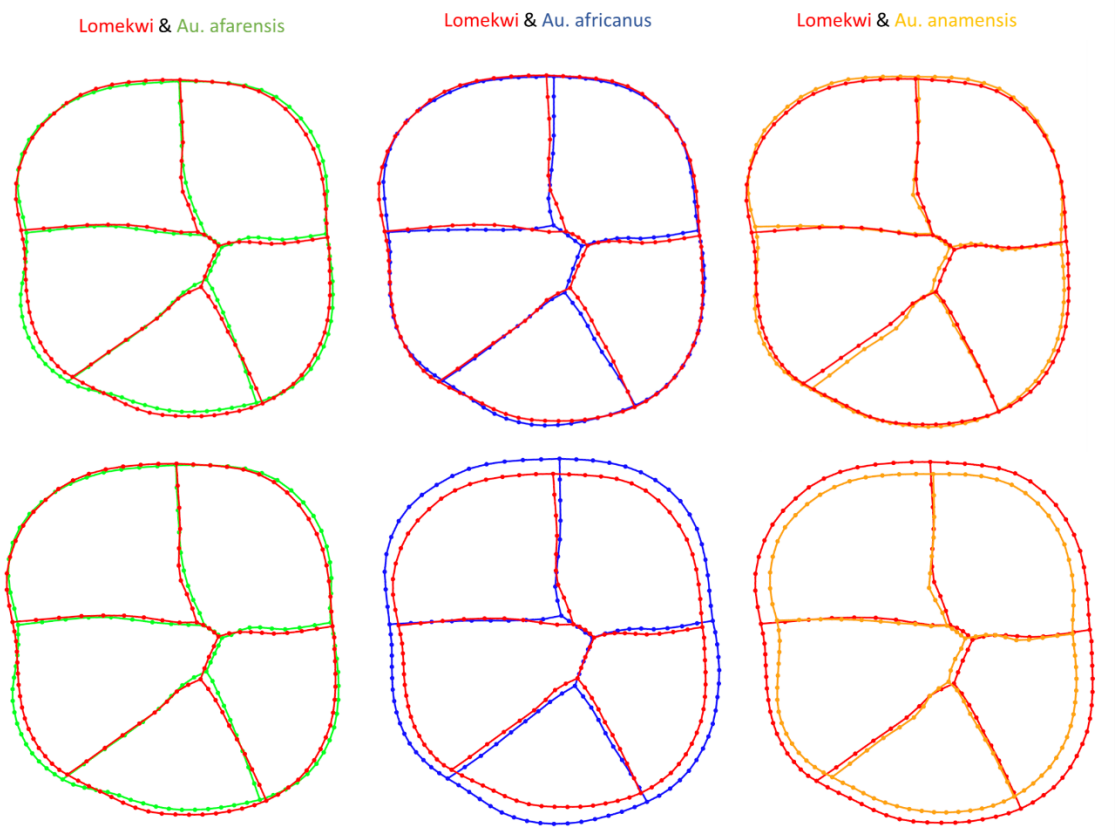

Figure 3.23. Top: the mean shape of Lomekwi M_1s (red) compared to the mean shape of the M_1s of *Au. afarensis* (green), *Au. africanus* (blue), and *Au. anamensis* (orange). Bottom: the mean shape *and* size of Lomekwi M_1s (red) compared to the mean shape *and* size of the M_1s of *Au. afarensis* (green), *Au. africanus* (blue), and *Au. anamensis* (orange)

Second molars

Among the Lomekwi M_2s and KNM-WT 38339, KNM-WT 38333 and KNM-WT 38349 showed a strong tendency to classify as Lomekwi in both Procrustes shape and form CVAs with cross-validation (Table 3.10). However, both molars are relatively different in shape: KNM-WT 38333 has and ovoid crown outline that tapers distally, whereas the crown shape of KNM-WT 38349 is more of a squared oval. The mesiobuccal fissure in KNM-WT 38333 is rather unique for its upward curve, while the fissure in KNM-WT 38349 is straight. However, both share a very small hypoconulid. Thus, it is likely that both molars classified as Lomekwi mainly due to their distinct

hypoconulid (see Discussion) that separates them from the other *Australopithecus* taxa in the sample. KNM-WT 38359b classified 8.3% of the time as Lomekwi, which could be explained by the relatively small hypoconulid of the molar as well (this can be observed in the shape of the molar when it is compared to the mean shape of *Australopithecus* M_2s, and its PC1 scores in the M_2s PCA plot (Figure 3.18)). KNM-WT 38339 classified as Lomekwi in 8.3% of the Procrustes shape CVAs probably due to its square shaped crown and the lack of distal tapering, which can be observed to some extent in the crown shape of KNM-WT 38349. The increase in the number of times KNM-WT 38359b and KNM-WT 38339 classified as Lomekwi in Procrustes form CVAs can be attributed to the similarity in the size of the molars.

Table 3.10
Classification results of CVAs with cross-validation using M_2s Procrustes form and shape data with Lomekwi molars treated as known. Shaded cells indicate the majority of the classification results.

	Procrustes shape (2-12 PCs)			
Specimen	*Au. afarensis*	*Au. africanus*	*Au. anamensis*	Lomekwi
KNM-WT 38333		8.3%		91.7%
KNM-WT 38349				100.0%
KNM-WT 38359b		83.3%	8.3%	8.3%
KNM-WT 38339		58.3%	33.3%	8.3%

	Procrustes form (2-8 PCs)			
Specimen	*Au. afarensis*	*Au. africanus*	*Au. anamensis*	Lomekwi
KNM-WT 38333		25.0%		75.0%
KNM-WT 38349				100.0%
KNM-WT 38359b	25.0%	25.0%	25.0%	25.0%
KNM-WT 38339	75.0%		12.5%	12.5%

PERMANOVA using Procrustes shape and form data found statistically significant differences between the mean shape of the M_2s of Lomekwi and *Au. afarensis* and *Au. africanus*, but not *Au. anamensis* (Table 3.11). In PERMANOVAs using Procrustes shape data, these are the only

significant results. The mean shape of Lomekwi M_2s is compared to the mean shapes of the M_2s of *Au. afarensis*, *Au. africanus*, and *Au. afarensis* in Figure 3.24. The mean shape of Lomekwi M_2s is most similar to the mean shape of *Au africanus* M_2s, and exhibits similar crown shape differences from the mean shapes of the molar in *Au. anamensis* and *Au. afarensis*. The mean shapes are not consistent with the PERMANOVA results for Lomekwi and *Au. anamensis*, which could be explained by the small sample size of n=3 of both groups, precluding the PERMANOVA from finding significant differences.

Lomekwi M_2s differ from the M_2s of the three taxa by having a larger metaconid, protoconid, hypoconid, and entoconid, as well as a smaller hypoconulid. The mesiobuccal fissure in Lomekwi M_2s shows a mesial deflection just before intersecting with the mesial longitudinal fissure, whereas in other taxa the fissure follows a relatively straight line. However, because of the small size of the Lomekwi sample, the morphology of fissure is representative of KNM-WT 38333 rather than that of the whole sample.

Table 3.11
Results of pairwise PERMANOVAs using Procrustes shape and form data for testing whether the mean shape of Lomekwi M_2s differ from the M_2s of *Au. anamensis*, *Au. afarensis*, *Au. africanus*. P-values in bold are significant. FDR corrected p-values are presented inside the parentheses. Note that KNM-WT 38339 was not included in the analyses due to the uncertainty regarding the position of the molar.

Procrustes shape pairwise permutational MANOVAs (1000 permutations)

	Au. afarensis	*Au. africanus*	*Au. anamensis*
Au. africanus	0.126 (0.187)	-	-
Au. anamensis	0.338 (0.319)	0.121 (0.187)	-
Lomekwi	**0.002 (0.015)**	**0.005 (0.015)**	0.100 (0.187)

Procrustes form pairwise permutational MANOVAs (1000 permutations)

	Au. afarensis	*Au. africanus*	*Au. anamensis*
Au. africanus	**0.033** (0.052)	-	-
Au. anamensis	0.500 (0.508)	0.380 (0.408)	-
Lomekwi	**0.017** (0.051)	**0.002 (0.012)**	0.100 (0.150)

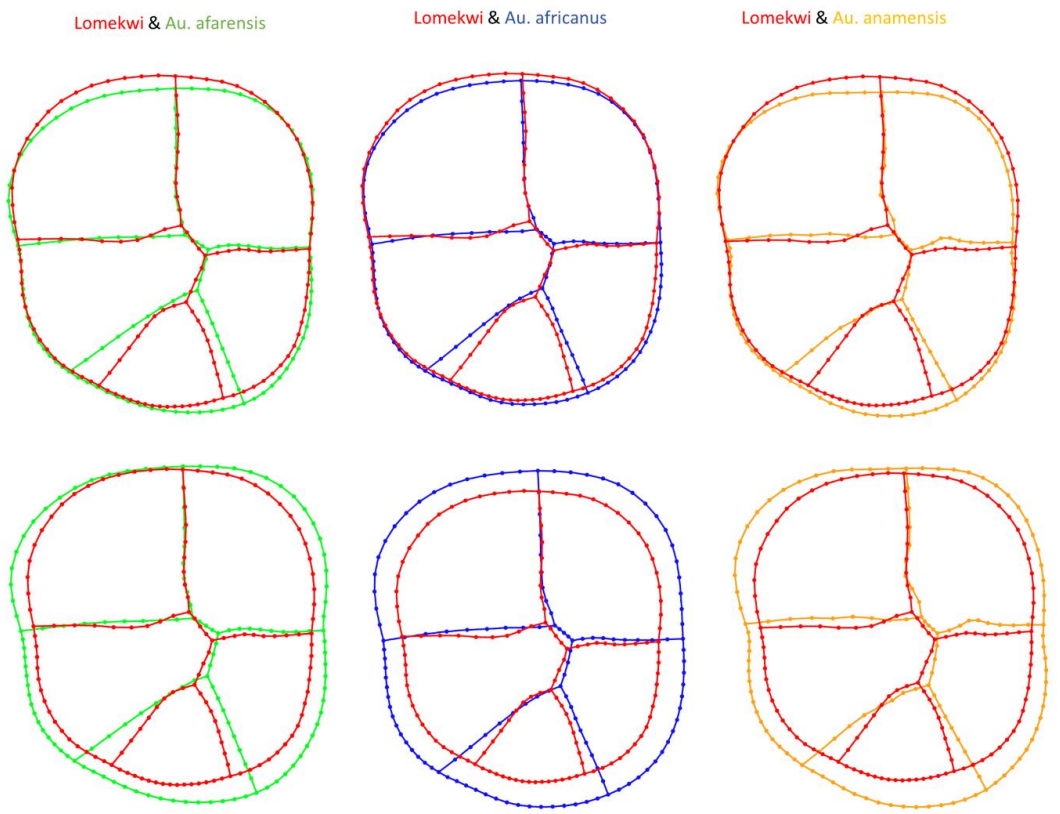

Figure 3.24. Top: the mean shape of Lomekwi M_2s (red) compared to the mean shape of the M_2s of *Au. afarensis* (green), *Au. africanus* (blue), and *Au. anamensis* (orange). Bottom: the mean shape *and* size of Lomekwi M_2s (red) compared to the mean shape *and* size of the M_2s of *Au. afarensis* (green), *Au. africanus* (blue), and *Au. anamensis* (orange). Note the especially reduced hypoconulid in Lomekwi M_2s.

Third molars

In Procrustes shape CVAs with cross-validation, KNM-WT 16006 and KNM-WT 38347 classified as Lomekwi 36.4% and 27.3% of the time, respectively (Table 3.12). The relatively similar shape of the hypoconid and the mesial half of the metaconid in both molars could explain the results. In Procrustes form CVAs with cross-validation only KNM-WT 38347 classified as Lomekwi (100%). The interpretation of these results is more difficult. While the size of KNM-WT 16006 is relatively small, it is not the smallest molar in the sample. However, the size of the molar, in conjunction with crown morphology, may have been sufficient to classify KNM-WT 38347 as Lomekwi.

Table 3.12
Classification results of CVAs with cross-validation using M_3s Procrustes form and shape data with Lomekwi molars treated as known. Shaded cells indicate the majority of the classification results.

	Procrustes shape (2-11)			
Specimen	*Au. afarensis*	*Au. africanus*	*Au. anamensis*	*Lomekwi*
KNM-WT 16006	36.4%		18.2%	36.4%
KNM-WT 38347	9.1%	45.5%	9.1%	27.3%

	Procrustes form (2-8)			
Specimen	*Au. afarensis*	*Au. africanus*	*Au. anamensis*	*Lomekwi*
KNM-WT 16006	71.4%		28.6%	
KNM-WT 38347				100.0%

No statistically significant differences were found between the Lomekwi M_3s and *Au. afarensis*, *Au. africanus*, and *Au. anamensis* in PERMANOVAs using Procrustes shape data, whereas a statistically significant difference was found between Lomekwi and *Au. africanus* M_3s ($p=0.028$, df=(1,11), Pseudo-F=7.4389, SS=0.1217, $R^2=0.404$) in PERMANOVA using Procrustes form data (Table 3.13). The Procrustes shape data results are consistent with the overlap between the mean shape of Lomekwi M_3s and the mean shapes of the molar in the *Australopithecus* taxa in

the sample (Figure 3.25). The crown shape of Lomekwi M_3s is subrectangular and tapers distally, which is more similar to the shape of the crown in *Au. afarensis* and *Au. anamensis*. The shape and position of the hypoconulid relative to the other cusps in Lomekwi M_3s are more similar to *Au. africanus*, whereas the shape of the entoconid is shared with *Au. afarensis*. The morphology of the mesial longitudinal fissure and the occlusal outline of the crown mostly resemble that of *Au. anamensis*.

Table 3.13
Results of pairwise PERMANOVAs using Procrustes shape and form data for testing whether the mean shape of Lomekwi M_3s differ from the M_3s of *Au. anamensis*, *Au. afarensis*, *Au. africanus*. P-values in bold are significant. FDR corrected p-values are presented inside the parentheses.

Procrustes shape pairwise permutational MANOVAs (1000 permutations)			
	Au. afarensis	*Au. africanus*	*Au. anamensis*
Au. africanus	0.166 (0.350)	-	-
Au. anamensis	0.708 (0.710)	**0.028** (0.190)	-
Lomekwi	0.539 (0.640)	0.425 (0.570)	0.300 (0.570)

Procrustes form pairwise permutational MANOVAs (1000 permutations)			
	Au. afarensis	*Au. africanus*	*Au. anamensis*
Au. africanus	**0.017** (0.072)	-	-
Au. anamensis	0.923 (0.937)	**0.035** (0.072)	-
Lomekwi	0.215 (0.240)	**0.028** (0.072)	0.200 (0.240)

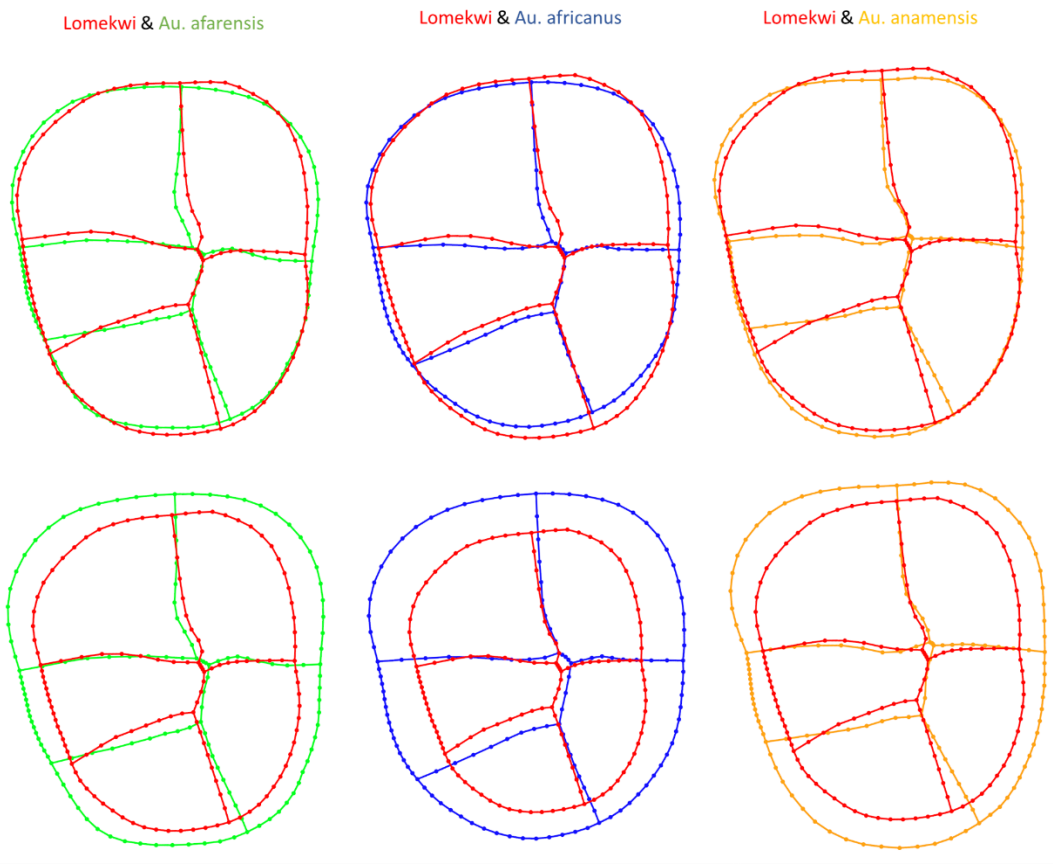

Figure 3.25. Top: the mean shape of Lomekwi M_3s (red) compared to the mean shape of the M_3s of *Au. afarensis* (green), *Au. africanus* (blue), and *Au. anamensis* (orange). Bottom: the mean shape *and* size of Lomekwi M_3s (red) compared to the mean shape *and* size of the M_3s of *Au. afarensis* (green), *Au. africanus* (blue), and *Au. anamensis* (orange).

CHAPTER 4: DISCUSSION

4.1 Taxonomic signal in traditional measurements of crown morphology

The results of the performance of different data types for capturing tooth crown morphology (GM shape and form, relative and absolute cusp areas, MD and BL measurements, and crown shape and crown size indices), suggest that GM data has the best ability to discriminate between the four taxa used in the analyses, and correctly classify a larger number of specimens to their respective taxonomic group. However, MD and BL measurements are the most commonly reported data when describing teeth and naming new species (e.g. Robinson, 1956; Johanson and White, 1979; Leakey et al., 1995, 2001). The utility of this data is good for differentiating between taxa that show marked differences in tooth size, but diminishes when the size of teeth are similar between taxa. Furthermore, the crown shape and crown size indices, which are derived from MD and BL data, provide only rudimentary information about tooth crown morphology. To realize the potential of dental remains in hominin taxonomic studies, Wood et al. (1983, 1987, 1988) conducted a series of analyses on the relative cusp areas of the dentition of East and South African hominins that were known at that time. In the current study, the performance of relative cusp area data was poor at both correctly classifying molars and detecting differences between group means. The performance improved in the analyses of the mandibular molar types of *Au. afarensis*, where each molar type showed a distinct relative cusp area pattern. The methods employed in this study slightly differed from those employed by Wood et al. (1983), who ran a number of t-tests using the relative cusp area

of each cusp. However, considering the large p-values returned by PERMANOVAs, it is highly unlikely that many significant differences would have been detected in t-tests.

Another consideration is the sample structure and size. Wood et al. (1983) compared between *P. robustus*, *P. boisei*, *Au. africanus*, *H. erectus*, and *H. habilis*, and had a relatively large sample size for each taxon. It is possible that differences between relative cusp areas are more marked between those taxa, than between the four taxa used in the current study. While relative cusp areas are able to provide more information about tooth crown morphology, and potentially distinguish between taxa at the genus level (Wood, Abbott and Graham, 1983; Grine et al., 2009), the current study revealed some limitations to this approach, with MD and BL data outperforming relative cusp areas in most analyses. However, absolute cusp area data performed nearly as well as GM data. The overall good performance of data types that capture size is most likely due to the composition of the sample, which included four taxa that exhibit marked differences in tooth size. Thus, MD and BL and absolute cusp area data may be useful in distinguishing between taxa that show significant differences in tooth size. However, pronounced sexual dimorphism and intra-sex variation in body size may increase the range of tooth size in a species and result in overlap in tooth size with other taxa. An example is the GDA2 mandibular second molar (Menter et al., 1999) that, in size, falls within the range of *P. boisei* and outside of *P. robustus*, while an analysis of the relative cusp areas of the molar suggests that it is more similar to *P. robustus* (Grine et al., 2012). Thus MD and BL data, and to some extent absolute cusp area data, may lead to unreliable or incorrect taxonomic classifications.

Overall, in the present study GM data has shown a number of advantages over commonly employed methods for studying tooth crown morphology. These include a better power to correctly identify the taxonomic affinities of individual specimens; useful visual supplements to the results in the form of mean shapes and TPS grids that manage to convey a larger range of morphological detail than do linear measurements or cusp areas, and, subsequently, a better performance at finding differences between group means.

4.2 Challenges to 2D GM assessement of crown morphology

There are however a number of limitation to the 2D GM approach. GM requires anatomical landmarks to be homologous, that is, they must describe the same anatomical loci across all specimens (Zelditch et al., 2004). Adherence to this principal may not always be possible, since the same anatomical structure (e.g. teeth, bones, or the shape of an organism) may show variability in the expression or presence/absence of morphological features across and within taxa, an issue which has been encountered in this study as well. Hominin lower molars sometimes have accessory cusps: a C6, which usually lies within the distal fovea between the entoconid and hypoconulid, and a C7, which lies on the lingual border of the crown between the entoconid and metaconid. The rate of expression of these traits differs between taxa, e.g. C6 is most commonly observed in *Paranthropus* M_1s (Wood, Abbot and Graham, 1983), and C7 is more prevalent in the M_1s of early *Homo* (Wood, Abbot and Graham, 1983). Because landmarking accessory cusps would require placing additional landmarks on non-homologous biological structures, which would violate the assumption of homology and equal number of landmarks per specimen, it was not possible to account for such morphological variation in this study. Furthermore, because relative and absolute cusp areas were derived from landmark

data, the same issues applied to these datasets as well. Generally, cusp areas data can be used to account for the presence of accessory cusps and protostylid (Wood, Abbot and Graham, 1983; Wood et al., 2013).

Furthermore, because GM requires molars to have enough of the morphology preserved for a meaningful morphological comparison, sample sizes can be very small (e.g. Skinner et al., 2008). The GM approach employed in this study focused on fissures and crown shape and not on cusp tips (e.g. Martinon-Torres, 2006) due to the tendency for fissures to remain visible even the tooth is heavily worn. Thus, this approach can match the sample sizes used in studies of hominin cusp areas. However, sometimes wear does lead to the erosion of parts of the fissures, or their complete obliteration. For example, in the *Au. afarensis* M_1s sample in this study, it was common for the mesial longitudinal fissure to be heavily worn. Fissures corrected for wear may not always be able to catch nuances of the original morphology of the fissure. Furthermore, the projection of the fissures when the tooth is viewed from occlusal view changes with the rotation of the tooth, which necessitates that differences between rotations should be small. It is of note that the same issues are pertinent to cusp area measurements as well. However, both issues can be overcome by rotating and landmarking a tooth a number of times and testing for cusp delineation and rotation errors.

In GM studies it is common to reduce the dimensionality of the data (that is, landmark coordinates) via PCA. It is done when the number of variables exceeds the number of cases. If the Procrustes shape coordinates are used in a CVA when the sample size is smaller than the number of landmarks, it can lead to unreliable classification results (Mitteroecker and Bookstein, 2011). While PCA dramatically reduces the number of variables, their number may

still exceed the number of cases, which is especially common in hominin studies (Gomez-Robles et al., 2007, 2008, 2011, 2012; Skinner et al., 2008). This may require using a reduced number of PCs that do not account for all the morphological variation present in the sample. Large group differences are represented by the first few PCs, while smaller differences are represented by a larger number of PCs, which is usually unknown. Thus, the necessity to use a reduced number of PCs may diminish the ability of CVA to separate between groups. Furthermore, variable reduction by PCA prior to CVA does not always guarantee that small group differences will be accounted for (Mitteroecker and Bookstein, 2011).

Another issue in GM analysis is accounting for size. A Generalized Procrustes Analysis (GPA) is often used on the raw landmark coordinates in order to correct for orientation, location, and remove geometric size (Zelditch et al., 2004). Size is returned as centroid size, which is the square root of the sum of squared distances of all the landmarks of an object from their centroid. It can then be included in a PCA with the Procrustes shape coordinates in order to introduce size as a variable. In this instance, the first PC accounts only for size. However, size also accounts for the variance in subsequent PCs, although at different levels. Thus, the interpretation of what variation (that is, shape and/or size) is explained by each PC becomes difficult, which further complicates the interpretation of CVA results.

The small size of the sample, the number of variables and the number of CVAs have to be considered when interpreting the results. Even though the morphological variation explained by each PC diminishes with each subsequent PC, the distribution of specimens in shape space can change dramatically. Some PCs may account for morphological variation (however small) shared by two specimens, and subsequently assign them to the same group. For example,

KNM-WT 16006 and KNM-WT 38347 plot far apart from each other in PCs 1,2, and 3 (Figures 3.21 and 3.22). These PCs explain 68.3% of the morphological variation. The Lomekwi M_3s start to classify as their own group at PC7, which accounts for 5.5% of the variation. Thus, if any morphological features are shared between the two specimens, they might be very small and their significance in differentiating betwen taxa should be closely evaluated. In the case of KNM-WT 16006 and KNM-WT 38347, it is probably parts of the the metaconid and the hypoconulid that are similar between the two. However, it is difficult to interpret which exact morphological features are shared between the molars due to the dimensionality reduction in both PCA and CVA. Nevertheless, 2D GM shape analysis was still able to perform well and convey a detailed morphological representation of the molars compared to the linear measurements and cusp areas datasets.

4.3 Tooth position ambiguity

Determining the tooth position of isolated teeth can yield ambiguous results, even when a number of morphological features are assessed in multiple analyses (e.g. Suwa 1996, Skinner et al., 2008). In the present study, the determination of the tooth positions of the Lomekwi molars showed consistent classification results for most teeth, with both the GM and cusp areas datasets being largely in agreement with each other. The high correct CVA classification results of the tooth types using both GM and cusp areas data suggest that there is relatively little overlap between the molar types of *Australopithecus* in multivariate space across different configurations of PCs. This in turn suggests that the Lomekwi molars that consistently classified as one molar type were closer to the centroids of one of these groups across all analyses. Because the reference population (i.e. *Australopithecus*) determines the multivariate

distribution of the tooth type groups, it can be suggested that these Lomekwi molars show morphological features that are consistent with those of *Australopithecus* molar types. Thus, in a way, the tooth position results suggests that the crown morphology of most Lomekwi molars is consistent with that of *Australopithecus*. However, there are some uncertainties regarding the position of KNM-WT 38339, KNM-WT 38347, and potentially KNM-WT 38333. The ambiguity of the results may stem from the unusual morphology of KNM-WT 38339, which has a dramatically reduced entoconid, and that of KNM-WT 38333, which exhibits a very small hypoconulid and unusual fissure patterning. KNM-WT 38347 shares many of its tooth crown morphological characteristics with *Australopithecus* M_3s but is very small. The ambiguity in the tooth position classification results of these molars may suggest that they exhibit features that are unusual to the *Australopithecus* hypodigm.

4.4 Taxonomy of Lomekwi

4.4.1 Similarities to *Australopithecus*

Lomekwi molars did not show a tendency to classify as either one of the three *Australopithecus* taxa across all Procrustes shape analyses. Only the M_2s showed a strong trend towards *Au. africanus*. However, the Lomekwi M_2s are smaller than all the *Au. africanus* M_2s in the sample. In fact, the Lomekwi M_2s are smaller than all *Au. africanus* M_2s for which size measurements are available (Moggi-Cecchi et al., 2006; Grine et al., 2013). The age of the Lomekwi molars ranges from 3.53mya to 3.2mya (Leakey et al., 2001), which does not overlap with the age of *Au. africanus* bearing sites. The closest in time are Member 2 at Sterkfontein at 3.67mya (Granger et al., 2015), and Makapansgat Member 3 which has an earliest age of 3.03mya

(Herries et al., 2013). Thus based on the age and location of the Lomekwi molars, it is highly unlikely that the second molars, or the Lomekwi sample generally, belong to *Au. africanus*. A more likely explanation is that because the CVA cannot leave specimens unclassified, the high morphological variability in *Au. africanus* M_2s may allow the Lomekwi molars to find more common features with this taxon and classify as it. A more likely relationship to *Au. africanus* could be considered regarding KNM-WT 66291, KNM-WT 38339, and KNM-WT 38359a and KNM-WT 38359b, as they all share a well developed protostylid which is highly characteristic of *Au. africanus* and to a lesser degree of *Au. anamensis*, while it is uncommon in *Au. afarensis* (Hlusko, 2004). However, the current GM analysis was not able to account for the presence of a protosylid, and it is outside the scope of the present study to make phylogenetic inferences based on this trait. It is important to note that KNM-WT 66291 did classify as *Au. africanus* in the majority of CVAs and plotted within the taxon in shape space PCA, most likely because the molar shares an elongated oval crown shape and a centrally positioned mesial longitudinal fissure with the taxon. The same features probably underlie the classification of KNM-WT 38342 and KNM-WT 34334 as *Au. africanus* as well. However, only KNM-WT 66291 would comfortably fit within *Au. africanus* as the size of the other Lomekwi M_1s is outside the range of the taxon.

Some Lomekwi molars showed relatively consistent classification results as *Au. anamensis* in Procrustes shape CVAs, namely KNM-WT 66291, KNM-WT 38342, and especially KNM-WT 38359a. The latter two also classified as *Au. anamensis* in most Procrustes form CVAs. However, KNM-WT 66291 and KNM-WT 38342 also classified as *Au. afarensis* in approximately half of the analyses, and it is KNM-WT 38359a that classified as *Au. anamensis* the majority of the time

and may be of interest. When the molar is compared to the *Au. anamensis* M_1 KNM-KP 31712J, it is evident that they share a few similarities that may have influenced the Lomekwi molar to classify as *Au. anamensis* (Figure 4.1).

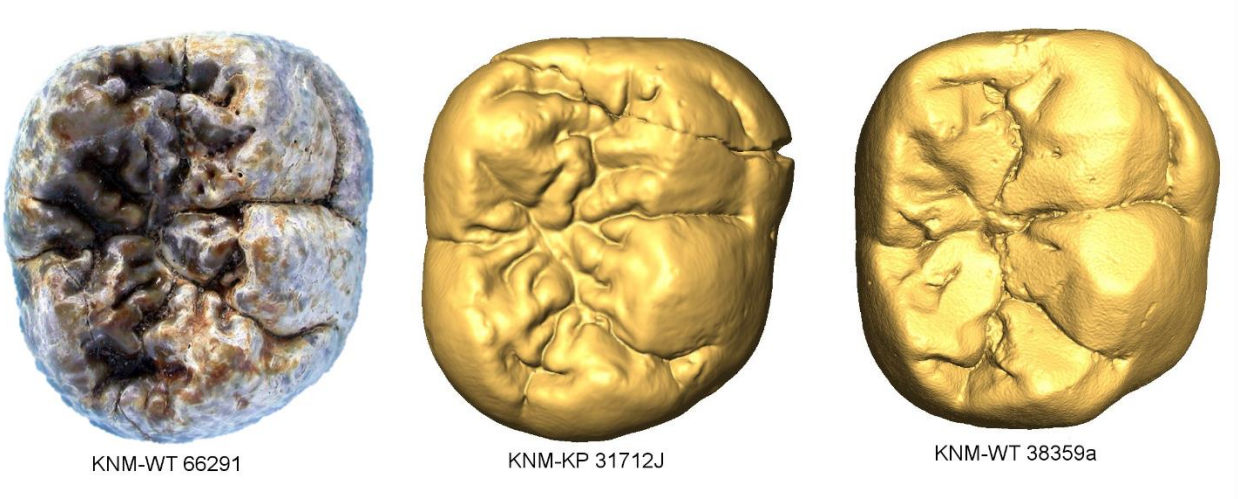

Figure 4.1. Two Lomekwi molars (far left and far right) compared to an *Au. anamensis* lower first molar (centre). Note the similarity in the protostylid and the numerous secondary fissures between the molars.

The cusp proportions of both molars are similar, and the well developed protostylids result in a buccal expansion of the mesiobuccal face of the crown. Furthermore, both exhibit a lingually expanded mesial fovea, and a distobuccal fissure that deflects disto-lingually due to the expansion of the hypoconid. KNM-WT 66291 is depicted as well to emphasize the crenulated enamel and the well developed protostylid, which are shared with KNM-KP 31712J.

This raises the question if some Lomekwi specimens might be phylogenetically related to *Au. anamensis*. The members of *Au. anamensis* lie within an age range of 4.2-3.8mya (Brown et al., 2013), which is ~300,000 years older than Lomekwi. However, representative fossils of *Au. anamensis* from Kanapoi, southwest of Lake Turkana (Leakey et al., 1995) share a temporal overlap with Lomekwi, which is situated west of Lake Turkana. Thus, if the Lomekwi specimens

mentioned above are *Au. anamensis*, then it would make them the latest known members of the taxon. Conversely, if the Lomekwi specimens represent a single species, they may have an evolutionary relationship with *Au. anamensis*, in this instance evolving from it.

Among all molars, KNM-WT 8556 showed the most consistent tendency to classify as *Au. afarensis* and plot near the taxon in shape space PCA. In the initial description of the mandible, Brown, Brown and Walker (2001) assigned it to *Au. afarensis* based on mandibular and dental morphological similarities with the taxon. Features that distinguish the mandible from *Au. afarensis*, such as the morphology of the P_3 and P_4, and the relative size of the P_4 to M_1, were noted by the authors, and later by Leakey et al. (2001). In their comparison of the M_1 of KNM-WT 8556 to A.L 333w-60 Brown, Brown and Walker (2001) noted that its hypocunulid is larger. The current study confirms that the hypoconulid of KNM-WT 8556 is larger than those of any *Au. afarensis* representatives from Hadar used in this study, and is matched by the only Laetoli specimen in the sample – LH3t. However, the hypoconulid of LH3t is wide at its base but otherwise narrow, whereas the hypoconulid in KNM-WT 8556 has a uniform triangular, wide outline (Figure 4.2).

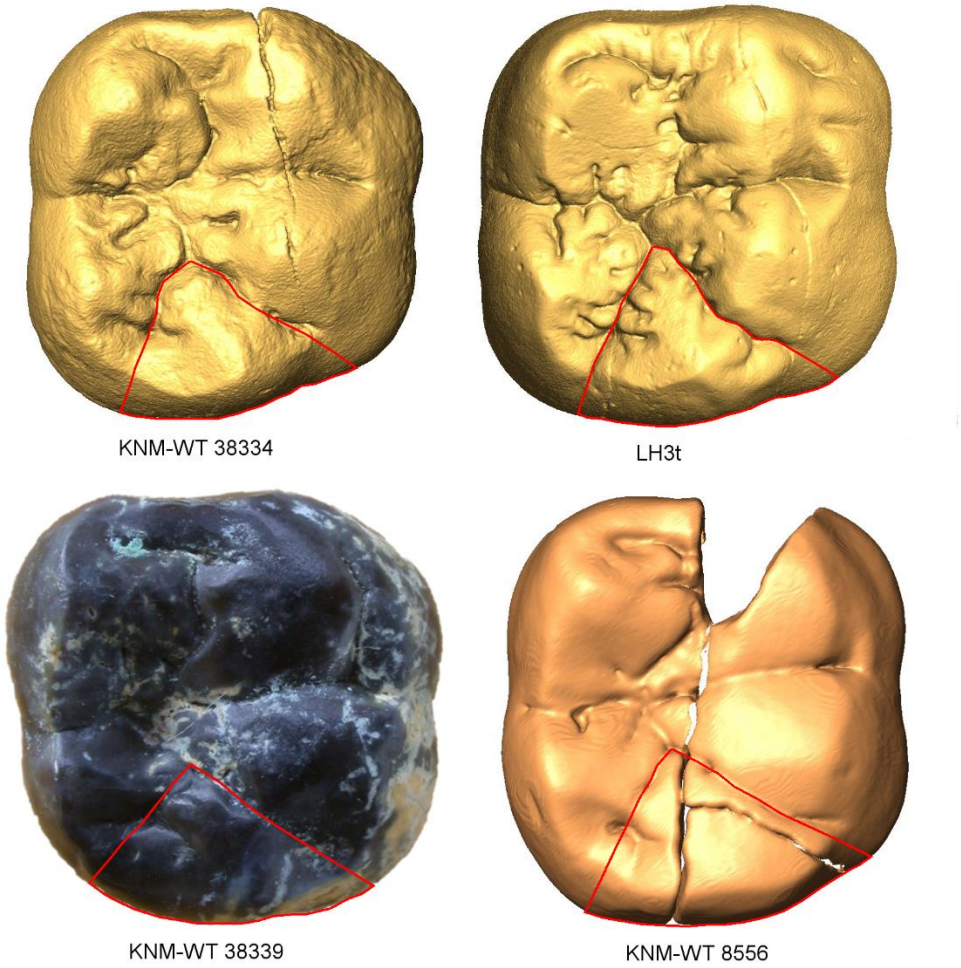

Figure 4.2. The relatively large hypoconulid in KNM-WT 8556, KNM-WT 39339, and KNM-WT 38334 compared to the largest hypoconulid in the *Au. afarensis* sample exhibited by the specimen LH3t.

Overall, KNM-WT 8556 exhibits a classic *Au. afarensis* M_1 shape, and the present study supports the close relation of KNM-WT 8556 to *Au. afarensis*. A GM study of the P_4 of KNM-WT 8556 also suggests similarities to *Au. afarensis* (Haile-Selassie, 2015), and the enamel thickness of the first molar places it close to *Au. africanus* and *Au. afarensis* (Skinner et al., 2015).

The KNM-WT 16006 mandible was also initially assigned to *Au. afarensis* (Brown, Brown and Walker, 2001), though the authors did enumerate ways in which the morphology of the mandible and the dentition departed from *Au. afarensis*, such as the large cingulum of its M_3

which is not seen in any Hadar or Laetoli specimens. Later, the mandible has been reassigned to cf. *Kenyanthropus platyops* (Wood and Leakey, 2011). In the shape space PCA, the molar plots near *Au. afarensis* and *Au. anamensis*, but does not fall within the distribution of either taxon. It departs from *Au. afarensis* mainly due to a more centrally placed distolingual fissure, and the relatively smaller metaconid and protoconid, which are shared with *Au. anamensis*. The reduction in the size of these two cusps probably led the molar to classify as *Au. anamensis* in half of the Procrustes shape CVAs. Overall, the result did not suggest that KNM-WT 16006 is more similar *to Au. afarensis* than to *Au. anamensis*.

4.4.2 Lomekwi as its own taxon

In Procrustes shape CVAs with cross-validation, some of the Lomekwi molars classified as their own group. The most significant results come from the M_2s, with KNM-WT 38333 and KNM-WT 38349, which classified as Lomekwi over 90% of the time. However, it is difficult to say whether these results can be interpreted to mean common taxonomy. Neither molar overlaps with other *Australopithecus* taxa, but the main morphological feature driving this separation is their small hypoconulids. This is especially evident by the classification results of KNM-WT 38339, which has a large hypoconulid, and classified only once out of 12 CVAs as Lomekwi. Apart from the size of their hypoconulids, their morphology is rather different. The crown shape of KNM-WT 38333 is ovoid with a bucco-lingually expanded mesial moiety, whereas KNM-WT 38349 is square shaped. KNM-WT 38333 has a large mesial fovea that expands buccally, and the molar lacks a protostylid. KNM-WT 38349 has a well developed protostylid and smaller, symmetrical mesial fovea. Both share a highly crenulated enamel surface. Thus, the classification results do not necessarily imply a close evolutionary relationship. Among the other two molar types,

KNM-WT 38339, and to some extent KNM-WT 38347 and KNM-WT 16006, tended to classify as Lomekwi in Procrustes shape CVAs. KNM-WT 38339 favours Lomekwi probably due to its large hypoconulid, which is shared to some degree with KNM-WT 8556 and KNM-WT 38334 (see below).

Generally, based on Procrustes shape results, it is difficult to say if the Lomekwi sample as a whole can be considered as belonging to its own taxon. There is also a possibility that Lomekwi samples multiple taxa. The classification results do suggest some morphological commonalities between the Lomekwi specimens across tooth positions, but these may constitute small parts of the crown morphology. However, what unites the Lomekwi sample is their small size. Only KNM-WT 66291 and KNM-WT 8556 are an exception to that (Figure 3.12). All M_1s and M_2s plot within the lower range of the size of *Au. afarensis* M_1s and M_2s. The M_1s plot within the middle range of *Au. anamensis* M_1s, and in the lower end of *Au. anamensis* M_2s. The size of the only preserved upper second molar of KNM-WT 40000 falls outside the range of *Australopithecus,* which suggests that *K. platyops* had small teeth (Leakey et al., 2001). Thus, the small size of the Lomekwi specimens and some of the morphological features shared between them that distinguish the sample from known East African *Australopithecus*, may make *K. platyops* as one of the possible taxa candidates that the molars may belong to.

4.5 Lomekwi molars that could be considered as morphological outliers

KNM-WT 38333

The M_2 exhibits a dramatically reduced hypoconulid, which is unusual in *Australopithecus*. The molar strongly influenced the morphological variation associated with PC1 in shape space PCA and did not overlap with any taxa (Figure 3.17). Among the *Australopithecus* taxa, the *Au. afarensis* M_2 A.L 417-1a exhibits the smallest hypoconulid, but its size is still approximately twice as big as the cusp in KNM-WT 38333. A reduced hypoconulid is common in *H. neanderthalensis* M_2s, and sometimes it is absent altogether (Bailey, 2002). A lack of C5 is most common in *H. sapiens*, though there is intraspecies variability in the expression of the trait, with some individuals possessing the cusp (Scott and Turner, 1997). In the current sample, the Neanderthal M_2 KRP53 had the smallest hypoconulid, although it is still slightly larger than KNM-WT 38333 (Figure 4.3). Of note is also the difference in the morphology of the hypoconulids between KNM-WT 38333 and the two molars. In the Lomekwi molar, it is short and originates in the distal portion of the crown, whereas in the other taxa it is longer, and emanates from near the centre of the crown. Based on the size of the hypoconulid alone, it may be suggested that KNM-WT 38333 could be related to early *Homo*, but the relative size of the cusp (0.060; Table 2, Appendix) is two times smaller than the smallest relative area of the cusp in East-African *Homo* (0.127; Wood Abbott and Graham, 1983). The recent discovery of a 2.8mya *Homo* mandible at Ledi-Geraru in Afar, Ethiopia (Villmoare et al., 2015) reduces the distance in time between *Homo* and the Lomekwi sample to ~400-500kya. While it is a considerable gap, comparing KNM-WT 38333 to the Ledi-Geraru mandible may allow elucidating the possible relation of the molar to early *Homo*.

KNM-WT 38333 also possess an unusual mesiobuccal fissure that strongly deflects mesially at the midpoint of the fissure due to the mesial and lingual-ward expansion of the hypoconid. Some degree of deflection is present in most molars regardless of taxa (which can also be seen in the KRP 53 and A.L 417-1a (Figure 4.3). Note that this assertion is based on the visual inspection of the specimens in the sample), however none show such an extreme expression of the trait. Overall, the taxonomic affiliations of KNM-WT 38333 remain unclear.

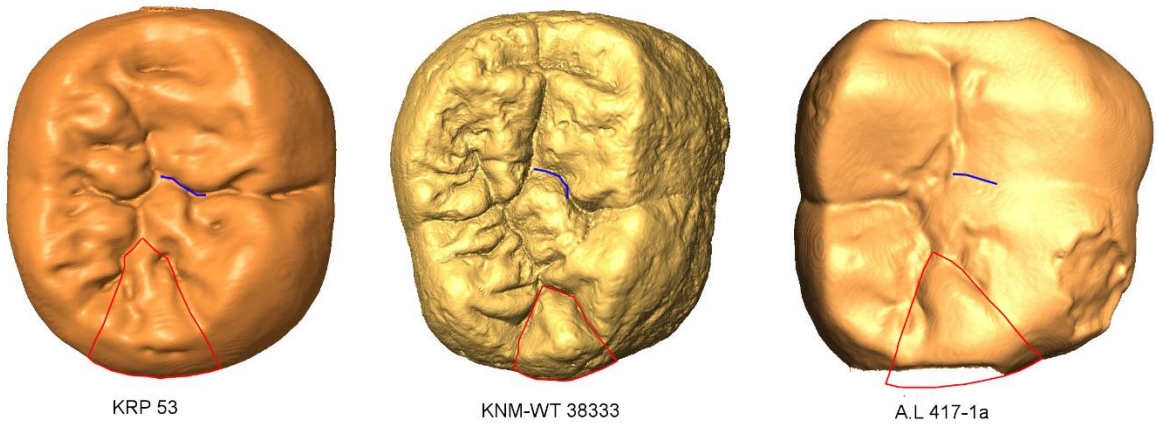

Figure 4.3. The hypoconulid (in red) of KNM-WT 38333 (middle) compared to the smallest hypoconulids of the M_2s *of H. neanderthalensis* (left) and *Au. afarensis* (right) in the sample. Note that both molars have a C6, which slightly inflates the size of the cusp. However, even without the C6 the- hypoconulid of both molars is larger than that of KNM-WT 38333. The upward deflection of the mesiobuccal fissure is depicted in blue.

KNM-WT 38339

The molar was not successfully assigned a position. It deviates from both the Lomekwi and *Australopithecus* samples for its relatively large BL dimension and the particularly reduced entoconid. The *Au. africanus* M_1 MLD2 has the smallest entoconid of all *Australopithecus* specimens used in the study and is compared to KNM-WT 38339 in Figure 4.4. Both molars also share a well developed protostylid and similar crown shape, albeit MLD2 have a more distally

projecting hypoconulid. KNM-WT 38339 is also compared to the M_1 STW 566, which was not used in this study since it has been attributed to *P. robustus* (Clarke, 1994; Kuman and Clarke, 2000). However, among the Sterkfontein Member 4 hominin M_1s, STW 566 exhibits the smallest entoconid (Grine, Delanty and Wood, 2013). Thus, KNM-WT 38339 and Stw 566 share a morphological feature that is unique among *Au. africanus*, and the *Au. afarensis* and *Au. anamensi*s representatives in the sample. KNM-WT 38339 is also compared to the *Au. africanus* M_2s STW 560E to show the similarities in the shape of the mesial longitudinal fissure and crown shape between them. The M_2s Procrustes shape CVA results did suggest that the molar is more similar to *Au. africanus*, whereas the M_1s results show that it is more similar to an *Au. afarensis* M_1. Its similarity to *Au. afarensis* is mostly due to the square shaped crown and the waisting at its midpoint. Overall, the taxonomy of KNM-WT 38339 remains unclear. It shares features with *Au. africanus*, mainly a well developed protostylid, which is usually absent or poorly expressed in *Au. afarensis* (Hlusko, 2004). However, its crown shape suggests affinities with *Au. afarensis*.

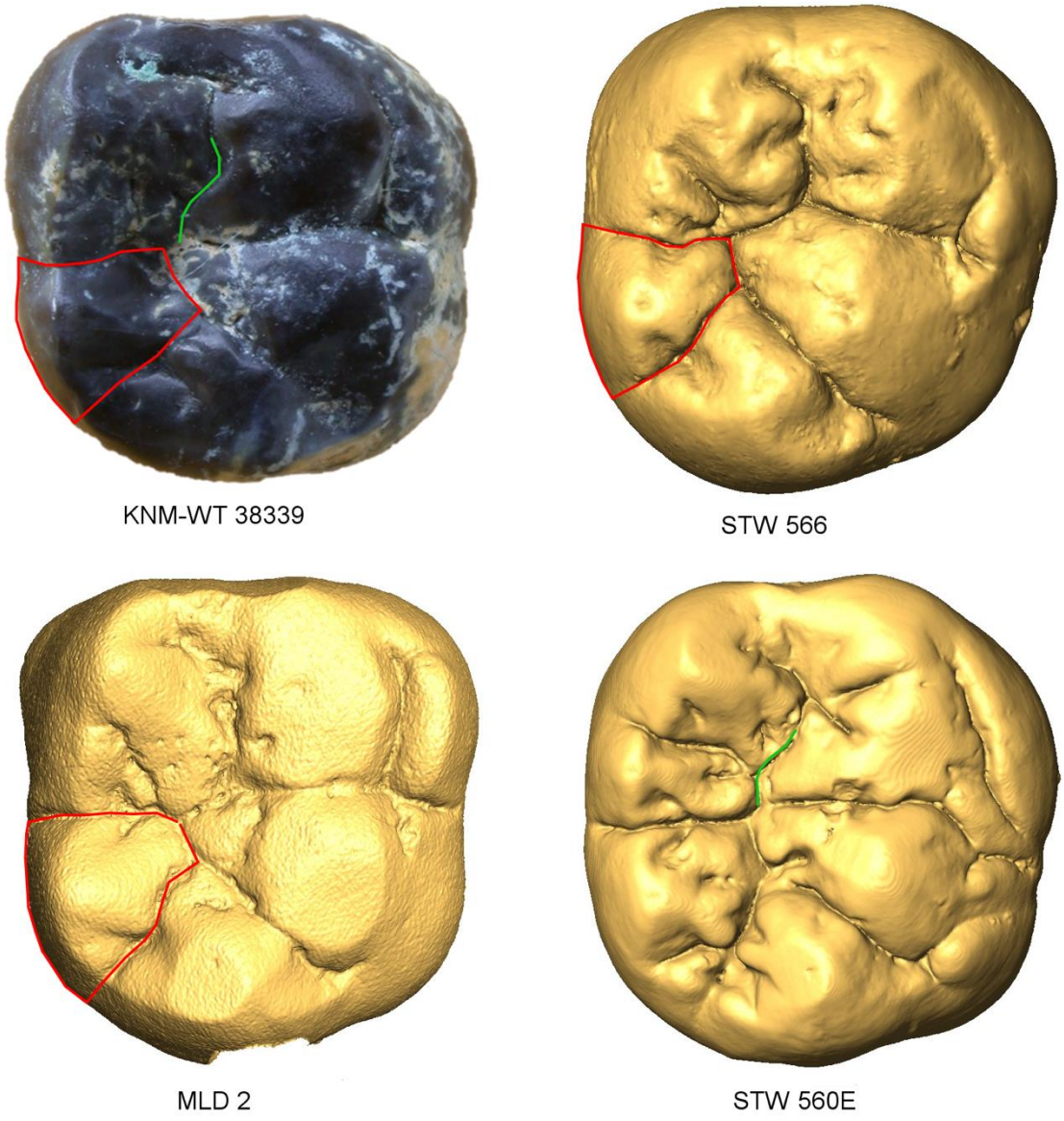

Figure 4.4. The entoconid (in red) and mesial longitudinal fissure (in green) of KNM-WT 38339 compared to *Au. africanus* specimens and STW 566.

KNM-WT 38347

Initially, the molar was described as a lower deciduous second molar (Leakey et al., 2001) and later confirmed as such (Wood and Leakey, 2011) based on its small size. The CVAs for determining tooth position consistently classified it as an M_3, and the molar has been assigned

to this position purely based on its crown morphology. However, it is the smallest molar in the sample (Figure 3.12). Its overall crown shape is more similar to *Au. afarensis* and *Au. anamensis*, whereas the size of the buccal base of the hypoconid is more similar to *Au. africanus*. The dentine horns of the cusps are high, which is characteristic of permanent teeth, as opposed to the low dentine horns in deciduous molars (Matthew Skinner, personal communication). The only preserved upper molar in the KNM-WT 40000 cranium is larger than KNM-WT 38347, and if the $M_3 > M_2 > M_1$ pattern holds true for *K. platyops*, then the M_3 would be expected to be larger. The dentition of K*. platyops* is considered to be smaller than that of any known *Australopithecus*. If KNM-WT 38347 is an M_3, as the results suggest, it may imply that in the occasion that the molar belongs to *K. platyops* or any other unknown taxa, the degree of sexual dimorphism may be very large in that species. Conversely, the members of that species could be small bodied as in *H. floresiensis* (Kaifu et al., 2015). If the molar is that of a known East African *Australopithecus*, then it would expand the known range of sexual dimorphism in that species considerably.

4.6 Future directions

One consideration would be to conduct a combined tooth types GM analyses, as the morphological variability along the molar row may be able to provide more information regarding the taxonomy or phylogeny of KNM-WT 8556, and KNM-WT 38359a and KNM-WT 38359b. This is especially pertinent since many tooth types are represented at Lomekwi. Currently, the Lomekwi sample is still in the process of being micro-CT scanned, and a combined 2D GM tooth type analysis would be the easiest to implement and would not require

any additional equipment. If diagenetic processes have not altered the structure of enamel and dentine to render their grey scale values indistinguishable, a study of the enamel-dentine junction morphology, which has shown to be useful in studies of hominin taxonomy (Skinner et al., 2008; Skinner, Wood and Hublin, 2009; Bailey et al., 2011), could further elucidate the taxonomy of the Lomekwi sample. Enamel thickness, which has been shown to distinguish between hominin taxa (Grine and Martin, 1988; Olejniczak et al., 2008; Skinner et al., 2015), may help clear the taxonomic ambiguities surrounding Lomekwi as well.

Another consideration would be to compare the Lomekwi sample to *Au. deyiremeda* and *Au. bahrelghazali*, which are contemporaneous with Lomekwi. Comparing the Lomekwi sample to the Woranso-Mille fossil material (Haile-Selassie, 2010) should also be considered. Both samples share a temporal and spatial overlap, and the Woranso-Mille material shows affinities with *Au. afarensis* and *Au. anamensis*, which the Lomekwi sample does as well.

An additional consideration would be to assess whether the Lomekwi sample samples a single species or multiple species. The results of the current analysis do suggest that there is a high degree of morphological variation within Lomekwi, especially in the M_2s. KNM-WT 38339 is particularly of interest, since in both the M_1s and M_2s PCAs the tooth plots far from all taxa and Lomekwi. Of note is the molar's position in the M_1s shape space PCA, where the closest specimen to it is the *Au. africnaus* M_1 MLD2, whose position in shape space is also distant from its taxon. A comparative study of Lomekwi and highly variable hominin taxa such as *Au. africanus*, may illuminate whether the variation observed in the mandibular molars of Lomekwi is within the range of other hominins. A further future direction, which is related to one of the limitations of the current study, would be to assess how often specimens from the comparative

sample (i.e. *Au. africanus, Au. anamensis*, and *Au. afarensis*) classify correctly in a CVA in order to provide more context to the Lomekwi classification results.

CHAPTER 5: Conclusion

The current thesis provided further support for the utility of 2D geometric morphometric analysis in realizing the potential of fossil dental remains in studies of hominin taxonomy compared to traditional measurements of crown morphology. The 2D GM shape data proved to be more accurate in classifying mandibular molars to their correct taxonomic group, and more powerful in finding significant differences between taxa than relative cusp area and crown shape index data. Because the 2D GM method employed here is similar in its approach to relative cusp areas by focusing on fissure pattern and crown shape rather than on cusp tips, future studies on hominin dentition may benefit from the greater power of this method without sacrificing sample size.

The current study cannot provide definitive answers to questions pertaining the taxonomy of Lomekwi, especially since it is unclear if the Lomekwi sample is even taxonomically coherent. However, it does raise interesting phylogenetic possibilities, especially with regards to *Au. anamensis*. The attribution of the specimens KNM-WT 8556 and KNM-WT 16006 to *Au. afarensis* by previous research (Brown, Brown and Walker, 2001) has been mostly supported in the current study, especially that of KNM-WT 8556. Further comparative studies of KNM-WT 16006 should be undertaken, considering that in the current study, it has shown some crown shape similarities with *Au. anamensis* and the only other known Lomekwi M_3 in the sample – KNM-WT 38347. Some of the similarities of the Lomekwi sample with *Au. africanus* that have

been noted by past researchers (Leakey et al., 2001), notably the presence of a protostylid in many of the molars, have been supported to some extent in the current study, especially with regards to the Lomekwi M_2s. Lomekwi specimens that exhibit unique morphological features among *Au. afarensis*, *Au. anamensis*, and *Au. africanus* have been identified in the analyses that have been undertaken in the thesis, and may open new future research directions regarding the Lomekwi sample. In terms of crown shape, of interest is KNM-WT 38333, which appears to exhibit some affinities with *Homo*. Overall, while the results of the current study are not definitive, they do suggest that the Lomekwi mandibular molar sample displays a number of unique morphological crown traits.

Appendix

Table A1
The complete sample of the specimens used in the Methods Comparison and Lomekwi analyses.

Accession	Taxon	Tooth	Basis	Citation	MD	BL	CSh	CSi
AL128-23	*Au. afarensis*	RM1	1	A	11.52	11.50	100.18	11.51
AL128-23	*Au. afarensis*	RM2	1	A	12.69	12.15	104.39	12.42
AL145-35	*Au. afarensis*	LM2	1	A	15.55	14.05	110.75	14.80
AL188-1	*Au. afarensis*	RM2	1	A	15.79	15.26	103.47	15.53
AL200-1b	*Au. afarensis*	RM1	2	A	13.07	12.38	105.59	12.73
AL207-13	*Au. afarensis*	LM2	1	A	13.77	12.30	111.94	13.03
AL225-8	*Au. afarensis*	LM3	1	B	13.35	11.28	118.38	12.31
AL241-14	*Au. afarensis*	LM2	3	A	14.64	13.12	111.58	13.88
AL266-1	*Au. afarensis*	LM1	1	A	12.88	11.75	109.61	12.32
AL266-1	*Au. afarensis*	RM2	1	A	13.60	13.71	99.23	13.66
AL266-1	*Au. afarensis*	RM3	1	A	15.13	13.48	112.24	14.31
AL330-5	*Au. afarensis*	RM1	1	B	12.68	12.16	104.28	12.42
AL330-5	*Au. afarensis*	RM2	1	B	12.93	12.75	101.46	12.84
AL330-5	*Au. afarensis*	RM3	1	B	13.81	12.75	108.30	13.28
AL333w-32	*Au. afarensis*	RM3	1	A	14.35	14.29	100.42	14.32
AL333w-1b	*Au. afarensis*	RM1	1	A	12.96	12.21	106.15	12.58
AL400-1a	*Au. afarensis*	RM2	1	B	15.76	14.51	108.59	15.14
AL400-1a	*Au. afarensis*	RM3	1	B	15.61	13.79	113.25	14.70
AL417-1a	*Au. afarensis*	LM2	1	B	13.78	13.08	105.37	13.43
AL440-1	*Au. afarensis*	RM2	2	B	15.49	13.75	112.71	14.62
AL996-1	*Au. afarensis*	LM1	1	B	14.08	13.31	105.79	13.69
AL996-1	*Au. afarensis*	LM2	1	B	16.08	14.86	108.20	15.47
AL1496-1	*Au. afarensis*	RM2	1	B	14.91	15.65	95.24	15.28
AL1496-1	*Au. afarensis*	RM3	1	B	16.79	15.34	109.46	16.07
AL1901	*Au. afarensis*	LM3	1	B	14.43	11.94	120.88	13.19
LH3t	*Au. afarensis*	LM1	2	E	13.52	13.40	100.88	13.46
KNM-ER 20422	*Au. anamensis*	LM1	3	C	11.96	11.08	107.93	11.52
KNM-KP 20428	*Au. anamensis*	LM3	3	C	15.87	13.55	117.12	14.71
KNM-ER 30201	*Au. anamensis*	LM1	3	D	11.72	10.09	116.08	10.91
KNM-ER 35233	*Au. anamensis*	LM2	3	D	14.90	13.29	112.09	14.10
KNM-KP 29286	*Au. anamensis*	LM2	1	D	14.61	14.07	103.84	14.34
KNM-KP 29286	*Au. anamensis*	LM3	1	D	14.99	13.21	113.47	14.10
KNM-KP 29281	*Au. anamensis*	RM3	1	D	14.70	12.11	121.40	13.40
KNM-KP 29286	*Au. anamensis*	RM1	1	D	12.63	12.21	103.45	12.42
KNM-KP 31712J	*Au. anamensis*	RM1	1	D	11.65	10.73	108.55	11.19
KNM-KP 34725R	*Au. anamensis*	RM1	1	D	13.98	12.24	114.20	13.11
KNM-KP 34725T	*Au. anamensis*	LM2	1	D	16.04	13.88	115.58	14.96

MLD2	*Au. africanus*	LM1	1	F	15.13	14.11	107.21	14.62
MLD2	*Au. africanus*	RM2	1	F	16.58	15.50	106.96	16.04
MLD19	*Au. africanus*	LM3	1	G	15.23	13.62	111.89	14.42
Sts9	*Au. africanus*	RM1	3	H	15.10	12.98	116.34	14.04
Sts18	*Au. africanus*	LM1	1	I	15.21	13.27	114.64	14.24
Sts52b	*Au. africanus*	RM2	1	J	14.81	13.21	112.12	14.01
Sts52b	*Au. africanus*	RM3	1	J	14.09	12.88	109.43	13.49
STW14	*Au. africanus*	RM2	1	K	16.22	14.49	111.99	15.36
STW14	*Au. africanus*	RM3	1	K	17.29	14.70	117.64	15.99
STW106	*Au. africanus*	RM1	1	K	12.32	11.57	106.56	11.94
STW109	*Au. africanus*	RM2	1	K	17.06	15.35	111.16	16.21
STW109	*Au. africanus*	RM3	1	K	17.58	15.86	110.79	16.72
STW131	*Au. africanus*	RM1	1	K	14.35	13.49	106.33	13.92
STW145	*Au. africanus*	RM2	3	K	13.88	12.67	109.52	13.28
STW234	*Au. africanus*	RM2	3	K	14.31	13.28	107.74	13.79
STW280	*Au. africanus*	RM3	3	K	16.78	16.29	103.05	16.54
STW309A	*Au. africanus*	RM1	2	K	14.61	13.89	105.19	14.25
STW327	*Au. africanus*	LM2	1	K	16.94	14.41	117.51	15.67
STW364	*Au. africanus*	RM1	3	K	13.95	12.55	111.19	13.25
STW384	*Au. africanus*	RM3	1	K	18.25	16.70	109.34	17.48
STW404	*Au. africanus*	RM2	1	K	14.76	13.88	106.35	14.32
STW404	*Au. africanus*	RM3	1	K	14.70	14.13	104.08	14.42
STW491	*Au. africanus*	LM2	1	K	14.83	13.78	107.61	14.30
STW491	*Au. africanus*	LM3	1	K	15.71	14.11	111.35	14.91
STW498c	*Au. africanus*	LM2	1	K	17.73	15.96	111.14	16.84
STW498c	*Au. africanus*	LM3	1	K	18.87	16.21	116.41	17.54
STW529	*Au. africanus*	RM3	3	K	15.10	14.37	105.09	14.73
STW537	*Au. africanus*	RM2	2	K	16.53	15.35	107.66	15.94
STW560A	*Au. africanus*	RM3	2	K	16.37	15.77	103.85	16.07
STW560E	*Au. africanus*	RM2	2	K	17.12	16.34	104.77	16.73
STW133	*Au. africanus*	LM3	2	K	16.38	14.99	109.25	15.69
STW213	*Au. africanus*	LM2	2	K	14.63	13.20	110.82	13.91
STW246	*Au. africanus*	LM1	2	K	15.42	13.07	117.95	14.25
STW421B	*Au. africanus*	LM1	2	K	15.18	13.64	111.30	14.41
Taung 1	*Au. africanus*	LM1	1	K	14.26	13.30	107.19	13.78
Abri-Suard 14	*H. neanderthalensis*	RM1	2	L	12.05	10.85	111.05	11.45
Abri-Suard 36	*H. neanderthalensis*	LM2	1	L	11.13	10.05	110.71	10.59
Abri-Suard 36	*H. neanderthalensis*	LM3	1	L	11.03	9.62	114.58	10.33
Abri-Suard 43	*H. neanderthalensis*	RM3	3	L	11.07	9.66	114.61	10.37
Combe Grenal I	*H. neanderthalensis*	RM1	1	M	12.59	10.89	115.65	11.74
G_1010_69	*H. neanderthalensis*	LM3	1	N	12.94	10.84	119.45	11.89
KRP 55	*H. neanderthalensis*	LM2	1	O	13.19	11.54	114.36	12.36
KRP D1	*H. neanderthalensis*	RM2	2	O	13.90	12.47	111.52	13.19

KRP D10	*H. neanderthalensis*	RM2	2	O	13.09	11.86	110.36	12.48
KRP 53	*H. neanderthalensis*	RM2	1	O	13.68	12.26	111.60	12.97
KRP D77	*H. neanderthalensis*	RM1	2	O	12.82	12.14	105.59	12.48
Le Moustier	*H. neanderthalensis*	LM2	1	P	12.37	11.61	106.59	11.99
Le Moustier_M2	*H. neanderthalensis*	LM1	1	P	12.89	11.69	110.25	12.29
Le Moustier_M3	*H. neanderthalensis*	LM2	1	P	12.83	11.76	109.13	12.30
La Quina Q760_H9	*H. neanderthalensis*	LM3	1	Q	12.42	11.90	104.37	12.16
Roc de Marsal	*H. neanderthalensis*	RM1	1	R	12.22	10.91	112.02	11.57
Scladina4A-1	*H. neanderthalensis*	RM1	1	S	11.74	10.69	109.78	11.22
Scladina4A-1	*H. neanderthalensis*	RM3	1	S	11.48	11.28	101.79	11.38
Scladina4A9	*H. neanderthalensis*	LM2	1	S	12.27	10.88	112.78	11.57
SD540	*H. neanderthalensis*	LM2	2	T	12.98	11.57	112.17	12.28
SD780	*H. neanderthalensis*	LM1	2	T	12.50	11.57	108.05	12.03
St. Cesaire 1	*H. neanderthalensis*	RM2	1	U	11.52	10.23	112.61	10.88
Vi_11_39	*H. neanderthalensis*	RM3	1	V	12.03	11.88	101.24	11.95
ZMB 6983	*P. troglodytes*	LM1	1	W	11.22	9.87	113.77	10.54
MRAC 10733	*P. troglodytes*	RM1	1	X	11.73	10.74	109.29	11.24
MRAC 10800	*P. troglodytes*	LM2	1	X	12.02	10.53	114.16	11.27
MPI 11776	*P. troglodytes*	RM2	1	Y	10.47	9.93	105.50	10.20
MPI 11778	*P. troglodytes*	LM3	1	Y	10.93	11.05	98.95	10.99
MPI 11779	*P. troglodytes*	RM2	1	Y	11.83	11.68	101.28	11.75
MPI 11790	*P. troglodytes*	RM2	1	Y	11.08	11.27	98.33	11.18
ZMB 15849	*P. troglodytes*	LM3	1	W	10.19	9.30	109.51	9.74
ZMB 17011	*P. troglodytes*	LM1	1	W	11.02	10.57	104.19	10.79
ZMB 24838	*P. troglodytes*	LM3	1	W	11.56	10.77	107.39	11.17
ZMB 27054	*P. troglodytes*	LM2	1	W	12.12	10.52	115.21	11.32
ZMB 30846	*P. troglodytes*	RM2	1	W	12.95	11.68	110.90	12.32
ZMB 31279	*P. troglodytes*	RM2	1	W	10.63	9.18	115.79	9.91
ZMB 32356	*P. troglodytes*	RM2	1	W	11.70	9.93	117.73	10.81
ZMB 35526	*P. troglodytes*	RM1	1	W	12.09	10.34	116.83	11.21
ZMB 46095	*P. troglodytes*	RM1	1	W	11.26	9.91	113.65	10.59
ZMB 72844	*P. troglodytes*	LM2	1	W	11.28	10.54	106.94	10.91
ZMB 83604	*P. troglodytes*	RM1	1	W	11.76	10.44	112.65	11.10
ZMB 83619	*P. troglodytes*	LM1	1	W	11.16	9.66	115.54	10.41
ZMB 83635	*P. troglodytes*	RM3	1	W	12.09	10.44	115.83	11.27
ZMB 83639	*P. troglodytes*	LM2	1	W	10.38	9.15	113.43	9.77
ZMB A16207	*P. troglodytes*	RM3	1	W	10.31	9.53	108.20	9.92
MPI 11903	*P. troglodytes*	LM3	1	Y	10.71	10.13	105.63	10.42
ZMB 83610	*P. troglodytes*	RM3	1	W	10.81	11.20	96.48	11.00
KNM-WT 8556	*cf. K. platyops*	RM1	1	Z	13.80	12.98	106.34	13.39
KNM-WT 16006	*cf. K. platyops*	LM3	1	Z	14.97	12.48	119.94	13.72
KNM-WT 38333	*cf. K. platyops*	LM2	3	WL	13.25	12.20	108.57	12.72
KNM-WT 38334	*cf. K. platyops*	LM1	3	WL	12.26	11.80	103.89	12.03

KNM-WT 38339	*cf. K. platyops*	LM1/2	3	WL	12.56	12.27	102.40	12.42
KNM-WT 38342	*cf. K. platyops*	LM1	3	WL	12.68	11.34	111.81	12.01
KNM-WT 38347	*cf. K. platyops*	LM3	3	WL	11.49	9.38	122.45	10.44
KNM-WT 38349	*cf. K. platyops*	RM2	3	WL	13.65	12.72	107.32	13.19
KNM-WT 38359a	*cf. K. platyops*	RM1	2	WL	12.93	11.80	109.58	12.36
KNM-WT 38359b	*cf. K. platyops*	RM2	2	WL	14.05	12.32	114.04	13.18
KNM-WT 66291	*cf. K. platyops*	LM2	3	WL	14.83	13.31	111.41	14.07

MD – mesiodistal; BL – buccolingual. Both measurements are in millimeters. CSh – crown shape index; CSi – crown size index.

Citations: A - Johanson et al., 1982; B - Kimbel et al., 2004; C - Coffing et al., 1994; D - Ward et al., 2001;E - Dart, 1948; F - White, 1980; G - WITS records; H - Suwa, 1996; I - Brain, 1981; J - Dart, 1954; K- Moggi-Cecchi, 2006; L - Telihol, 2001; M - Geralda and Vandermeetsch, 2000; N - Vlcek, 1993;O - Radovcic et al., 1987; P - Klaatsch and Hauser, 1908; Q - TNT records; R - Bordes, 1975; S - Toussaint et al., 1988; T - Rosas et al., 2009; U - Laveque and Vandermeersch, V - 1980; Wolpoff et al., 1981; W - ZMB records; X - MRAC records; Y - MPI records; WL – Wood and Leakey, 2011.

Table A2
Relative (RCA) and absolute (ACA) cusp area measurements.

			RCA					ACA				
Accession	Taxon	Tooth	Hld	Med	End	Hyd	Prd	Hld	Med	End	Hyd	Prd
AL128-23	*Au. afarensis*	RM1	0.153	0.199	0.174	0.232	0.242	17.15	22.26	19.43	25.97	27.07
AL128-23	*Au. afarensis*	RM2	0.132	0.192	0.183	0.227	0.267	17.06	24.76	23.74	29.45	34.57
AL145-35	*Au. afarensis*	LM2	0.170	0.231	0.135	0.203	0.261	30.89	41.82	24.41	36.83	47.23
AL188-1	*Au. afarensis*	RM2	0.155	0.217	0.143	0.184	0.301	30.53	42.71	28.05	36.35	59.50
AL200-1b	*Au. afarensis*	RM1	0.154	0.227	0.160	0.227	0.232	21.04	31.07	21.82	31.15	31.68
AL207-13	*Au. afarensis*	LM2	0.164	0.202	0.174	0.205	0.255	23.02	28.25	24.44	28.75	35.73
AL225-8	*Au. afarensis*	LM3	0.194	0.231	0.133	0.179	0.263	23.65	27.97	16.12	21.62	31.95
AL241-14	*Au. afarensis*	LM2	0.168	0.234	0.159	0.190	0.248	27.08	37.55	25.49	30.49	39.80
AL266-1	*Au. afarensis*	LM1	0.153	0.213	0.175	0.223	0.236	20.10	28.01	23.00	29.27	30.95
AL266-1	*Au. afarensis*	RM2	0.158	0.259	0.147	0.176	0.260	24.24	39.84	22.62	27.02	39.85
AL266-1	*Au. afarensis*	RM3	0.221	0.247	0.147	0.132	0.253	36.70	40.62	24.17	21.45	41.67
AL330-5	*Au. afarensis*	RM1	0.142	0.224	0.159	0.215	0.260	18.79	29.51	20.95	28.38	34.44
AL330-5	*Au. afarensis*	RM2	0.153	0.223	0.157	0.198	0.269	20.99	30.67	21.60	27.23	37.05
AL330-5	*Au. afarensis*	RM3	0.159	0.234	0.154	0.182	0.271	22.60	33.14	21.81	25.74	38.49
AL333w-32	*Au. afarensis*	RM3	0.137	0.245	0.192	0.163	0.263	23.09	41.34	32.33	27.31	44.22
AL333w-1b	*Au. afarensis*	RM1	0.128	0.215	0.160	0.242	0.255	17.40	29.34	21.89	33.16	34.79
AL400-1a	*Au. afarensis*	RM2	0.119	0.261	0.146	0.210	0.263	21.72	47.61	26.60	38.40	48.03
AL400-1a	*Au. afarensis*	RM3	0.126	0.242	0.174	0.176	0.282	22.06	42.30	30.47	30.69	49.43
AL417-1a	*Au. afarensis*	LM2	0.105	0.232	0.157	0.244	0.261	15.73	34.76	23.51	36.61	39.15
AL440-1	*Au. afarensis*	RM2	0.151	0.230	0.164	0.203	0.252	26.69	40.53	28.87	35.86	44.43
AL996-1	*Au. afarensis*	LM1	0.158	0.228	0.170	0.207	0.237	25.50	36.76	27.48	33.43	38.31
AL996-1	*Au. afarensis*	LM2	0.169	0.242	0.153	0.194	0.242	34.58	49.31	31.12	39.57	49.42
AL1496-1	*Au. afarensis*	RM2	0.136	0.232	0.149	0.210	0.273	26.13	44.37	28.50	40.25	52.25
AL1496-1	*Au. afarensis*	RM3	0.193	0.225	0.163	0.142	0.277	41.65	48.51	34.98	30.34	59.83
AL1901	*Au. afarensis*	LM3	0.161	0.216	0.184	0.177	0.262	22.60	30.24	25.79	24.74	36.66
LH3t	*Au. afarensis*	LM1	0.155	0.225	0.170	0.219	0.231	24.56	35.40	26.76	34.57	36.44

KNM-ER 20422	*Au. anamensis*	LM1	0.141	0.200	0.148	0.245	0.265	15.89	22.54	16.70	27.73	29.94
KNM-KP 20428	*Au. anamensis*	LM3	0.209	0.217	0.169	0.140	0.265	37.12	38.17	29.47	24.94	46.43
KNM-ER 30201	*Au. anamensis*	LM1	0.162	0.238	0.147	0.231	0.222	16.20	23.87	14.67	23.20	22.18
KNM-ER 35233	*Au. anamensis*	LM2	0.145	0.205	0.165	0.227	0.258	24.09	34.14	27.53	37.75	42.96
KNM-KP 29286	*Au. anamensis*	LM2	0.164	0.196	0.141	0.221	0.278	28.34	33.73	24.24	38.11	48.03
KNM-KP 29286	*Au. anamensis*	LM3	0.188	0.192	0.171	0.169	0.278	30.18	30.69	27.38	27.00	44.57
KNM-KP 29281	*Au. anamensis*	RM3	0.204	0.231	0.153	0.134	0.278	30.11	33.80	22.40	19.44	40.76
KNM-KP 29286	*Au. anamensis*	RM1	0.155	0.211	0.148	0.235	0.251	20.44	27.70	19.44	30.90	32.95
KNM-KP 31712J	*Au. anamensis*	RM1	0.127	0.231	0.167	0.215	0.260	13.22	24.03	17.35	22.36	27.00
KNM-KP 34725R	*Au. anamensis*	RM1	0.142	0.238	0.180	0.231	0.209	20.52	34.54	26.04	33.49	30.31
KNM-KP 34725T	*Au. anamensis*	LM2	0.138	0.223	0.167	0.211	0.262	25.54	41.17	30.87	39.04	48.57
MLD2	*Au. africanus*	LM1	0.163	0.239	0.115	0.232	0.252	29.30	43.04	20.52	41.72	45.27
MLD2	*Au. africanus*	RM2	0.123	0.248	0.124	0.238	0.267	26.76	54.28	27.10	52.26	58.41
MLD19	*Au. africanus*	LM3	0.161	0.241	0.160	0.180	0.258	27.51	41.18	27.29	30.79	44.01
Sts9	*Au. africanus*	RM1	0.127	0.236	0.149	0.222	0.266	20.92	38.94	24.54	36.65	43.79
Sts18	*Au. africanus*	LM1	0.148	0.216	0.185	0.209	0.242	25.16	36.65	31.32	35.34	40.98
Sts52b	*Au. africanus*	RM2	0.132	0.250	0.149	0.194	0.275	20.98	40.02	23.69	31.00	43.89
Sts52b	*Au. africanus*	RM3	0.141	0.254	0.157	0.160	0.287	20.65	37.20	22.88	23.35	42.02
STW14	*Au. africanus*	RM2	0.128	0.259	0.159	0.199	0.255	24.95	50.41	30.95	38.78	49.65
STW14	*Au. africanus*	RM3	0.142	0.257	0.196	0.172	0.232	30.52	55.28	42.25	36.79	49.74
STW106	*Au. africanus*	RM1	0.133	0.222	0.199	0.213	0.234	15.90	26.58	23.93	25.58	28.00
STW109	*Au. africanus*	RM2	0.151	0.242	0.154	0.180	0.273	32.89	52.67	33.47	39.02	59.29
STW109	*Au. africanus*	RM3	0.128	0.229	0.171	0.176	0.295	27.80	49.62	37.18	38.19	64.07
STW131	*Au. africanus*	RM1	0.134	0.201	0.174	0.216	0.275	22.13	33.28	28.83	35.89	45.54
STW145	*Au. africanus*	RM2	0.108	0.240	0.192	0.216	0.244	16.23	36.14	29.00	32.48	36.74
STW234	*Au. africanus*	RM2	0.114	0.217	0.165	0.237	0.266	18.10	34.60	26.21	37.86	42.47
STW280	*Au. africanus*	RM3	0.139	0.194	0.142	0.198	0.327	30.65	42.96	31.46	43.85	72.77
STW309A	*Au. africanus*	RM1	0.157	0.198	0.188	0.221	0.236	26.67	33.60	31.85	37.54	40.05
STW327	*Au. africanus*	LM2	0.136	0.250	0.170	0.193	0.250	27.24	50.05	34.03	38.59	50.03
STW364	*Au. africanus*	RM1	0.154	0.238	0.178	0.213	0.217	22.39	34.60	25.91	31.06	31.61
STW384	*Au. africanus*	RM3	0.174	0.216	0.172	0.152	0.287	43.18	53.51	42.37	37.84	70.42

STW404	*Au. africanus*	RM2	0.124	0.191	0.189	0.206	0.290	20.78	32.00	31.89	34.73	48.86
STW404	*Au. africanus*	RM3	0.139	0.213	0.194	0.193	0.261	23.92	36.75	33.51	33.41	44.99
STW491	*Au. africanus*	LM2	0.134	0.223	0.145	0.221	0.278	22.94	38.17	24.85	37.93	47.76
STW491	*Au. africanus*	LM3	0.145	0.222	0.148	0.216	0.269	25.89	39.81	26.52	38.73	48.18
STW498c	*Au. africanus*	LM2	0.156	0.230	0.131	0.211	0.271	37.51	55.22	31.36	50.74	65.02
STW498c	*Au. africanus*	LM3	0.153	0.249	0.157	0.182	0.259	39.00	63.56	39.97	46.50	66.31
STW529	*Au. africanus*	RM3	0.106	0.241	0.174	0.181	0.297	18.26	41.66	30.06	31.20	51.44
STW537	*Au. africanus*	RM2	0.143	0.227	0.166	0.196	0.269	30.08	47.85	34.91	41.22	56.61
STW560A	*Au. africanus*	RM3	0.149	0.218	0.146	0.228	0.259	30.71	44.82	30.11	47.01	53.35
STW560E	*Au. africanus*	RM2	0.155	0.221	0.138	0.209	0.278	35.61	50.46	31.43	47.86	63.75
STW133	*Au. africanus*	LM3	0.143	0.227	0.180	0.188	0.263	28.93	46.04	36.72	38.08	53.51
STW213	*Au. africanus*	LM2	0.123	0.212	0.184	0.212	0.269	19.94	34.49	30.04	34.55	43.81
STW246	*Au. africanus*	LM1	0.143	0.198	0.195	0.218	0.246	23.25	32.19	31.80	35.49	40.11
STW421B	*Au. africanus*	LM1	0.179	0.207	0.182	0.209	0.223	31.10	35.88	31.68	36.21	38.76
Taung 1	*Au. africanus*	LM1	0.157	0.220	0.188	0.204	0.231	24.91	34.82	29.88	32.35	36.57
Abri-Suard 14	*H. neanderthalensis*	RM1	0.151	0.199	0.183	0.204	0.263	16.25	21.38	19.70	21.89	28.30
Abri-Suard 36	*H. neanderthalensis*	LM2	0.126	0.190	0.169	0.228	0.288	11.62	17.54	15.62	21.09	26.63
Abri-Suard 36	*H. neanderthalensis*	LM3	0.159	0.207	0.179	0.151	0.304	13.75	17.91	15.46	13.00	26.22
Abri-Suard 43	*H. neanderthalensis*	RM3	0.126	0.224	0.154	0.177	0.318	10.72	19.13	13.19	15.14	27.18
Combe Grenal I	*H. neanderthalensis*	RM1	0.167	0.197	0.185	0.185	0.265	18.53	21.85	20.52	20.50	29.39
G_1010_69	*H. neanderthalensis*	LM3	0.137	0.201	0.163	0.225	0.274	15.54	22.84	18.54	25.51	31.08
KRP 55	*H. neanderthalensis*	LM2	0.113	0.180	0.223	0.225	0.260	14.21	22.54	27.95	28.19	32.60
KRP D1	*H. neanderthalensis*	RM2	0.112	0.193	0.194	0.232	0.268	16.05	27.56	27.79	33.22	38.27
KRP D10	*H. neanderthalensis*	RM2	0.123	0.172	0.238	0.195	0.272	15.78	22.03	30.50	25.05	34.97
KRP 53	*H. neanderthalensis*	RM2	0.101	0.214	0.156	0.237	0.292	14.22	30.06	21.86	33.35	40.96
KRP D77	*H. neanderthalensis*	RM1	0.097	0.199	0.231	0.204	0.269	12.84	26.31	30.53	26.93	35.56
Le Moustier	*H. neanderthalensis*	LM2	0.132	0.233	0.182	0.213	0.241	15.42	27.29	21.38	24.93	28.20
Le Moustier_M2	*H. neanderthalensis*	LM1	0.122	0.186	0.212	0.223	0.257	15.02	22.89	26.07	27.46	31.68
Le Moustier_M3	*H. neanderthalensis*	LM2	0.149	0.235	0.193	0.202	0.221	17.82	27.99	23.00	24.15	26.35
La Quina Q760_H9	*H. neanderthalensis*	LM3	0.130	0.189	0.173	0.239	0.268	16.16	23.49	21.55	29.74	33.29
Roc de Marsal	*H. neanderthalensis*	RM1	0.180	0.218	0.180	0.183	0.240	19.32	23.32	19.22	19.56	25.65

Scladina4A-1	*H. neanderthalensis*	RM1	0.118	0.220	0.190	0.204	0.268	12.08	22.46	19.45	20.89	27.37
Scladina4A-1	*H. neanderthalensis*	RM3	0.132	0.207	0.152	0.188	0.321	13.75	21.47	15.77	19.47	33.38
Scladina4A9	*H. neanderthalensis*	LM2	0.136	0.194	0.171	0.207	0.293	14.60	20.92	18.38	22.28	31.51
SD540	*H. neanderthalensis*	LM2	0.145	0.187	0.224	0.196	0.249	17.86	23.02	27.58	24.17	30.67
SD780	*H. neanderthalensis*	LM1	0.147	0.224	0.168	0.221	0.239	17.20	26.14	19.57	25.84	27.93
St. Cesaire 1	*H. neanderthalensis*	RM2	0.107	0.239	0.151	0.243	0.259	10.49	23.43	14.81	23.76	25.39
Vi_11_39	*H. neanderthalensis*	RM3	0.079	0.201	0.192	0.239	0.290	9.07	23.00	21.98	27.39	33.26
ZMB 6983	*P. troglodytes*	LM1	0.138	0.212	0.184	0.221	0.244	12.96	19.88	17.20	20.68	22.87
MRAC 10733	*P. troglodytes*	RM1	0.157	0.240	0.162	0.207	0.234	16.93	25.82	17.39	22.28	25.15
MRAC 10800	*P. troglodytes*	LM2	0.141	0.223	0.183	0.205	0.247	15.08	23.80	19.54	21.85	26.34
MPI 11776	*P. troglodytes*	RM2	0.090	0.257	0.201	0.186	0.266	7.81	22.37	17.52	16.21	23.11
MPI 11778	*P. troglodytes*	LM3	0.115	0.223	0.156	0.202	0.303	11.61	22.53	15.80	20.46	30.65
MPI 11779	*P. troglodytes*	RM2	0.140	0.205	0.184	0.199	0.272	15.93	23.29	21.01	22.65	30.98
MPI 11790	*P. troglodytes*	RM2	0.122	0.261	0.186	0.164	0.266	12.78	27.24	19.39	17.13	27.78
ZMB 15849	*P. troglodytes*	LM3	0.148	0.233	0.160	0.220	0.239	11.59	18.17	12.49	17.21	18.63
ZMB 17011	*P. troglodytes*	LM1	0.160	0.198	0.187	0.198	0.257	15.32	18.88	17.87	18.92	24.53
ZMB 24838	*P. troglodytes*	LM3	0.148	0.244	0.156	0.210	0.241	15.64	25.80	16.47	22.22	25.45
ZMB 27054	*P. troglodytes*	LM2	0.189	0.214	0.163	0.193	0.241	20.53	23.24	17.70	21.02	26.25
ZMB 30846	*P. troglodytes*	RM2	0.163	0.237	0.158	0.182	0.260	20.24	29.56	19.67	22.73	32.37
ZMB 31279	*P. troglodytes*	RM2	0.136	0.216	0.177	0.208	0.262	10.93	17.40	14.24	16.72	21.10
ZMB 32356	*P. troglodytes*	RM2	0.163	0.240	0.190	0.172	0.236	15.50	22.83	18.08	16.36	22.48
ZMB 35526	*P. troglodytes*	RM1	0.131	0.227	0.189	0.231	0.223	13.81	23.91	19.95	24.34	23.47
ZMB 46095	*P. troglodytes*	RM1	0.115	0.265	0.146	0.199	0.275	10.80	24.83	13.72	18.69	25.80
ZMB 72844	*P. troglodytes*	LM2	0.123	0.221	0.195	0.202	0.259	12.16	21.92	19.37	19.99	25.72
ZMB 83604	*P. troglodytes*	RM1	0.156	0.216	0.187	0.202	0.240	15.49	21.43	18.53	20.04	23.85
ZMB 83619	*P. troglodytes*	LM1	0.112	0.203	0.161	0.175	0.349	9.56	17.42	13.79	15.02	29.86
ZMB 83635	*P. troglodytes*	RM3	0.141	0.233	0.189	0.196	0.242	14.87	24.55	19.90	20.71	25.48
ZMB 83639	*P. troglodytes*	LM2	0.088	0.232	0.186	0.217	0.278	6.95	18.35	14.73	17.16	22.04
ZMB A16207	*P. troglodytes*	RM3	0.138	0.242	0.175	0.191	0.254	11.14	19.53	14.09	15.44	20.50
MPI 11903	*P. troglodytes*	LM3	0.144	0.235	0.174	0.179	0.269	12.82	20.94	15.51	16.00	23.99
ZMB 83610	*P. troglodytes*	RM3	0.140	0.244	0.135	0.192	0.289	13.77	24.01	13.31	18.85	28.40

KNM-WT 8556	*cf. K. platyops*	RM1	0.185	0.231	0.149	0.215	0.221	28.47	35.55	22.94	33.08	34.01
KNM-WT 16006	*cf. K. platyops*	LM3	0.191	0.214	0.180	0.141	0.274	29.17	32.67	27.52	21.53	41.94
KNM-WT 38333	*cf. K. platyops*	LM2	0.060	0.236	0.168	0.232	0.304	7.78	30.76	21.95	30.29	39.73
KNM-WT 38334	*cf. K. platyops*	LM1	0.152	0.203	0.176	0.241	0.228	18.52	24.74	21.44	29.44	27.86
KNM-WT 38339	*cf. K. platyops*	LM1/2	0.158	0.241	0.104	0.225	0.273	20.25	30.94	13.37	28.84	35.01
KNM-WT 38342	*cf. K. platyops*	LM1	0.154	0.218	0.143	0.239	0.246	18.74	26.48	17.42	29.05	29.95
KNM-WT 38347	*cf. K. platyops*	LM3	0.161	0.210	0.178	0.195	0.256	14.67	19.15	16.21	17.73	23.29
KNM-WT 38349	*cf. K. platyops*	RM2	0.106	0.243	0.149	0.233	0.269	15.69	35.97	22.00	34.39	39.81
KNM-WT 38359a	*cf. K. platyops*	RM1	0.119	0.223	0.165	0.223	0.270	15.29	28.64	21.20	28.64	34.76
KNM-WT 38359b	*cf. K. platyops*	RM2	0.131	0.241	0.147	0.204	0.277	18.69	34.39	21.02	29.04	39.53
KNM-WT 66291	*cf. K. platyops*	LM2	0.164	0.227	0.183	0.190	0.236	26.64	36.75	29.60	30.78	38.31

Hld – hypoconulid; Med – metaconid; End – entoconid; Hyd – hypoconid; Prd – protoconid.

Table A3

Classification results of specimens that have been rotated and landmarked three times. Classification accuracy indicates the percentage of time each specimen classified as belonging to the group containing the other two repatead measures specimens.

Specimen	Classification accuracy
AL128-23	95%
AL128-23	99%
AL128-23	98%
KNM-ER 20422	95%
KNM-ER 20422	88%
KNM-ER 20422	90%
LH3t	91%
LH3t	98%
LH3t	93%
STW234	88%
STW234	89%
STW234	88%
STW285b	100%
STW285b	99%
STW285b	100%
STW308	89%
STW308	99%
STW308	86%
STW412B	87%
STW412B	89%
STW412B	96%
STW424	100%
STW424	100%
STW424	99%
STW 123	88%
STW 123	89%
STW 123	99%
STW 213	86%
STW 213	87%
STW 213	87%

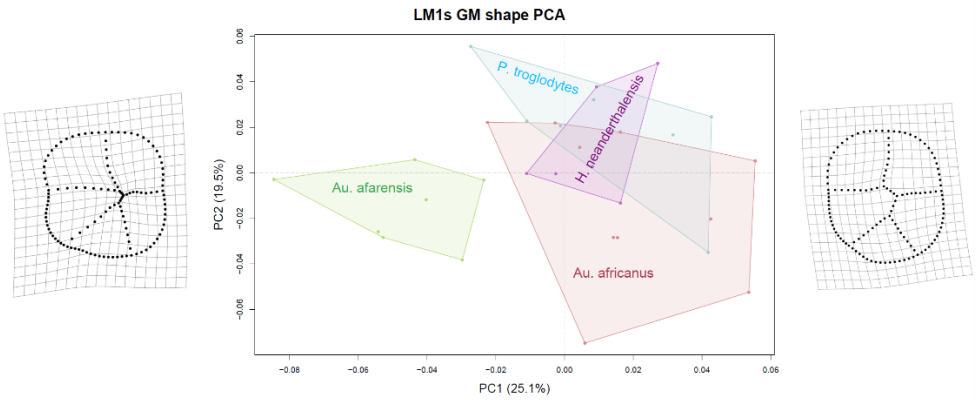

Figure A1. TPS grids depicting the morphological variation along the first PC in the M_1s Shape space PCA of the methods comparison sample. Note the square shaped outline of the M_1s of *Au. afarensis*, which separates the species from *Au. anamensis*, *P. troglodytes*, and *H. neanderthalensis*, which all share an elongated oval crown shape.

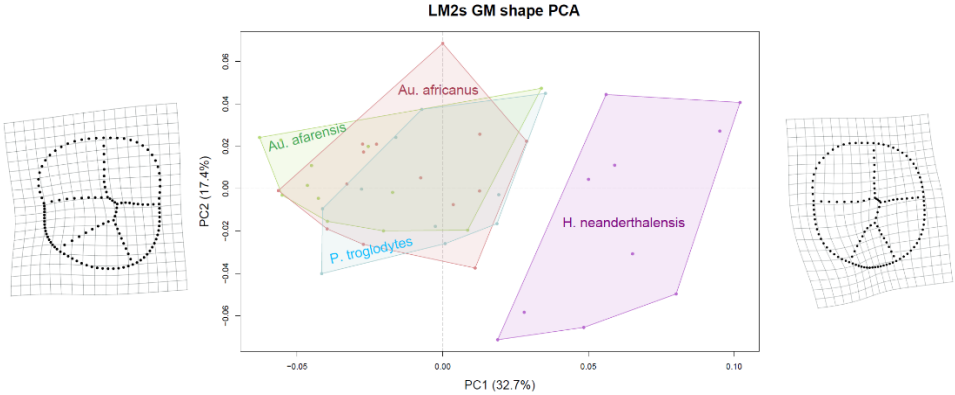

Figure A2. TPS grids depicting the morphological variation along the first PC in the M_2s Shape space PCA of the methods comparison sample. Note the oval shape of of *H. neanderthalensis* M2s which separates the taxon from *Australopithecus* and *P. troglodytes* M_2s.

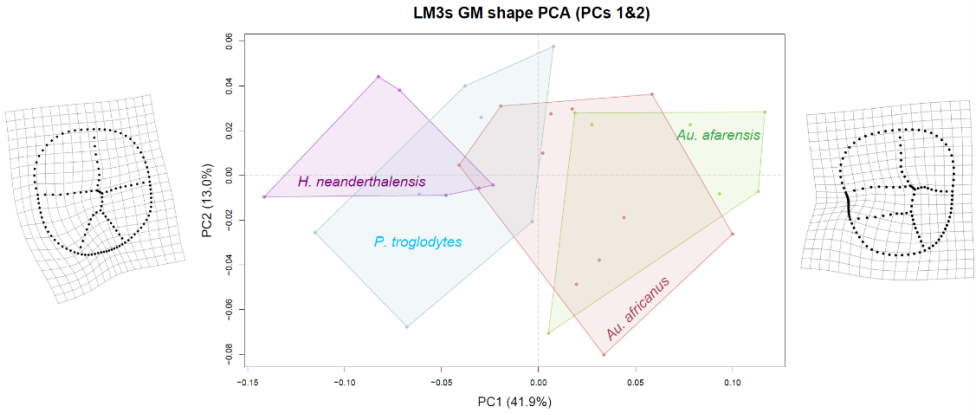

Figure A3. TPS grids depicting the morphological variation along the first PC in the M_3s Shape space PCA of the methods comparison sample. Note the separation between *H. neanderthalensis*, *P. trogldyes* and the two *Australopithecus* taxa.

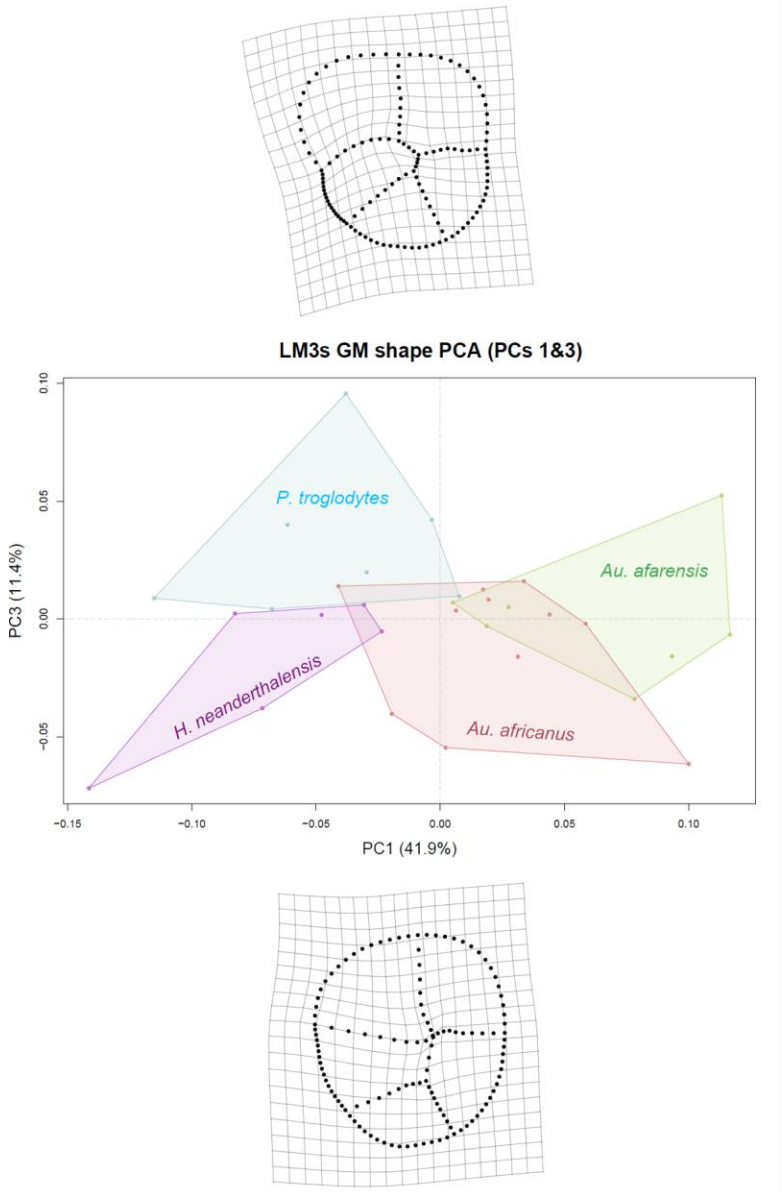

Figure A4. TPS grids depicting the morphological variation along the third PC in the M_3s Shape space PCA of the methods comparison sample. Note the separation between *H. neanderthalensis* and *P. trogldyes* along these PC.

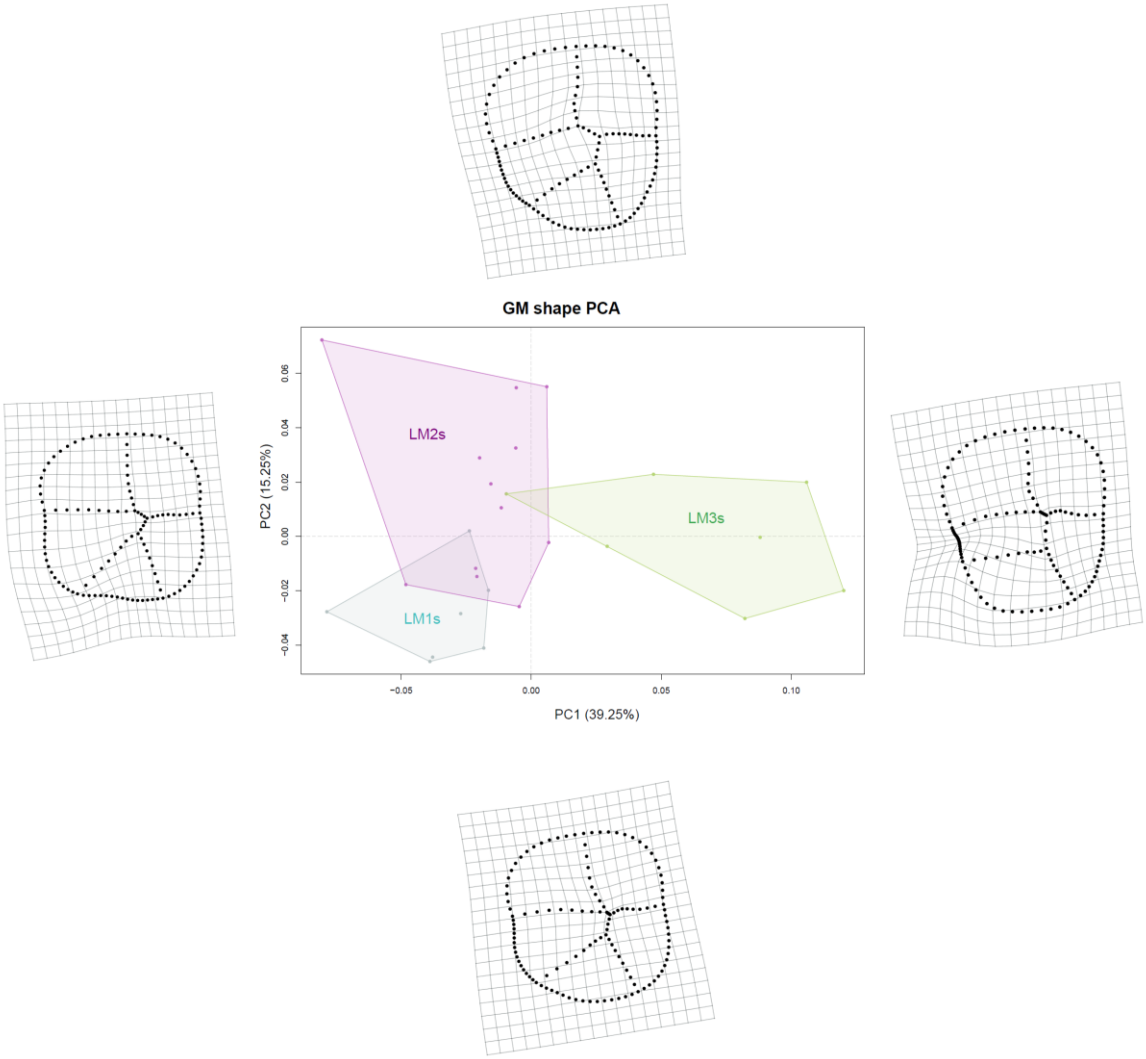

Figure A5. TPS grids depicting the morphological variation along the first and second PCs in the *Au. afarensis* molar type Shape space PCA of the methods comparison sample.

Landmarked teeth

The following section contains the landmarks molars for each taxon used in the analyses. The accession ID and the position of the molar are indicated above each tooth. Here, LLM1 would mean lower left first molar. Scale is in 10 millimeters. Note that all right molars have been mirrored.

P. troglodytes

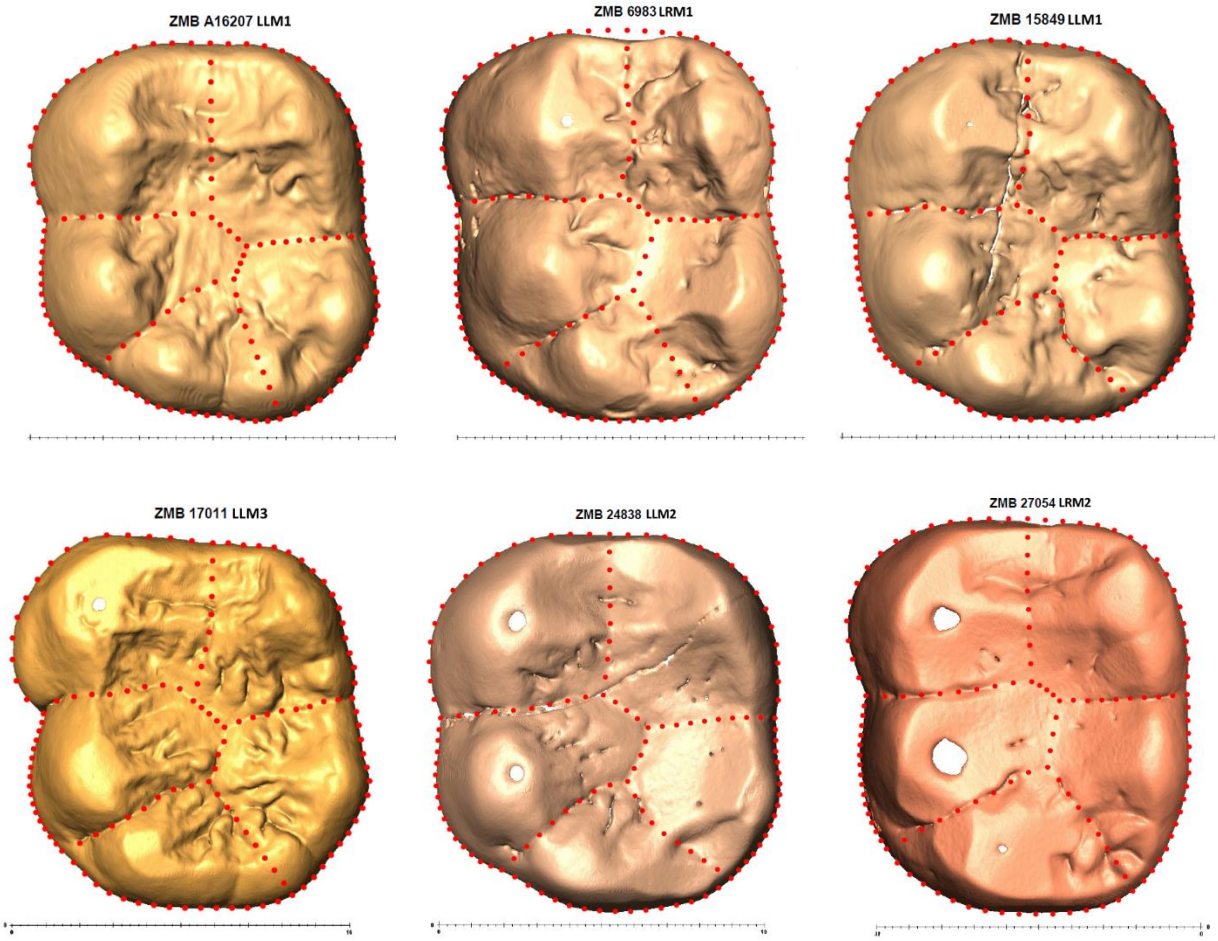


ZMB 30846 LRM2
ZMB 31279 LRM2
ZMB 32356 LRM1
ZMB 35526 LRM1
ZMB 46095 LLM2
ZMB 72844 LRM1
ZMB 83604 LLM1
ZMB 83610 LRM3
ZMB 83619 LRM3


ZMB 83635 LLM2
ZMB 83639 LRM3
MPI 11776 LLM3
MPI 11778 LRM2
MPI 11779 LRM2
MPI 11790 LLM3
MRAC 10733 LLM2
MRAC 10800 LRM2

Au. afarensis

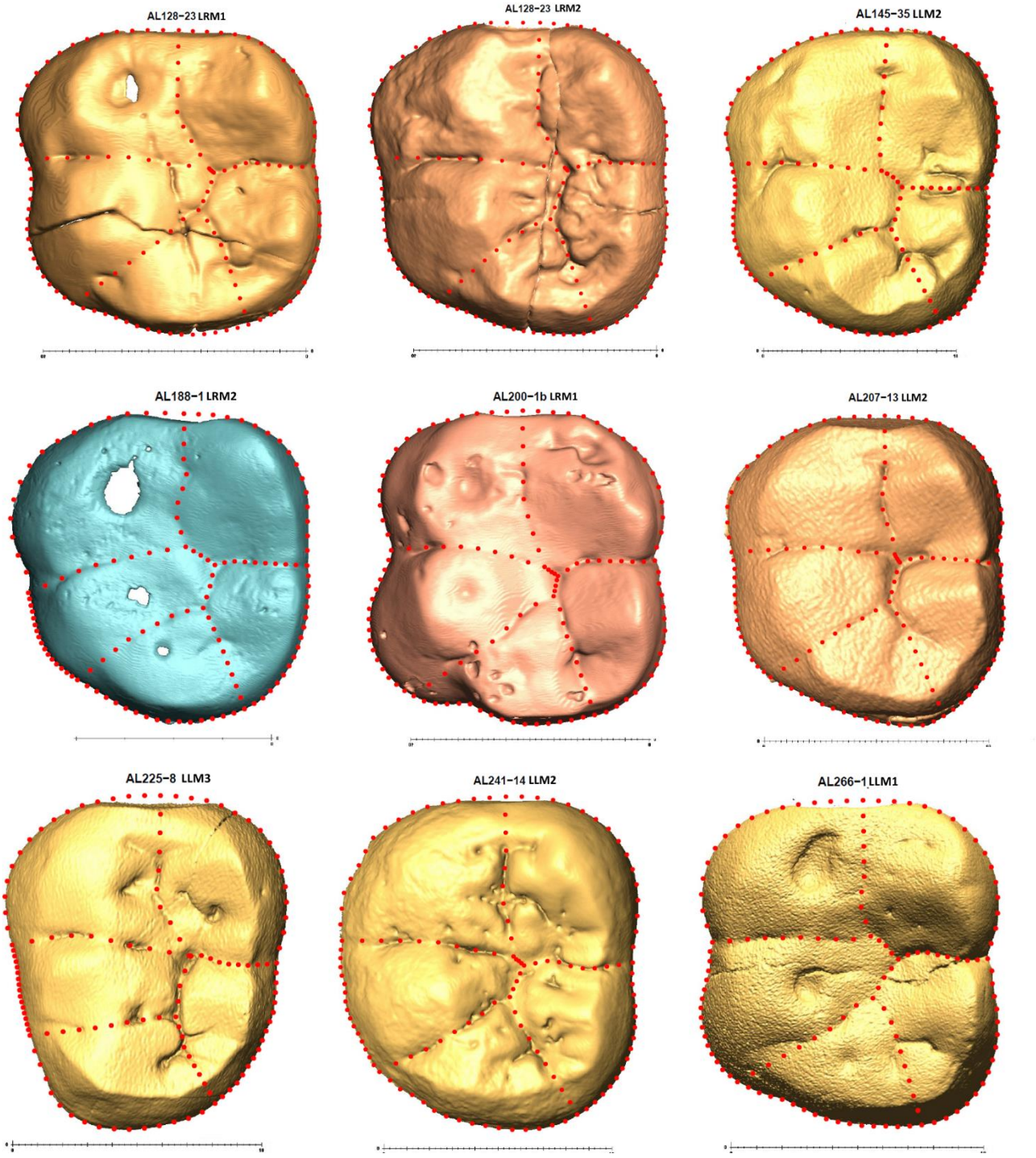

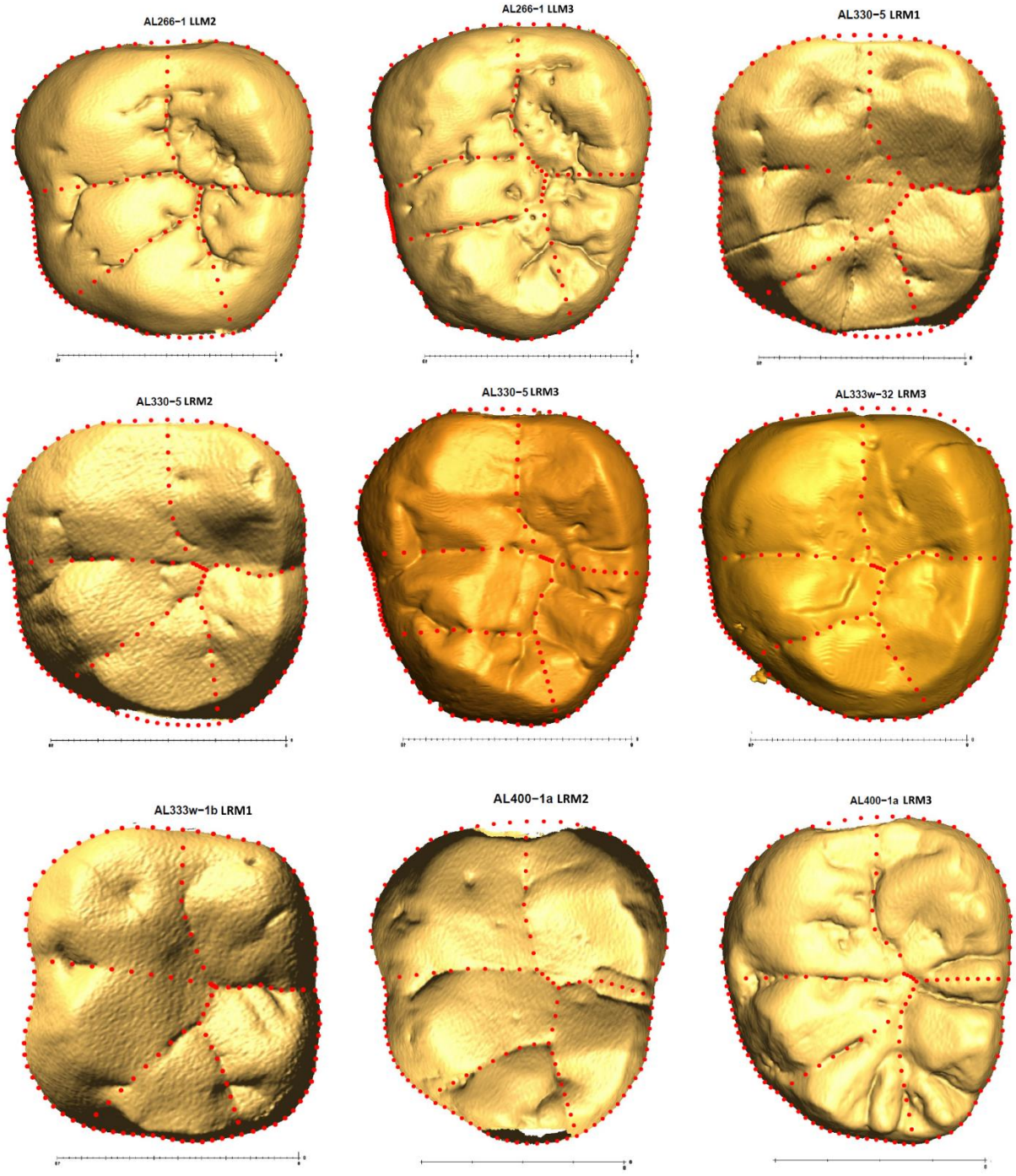
AL266-1 LLM2
AL266-1 LLM3
AL330-5 LRM1
AL330-5 LRM2
AL330-5 LRM3
AL333w-32 LRM3
AL333w-1b LRM1
AL400-1a LRM2
AL400-1a LRM3


AL417-1a LLM2
AL440-1 LRM2
AL996-1 LLM1
AL996-1 LLM2
AL1496-1 LRM2
AL1496-1 LRM3
AL1901 LLM3
LH3t LLM1

Au. africanus

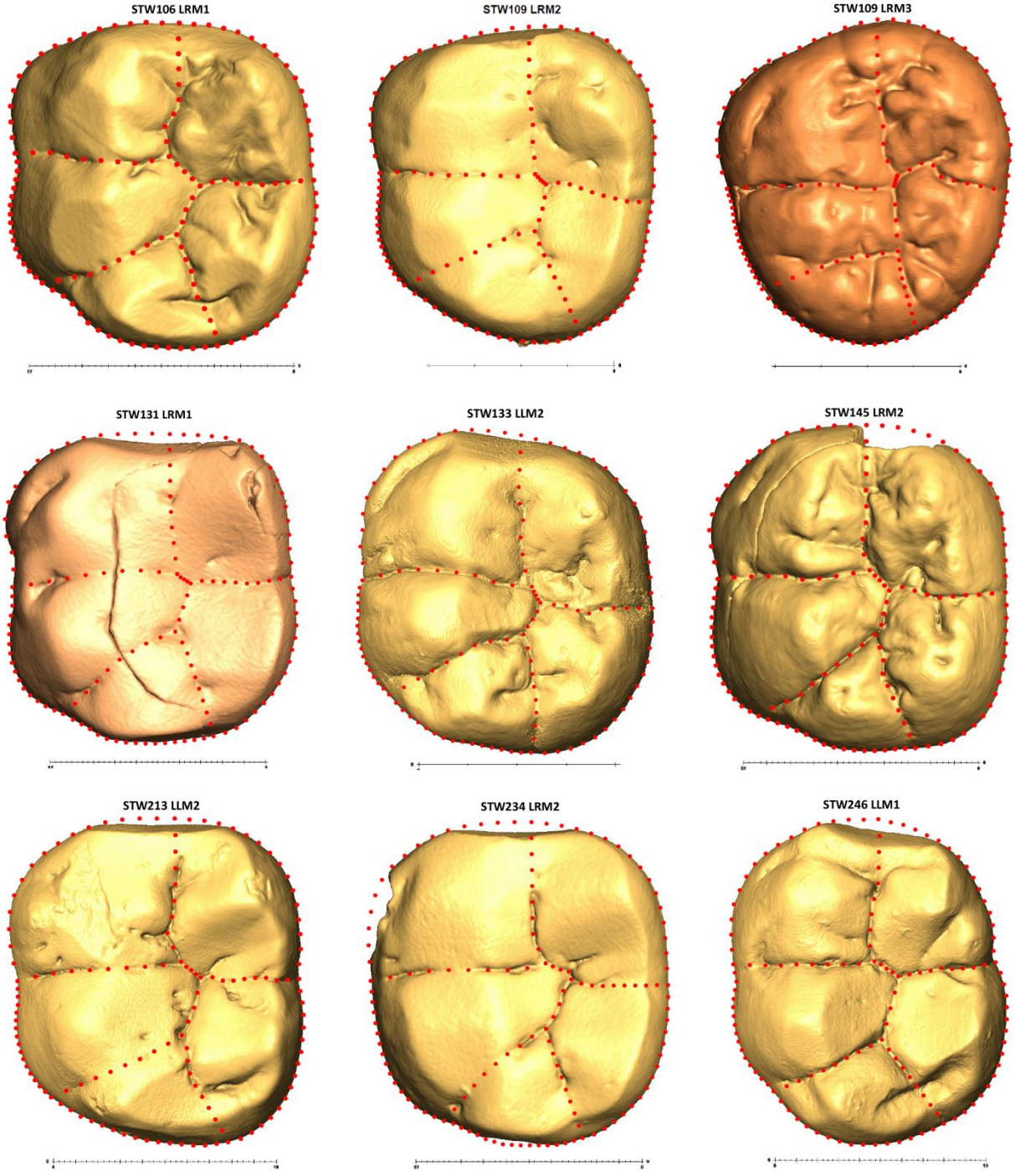
STW106 LRM1
STW109 LRM2
STW109 LRM3
STW131 LRM1
STW133 LLM2
STW145 LRM2
STW213 LLM2
STW234 LRM2
STW246 LLM1

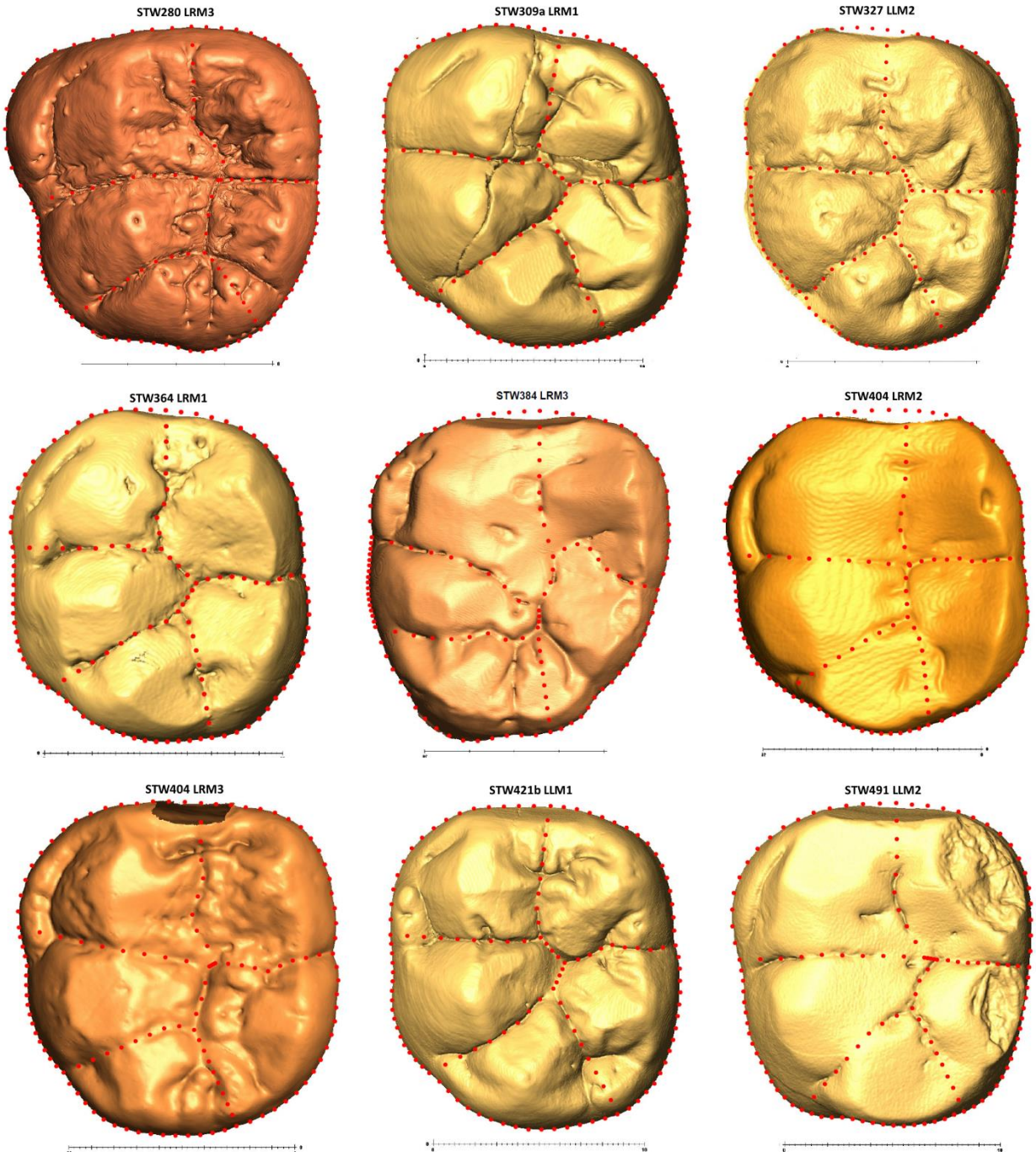
STW280 LRM3
STW309a LRM1
STW327 LLM2
STW364 LRM1
STW384 LRM3
STW404 LRM2
STW404 LRM3
STW421b LLM1
STW491 LLM2


STW491 LLM3
STW498c LLM2
STW498c LLM3
STW529 LRM3
STW537 LRM2
STW560a LRM3
STW560E LRM2
Taung 1 LLM1

Au. anamensis

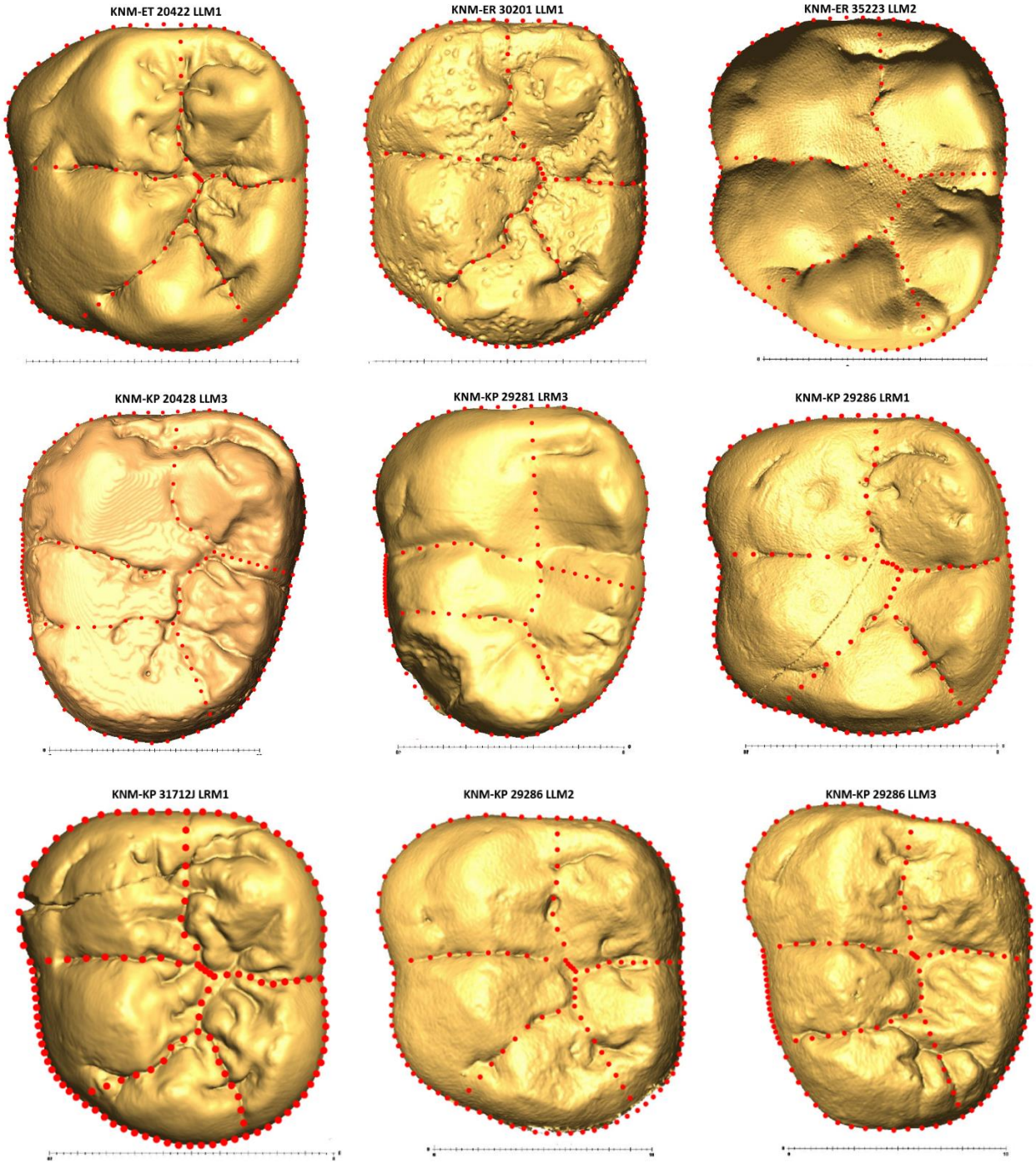

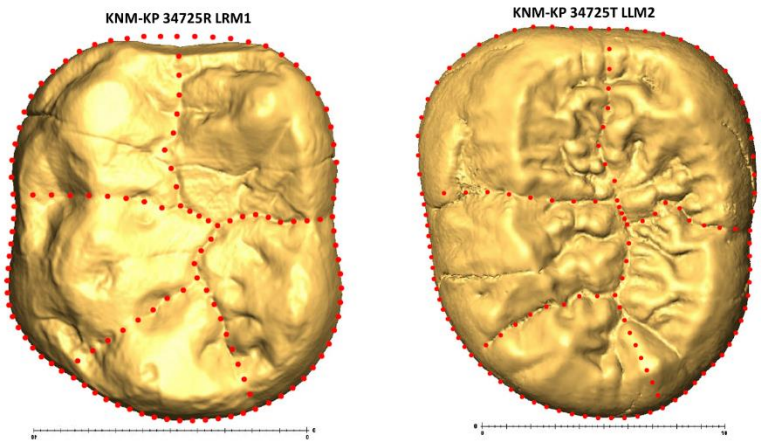

H. neanderthalensis

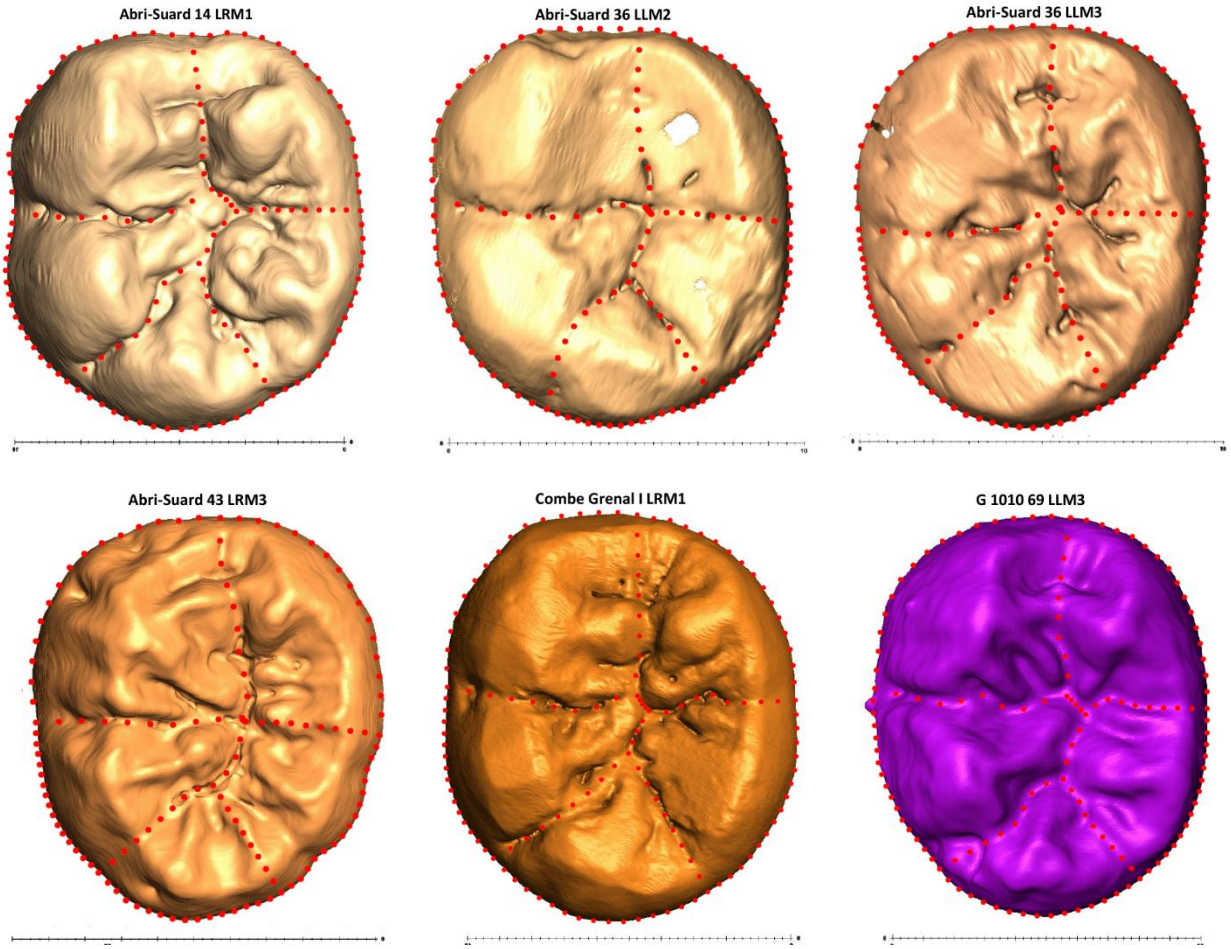


KRP 55 LLM2
KRP D1 LRM2
KRP 10 LRM2
KRP 53 LRM2
KRP D77 LRM1
La Quina Q760 H9 LLM2
Le Moustier LLM1
Le Moustier LLM2
Le Moustier LLM3

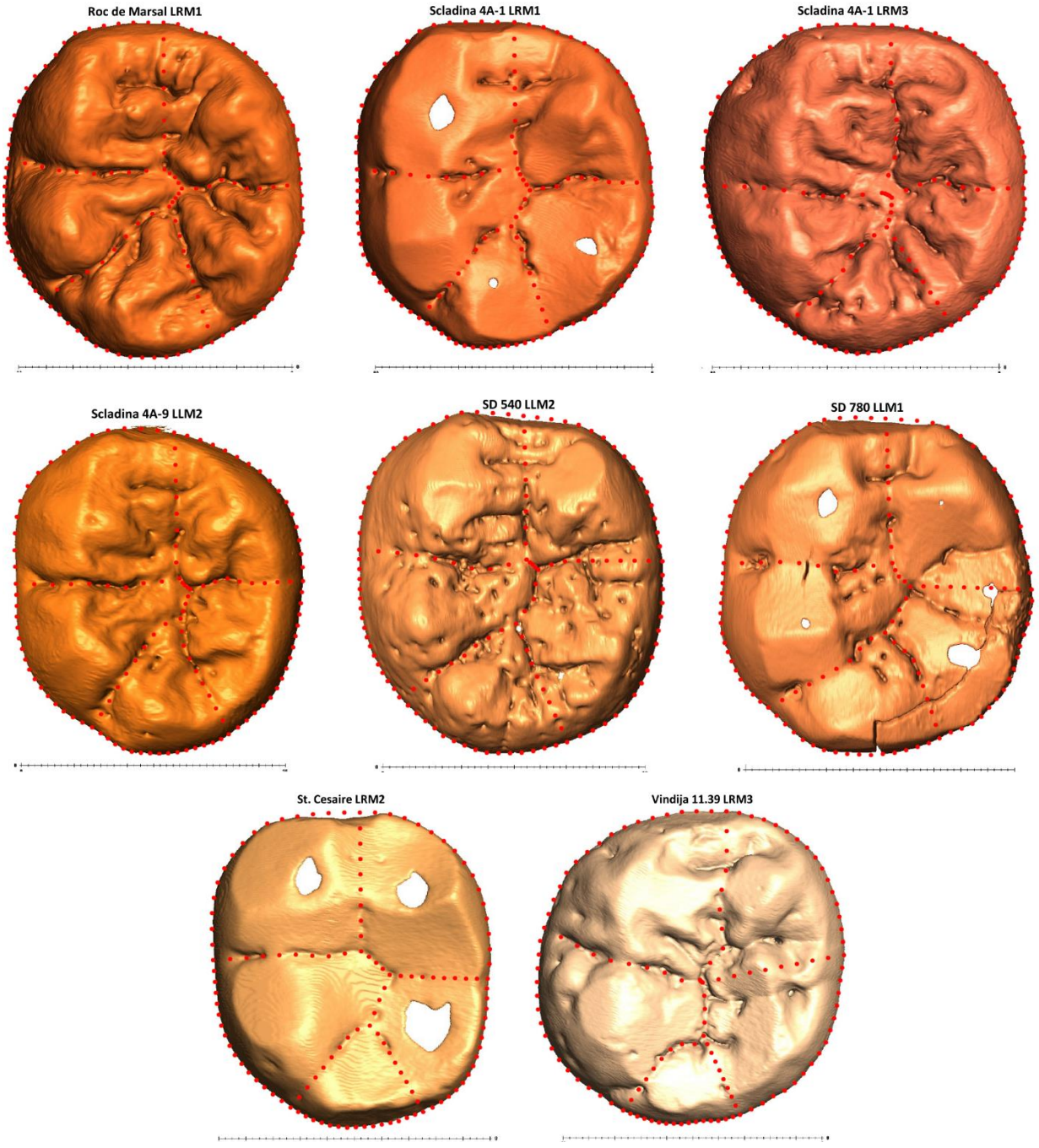
Roc de Marsal LRM1
Scladina 4A-1 LRM1
Scladina 4A-1 LRM3
Scladina 4A-9 LLM2
SD 540 LLM2
SD 780 LLM1
St. Cesaire LRM2
Vindija 11.39 LRM3

Bibliography

Adams, D. C., Rohlf, F. J., & Slice, D. E. (2004). Geometric morphometrics: ten years of progress following the 'revolution'. *Italian Journal of Zoology, 71*(1), 5-16.

Aguirre, E. (1970). Identificacion de ''Paranthropus'' en Makapansgat. *Crónica del XI Congreso Nacional de Arqueologia*, 98-124. Merida.

Alsberg, P. (1934). The Taungs Puzzle. A Biological Essay. *Man, 34*, 154-159.

Anderson, M. J. (2001). A new method for non-parametric multivariate analysis of variance. *Austral Ecology: A Journal of Ecology in the Southern Hemisphere, 26*(1), 32-46.

Antón, S. C. (2012). Early Homo: who, when, and where. *Current Anthropology, 53*(S6), S278-S298.

Asfaw, B., White, T., Lovejoy, O., Latimer, B., Simpson, S., & Suwa, G. (1999). Australopithecus garhi: a new species of early hominid from Ethiopia. *Science, 284*(5414), 629-635.

Ashton, E. H., & S. Zuckerman, F. R. (1950). Some quantitative dental characters of fossil anthropoids. *Phil. Trans. R. Soc. Lond. B, 234*(617), 485-520.

Benjamini, Y., & Hochberg, Y. (1995). Controlling the False Discovery Rate: A practical and powerful approach to multiple testing. *Journal of the Royal Statistical Society. Series B (Methodological), 57*(1), 289-300.

Berger, L. R., Ruiter, D. J., Churchill, S. E., Schmid, P., Carlson, K. J., Dirks, P. H., & Kibii, J. M. (2010). Australopithecus sediba: a new species of Homo-like australopith from South Africa. *Science, 328*(5975), 195-204.

Blumenberg, B., & Lloyd, A. T. (1983). Australopithecus and the origin of the genus Homo: Aspects of biometry and systematics with accompanying catalog of tooth metric data. *BioSystems, 16*(2), 127-167.

Bookstein, F. L. (1991). *Morphometric tools for landmark data: geometry and biology.* Cambridge University Press.

Bordes, F. (1975). Le gisement de Pech de l'Azé IV. Note Préliminaire. *Bulletin de la Societé Préhistorique Française, 72*, 293-308.

Broom, R. (1929). Note on the milk dentition of Australopithecus. *Journal of Zoology, 99*(1), 85-88.

Broom, R. (1936). New fossil anthropoid skull from South Africa. *Nature, 138*(3490), 486-488.

Broom, R. (1938). The pleistocene anthropoid apes of South Africa. *Nature, 142*(3591), 377-379.

Broom, R. (1943). An ankle-bone of the ape-man, Paranthropus robustus. *Nature, 152*(689), 690.

Broom, R. (1947). Discovery of a new skull of the South African ape-man, Plesianthropus. *Nature, 159*(4046), 672.

Broom, R. (1949). Another new type of fossil ape-man. *Nature, 163*(4132), 57.

Broom, R. (1950). The genera and species of the South African fossil ape-men. *American journal of physical anthropology, 8*(1), 1-14.

Broom, R., & Robinson, J. (1947). Jaw of the male Sterkfontein ape-man. *Nature, 160*, 153.

Broom, R., & Robinson, J. T. (1949). A new type of fossil man. *Nature, 164*(4164), 322-323.

Broom, R., & Robinson., J. T. (1952). *Swartkrans ape-man: Paranthropus crassidens. No. 6.* Transvaal Museum.

Broom, R., & Schepers, G. (1946). *The South African fossil ape-men: the Australopithecinae.* Pretoria: Transvaal Museum.

Broom, R., & Schepers, G. W. (1946). *The South African fossil ape-men: the Australopithecinae. No. 2.* Pretoria: Transvaal Museum.

Brown, B., Brown, F. H., & Walker, A. (2001). New hominids from the Lake Turkana basin, Kenya. *Journal of human evolution, 41*(1), 29-44.

Brunet, M. (1996). Australopithecus bahrelghazali, une nouvelle espece d'Hominid ancien de la region de Koro Toro (Tchad). *Comptes Rendus de l'Academie des Sciences, Paris, series II a 322*, 907-913.

Brunet, M. A., Coppens, Y., Heintz, E., Moutaye, A. H., & Pilbeam, D. (1995). The first australopithecine 2,500 kilometres west of the Rift Valley (Chad). *Nature, 378*(6554), 273-275.

Buchanan, B., & Collard, M. (2010). A geometric morphometrics-based assessment of blade shape differences among Paleoindian projectile point types from western North America. *Journal of Archaeological Science, 37*, 350–359.

Carney, J., Hill, A., Miller, J. A., & Walker., A. (1971). Late australopithecine from Baringo district, Kenya. *Nature, 230*(5295), 509-514.

Changbunjong, T., Sumruayphol, S., Weluwanarak, T., Ruangsittichai, J., & Dujardin, J. P. (2016). Landmark and outline-based geometric morphometrics analysis of three *Stomoxys* flies (Diptera: Muscidae). *Folia Parasitologica, 63*, 037.

Clark, L. G. (1947). Observations on the anatomy of the fossil Australopithecinae. *Journal of Anatomy* , 300-333.

Clark, W. L. (1950). Hominid characters of the australopithecine dentition. *Journal of the Anthropological Institute of Great Britain and Ireland, 80*(1), 37-54.

Clark, W. L. (1950). South African Fossil Hominoids. *Nature, 166*(4227), 893-894.

Clarke, R. J. (1985). Australopithecus and early Homo in southern Africa. In E. Delson (Ed.), *Ancestors: The hard evidence* (pp. 171-177). New York: Alan R. Liss.

Clarke, R. J. (1988). A new Australopithecus cranium from Sterkfontein and its bearing on the ancestry of Paranthropus. In F. E. Grine (Ed.), *Evolutionary history of the ‘‘robust’’ australopithecines* (pp. 285-292). New York: Aldine de Gruyter.

Clarke, R. J. (2008). Latest information on Sterkfontein's Australopithecus skeleton and a new look at Australopithecus. *South African Journal of Science, 104*(11-12), 443-449.

Cocos, A., & Halazonetis, D. J. (2017). Craniofacial shape differs in patients with tooth agenesis: geometric morphometric analysis. *European Journal of Orthodontics, 39*(4), 345–351.

Coffing, K., Feibel, C., Leakey, M., & Walker, A. (1994). Four-million-year-old hominids from East Lake Turkana, Kenya. *American Journal of Physical Anthropology, 93*, 55-65.

Dart, R. A. (1925). Australopithecus africanus the man-ape of South Africa. *Nature, 115*(2884), 195-199.

Dart, R. A. (1934). The Dentition of Australopithecus Africanus. *Folia anatomica japonica, 12*(4), 207-221.

Dart, R. A. (1948). The adolescent mandible of Australopithecus prometheus. *American journal of physical anthropology, 6*(4), 391-412.

Dart, R. A. (1948). The Makapansgat proto-human australo-pithecus prometheus. *American Journal of Physical Anthropology, 6*(3), 259-284.

Dart, R. A. (1949). The cranio-facial fragment of Australopithecus prometheus. *American journal of physical anthropology, 7*(2), 187-214.

de Ruiter, D. J., DeWitt, T. J., Carlson, K. B., Brophy, J. K., Schroeder, L., Ackermann, R. R., . . . Berger, L. R. (2013). Mandibular remains support taxonomic validity of Australopithecus sediba. *Science, 340*(6129), 1232997.

Delezene, L. K., & Kimbel, W. H. (2011). Evolution of the mandibular third premolar crown in early Australopithecus. *Journal of human evolution, 60*(6), 711-730.

Delezene, L. K., & Kimbel, W. H. (2011). Evolution of the mandibular third premolar crown in early Australopithecus. *Journal of human evolution, 60*(6), 711-730.

Dykes, S. J. (2016). A morphometric analysis of hominin teeth attributed to Australopithecus, Paranthropus and Homo. *South African Journal of Science, 112*(11/12), 1-15.

Garralda, M., & Vandermeersch, B. (2000). Les Néandertaliens de la grotte de Combe-Grenal (Domme, Dordogne, France)/The Neanderthals from Combe-Grenal cave (Domme, Dordogne, France). *Paléo, Revue d'Archéologie Préhistorique, 12*(1), 213-259.

Gómez-Robles, A., Martinón-Torres, M., Castro, J. B., Margvelashvili, A., Bastir, M., Arsuaga, J. L., . . . Martínez, L. M. (2007). A geometric morphometric analysis of hominin upper first molar shape. *Journal of Human Evolution, 53*(3), 272-285.

Gómez-Robles, A., Martinón-Torres, M., Castro, J. M., Prado-Simón, L., & Arsuaga, J. L. (2011). A geometric morphometric analysis of hominin upper premolars. Shape variation and morphological integration. *Journal of human evolution, 61*(6), 688-702.

Gomez-Robles, A., Martinon-Torres, M., de Castro, J., Prado, L. S., S, & Arsuaga, J. (2008). Geometric morphometric analysis of the crown morphology of the lower first premolar of hominins, with special attention to Pleistocene Homo. *Journal of human evolution, 55*(4), 627-638.

Greenfield, L. O. (1990). Canine “honing” in Australopithecus afarensis. *American journal of physical anthropology, 82*(2), 135-143.

Gregory, M., & William., K. (1939). The dentition of the extinct South African man-ape Australopithecus (Plesianthropus) transvaalensis Broom. A comparative and phylogenetic study. Part 1. *Annals of the Transvaal Museum, 19*(4), 339-352.

Gregory, W. K., & Hellman., M. (1939). The South African fossil man-apes and the origin of the human dentition. *The Journal of the American Dental Association, 26*(4), 558-564.

Grine, F. E. (2013). The Alpha Taxonomy of Australopithecus africanus. In K. E. Reed, J. G., & R. E. Leakey (Eds.), *The Paleobiology of Australopithecus* (pp. 73-104). Springer Netherlands.

Grine, F. E., & Martin, L. B. (1988). Enamel thickness and development in. In G. FE (Ed.), *Evolutionary history of the robust australopithecines* (pp. 3-42). New York: Aldine de Gruyter.

Grine, F. E., Delanty, M. M., & Wood, B. A. (2013). Variation in Mandibular Postcanine Dental Morphology and Hominin Species Representation in Member 4,Sterkfontein, South Africa. In K. E. Reed, J. G. Fleagle, & R. E. Leakey (Eds.), *The paleobiology of Australopithecus* (pp. 125-146). Springer Netherlands.

Grine, F. E., F., S. H., Heesy, C. P., & Smith, E. J. (2009). Phenetic affinities of Plio-Pleistocene Homo fossils from South Africa: molar cusp proportions. In *The First Humans–Origin and Early Evolution of the Genus Homo* (pp. 49-62). Dordrecht: Springer.

Grine, F. E., Jacobs, R. L., Reed, K. E., & Plavcan, J. M. (2012). The enigmatic molar from Gondolin, South Africa: implications for Paranthropus paleobiology. *Journal of human evolution, 63*(4), 597-609.

Grine, F. E., Ungar, P. S., & Teaford., M. F. (2006). Was the Early Pliocene hominin'Australopithecus' anamensis a hard object feeder? *South African Journal of Science, 102*(7-8), 301-310.

Guatelli-Steinberg, D. (2016). *What teeth reveal about human evolution.* Cambridge University Press.

Guatelli-Steinberg, D., & Irish, J. (2005). Brief communication: early hominin variability in first molar dental trait frequencies. *American Journal of Physical Anthropology, 128*(2), 477-484.

Gunz, P., & Mitteroecker, P. (2013). Semilandmarks: a method for quantifying curves and surfaces. *Hystrix, the Italian Journal of Mammalogy, 24*(1), 103-109.

Guy, F., Mackaye, H. T., Likius, A., Vignaud, P., Schmittbuhl, M., & Brunet, M. (2008). Symphyseal shape variation in extant and fossil hominoids, and the symphysis of Australopithecus bahrelghazali. *Journal of human evolution, 55*(1), 37-47.

Haile-Selassie, Y. (2010). Phylogeny of early Australopithecus: new fossil evidence from the Woranso-Mille (central Afar, Ethiopia). *Philosophical Transactions of the Royal Society of London B: Biological Sciences, 365*(1556), 3323-3331.

Haile-Selassie, Y., & Melillo, S. M. (2015). Middle Pliocene hominin mandibular fourth premolars from Woranso-Mille (Central Afar, Ethiopia). *Journal of human evolution, 78*, 44-59.

Haile-Selassie, Y., Gibert, L., Melillo, S. M., Ryan, T. M., Alene, M., Deino, A., . . . Saylor, B. Z. (2015). New species from Ethiopia further expands Middle Pliocene hominin diversity. *Nature, 521*(7553), 483-488.

Hlusko, L. J. (2004). Protostylid variation in Australopithecus. *Journal of Human Evolution, 46*(5), 579-594.

Irish, J. D., Guatelli-Steinberg, D., Legge, S. S., Ruiter, D. J., & Berger, L. R. (2013). Dental morphology and the phylogenetic "place" of Australopithecus sediba. *Science, 340*(6129), 1233062.

Johanson, D. C., & Taieb, M. (1976). Plio-pleistocene hominid discoveries in Hadar, Ethiopia. *Nature, 5549*(260), 293-297.

Johanson, D. C., White, T. D., & Coppens, Y. (1978). A new species of the genus Australopithecus (Primates: Hominidae) from the Pliocene of eastern Africa. *Kirtlandia, 28*, 1-14.

Johanson, D. C., White, T. D., & Coppens, Y. (1982). Dental remains from the Hadar Formation, Ethiopia: 1974–1977 collections. *American Journal of Physical Anthropology, 57*(4), 545-603.

Kaifu, Y., Kono, R. T., Sutikna, T., Saptomo, E. W., & Awe, R. D. (2015). Unique dental morphology of Homo floresiensis and its evolutionary implications. *PloS one, 10*(11), e0141614.

Keith, A. (1931). *New discoveries relating to the antiquity of man.* WW Norton, Incorporated.

Keith, A. (1948). *A new theory of human evolution.* London: Watts And Co.

Keith, A., & Smith., G. E. (1925). The fossil anthropoid ape from Taungs. *Nature, 115*(2885), 234-236.

Kimbel, W. H., & Delezene., L. K. (2009). "Lucy" redux: A review of research on Australopithecus afarensis. *American journal of physical anthropology, 140*(S49), 2-48.

Kimbel, W. H., Lockwood, C. A., Ward, C. V., Leakey, M. G., Rak, Y., & Johanson, D. C. (2006). Was Australopithecus anamensis ancestral to A. afarensis? A case of anagenesis in the hominin fossil record. *Journal of human evolution, 51*(2), 134-152.

Kimbel, W. H., Rak, Y., & Johanson, D. C. (2004). *The skull of Australopithecus afarensis.* Oxford University Press.

Klaatsch, H., & Hauser, O. (1908). Homo mousteriensis Hauseri: ein altdiluvialer Skelettfund im Departement Dordogne und seine Zugehörigkeit zum Neandertaltypus. *Arch Anthropol (new series), 7*, 287–297.

Kovarovic, K., Aiello, L. C., Cardini, A., & Lockwood, C. A. (2011). Discriminant function analyses in archaeology: are classification rates too good to be true? *Journal of Archaeological Science, 38*(11), 3006-3018.

Leakey, L. (1959). A new fossil skull from Olduvai. *Nature, 184*(4685), 491-493.

Leakey, L. (1960). Recent discoveries at Olduvai gorge. *Nature, 188*(4755), 1050-1052.

Leakey, L. (1961). The juvenile mandible from Olduvai. *Nature, 191*(4786), 417-418.

Leakey, L. S. (1958). Recent discoveries at Olduvai Gorge, Tanganyika. *Nature, 181*(4616), 1099-1103.

Leakey, L., Tobias, P., & Napier, J. (1964). A new species of the genus Homo from Olduvai Gorge. *Nature, 202*(4927), 7-9.

Leakey, M. D., Hay, R. L., Curtis, G. H., Drake, R. E., Jackes, M. K., & White, T. D. (1976). Fossil hominids from the Laetolil Beds. *Nature, 5568*(262), 460-466.

Leakey, M. D., Hay, R. L., Curtis, G. H., Drake, R. E., Jackes, M. K., & White, T. D. (1976). Fossil hominids from the Laetolil Beds. *Nature, 262*(5568), 460-466.

Leakey, M. G., Feibel, C. S., McDougall, I., & Walker., A. (1995). New four-million-year-old hominid species from Kanapoi and Allia Bay, Kenya. *Nature, 376*(6541), 565-571.

Leakey, M. G., Spoor, F., Brown, F. H., Gathogo, P. N., Kiarie, C., Leakey, L. N., & McDougall, I. (2001). New hominin genus from eastern Africa shows diverse middle Pliocene lineages. *Nature, 410*(6827), 433-440.

Lee-Thorp, J., Likius, A., Mackaye, H. T., Vignaud, P., Sponheimer, M., & Brunet, M. (2012). Isotopic evidence for an early shift to C4 resources by Pliocene hominins in Chad. *Proceedings of the National Academy of Sciences, 109*(50), 20368-20372.

Leveque, F., & Vandermeersch, B. (1980). Les découvertes de restes humains dans un horizon castelperronien de Saint-Césaire (Charente-Maritime). *Bulletin de la Société Préhistorique Française. Comptes Rendus des Séances Mensuelles Paris, 77*(2), 187-189.

Lockwood, C. A., Kimbel, W. H., & Johanson, D. C. (2000). Temporal trends and metric variation in the mandibles and dentition of Australopithecus afarensis. *Journal of Human Evolution, 39*(1), 23-55.

Manthi, F. K., Plavcan, J. M., & Ward, C. V. (2012). New hominin fossils from Kanapoi, Kenya, and the mosaic evolution of canine teeth in early hominins. *South African Journal of Science, 108*(3-4), 1-9.

Martin, R. M., Hublin, J.-J., Gunz, P., & Skinner, M. M. (2017). The morphology of the enamel–dentine junction in Neanderthal molars: Gross morphology, non-metric traits, and temporal trends. *Journal of human evolution, 103*, 20-44.

Martinón-Torres, M., Bastir, M., De Castro, J., Gómez, A., Sarmiento, S., Muela, A., & Arsuaga, J. (2006). Hominin lower second premolar morphology: evolutionary inferences through geometric morphometric analysis. *Journal of human evolution, 50*(5), 523-533.

Mayr, E. (1950, January). Taxonomic categories in fossil hominids. *Cold Spring Harbor Symposia on Quantitative Biology, 15*, 109-118. Cold Spring Harbor Laboratory Press.

Mitteroecker, P., & Bookstein, F. (2011). Linear discrimination, ordination, and the visualization of selection gradients in modern morphometrics. *Evolutionary Biology, 38*(1), 100-114.

Moggi-Cecchi, J., Grine, F. E., & Tobias, P. V. (2006). Early hominid dental remains from Members 4 and 5 of the Sterkfontein Formation (1966–1996 excavations): catalogue, individual associations, morphological descriptions and initial metrical analysis. *Journal of Human Evolution, 50*(3), 239-328.

Narum, S. R. (2006). Beyond Bonferroni: Less conservative analyses for conservation genetics. *Conservation Genetics, 7*(5), 783–787.

Nicholson, E., & Harvati, K. (2006). Quantitative analysis of human mandibular shape using three-dimensional geometric morphometrics. *American Journal of Physical Anthropology, 131*(3), 368-383.

Olejniczak, A. J., Smith, T. M., Skinner, M. M., Grine, F. E., Feeney, R. N., Thackeray, J. F., & Hublin, J. J. (2008). Three-dimensional molar enamel distribution and thickness in Australopithecus and Paranthropus. *Biology Letters, 4*(4), 406-410.

R Core Team (2017). *R: A language and environment for statistical computing*. R Foundation for Statistical: https://www.R-project.org/

Radovčić, J. (1988). *The Krapina hominids: an illustrated catalog of skeletal collection.* Mladost.

Robinson, J. (1953). Telanthropus and its phylogenetic significance. *American Journal of Physical Anthropology, 11*(4), 445-502.

Robinson, J. (1954). The genera and species of the Australopithecinae. *American Journal of Physical Anthropology, 12*(2), 181-200.

Robinson, J. (1965). Homo 'habilis' and the australopithecines. *Nature, 205*(4967), 121-124.

Robinson, J. T. (1953). Telanthropus and its phylogenetic significance. *American Journal of Physical Anthropology, 11*(4), 445-502.

Robinson, J. T. (1956). The dentition of Australopithecinae. *Transvaal Museum Memoir, 9*, pp. 1-179.

Robinson, J. T. (1960). The affinities of the new Olduvai australopithecine. *Nature, 186*(1960), 456-458.

Robinson, J. T. (1963). Adaptive radiation in the australopithecines and the origin of man. In F. C. Howell, & F. Bourliere (Eds.), *African ecology and human evolution* (pp. 385-416). Chicago: Aldine Pub.

Robinson, J. T. (1972). *Early hominid posture and locomotion.* University of Chicago Press.

Rosas, A., Martínez-Maza, C., Bastir, M., García-Tabernero, A., Lalueza-Fox, C., Huguet, R., . . . Martínez, E. (2006). Paleobiology and comparative morphology of a late Neandertal sample from El Sidrón, Asturias, Spain. *Proceedings of the National Academy of Sciences, 103*(51), 19266-19271.

Sanchez, M. V., Bastir, M., & Roldan, E. R. (2013). Geometric morphometrics of rodent sperm head shape. *PLoS ONE, 8*(11), e80607.

Senut, B. (1996). Pliocene hominid systematics and phylogeny. *South African journal of science, 92*(4), 165-166.

Skinner, M. M., Gunz, P., Wood, B. A., & Hublin, J. J. (2008). Enamel-dentine junction (EDJ) morphology distinguishes the lower molars of Australopithecus africanus and Paranthropus robustus. *Journal of Human Evolution, 55*(6), 979-988.

Spoor, F., Leakey, M. G., & Leakey, L. N. (2010). Hominin diversity in the Middle Pliocene. *Philosophical Transactions of the Royal Society B: Biological Sciences, 365*(1556), 3377-3388.

Spoor, F., Leakey, M. G., & Leakey, L. N. (2010). Hominin diversity in the Middle Pliocene of eastern Africa: the maxilla of KNM-WT 40000. *Philosophical Transactions of the Royal Society B: Biological Sciences, 365*(1556), 3377-3388.

Strait, D. S., & Grine, F. E. (2004). Inferring hominoid and early hominid phylogeny using craniodental characters: the role of fossil taxa. *Journal of human evolution, 47*(6), 399-452.

Suwa, G. (1988). Evolution of the "robust" australopithecines in the Omo succession: evidence from mandibular premolar morphology. In F. E. Grine (Ed.), *Evolutionary history of the "robust" australopithecines* (pp. 199-222). New York: Aldine de Gruyter.

Suwa, G. B. (1994). "Further analysis of mandibular molar crown and cusp areas in Pliocene and early Pleistocene hominids. *American Journal of Physical Anthropology, 93*(4), 407-426.

Suwa, G., Asfaw, B., Beyene, Y., White, T. D., Katoh, S., Nagaoka, S., . . . WoldeGabriel., G. (1997). The first skull of Australopithecus boisei. *Nature, 389*(6650), 489-492.

Tobias, P. V. (1965). Early man in east Africa. *Science, 149*(3679), 22-33.

Tobias, P. V. (1967). *The cranium and maxillary dentition of Australopithecus (Zinjanthropus) boisei. Olduvai Gorge, Vol. 2.* Cambridge: Cambridge University.

Tobias, P. V. (1980). Australopithecus afarensis" and A. Africanus: Critique and an alternative hypothesis. *Palaeontologia africana, 23*, 1-17.

Tobias, V. P. (1966). The distinctiveness of Homo habilis. *Nature, 209*(5027), 953-957.

Toussaint, M., Otte, M., Bonjean, D., Bocherens, H., Falgueres, C., & Yokoyama, Y. (1988). Immature Neandertal Remains of Level 4A of the Scladina cave (Andenne, Belgium). *C. R. Académie des Sciences - Series IIA - Earth Planetary Science, 326*, 737-742.

Turvey, S. T., Brunn, K., Ortiz, A., Hansford, J., Hu, S., Ding, Y., . . . Chatterjee, H. J. (2018). New genus of extinct Holocene gibbon associated with humans in Imperial China. *Science, 360*(6395), 1346-1349.

Ungar, P. S. (2011). Dental evidence for the diets of Plio-Pleistocene hominins. *American journal of physical anthropology, 146*(S53), 47-62.

Villmoare, B., Kimbel, W. H., Seyoum, C., Campisano, C. J., DiMaggio, E. N., R. J., & Reed, K. E. (2015). Early Homo at 2.8 Ma from Ledi-Geraru, Afar, Ethiopia. *Science, 347*(6228), 1352-1355.

Vlcek, E. (1993). *Fossile Menschenfunde von Weimar-Ehringsdorf.* Stuttgart: Konrad Theiss Verlag.

Ward, C. V., Leakey, M. G., & Walker, A. (2001). Morphology of Australopithecus anamensis from Kanapoi and Allia Bay, Kenya. *Journal of human evolution, 41*(4), 255-368.

Ward, C. V., Manthi, F. K., & Plavcan, J. M. (2013). New fossils of Australopithecus anamensis from Kanapoi, West Turkana, Kenya (2003–2008). *Journal of human evolution, 65*(5), 501-524.

Ward, C. V., Plavcan, J. M., & Manthi, F. K. (2010). Anterior dental evolution in the Australopithecus anamensis–afarensis lineage. *Philosophical Transactions of the Royal Society B: Biological Sciences, 365*(1556), 3333-3344.

Weinert, H. (1950). Uber die Neuen Vor-und Fruhmenschenfunde aus Afrika, Java. *Zeit. Morph. Anthrop, 42*, 113-148.

White, T. (2003). Early Hominids--Diversity or Distortion? *Science, 299*(5615), 1994-1997.

White, T. D. (1980). Additional fossil hominids from Laetoli, Tanzania: 1976–1979 specimens. *American Journal of Physical Anthropology, 53*(4), 487-504.

White, T. D. (1985). The hominids of Hadar and Laetoli: an element-by-element comparison of dental samples. In E. Delson (Ed.), *Ancestors: The Hard Evidence* (pp. 138-152). New York: Alan R. Liss.

White, T. D., Suwa, G., Simpson, S., & Asfaw, B. (2000). Jaws and teeth of Australopithecus afarensis from Maka, Middle Awash, Ethiopia. *American Journal of Physical Anthropology, 111*(1), 45-68.

White, T., WoldeGabriel, G., Asfaw, B., Ambrose, S., Beyene, Y., Bernor, R., . . . Hart, W. (2006). Asa Issie, Aramis and the origin of Australopithecus. *Nature, 440*(7086), 883-889.

Wolpoff, M. H., Smith, F. H., Malez, M., Radovčić, J., & Rukavina, D. (1981). Upper pleistocene human remains from Vindija cave, Croatia, Yugoslavia. *American Journal of Physical Anthropology, 54*(4), 499-545.

Wood, B. A., & Uytterschaut, H. (1987). Analysis of the dental morphology of Plio-Pleistocene hominids. III. Mandibular premolar crowns. *Journal of Anatomy, 154*, 121-155.

Wood, B. A., Abbott, S. A., & Graham., S. H. (1983). Analysis of the dental morphology of Plio-Pleistocene hominids. II. Mandibular molars--study of cusp areas, fissure pattern and cross sectional shape of the crown. *Journal of Anatomy, 137*, 287-314.

Wood, B. A., Abbott, S. A., & Uytterschaut, H. (1988). Analysis of the dental morphology of Plio-Pleistocene hominids. IV. Mandibular postcanine root morphology. *Journal of anatomy, 156*, 107-139.

Wood, B., & Constantino, P. (2007). Paranthropus boisei: fifty years of evidence and analysis. *American journal of physical anthropology, 134*(S45), 106-132.

Wood, B., & Leakey, M. (2011). The Omo-Turkana Basin Fossil Hominins and Their Contribution to Our Understanding of Human Evolution in Africa. *Evolutionary Anthropology: Issues, News, and Reviews, 20*(6), 264-292.

Wood, B., & Lonergan., N. (2008). The hominin fossil record: taxa, grades and clades. *Journal of Anatomy, 212*(4), 354-376.

Zelditch, M. L., Swiderski, D. L., & Sheets, H. D. (2004). *Geometric morphometrics for biologists: a primer.* New York: Elsevier Academic Press.

```
library(gtools)
library(geomorph)
library(splancs)
library(geometry)
#Creates a filelist in R that contains all the .txt files of the coordinates
of each curve
filelist <- list.files(pattern = ".c.*.txt")

#To be used for creating a .csv file in excel with accession ID and group
membership
filenames <- list.files(pattern = ".c10.*.txt")

#Sorts the files in both lists in numerical order.
sorted <- mixedsort(sort(filelist))
sortednames <- mixedsort(sort(filenames))


#Imports each curve text file into R as a table and compiles them into a
single list
data_list = lapply(sorted, read.table, sep = "")

#Coverts each table into a matrix
datamat <- sapply(data_list, as.matrix, simplify=FALSE)


#Code for generating equidistant semilandmarks. The part of the code that
generates semilandmarks is taken from digit.curves() from the package
'geomorph'. mysequence variables correspond to each curve. E.g. mysequence1
is curve 8, mysequence2 is curve 10, etc. This is a way to tell R to generate
the desired number of equdistant semilandmards for specific curves.
digiCurves <- function(i, X)
{
    mysequence1 = seq(8, length(datamat), by = 12)
    mysequence2 = seq(10, length(datamat), by = 12)
    mysequence3 = seq(6, length(datamat), by = 12)
    mysequence4 = seq(7, length(datamat), by = 12)
    mysequence5 = seq(9, length(datamat), by = 12)
    mysequence6 = seq(11, length(datamat), by = 12)
    mysequence7 = seq(12, length(datamat), by = 12)
    curve = X
    start = X[1,]
     if(i %in% mysequence1 | i %in% mysequence2){
         nPoints = 5
    } else if(i %in% mysequence3 | i %in% mysequence4| i %in% mysequence5| i
%in% mysequence6| i %in% mysequence7){
         nPoints = 10
    }  else
         nPoints = 17
    checkmat <- is.matrix(curve)
    if (checkmat == FALSE) {
        stop("Input must be a p-x-k matrix of curve coordinates")
    }
    checkdim <- dim(curve)[2]
    nCurvePoints = nrow(curve)
    start <- as.numeric(start)
```

```
    newPoints <- matrix(NA, ncol = checkdim, nrow = nPoints)
    start <- which.min(sqrt((start[1] - curve[, 1])^2 + (start[2] -
        curve[, 2])^2))
    newPoints[1, ] <- curve[start, ]
    if (start != 1 && start != nCurvePoints) {
        curve <- rbind(curve[start:nCurvePoints, ], curve[1:(start -
            1), ])
    }
    if (start == nCurvePoints) {
        curve <- curve[nCurvePoints:1, ]
    }
    newPoints[nPoints, ] <- curve[nrow(curve), ]
    B <- rep(0, nCurvePoints)
    for (i in 1:(nCurvePoints - 1)) {
    Interval <- sqrt((curve[i, 1] - curve[i + 1, 1])^2 +
                (curve[i, 2] - curve[i + 1, 2])^2)
        B[i + 1] <- B[i] + Interval
    }
    TotalLength <- B[nCurvePoints]
    j = 2
    for (i in 2:(nPoints - 1)) {
        NextLength <- TotalLength * (i - 1)/(nPoints - 1)
        while (B[j - 1] < NextLength) {
            j = j + 1
        }
        xy0 <- curve[j - 2, ]
        xy <- curve[j - 1, ]
        CurrInterval <- B[j - 1] - B[j - 2]
        if (CurrInterval > 0) {
            p <- (NextLength - B[j - 2])/CurrInterval
        }
        else p <- 0
        newPoints[i, 1] <- round((1 - p) * xy0[1] + p * xy[1],
            digits = 4)
        newPoints[i, 2] <- round((1 - p) * xy0[2] + p * xy[2],
            digits = 4)
        if (checkdim == 3) {
            newPoints[i, 3] <- round((1 - p) * xy0[3] + p * xy[3],
                digits = 4)
        }
    }
        return(newPoints[1:nPoints, ])
}
```

```
#Generates equidistant semilandmarks for each curve
semis = lapply(seq_along(datamat), function(i) digiCurves(i, datamat[[i]]))

#Combines all the landmarks of each specimen into a single matrix
CombinedLandmarks=lapply(seq(1,length(semis),by=12),function(x)do.call("rbind
", semis[x:(x+11)]))
CombinedCurves=lapply(seq(1,length(datamat),by=12),function(x)do.call("rbind"
, datamat[x:(x+11)]))
```

```
#Deletes duplicated fixed landmarks (in this case it's either the last or
first landmark of each curve). The duplicated landmarks have to be manually
selected.
NewCoords <- lapply(CombinedLandmarks, function(x)x[-c(18, 35, 52, 69, 85:86,
96, 105:106, 111,120, 121,126, 135,136, 145), ])

#Turns the list into a 3D array
NewCoordsArray <- array(as.numeric(unlist(NewCoords)),
dim=c(nrow(NewCoords[[1]]), ncol(NewCoords[[1]]) ,length(NewCoords)))

#Extraction of specimen names and group factors from a .csv file that was
created in excel.
classifier <- read.csv("HighestCVLabels2.csv", header=TRUE,stringsAsFactors =
FALSE)
keep<-classifier$Exclude!="ex"
classifier2<-classifier[keep,]
gp <- as.factor(paste(classifier2$Species))

#Names each matrix in the array
dimnames(NewCoordsArray)[[3]] <- classifier$Accession


#Loading a .csv file that indicates which landmarks are to be slid. Defining
sliders is done prior with the function define.slider from the package
'geomorph' and it is not presented here. See 'Quick Guide to Geomorph' for
more detailed instructions and infromation.
sliders <- read.csv("Sliders.csv", header=T, row.names=1)
sliders <- as.matrix(sliders)
#Sliding and GPA using function from the package 'geomorph'
B <- gpagen(NewCoordsArray,
curves=sliders,
ProcD=FALSE, print.progress = FALSE)


##Cusp areas

#Manually select the coordinates that make up each cusp. The order in which
they are typed in is important since the polygon should not be self
intersecting.
hypoconid <- NewCoordsArray[c(1:17, 121:110,101:98,89:97),,]
metaconid <- NewCoordsArray[c(49:65, 81:89, 98:109,49),,]
protoconid <-NewCoordsArray[c(65:80,1,97:81),,]
entoconid <- NewCoordsArray[c(33:49,109:101,110:113,122:129),,]
hypoconulid <- NewCoordsArray[c(17:33,129:122,113:121),,]

#Use the areapl function from the package 'splancs' to calculate the absolute
cusp areas for each specimen.
hypd.area <- apply(hypoconulid, 3, areapl)
met.area <- apply(metaconid, 3, areapl)
ent.area <- apply(entoconid, 3, areapl)
pro.area <- apply(protoconid, 3, areapl)
hyp.area <- apply(hypoconid, 3, areapl)

#Create a matrix where each column represents the absolute area of each cusp

crown <- cbind(hypd.area,met.area,ent.area,hyp.area,pro.area)
```

```
size <- apply(crown,1,sum)
B.crown <- cbind(hypd.area,met.area,ent.area,hyp.area,pro.area,size)

#Divide the absolute area of each cusp by the total area of the crown for
each specimen to calculate relative cusp areas
relative.cusp <- sweep(crown[,1:5], 1, rowSums(crown[,1:5]), FUN="/")


##MD and BL measurements

#Creates an empty matrix to contain the MD and BL measurements
MD.BL.mat <- matrix(0, nrow=dim(NewCoordsArray)[3],ncol=4)

#A loop for finding the smallest and largest X and Y values, and substracting
them from each other for each respective axis using the raw (that is pre
generalized Procrustes analysis) landmark coordinates.
for(i in 1:dim(NewCoordsArray )[3]){
      wmin <- which.min(NewCoordsArray [,2,i])
      wmax <- which.max(NewCoordsArray [,2,i])
      MDdis <- dist(NewCoordsArray [c(wmin,wmax),2,i])
      MD.BL.mat[i,1] <- MDdis
      w2min <- which.min(NewCoordsArray [,1,i])
      w2max <- which.max(NewCoordsArray [,1,i])
      BLdis <- dist(NewCoordsArray [c(w2min,w2max),1,i])
      MD.BL.mat[i,2] <- BLdis
      MD.BL.mat[i,3] <- MD.BL.mat[i,1]/MD.BL.mat[i,2]*100
      MD.BL.mat[i,4] <- (MD.BL.mat[i,1]+MD.BL.mat[i,2])/2
      }

rownames(MD.BL.mat) <- dimnames(NewCoordsArray)[[3]]
colnames(MD.BL.mat) <- c("MD","BL","Crown shape", "Crown size")
```